



The
University
Of
Sheffield.

Manipulation of Flames with Electric Fields

TIMOTHY DOLMANSLEY

March 2008

Supervisors: Professor C W Wilson & Dr D A Stone

**Report Submitted to the University of Sheffield in partial
fulfilment for the degree of Doctor of Philosophy in the Faculty
of Engineering**

THE UNIVERSITY OF SHEFFIELD

Abstract

An electric field is shown to have a strong affect on the blow off limits using both DC and pulsed fields. However, the DC fields only affects stochiometric and rich flames whereas pulsed fields also affect lean flames. The modifications using a DC field have been shown to originate from an aerodynamic body force created by the field, known as an ionic wind. The ionic wind has been experimentally measured, using particle image velocimetry (PIV). Its direction has also been modelled by analysing the field produced by the apparatus geometry.

There is no standard apparatus used by researchers in this field. It has been shown using electric field modelling techniques that the field will vary significantly between different geometries. It is suggested that a uniform field should be used ensuring that the affects of the field on a flame can be related to the field strength. The most uniform field is produced by parallel plates. However, it is suggested that if one of the electrodes is in the flow path it should be replaced with a mesh as the flow will not be disturbed aerodynamically. It is also proposed that the results be conducted in a Faraday cage to ensure there is no electrical interference.

The modelling work was supported by experimental data that showed a greater increase in the blow off limits with field strengths that were amplified by the apparatus geometry. The model also predicted the approximate change to the field when a flame was present. The results showed a close comparison with the ionic wind measured by PIV.



The
University
Of
Sheffield.

Manipulation of Flames with Electric Fields

TIMOTHY DOLMANSLEY

March 2008

Supervisors: Professor C W Wilson & Dr D A
Stone

Report Submitted to the University of Sheffield in partial fulfilment for the
degree of Doctor of Philosophy in the Faculty of Engineering

THE UNIVERSITY OF SHEFFIELD

Abstract

An electric field is shown to have a strong effect on the blow off limits of flames using both DC and pulsed fields. However, the DC fields only effects stoichiometric and rich flames whereas pulsed fields also effect lean flames. The modifications using a DC field have been shown to originate from an aerodynamic body force created by the field, known as an ionic wind. The ionic wind has been experimentally measured, using particle image velocimetry (PIV). Its direction has also been modelled by analysing the field produced by the apparatus geometry.

There is no standard apparatus used by researchers in this field. It has been shown using electric field modelling techniques that the field will vary significantly between different geometries. It is suggested that a uniform field should be used, ensuring that the effects of the field on a flame can be related to the field strength. The most uniform field is produced by parallel plates. However, it is suggested that if one of the electrodes is in the flow path it should be replaced with a mesh to minimise the aerodynamic disturbance to the flow. It is also proposed that the experiments be conducted in a Faraday cage to ensure there is no electrical interference.

The modelling work was supported by experimental data that showed a greater increase in the blow off limits with field strengths that were amplified by the apparatus geometry. The model also predicted the approximate change to the field when a flame was present. The results showed a close comparison with the ionic wind measured by PIV.

The pulsed fields increased the blow off limits more than DC fields. The greatest effect was found with a square wave, however the results varied very little when the pulse was activated for between 25 and 75% of the time period. Up to 5kHz (equipment limit) the increase in blow off velocity was greater for higher frequencies. The increase in blow off velocity occurred for all equivalence ratios (although it was stronger for rich flames). The results were shown to be independent of the ionic wind and were therefore caused by chemistry changes within the flame. The mechanism for this is discussed.

Table of contents

Abstract.....	i
Table of contents.....	ii
Acknowledgements.....	vi
Glossary of Terms.....	vii
Chapter 1 Introduction	1
1.1 Overview of the thesis	1
1.1.1 Contribution to knowledge.....	1
1.2 Background	2
1.2.1 Combustion	2
1.2.2 Electric field effects on combustion	8
1.2.3 Ions in flames	9
Chapter 2 Literature review.....	10
2.1 Ions in flames and how they get there.....	10
2.1.1 Method of ion formation - Chemi ionisation	10
2.2 How ions can be moved and excited by electric fields.....	15
2.2.1 Ionic wind.....	15
2.2.2 AC electric fields	17
2.3 How an electric field can influence a flame.....	19
2.3.1 Extinction	19
2.3.2 Increased stability	23
2.3.3 Emissions and flame temperature.....	27
2.3.4 Flame conduction of electricity	33
2.3.5 Heat transfer.....	34
2.3.6 Power consumption	36
2.4 Ionic wind vs chemical change debate	36
2.4.1 DC fields and AC fields up to 50Hz.....	37
2.4.2 AC and Pulsed Fields	38
2.4.3 Plasmas and Coronas	40
2.5 Modelling	41

2.6	Type/orientation of electrodes	41
2.7	Scope of the work	47
Chapter 3	Electrostatic Field Modelling.....	48
3.1	Introduction.....	48
3.2	Settings used for modelling	49
3.2.1	Theory	49
3.2.2	Model, meshing and materials	50
3.2.3	Boundary Conditions	52
3.2.4	Field orientation	56
3.2.5	Faraday cage position	56
3.2.6	Solver used.....	59
3.2.7	Program used	59
3.3	Field produced by experimental set ups used in the literature.....	62
3.4	Ionic wind direction	72
3.5	Effect of the upper electrode.....	73
3.6	Bunsen burner material	76
3.7	Cutting a hole in the plate	78
3.8	Effect of a conductive flame on field.....	80
3.9	Conclusions.....	90
Chapter 4	Experimental Study into the Effect of a DC Fields on a Flame.....	91
4.1	Introduction.....	91
4.2	Experimental set up.....	92
4.2.1	Apparatus	92
4.2.2	Figure 4.5 Picture of the Bunsen assembled.....	95
4.2.3	Mixer.....	95
4.2.4	Mass flow rate.....	99
4.2.5	Measurement.....	100
4.2.6	Procedure	101
4.3	Results of applying a DC field.....	102
4.4	Change of field direction	107
4.5	Different set ups (ring Bunsen, tube wire and plates).....	109

4.5.1	Aerodynamic effect	110
4.5.2	Applied electric field effect.....	116
4.6	Ignition tests	120
4.7	Discussion.....	122
4.8	Conclusions	127
Chapter 5	Effect of Pulsed Fields.....	128
5.1	Introduction and apparatus	128
5.2	Effect of frequencies with a square wave.....	130
5.2.1	Results	130
5.3	Pulse width effect.....	133
5.3.1	Rich mixture results.....	136
5.3.2	Around stoichiometric mixture results	138
5.3.3	Lean mixture results	139
5.4	Effect of both frequency and pulse width.....	141
5.5	Reverse polarity	144
5.6	Discussion.....	147
5.7	Conclusions	155
Chapter 6	High Speed Camera Work.....	156
6.1	Particle image velocimetry (PIV)	156
6.2	Seeding	160
6.2.1	Apparatus selection.....	160
6.3	Results.....	167
6.3.1	Adaptive correlation	169
6.3.2	Moving Average	170
6.3.3	Velocity profile and regions of poor seeding.....	172
6.3.4	Comparison of PIV with and without an applied field.....	180
6.3.5	Streamlines	185
6.3.6	Ionic wind.....	188
6.4	Particle tracking	199
6.4.1	Method.....	199
6.4.2	Results	202

6.5	Conclusions.....	205
Chapter 7	Conclusions.....	206
7.1	Future work.....	209
	References.....	212
	Appendix 1.....	224
	Ionic Species in Flames	224
	Appendix 2.....	225
	5kV comparison of apparatus	225
	5kV Ignition tests.....	226
	Appendix 3.....	227
	Particle Image Velocimetry (PIV).....	227
	Lean flame no field	227
	5kV DC lean flame	228
	10kV DC lean flame	230
	Rich flame no field.....	232
	Rich flame 5kV	234
	Rich flame 10kV	236
	Stoichiometric flame no field.....	238
	Stoichiometric flame 10kV	240
	Appendix 4.....	243
	Particle tracking	243
	DC Results	243
	Pulse Results	244
	3 Dimensional Graphs of Particle Tracking.....	246

Acknowledgements

I would like to thank several members of staff in the departments of Mechanical and Electrical Engineering, Dr Stephen Beck, Dr Simon Blakey, Dr Martin Foster and Dr Robert Woolley for valuable time they have spent explaining difficult topics. I would also like to thank Simon Choppin for his assistance with the particle tracking work.

I am very grateful to Robert Yaracheski of Dantec Dynamics for the loan and use of their PIV software. Robert was very generous with his time and expertise.

Many of the experiments conducted in this report have used apparatus built by Malcolm Nettleship. I would like to thank him for all of his efforts and patience with me when apparatus had to be altered.

I would also like to thank both of my supervisors, Prof. Christopher Wilson and Dr David Stone. Both of whom have managed to provide valuable equipment at crucial times. It is with deep gratitude that I thank Prof Wilson for financial support when the project took longer than expected to complete. Both of my supervisors have been full of words of wisdom and encouragement.

There are many people who have given me support through difficult times. However, I wish particularly to thank my parents and Uncle John Mockford for encouraging me to finish.

Lastly I would like to thank my wife Hannah. She has always been there to encourage me, as well as staring at flames in the lab for weeks on end and proof reading the final product. Words cannot begin to say how grateful I am to you.

Glossary of Terms

Blow off	A term referring to a burner stabilised flame. The burner prevents the flame propagating upstream due to the quenching effect of the burner. Blow off is the term for when the flame speed is less than the fluid velocity and combustion cannot be sustained and the flame is extinguished. Blow off may be preceded by “lift off” for rich flames (see below)
Chemion	An ion formed by chemical reaction of a hydrocarbon
Corona	Local ionisation of gas. As the voltage is increased this can lead to the total ionisation of the gas between the electrodes, causing dielectric breakdown
Equivalence ratio	The actual fuel/air ratio divided by the stoichiometric fuel/air ratio
Free ion	Ion produced by a corona
Flashback	Burner stabilised combustion term referring to the point at which a flame propagated back along the burner
Ionic wind	An aerodynamic body force resulting from the attraction of ions to electrodes
Lean	Premixed combustion term meaning deficiency in fuel (excess air)
Rich	Premixed combustion term meaning deficiency in air (excess fuel)
Stoichiometric	This is when there is exactly enough air for complete combustion of all the products

Chapter 1 Introduction

1.1 Overview of the thesis

Ions are produced in the combustion of hydrocarbons. These ions can be moved within the flame using an external electric field. The aim of this work is to further research the effect electric fields have on flames. The ultimate goal is to see electrically controlled combustion, but this is beyond the scope of the present work. There has already been extensive research on this topic which is reviewed in Chapter 2 and gives the reader an impression of how electric fields have been used to modify the combustion of hydrocarbons.

Due to the effect on a flame being dependant on the field strength applied, the field is modelled in Chapter 3 for a range of apparatus geometries. The most uniform field has been chosen for the experiments conducted in this work to ensure the affect can be directly related to the field strength. Altering the geometry of the apparatus could be used to amplify the field with no additional power input.

Once the apparatus has been chosen the effect of an electric field on a flame can be measured for direct current (DC) fields (Chapter 4) and for pulsed fields (Chapter 5). These effects were measured for flames with a range of equivalence ratios.

The flame was then analysed using particle imaging velocimetry (PIV) and particle tracking (Chapter 6) to identify whether the cause of the effects are aerodynamic or chemical. The results of this was used to asses the quality of the field predicted by the modelling.

1.1.1 Contribution to knowledge

This work has made the following contributions to knowledge;

- Identified the differences between the electric field produced by the various apparatus used by researchers to date
- Modelled the field without the flame present and estimated the change in the field when a flame is present
- Suggested apparatus that produces an uniform field where the effects of an electric field on a flame can be related to the field strength
- Qualitatively validated these results by using particle image velocimetry to model the ionic wind and shown how different apparatus have a greater or lesser effect on a flame, depending on the field strength they produce
- Shown how a DC field can increase the rich burning limits (blow off limits)
- Shown that the increase in blow off limits of a flame by DC fields is due to the ionic wind
- Shown that AC and pulsed fields can increase the blow off limits of a flame in lean, stoichiometric and rich flames
- Shown that the increase in the blow off limits of a flame is greater for higher frequencies (up to 5kHz) and for pulse durations that are 25-75% of time between the pulses(peaking at 50% or a square waveform)
- Shown that the increase in the blow off limits of a flame by AC and pulsed fields is due to changes to the flame chemistry, not from the ionic wind

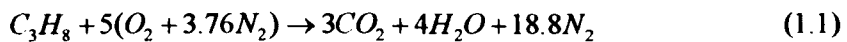
1.2 Background

1.2.1 Combustion

Mankind has been building fires for as long as we can trace our history. The methods for doing this have become increasingly complex as we try to increase the efficiency and understand the impact of combustion on our environment. Combustion is simply the oxidation of a fuel. The introduction of fuel and oxygen into the system can greatly change the characteristics of combustion. For example this could be the method of fuel vaporisation (for a liquid fuel) or the point at which air is introduced into the system (before or after combustion). If the air is not introduced into the flow before combustion then the flame becomes a diffusion flame, so called as the air has to diffuse into the flame from one side of the flame while fuel is introduced from the other side. This type of

combustion has a distinct flame boundary with unburnt fuel on one side and oxygen (usually in the form of air) on the other side. If oxygen is introduced before combustion the flame is known as a premixed flame. A good example of the difference between the two types is a Bunsen burner; the yellow diffusion flame can be turned into a blue premixed flame by opening the air inlet at the base of the Bunsen.

The amount of air introduced into the flow also has a great impact on the combustion characteristics. The exact amount of air required for complete combustion can be calculated as shown below for propane. The simplified reaction can be given by;



Therefore for 1 mol of propane (C_3H_8) 5 mol of (O_2) are required. The oxygen is supplied by air ($O_2 + 3.76N_2$). To supply 5 mol of O_2 requires, $(5*1)O_2 + (5*3.76)N_2 = 23.8air$.

This means that if 1 mol of fuel is present and 23.8mol air is mixed with it then it will burn completely with no fuel or oxygen left over. This case is called stoichiometric combustion. If more air is introduced then fuel will be deficient and there will be excess air; this case is called lean combustion. If there is less air than required for stoichiometric combustion air is deficient and fuel is in excess; this is called rich combustion. It is common to refer to the air to fuel ratio (the mass of air divided by the mass of fuel). This can be made into a non dimensional number (called the equivalence ratio, Φ) by dividing the actual air fuel ration by the stoichiometric air fuel ratio. This gives a value of 1 for stoichiometric, less than 1 for lean and greater than 1 for rich.

The velocity and temperature of the flame is altered by the equivalence ratio. Any excess air will quench the flame, lowering the temperature and dilute the reactants, taking longer for them to mix. Excess fuel will require oxygen to be absorbed from the surroundings, increasing the size of the flame; this can reduce the temperature due to the increased radiation losses.

A flame will travel along a mixture of fuel and air at a given speed, called the flame speed. This can make it very difficult to observe the flame or keep it in a given place. In domestic and industrial systems flames are made stable by attaching the flame to a

burner. The burner quenches the flame at the burner mouth, preventing it from travelling back along the incoming flow, down the burner tube (known as flash back) under most circumstances. However, if the flow rate from the burner is greater than the flame speed the flame will “lift off” the burner until it is far enough away for the burner quenching effect to become reduced and the flame speed increase again. However, this lift off will entrain air into the flow, diluting the flow. For lean flames this will cause a further decrease in the burning velocity and cause the flame to “blow off” (or be extinguished).

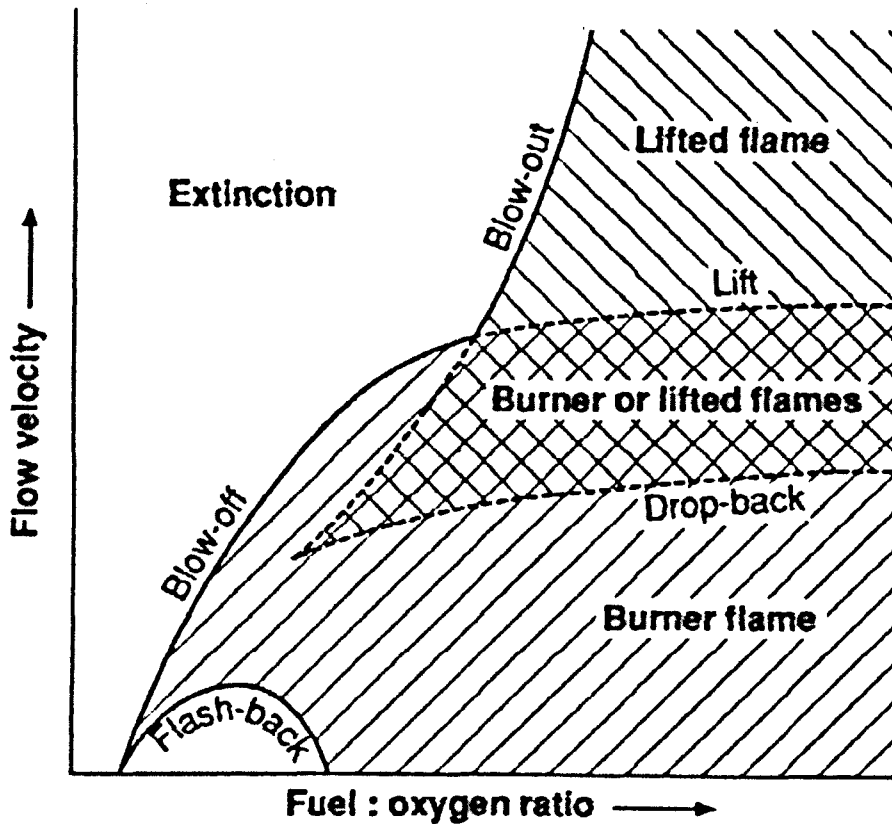


Figure 1.1 Blow off velocity against fuel/air ratio from Griffiths and Barnard [1]

However, for a rich flame the additional air entrainment brings the mixture closer to stoichiometric and increases the flame velocity, allowing a “lifted flame” to form some distance above the burner. The relationship is shown clearly by Griffiths and Barnard [1], shown in Figure 1.1.

These results represent the limits of combustion for burner systems. The aim of this work is to extend these limits, allowing leaner flames and faster flow rates.

The effect of combustion of the environment can be defined as the pollutants that it emits. The emissions from hydrocarbon combustion that are considered to be undesirable are oxides of nitrogen, unburned or partially burned hydrocarbons, carbon monoxide and soot. The carbon dioxide emission is also important but this is a product of complete combustion and the only way in which it can be reduced is to increase the efficiency of the flame, reducing the amount of fuel required. Oxides of sulphur are not mentioned as the combustion engineer is not concerned with the production of sulphur oxides as their emission is mainly dependant on the sulphur content of the fuel. Almost all premixed combustion deals with low sulphur content fuel (natural gas contains virtually no sulphur and gasoline contains less than 600ppm by weight sulphur [2]) so sulphur oxides can be neglected for this case. Nitrogen oxides (often called NO_x) are formed by 3 mechanisms;

1. Thermal (or Zeldovich) NO_x . This is the slow oxidation of nitrogen by oxygen. The thermal formation mechanism is shown below in equations (1.2), (1.3) and (1.4);



The rate of this reaction is highly temperature dependant.

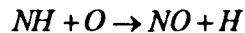
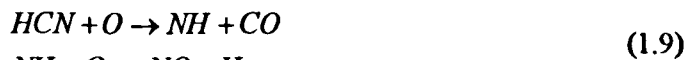
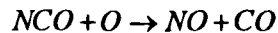
2. Prompt (or Femmore) NO_x . This mechanism produces less NO_x in high temperature combustors than the thermal mechanism. However, many modern, low NO_x burners have so successfully reduced thermal NO_x that this may be the major method of production. It forms differently for lean and rich systems. For lean systems;



The oxygen radical formed then attacks the N_2 molecule to form NO. In fuel rich systems;



The N from (1.6) then goes on to form NO by the thermal mechanisms shown in (1.3) and (1.4). NH formed by (1.7) is oxidised by the following mechanisms;



3. Fuel NO_x . Nitrogen bound in the fuel is released during combustion to form NH_3 or HCN. NH_3 broken down to NH_2 , followed by NH which is oxidised to NO_x . HCN is converted to NO_x as previously described in (1.8) and (1.9).

In a simple burner almost all the NO_x will originate from the thermal mechanism. However, most modern burners are designed to reduce this by decreasing the temperature of combustion by burning lean or staging the air or fuel input (this is discussed in detail in Turns [2], Chapter 15 and will not be repeated here).

The production of soot is also temperature dependant. The production of soot increases with temperature before reaching a plateau. However, soot is also oxidised in the flame and the rate at which this occurs is also temperature dependant. However reduction in soot emission is favoured by higher temperatures. This can be seen in Figure 1.2 and the regions of soot emission are shown below the graph.

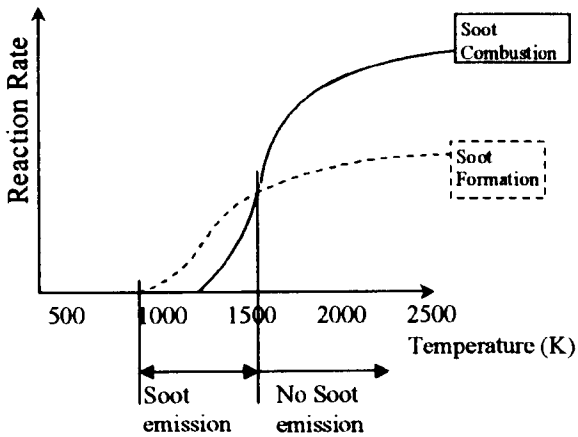


Figure 1.2 Graph of reaction rate against temperature for soot and nitrogen formation taken from Griffiths and Barnard [1]

Particulate emission or unburnt hydrocarbon emission results only from rich combustion (not enough air to completely burn all the fuel). For this reason many modern combustors choose to burn lean.

As the system burns leaner the temperature of the exhaust gasses decreases. As the temperature decreases the ratio of specific heats (pressure and volume), γ , increases. For an ideal gas, the ratio of temperatures is related to the ratio of volumes by;

$$\frac{T_2}{T_1} = \left(\frac{V_1}{V_2} \right)^{\gamma-1} \quad (1.10)$$

For a system such as an internal combustion engine, where the volume ratio is fixed the temperature ratio must therefore increase for leaner equivalence ratios. This gives more work per unit mass. The result of this can be seen by looking at the otto cycle for diesel engines. This can be seen below in Figure 1.3.

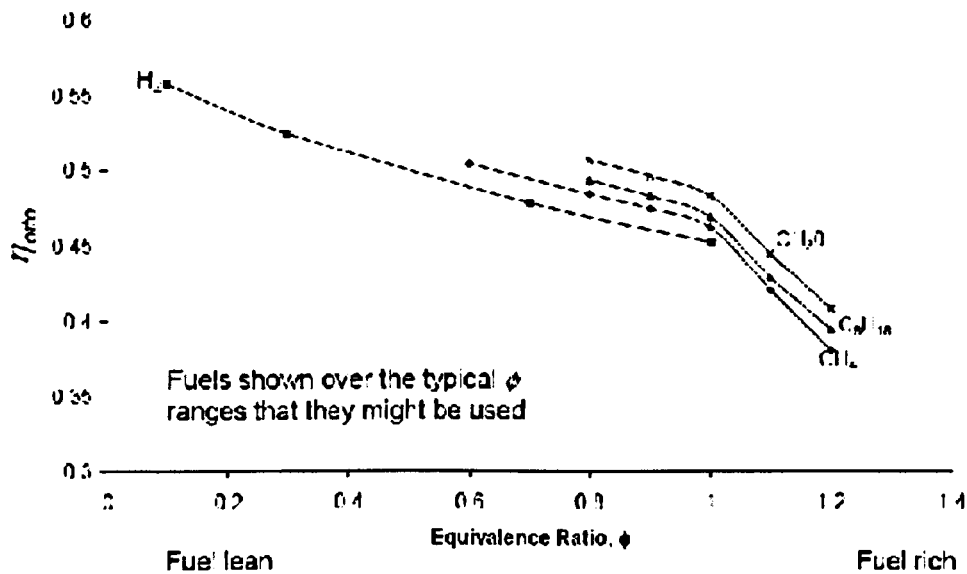


Figure 1.3 Otto efficiency for various equivalence ratios for non constant specific heat ratio

For leaner systems the efficiency is increased as well as decreasing the NO_x and soot. Therefore it is very advantageous to burn leaner and the aim of this work is to increase the combustion limits, particularly in the lean region.

1.2.2 Electric field effects on combustion

Interest in how electric fields could be used to manipulate combustion began as early as 1600 when William Gilbert first used charged furs and rods to attract flames [3]. Hauksbee [4] in 1709, followed by Brande [5] in 1814 was the first to scientifically analyse the influence of an electric field on a flame. However, the earliest work of real significance was Chattock [6] in 1899, who identified an aerodynamic body force created when charged particles were subjected to an external electric field. In honour of his discovery some researchers still use the term “Chattock wind” for this body force, although it is becoming increasingly popular to refer to it as the ionic wind. This will be further discussed in Chapter 2 as the effects of the ionic wind is still the subject of debate.

Despite the length of time that it has been known that electric fields can influence flames no practical use has been found. The effects are still not fully understood and there is still

extensive discussion in the literature about what causes them. The aim of this work is to further understand the effect of electric fields on flames and try to assess their source.

1.2.3 Ions in flames

Ions are formed in flames as part of the combustion of hydrocarbons (see section 2.1). These ions are often called chemi ions. Ions can also be formed by the application of an electric field. This can be by two methods; chemi ion collision/attachment or corona discharge. Chemi ions are pulled towards the electrodes and collide with neutral particles. Inelastic collisions with electrons or high energy collisions where enough energy is released to free an electron will further ionise the medium [7-9]. Corona discharge is created when the local field strength is above the dielectric breakdown voltage. For air the dielectric breakdown is approximately 3MV/m. The results of this work use a maximum of 170kV/m and with the dielectric breakdown measured as approximately 330kV/m. The reason that this measured value is so much lower than for air is due to the presence of the flame. At this voltage the medium will begin to ionise, leading to a spark discharge. However, if the geometry of the electrodes is such that there is a high concentration of the field at one electrode then the ionisation voltage can be reached close to that electrode but not for the whole medium (which is required for a spark). Coronas were commonly used in photocopiers and are responsible for the “fresh air” smell in thunderstorms (where O₃ is formed by the coronas). Early researchers used coronas as a method of producing ions [6] and can be used to produce a locally strong velocity which can be used to cool parts of a combustor, shown by Sandhu and Weinberg [10] (this will be further discussed in section 2.3.5). Ion movement, such as from a corona, are even used for the thrusters on space craft [11]. The use of coronas, although still very small, requires higher power consumptions than manipulation of the chemi ions already present in the flame (in the order of 60μA for coronas compared to 1μA for manipulation of chemi ions). This work therefore uses the chemi ions created from the combustion process. In the remainder of the thesis the term ionic wind will be used to refer to the ionic wind created from the chemi ions and not from free ions from coronas, unless specifically stated.

Chapter 2 Literature review

There have been several papers that give an overview on how electric fields can influence flames. Extensive reviews of this can be found in Lawton and Weinberg [7], Fialkov [12] and Huneiti Balachndran [13]. However, there have been no recent papers that review the subject. The aim of this chapter is to review the current understanding of this subject and identify the areas where the knowledge base is incomplete.

2.1 Ions in flames and how they get there

Ions are naturally formed in the combustion of hydrocarbons. However, when a field is applied ions can also be produced by secondary ionisation or coronas. The major interest of this work is to manipulate the ions that are formed as a natural part of the combustion process. This requires small power inputs while achieving large changes to the combustion process (ion formation by corona requires a lot more power than manipulation of chemi ions, as discussed in section 1.2.3).

This study is also mainly concerned with how ions in flames can be used and manipulated rather than how they get there. Therefore only a brief outline of how ions are formed in flames will be given here. More interested readers should look particularly at Pedersen [14] as well as Pederson and Brown [15], Lawton and Weinberg [7] page 218, Calcote [16] and Peeters et al [17].

2.1.1 Method of ion formation - Chemi ionisation

Early experiments [18-20] identified that flames have a much greater number of ions in the flame than equilibrium conditions would suggest (there can be as many as 10^9 ions/cm³ in the flame front [21]). A reaction involving a hydrocarbon or a hydrocarbon radical must be involved as combustion of pure hydrogen contains far fewer ions than

that of hydrocarbon combustion (thermal ionisation is dominant [22]) and many of these ions are accounted for by hydrocarbon impurities in the hydrogen [22-3].

Calcote [16] looked at the methods proposed for the source of ions in flames (thermal ionisation of impurities, radical species, carbon atoms, translational energy, and cumulative excitation) and was able to prove that the only explanation is that the ions are formed by chemi-ionisation. The reasons why are best explained by Calcote himself [16] so interested readers are directed there.

Chemi-ionisation is when enough energy is released during a chemical rearrangement to ionise one of the products. This method is the only one where the concentrations of ions produced are in the order of those observed [16]. Much work has been done to prove this (see Lawton and Weinberg for a review [7]).

The importance of Calcote's work was not only to present chemi-ionisation as the primary method for ion formation in flames but to identify CHO^+ as the major source of ions in flames by the chemi-ionisation reaction (2.1).



Calcote proposed that the other ions observed in flames were the result of charge transfer reactions involving CHO^+ . For example the most abundant ion found in flames H_3O^+ can be shown to form from CHO^+ (2.2).



Since Calcote's work several others have tried to find other primary ions in flames and confirm Calcote's theory. It is now generally accepted that reaction (2.1) is the major reaction to occur [7], [8], [17], [24].

Peeters et al [17] have a good summary of the work after Calcote, along with reaction (2.1), they suggest the following reactions may also result in ionisation;





There has been some discussion as to whether the ion $C_3H_3^+$ is a primary ion [7] [8]. However, what is important for this study is that although reactions (2.3), (2.4), (2.5) and (2.6) are possible (and may occur in the flame) the most important chemi-ion is CHO^+ , produced through reaction (2.1) and the majority of other ions present in flames are derived from this ion. This work is supported by Fialkov et al [8] who experimentally found that CHO^+ , CHO_2^+ and an ion of mass 32amu, probably O^+ , are the only primary ions present in strong electric fields which pulls the primary ions out before they have time to react with other species [25]. Several authors have reported that when the field strength is strong enough the variety of ionic species drops and CHO^+ is the main ion found. Good reviews of the above can be found in Huneiti and Balachandran [13], Hu et al [24] and Lawton and Weinberg [7] [25].

Several authors have found the effects of electric fields on flames are greatly decreased when the carbon content of the burning gas is decreased [26] [27]. This supports the theory of reaction (2.1) as carbon is required for the reaction.

The most abundant ion present in flames is H_3O^+ [7] [14] [24], formed by reaction (2.2) [16]. The principle method for the recombination of ions is the highly exothermic reaction (2.7) [16] [28].

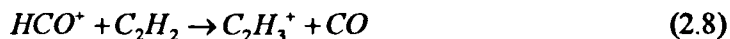


Further studies identified the positive ions present in flames, most notably the works of Sugden [23] and van Tiggelen [17]. An extensive, critical review is available by Lawton and Weinberg [7] page 218. See Appendix 1 for a list of the positive ions identified in flames. The regions where these ions exist is also presented in Lawton and Weinberg [7] chapter 6. Further work of interest can be found in Kinbara and Nakamura [29], Green and Sugden [23] and Sugden et al [30]. The methods of formation of these ions is too long to be presented here but can be found in Van Tiggelen et al [17], Green and Sugden

[23], Sugden et al [30] and Vinckier et al [31]. Application of an electric field will hinder the formation of these downstream ions, but this point will be discussed later.

As mentioned above, CHO^+ goes on to produce the majority of ions within the flame. Figure 2.1, above, gives a visual idea of how many ions are produced and how.

The reaction leading to polymerization is



$\text{C}_{2n}\text{H}_{2n-1}^+$ and $\text{C}_{2n}\text{H}_{2n+1}^+$ are then formed as shown below in Figure 2.2;

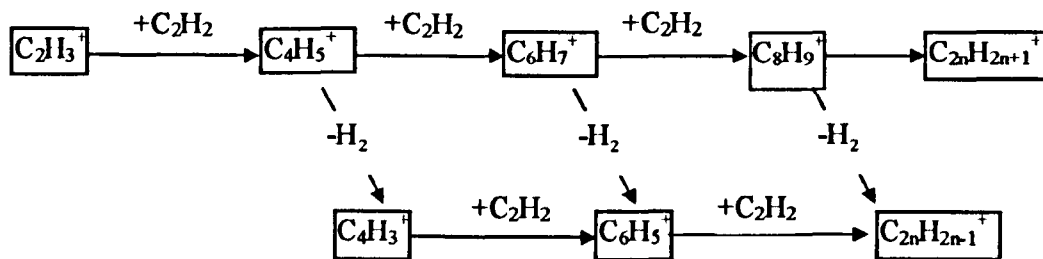


Figure 2.2 Reaction mechanism for polymerization (taken from Vinckier et al [31])

As the reaction progresses, the ions are more likely to lose a H_2 atom, so the larger molecules tend to be of the form $\text{C}_{2n}\text{H}_{2n-1}^+$. For much greater detail on ionic reactions, Fialkov [12] has a very extensive review and a good table of reactions involving ions.

It has been well established that the positive ions in flames are ionic species but the negative ions are mainly free electrons [7], [20], [25], [33], [34]. The major affect of this is on the relative mobility of the positive and negative ions, which will be discussed further in Section 2.2.1.

2.2 How ions can be moved and excited by electric fields

2.2.1 Ionic wind

The ionic wind (also known as “electric”, “Chattock” or “corona” wind) is the term used for a bulk gas movement caused by an electric field (first discovered by Chattock [6] in 1899). Whilst being pulled towards the anode, large positive ions collide with neutral particles and cause them to move in the same direction. As mentioned previously the negative ions are mainly electrons so their movement has little effect on the shape of the flame (proved in 1964 by Lawton and Weinberg [25]). This movement caused by ions can make the flame bend (Figure 2.3 and Figure 2.4), force air entrainment or even increase the heating effect on a surface. These will be discussed later.

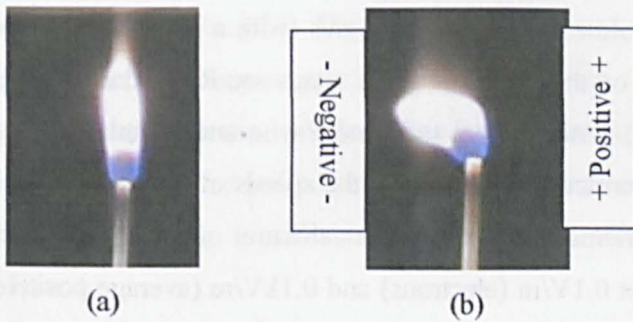


Figure 2.3 (a) Normal flame, (b) Flame bending to anode

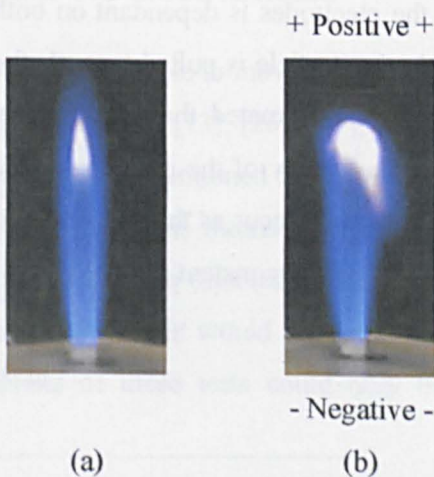


Figure 2.4 Electrodes parallel to flow (a) No field, (b) Applied field

It has been suggested that the ionic wind could be used for a propulsion device [36] with ions formed by coronas. However, it was found that the velocity of the gas can be approximated as proportional to the square root of the corona current [36], meaning high velocities require very large currents making it very inefficient. Ionic winds even have difficulty in over coming even low pressure restrictions [37], making it difficult to speed the flow up by other means such as reducing the flow diameter. They can however be used to produce a highly localised air flow which could be used to cool parts of combustors [33], increase the flame speed by creating a flow opposite to the flow rate [38]. Coronas can also be used to pull the radicals in the early part of a flame [39] [40].

The ionic wind velocity is in the order of 2m/s (100kV/m) [37] (consistent with measurements taken by Saito et al of 1-4m/s [41] and calculations by Mitchell and Wright [21] which estimated an absolute maximum of 5.5 m/s (with a practical velocity well below this). For further details on the speeds of ionic winds see Rickard et al [37], Lawton and Weinberg [7] and [25], Lawton et al [42] and Payne and Weinberg [33], where detailed calculations are performed into predicting the speeds of ionic winds and air entrainment. However, the ions themselves can achieve velocities of 1/3 of the speed of sound with a field strength of just 0.1V/m (electrons) and 0.1kV/m (average positive ion) [33], [34].

The speed with which a particle will move towards the electrodes is dependant on both the mass of the particle and the charge it possesses. As the particle is pulled towards the electrode it will collide many times (in 10^{-6} s it has been estimated that an ion may undergo as many as 5000 elastic collisions [7], [16]). The energy of the particle will be entirely given up to the neutral gas in the many collisions that occur as the ion is pulled towards the field. This resistance will cause the ion to travel at a constant speed [7], [12] [9]. The speed can be given by

$$v = KE \quad (2.9)$$

where K is the mobility of the ion in the direction of the applied force (it is not usual to distinguish mobilities of opposite charges by sign) and E is the field strength¹. Wilson [20] and Kinbara and Ikegemi [34], suggest an average ion mobility of $1 \times 10^{-4} \text{m}^2 \text{V}^{-1} \text{s}^{-1}$ for positive ions and $0.0103 \text{m}^2 \text{V}^{-1} \text{s}^{-1}$ for electrons.

It has been suggested [43] that the ionic wind is created in the later part of the flame. This seems logical as the majority of the ionic species present are in the form of H_3O^+ which is mainly found later in the combustion process (see section 2.1). The movement of H_3O^+ may therefore be the major factor in creating the ionic wind.

The ionic wind is not immediately established. It takes between 5 [39] and 14ms [44] for the ionic wind to become established, verified by experimental results (verified with experimental results [39]). This is very important when it comes to looking at AC fields as the ionic wind may or may not effect the results, depending on the frequency applied and whether the ionic wind has time to become established. This is also an important factor relating to the pulsed power supplies described later in this report (Section 2.2.2) and may be a way to differentiate between the effect of the ionic wind and chemical effects.

2.2.2 AC electric fields

It is also possible to move or excite the ions in a flame with an AC field. There have been several reports [13], [26], [39], [45-55] showing that AC fields can significantly modify flames. As mentioned previously, the ionic wind takes about 10-14ms to become established. This means that an AC or pulsed field with an “on time” shorter than the time required to establish the ionic wind would result in the effects being independent of ionic wind (this would require a frequency of 70-100Hz or greater being used). The results of these tests could only be explained by modifications to the chemistry of

¹ For uniform fields; $\text{Field strength} = \frac{\text{Potential difference between electrodes}}{\text{Distance between electrodes}}$

combustion. This distinction is particularly important as the changes can be shown to be chemical or caused by the ionic wind. The cause of the effects has caused much controversy in the literature. The use of pulsed and AC power supplies may provide a way to isolate the aerodynamic from the chemical effects to establish the cause of the flame modifications by an electric field.

The use of pulsed power supplies has not been extensively used in this area but has been used in other areas successfully to excite particles, for example to excite mercury for backlighting LCD screens [56]. Their results show that a considerable increase in the excitation of the mercury is possible for much less power when a pulse is used instead of a square wave at the resonant frequency of mercury. If the resonant frequencies of the flame ions could be found then particular ions could be greatly excited while others remain unexcited. This could allow large chemical modifications for very little power consumption.

As you would expect, the charged particles will oscillate within an AC field; the slower the frequency the larger the amplitude of oscillation (the particles take a finite time to be accelerated in the direction of the field so the longer the field is present in each direction the longer the particles are accelerated in that direction). The mass of the ion and its charge will also greatly effect the amplitude (see the discussion on mobility above). Anything less than 50Hz (see Figure 2.5) and all the charged particles in the flame will behave in a similar way to how they would in a DC field. So as the frequency is increased the effect will differ on particles of different mobilities. A good illustration of this can be found in Weinberg [47]. Among his findings are those shown in Figure 2.5, which shows how an AC field could be used to remove the ions/particles of a given size at a particular frequency. For example at 10MHz electrons would be pulled out of the flame and recombined at the electrodes, leaving all other ions and charged particles within the flame. However, at 10kHz both large ions and electrons could be removed, leaving only the charged particles.

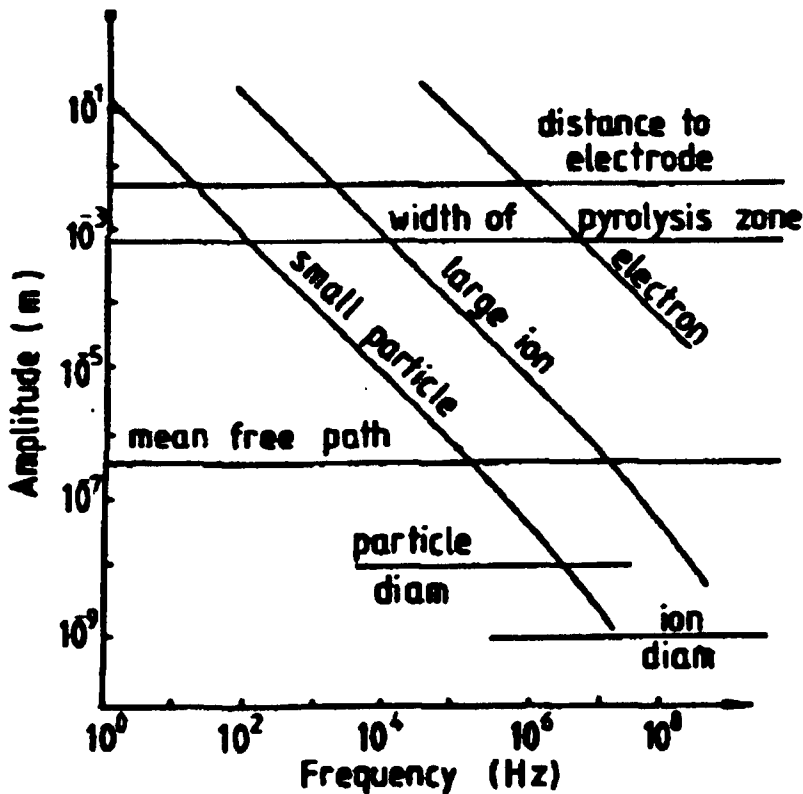


Figure 2.5 Field strength of 103V/m. Taken from Weinberg [47] who used results from Kono et al [57]

2.3 How an electric field can influence a flame

2.3.1 Extinction

The use of electric fields to extinguish flames offers some real advantages for the extinction of fires in aggressive environments or where conventional fire retardants are not possible. A good example of this is a nuclear submarine where water or gaseous extinction methods are unfavourable but large amounts of electricity are available.

The orientation of the electrodes is very important for extinction to occur. Extinction only occurs when the negative electrode is above the flame for uniform fields [36], [58], [59]

or there is a transverse DC field applied to the flame [60] (Figure 2.6). The effect of AC fields is less than DC and is only noticeable at low frequencies (50Hz was observed in [51]). Higher frequencies actually seem to enhance combustion and stabilise the flame. See Section 2.3.2 for further details on this.

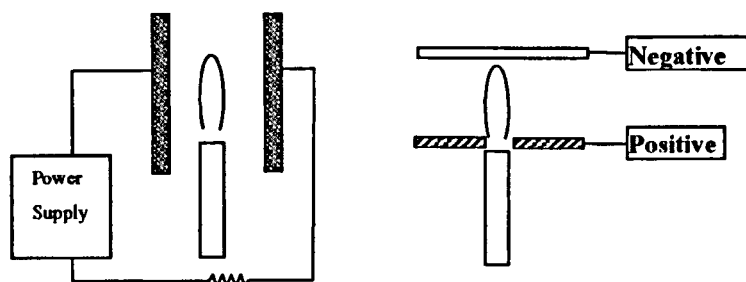


Figure 2.6 Electrode orientation favouring extinction

Work by Sher et al [36] and Calcote and Pease [58], supported by previous unpublished work by the author [60] and by Huneiti and Balachandran [13] showed that the extinction of flames occurred in two phases. First the flame began to move towards the negative electrode, stretching the flame. The end of this first phase in [60] was characterised by the flame lifting off the Bunsen (in some cases causing extinction Figure 2.7). Secondly, at a critical field strength the flame suddenly contracted. Calcote and Pease [58] also reported the flame becoming unstable, before restabilising and dropping back to the Bunsen as the voltage is increased. The flame then becomes increasingly smaller until the final extinction occurs. As mentioned above, it was found that extinction could occur by either a lifted flame (Figure 2.8), although this was not instantaneous, or the flame being blow out at higher voltages Figure 2.9 [60]. The difference can be seen in Figure 2.7.

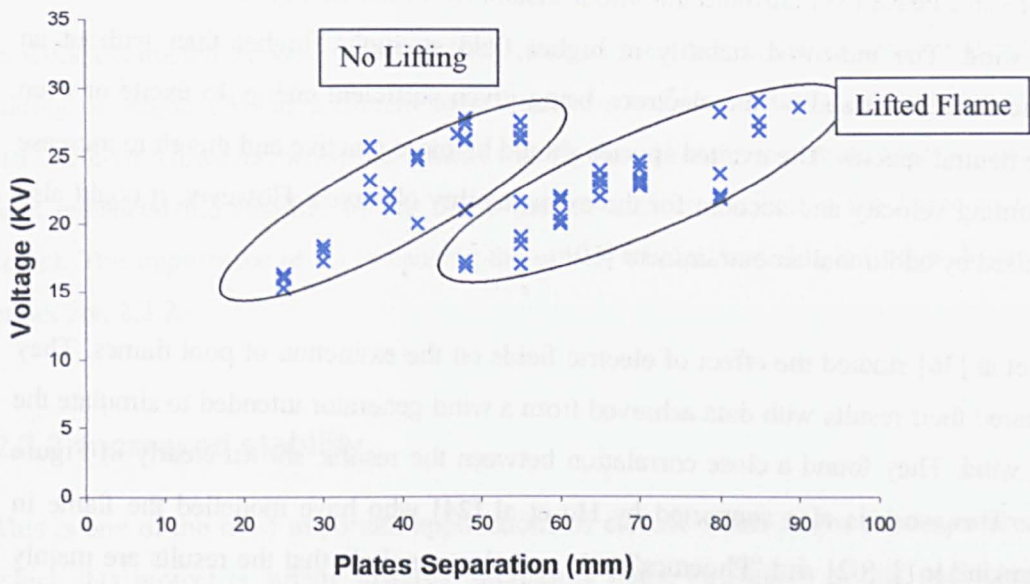


Figure 2.7 Graph of Extinction Voltage against the distance between the plates [60]

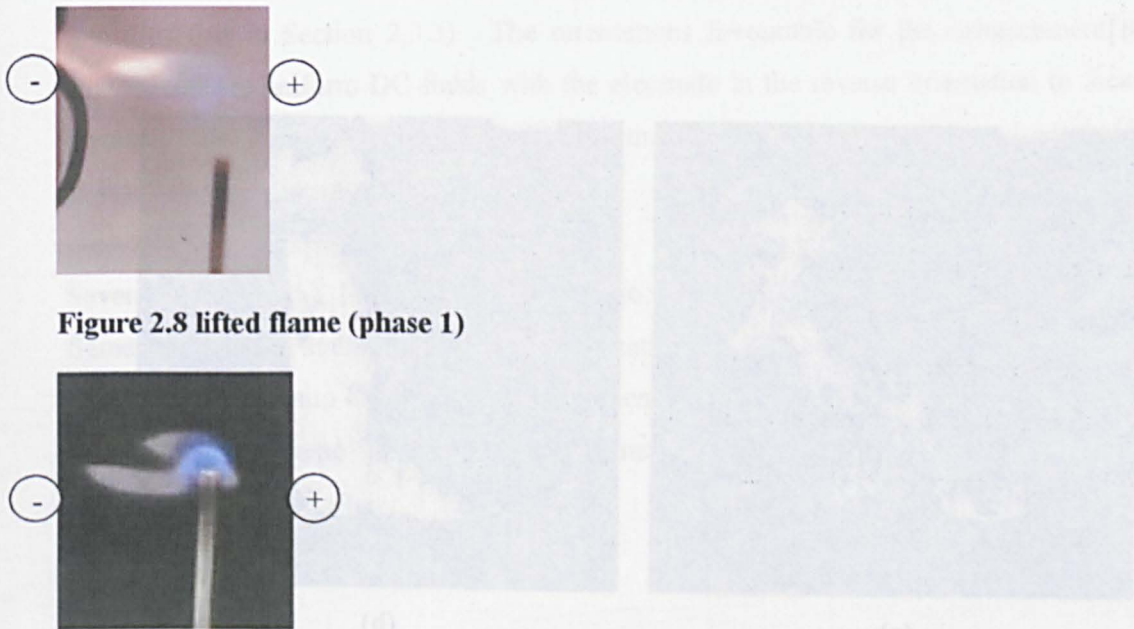


Figure 2.8 lifted flame (phase 1)

Figure 2.9 Restabilised flame prior to lift off (phase 2)

Calcote and Pease [58] attribute the initial instability to the aerodynamic effects of the ionic wind. The increased stability at higher field strengths (higher than without an electric field) is caused by the electrons being given sufficient energy to excite or even ionise neutral species. The excited species should be more reactive and therefore increase the burning velocity and account for the extra stability observed. However, it could also be caused by additional air entrainment [60].

Sher et al [36] studied the effect of electric fields on the extinction of pool flames. They compared their results with data achieved from a wind generator intended to simulate the ionic wind. They found a close correlation between the results, shown clearly in Figure 2.10. This work is also supported by Hu et al [24] who have modelled the flame in “Chemkin” [61], [62] and “Phoenix” [63] and also conclude that the results are mainly aerodynamic effects due to the ionic wind. Further weight is added to this argument as AC fields have a decreased extinguishing effect compared with DC fields and has not been observed at higher frequencies where the ionic wind will not play an important role [51].

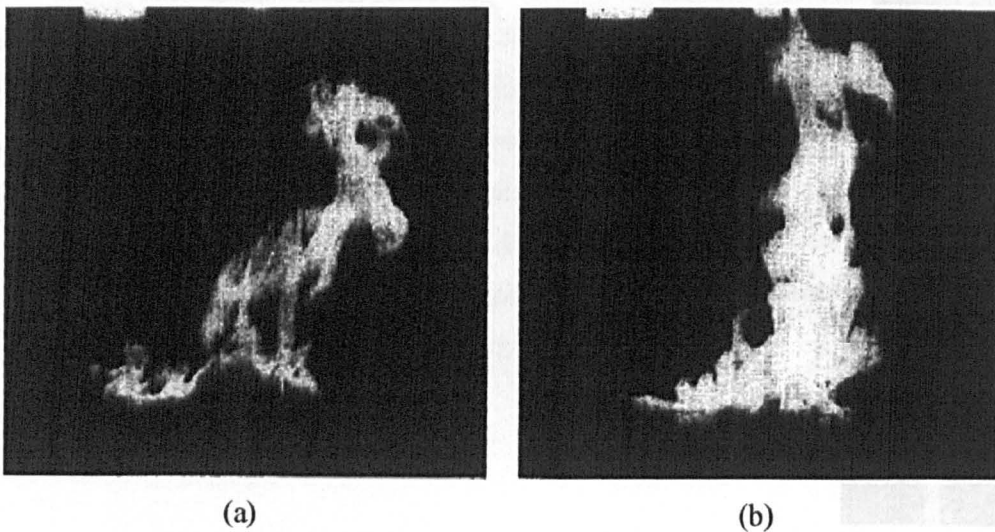


Figure 2.10 Comparison of ionic wind at 25kV (a) and wind generator at 2.5m/s (b) taken from [36]

In work conducted by Gulyaev et al [64], it was found that the extinguishing effect of adding of Argon (Ar) as a diluent to a flame was enhanced by the application of an electric field. However, when the diluent was N₂ the effect was reversed and the electric field enhanced the stability of the flame (negative electrode below the flame in both cases). The importance of N₂ in causing the effects of electric fields is further discussed in Section 2.3.2.

2.3.2 Increased stability

This is one of the most important applications of electric fields and is the major area in which this project is aiming towards. Increasing flame strengths² would enable more power to be outputted from a combustor of the same volume or allow a smaller combustor to be used for the same power. It would also allow faster transit of the gases through the flame, meaning less time at high temperature and therefore less thermal NO_x (more of this in Section 2.3.3). The orientations favourable for the enhancement of combustion are uniform DC fields with the electrode in the reverse orientation to those favourable for extinction (negative below) or the use of AC (and possibly pulsed) fields in several orientations.

Several authors [26], [41], [54], [58], [59], [65], [66], [67] have reported a change to flame strength or stability under the application of DC electric field. The effect is demonstrated by Saito et al [41] and can be seen in the picture below (Figure 2.11) where the size of the flame can be seen to dramatically decrease, thereby increasing the intensity.

$$^2 \text{ Flame strength} = \frac{\text{Fuel mass consumption}}{\text{Flame surface area}}$$

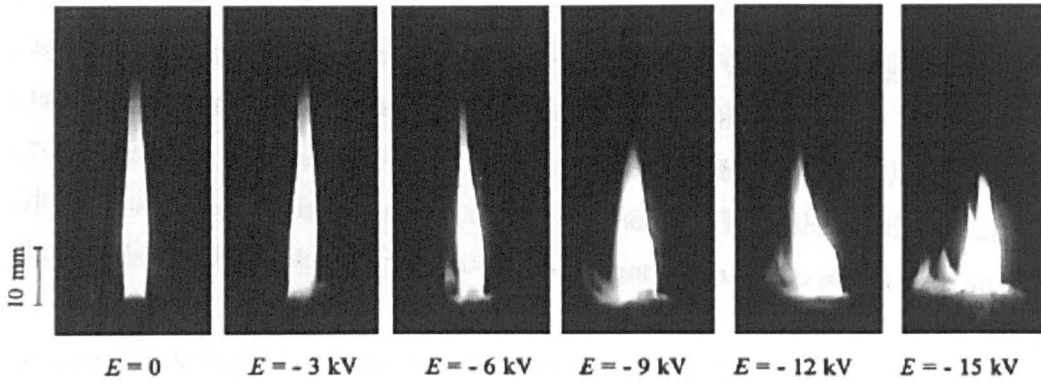


Figure 2.11 Picture of flame shape of acetylene flame subject to negative burner voltage and earth ring above the flame ($M_f=3.09\text{mg/s}$, distance between electrode = 50mm). Taken from Saito et al [41]

It is also possible to increase a flames' strength by using the aerodynamic properties of an electric field to entrain air (the velocity of entrainment can be as much as 10 times the burning velocity [42]), increase mixing [25] or suppress the flow velocity [60].

The lean blow off limit (velocity to cause extinction for a given equivalence ratio [the equivalence ratio is a non dimensional number for the fuel/air ratio]) can be extended by a DC electric field [38], [54], [58], [59], [66], [67]. The effects are attributed to the aerodynamic forces and can be as great as a 100% increase in flow speed before blow off occurs. However, if the flame lifts above the Bunsen and corona forms in the air below it, the flow rate can be increased to as much as 200% [38]. Also the equivalence ratio where blow off occurs can be extended for lean flames (the flames can be made to burn much leaner at a given velocity). It was also found that the mass flow rate where combustion could be sustained for a given equivalence ratio was increased by about 50%.

Another method to increase a flames' stability/strength is to use bluff bodies/obstacles in the flow path of flames [42] or a swirler [68], [69] to recirculate the hot combustion products. Both bluff bodies and swirlers increased the temperature (see Section 2.3.3 for more details on this) and consequently the reaction rate [42] (the decrease due to dilution of the combustion products being negligible in comparison). It may be possible to do the

same thing with electric fields. Problems associated with these techniques such as pressure loss associated with causing turbulence and heat transfer to the bluff body are avoided by using electric fields. The electric fields will also not wear out in the way in which solid bodies in the flow path will.

Two reports have been written recently regarding the use of pulsed fields [39] and DC fields [40] to stabilise combustion. They have discovered that the flame speed can be modified by the application of an electric field. It has been suggested that the electric field pulls ions such as HCO^+ and H_3O^+ , which are present at the base of the flame, into the preheat region of the flame. The ions then recombine by dissociative recombination. This type of recombination can lead to the production of radicals such as OH^\cdot [28] which are normally deficient in this region. It has been shown that the pace of many combustion systems is set by the elementary reaction (2.10) between H atoms and O_2 molecules [70];



An increase in the OH concentration in the initial stages of combustion will reduce the importance of reaction (2.10) and increase the overall rate of combustion (this will be further discussed in section 2.4.2).

Despite these results being very significant they are then interpreted by the use of the Lewis number. The Lewis number is a non dimensional number which relates the burning velocity to the diffusion of species. It assumes that the whole process can be characterised by the diffusion rate of one species. However, the theoretical calculation of the Lewis number creates a discontinuity at equivalence ratios of unity, which is not seen experimentally. To avoid this discontinuity many authors prefer to use the Markstein number as it is a direct measurement of flame behaviour [71-3].

Determination of both the Lewis number and Markstein number require an accurate measurement of the burning velocity. This is very difficult to do practically (see Andrews and Bradley [74] for a description of how to measure burning velocities and their accuracy). Marcum and Ganguly [39] and Wiseman et al [40] use the cone angle within the flame to calculate the burning velocity. It is known that the flame is distorted by the

electric field. This distortion will also distort the cone of the flame making accurate measurement of the burning velocity very difficult. The ionic wind may also be the cause of the increased speed by creating turbulence within the flame or slowing the flow rate down, depending on the orientation of the electrodes. The use of a non dimensional number in this case does not appear to be useful. There are too many assumptions as well as the difficulty of an accurate determination of the burning velocity.

Jaggers and Von Engel [26] have also documented changes to the burning velocity. They found that the burning velocity appeared to increase with the application of an AC electric field. They attributed the results to an increase in electron cross section and thereby an increase in the reaction rates of the flame. Further study [45], [46] was however, unable to replicate the results and there remains some confusion as to whether the burning rates are actually changed by electric fields.

Jaggers and von Engel [26], Criner *et al* [54] and Lee *et al* [55] have used electric fields on lifted flames. All of the researchers showed that a lifted flame could be brought closer to a burner by the application of an electric field. This has been used as justification that an electric field can increase the speed of combustion. The effects could not be due to ionic wind effects as the flame shape was not altered [26] (as it would be if the effect was aerodynamic) and also the frequency used means that an ionic wind would not be established. The reason for the flame speed increase occurring were attributed to the electrons cross becoming vibrationally excited. These results are consistent with the work of others who have seen an increase in electron excitation [44], [47], [49], [57], characterised by greater luminosity of the flame.

Recently some researchers have used plasmas and the electric fields they create to modify flames, most notably Starikovskii [50]. He shows how a pulsed plasma can greatly increase the burning velocity. The increase was attributed to chemical effects instead of aerodynamic. The burning velocities have also only been observed with combustion in air (containing N₂). The same effect is not observed with O₂ and Ar [50], [64], [75], [76]. This could be due to the high amounts of energy that N₂ absorbs from free electrons,

shown numerically in [48]. This is an important topic and will be discussed in much greater detail in Section 2.4.

2.3.3 Emissions and flame temperature

As mentioned in Chapter 1 soot and NO_x production are related to temperature. From Saito et al [77], the critical temperature for the onset of soot production was found to be 1080°C , while maximum soot production occurred at 1130°C . As the temperature increased above this the soot was oxidised and emissions went down. This is supported by Wagner [78] and Mizutani et al [79]. At low temperatures soot was produced less quickly and emissions were therefore lower.

As mentioned previously the recirculation of hot combustion products by a swirler or a bluff body increases the flame temperature and therefore can decrease the soot it contains. However, (as Figure 1.2 shows) the increase in temperature also causes an increase in the production of NO_x . Increasing legislation in this area means that the efficiencies gained by running at higher temperatures must be sacrificed for lower pollutant levels.

Saito et al [77] used the same experimental set up as Lawton *et al* [42], and measured the temperature and soot suppression. A decrease in the soot production was found but this was due to an increase in the temperature [42], [77] (see Figure 2.12). This increase in temperature can be explained by recirculation and air entrainment caused by the ionic wind.

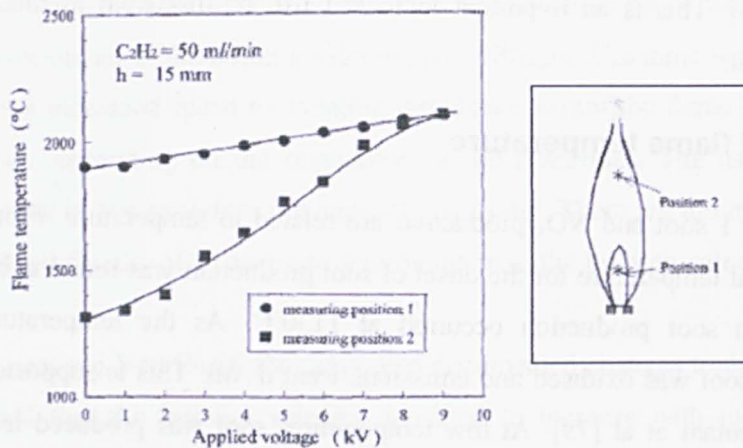


Figure 2.12 Change in flame temperature with applied voltage, Saito et al [77]

Visually this can be seen in the author's previous work [60] where a yellow diffusion flame was turned blue, indicating air entrainment (Figure 2.13). Sandhu and Weinberg [10], Payne and Weinberg [33] and Lawton, Mayo and Weinberg [42] have looked specifically at entraining air and how it can be used. This will be further discussed in Section 2.3.5.

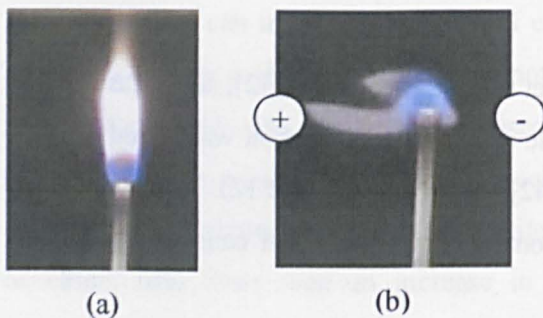


Figure 2.13 (a) Normal flame, (b) Ionic wind causing air to be entrained

There has been a great deal of work regarding soot particles and their formation. Payne and Weinberg [33] conducted several experiments that indicated that soot has a positive charge in the flame and can be attracted to the negative electrode. This work was later confirmed by others then reviewed by Weinberg [47].

Although it is established that soot particles have a positive charge it is not clear whether they attain this charge due to nucleation around a charge particle [80] or whether they nucleate around a neutral species [27], [81] and then attain charge by other methods such as diffusion charging. Introduction of neutral particles into a flame showed that they became charged [82]. The most likely explanation is that both may be occurring simultaneously [47], [83], [84]. However, under the application of DC electric fields where the flame is effectively wiped clean of charged particles, soot is likely to nucleate around uncharged particles and gain its charge when it reaches approximately 5nm in size [47].

The importance for this study is not how the soot becomes charged but simply that it does become charged. Practically, this means that soot can be influenced by an electric field either by removing ions for soot to nucleate around [47], [85], by holding the charged particles in the flame for longer allowing them to oxidise or by increasing the temperature and therefore the oxidation rate.

The application of uniform electric fields has been shown to reduce the soot formation in flames by up to 90% [35], [41] [77], [86], [87], [89]. The mechanism of soot suppression depends on the position of the electrodes.

If the experiment is set up with the negative electrode below the burner, as shown in Figure 2.14, then the positive soot particles will be held in the flame for longer and be oxidised. It has also been found by Yuan et al [35] that the flame became smaller, decreasing the rate of combustion per unit. This smaller area increased the radiation per unit flow rate, making radiation significant, as it cools the flame. This decrease in the flame temperature prevented soot and NO_x being formed.

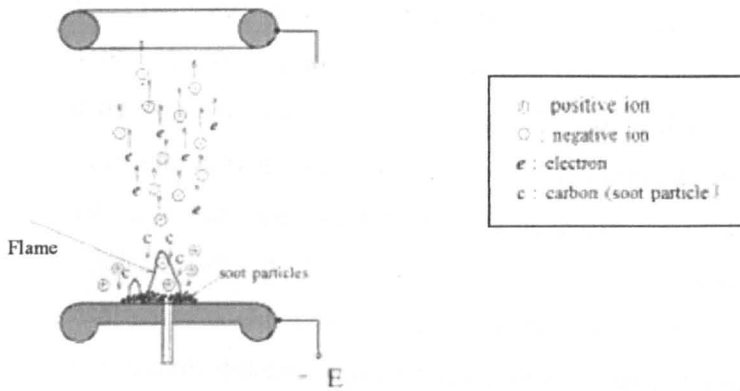


Figure 2.14 Negative electrode below the burner [41]

If the experiment is set up as in Figure 2.15, then there will be a dual effect caused by the electric field. Firstly the carbon particles will be removed from the reaction zone quickly and prevented from becoming as large [35], [47], [85], [89] and then they will be accelerated towards the ground electrode, inducing an ionic wind, entraining air and increasing the temperature. This pushes combustion into the region where the soot is oxidised more quickly than it is produced (see Figure 1.2). Also, it therefore has the negative effect of increasing NO_x production.

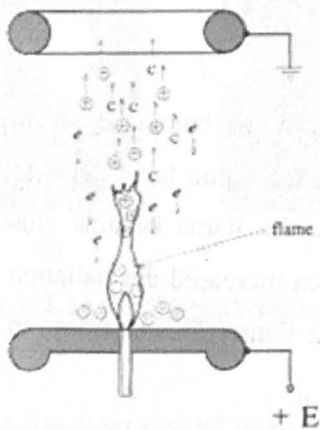


Figure 2.15 Positive electrode below the burner [41]

Two reliable studies have been conducted by Saito et al [41], [77]. They discovered that soot is reduced by 90% with a positive electrode below the flame, while a 70% reduction

in soot formation can be achieved with a negative electrode below the flame due to the reasons explained above. Their work is expressed concisely by the graph below (Figure 2.16), showing the reduction in soot emission with increased intensity of the electric field applied. Their work also shows that the mechanism of increasing the temperature of the flame is more effective than holding soot particles in the flame for longer to allow them to oxidise.

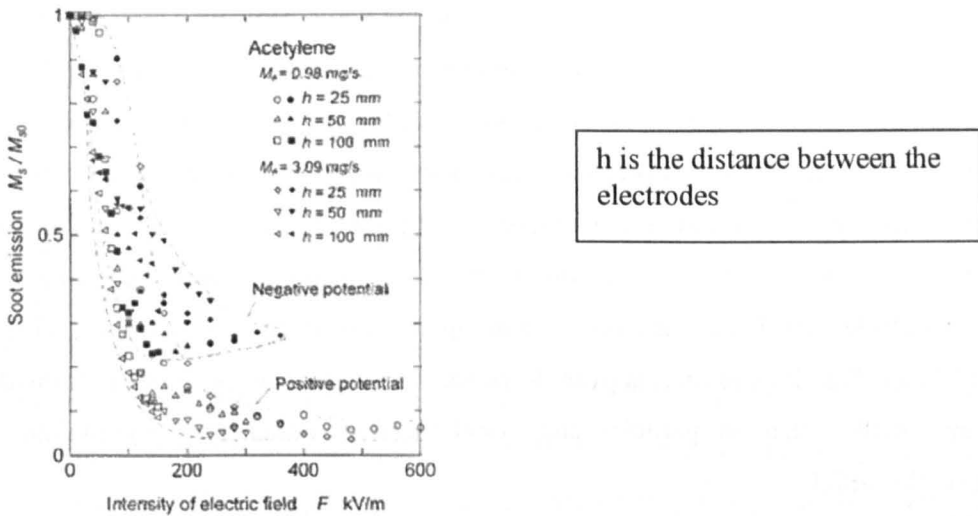


Figure 2.16 Relationship between electric field intensity and soot emission, Saito et al [41]

Bowser and Weinberg [86] studied the effect of electric fields during pyrolysis (a type of incineration where organic materials chemically decompose, typically occurring at temperatures in excess of 430°C) in the absence of oxygen. Soot emission could be controlled by the use of electric fields, as with combustion with oxygen. They also discovered that the production of ions, particularly CH^+ (which has only been known to form using oxygen products) was also present and that ionisation occurred even at very low temperatures, allowing electrical fields to be of great use in controlling the soot production.

There has been extensive research from aerosol researchers into using electric fields to control the size of particles formed in a flame. Pratsinis [87] shows a good example of

this. The effects of electric fields on fine tuning of the particle size are discussed. There has also been research into introducing charged particles into the exhaust of a flame, which combine with soot particles and provide a means to then remove them to charged electrodes. However, of more interest to the engineer is to eliminate soot entirely, rather than change its size.

AC fields have little effect on the output of soot from the flame. However, they do effect its production, tending to produce a greater number of smaller particles [44], [47], [49] [57]. The majority of these particles are oxidised before leaving the flame, increasing the luminosity of the flame. Despite this the AC field does tend to encourage the particles to collide and form larger soot particles. The larger soot particles are relatively unaffected by the AC field (as their mobility is low due to their large mass) and tend to combine to form larger particles which are less likely to bum up in the reaction zone [44], [47], [49], [57]. This means that the emission appears to be the same although the soot has formed from many smaller charged particles and conglomerated, rather than accumulating around a single particle.

The increase in the stability and blow off limits of the flame discussed previously in Section 2.3.2 also enables the flame to bum much leaner. This can reduce the NO_x produced by the flame [66]. However, turbulent flames tend to produce more NO_x [66]. The ionic wind can be used to increase turbulence so a balance is required between allowing the flame to bum leaner without causing too much turbulence which will increase the NO_x .

The use of AC fields at higher frequencies does not effect the pollutants created. However, the luminosity is increased by up to 230% [44], [57] and the effect is still appreciable as low as 108Hz [44], [47]. This may indicate that more soot is being produced but is burnt up before it leaves the flame. At lower frequencies (below 50 Hz) there is a reduction in the amount of soot formed [44], [47], [57].

2.3.4 Flame conduction of electricity

When a flame is subjected to an external electric field it will conduct electricity. This is due to the fact that ions in the flame are attracted towards the electrodes where they are neutralised (the positive ions accepting an electron and the negative ions giving up an electron), giving the appearance of a current flow. There were some early studies that attempted to use an electric field to create a current and generate electricity (see review in Lawton and Weinberg [7]) but this idea was soon rejected as it was found to be unpractical and not as efficient as the method of steam turbines that we use today.

The current increases with the applied voltage up to a limiting value, known as the saturation current [7], [25], [39-41]. When the saturation current is reached it is assumed that at this point all the ions in the flame are being removed before they are able to react with other species or recombine. This enabled early researchers to estimate the concentration of ions in a flame (see reviews in Lawton and Weinberg [7] and Fialkov [12]) and identify the primary ions (see section 2.1.1). Further increase to the voltage will accelerate the ions so much that when they knock into some neutral species they will release enough energy to ionise that species (known as secondary ionisation, see section 1.2.3 for further details). Saito et al [41] demonstrates the saturation current graphically (Figure 2.17).

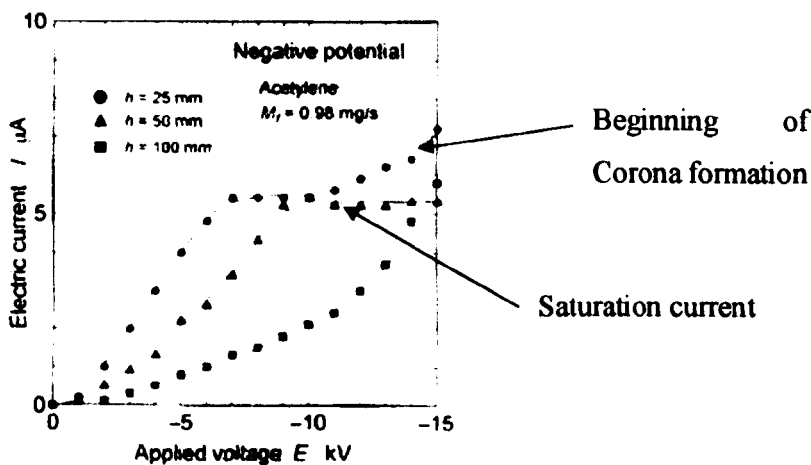


Figure 2.17 The effect of applied voltage on current conducted across the flame, Saito et al [41]

Using electrodes with the opposite polarity, the current continued to increase (the effect was attributed to the decrease in the size of the flame thereby increasing the insulation between the electrodes. The saturation current has been used as a method to ensure that the flame and the field are coupled with each other for a particular electrode orientation and geometry. This is discussed in section 2.6.

The conduction of electricity is related to the number of ions in the gas and also their mobility by the following equation;

$$\sigma = e(\mu_e n_e + \mu_i n_i) \quad (2.11)$$

where,

σ = conductivity

e = electron charge

$\mu_{e,i}$ = mobility_{electron, positive ion}

$n_{e,i}$ = concentration_{electron, positive ion}

The concentrations of both electrons and positive ions are very similar (ie $n_e = n_i$). However, the mobility of an electron ($\mu_e = 1\text{cm}^2\text{V}^{-1}\text{s}^{-1}$) and the mobility of an average positive ion ($\mu_i = 103\text{cm}^2\text{V}^{-1}\text{s}^{-1}$) are very different [33], [34]. In the context of equation (2.11) the positive side becomes negligible [12] and can therefore be reduced to;

$$\sigma = e\mu_e n_e \quad (2.12)$$

When a corona is formed (localised breakdown of the gas below the breakdown voltage of the entire gas) the current, I , can be related to the speed of the ionic wind, v , as shown in (2.13), see [36] for further details.

$$v \propto \sqrt{I} \quad (2.13)$$

2.3.5 Heat transfer

An electric field is known to induce an ionic wind on a flame. This can be directed towards a surface where heating is required [10] which can greatly improve the heat

transfer rate. Payne and Weinberg [33] show this in detail for Hydrogen, coal and ethylene flames. They surrounded the flame with a water jacket that was given a negative potential (see Figure 2.18).

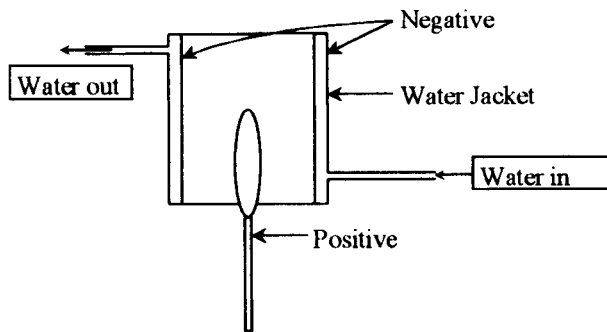


Figure 2.18 Experimental set up of Payne and Weinberg [33]

The power required to create this was very small compared to the increased heat transfer: 0.12cal/s was required electrically and caused an increase of 2 orders of magnitude in heat transfer (this will be further discussed in section 2.3.6). It was concluded that the major reason for the increase in heat transfer was because the positive ions were pulled radially by the field, resulting in a flow of other hot gases in that direction, heating the water jacket. Interestingly the removal of these hot gases caused a vortex, pulling in fresh combustion products. The use of this air entrainment were extensively investigated in Payne and Weinberg [33].

Further to this study Sandu and Weinberg [10] conducted a comprehensive study into heating effects that can be influenced by electric fields. They found that an electric field could be used to increase the heating of bodies normally outside the flame boundary. They also found a reduction of the heating of bodies inside the flame could be achieved. However, the relationship is not a simple one. The situation in which the flame is situated is very important. There are two competing effects occurring;

1. Hot gases are moved towards the body you wish to heat, which as expected increases the heat transfer.

2. The electric field increases the gas velocity, which with incompressible gasses is not possible unless ambient gasses are entrained. In the case of small unconfined flames these gases are cold and actually reduce the flame temperature as they are entrained reducing heat transfer.

The apparatus is therefore very important. For larger rich flames the additional air entrainment can increase the temperature by bringing the air/fuel ratio closer to stoichiometric. This could be very useful practically but the design cannot be generic and needs to be designed individually for each application.

2.3.6 Power consumption

As mentioned previously (in Section 2.3.5) the power required to cause the modifications to flames is small compared to the energy released from combustion. There have been several reports that state the percentage of the power used by the electric field to the power of combustion. The actual values vary between reports but a few typical examples are that an electric field uses 0.0001% [55], 0.01% [59], [66], 0.025% [90], 0.1% [54] of the energy produced in the combustion process to control it. It may be possible to reduce this further with the use of pulsed fields where it has been shown that they can cause greater excitation than AC fields with much less power consumption under the right conditions [56].

2.4 Ionic wind vs chemical change debate

There has been a great deal written in the literature about whether the effects caused by an electric field are chemical or aerodynamic in origin. Virtually all the papers written on this topic have an opinion on the matter. The reason for the variation could be due to both aerodynamic and chemical effects occurring. The dominant effect will be dependant on the apparatus used. It is likely that the effects of a low frequency field (under 50Hz) or DC fields are caused by aerodynamic effects. However, this is not possible for higher frequencies as the time that the electrode is charged is not long enough to create an ionic

wind (above 50Hz). The effect must therefore originate from a chemical modification. The reasons and evidence to show this is explained in sections 2.4.1, 2.4.2 and 2.4.3.

2.4.1 DC fields and AC fields up to 50Hz

The effect of a field on a flame for a DC voltage or a frequency up to 50Hz can be described by aerodynamic alterations to the flame flow paths. There are many authors who also support this theory [21], [24], [36], [38], [45], [58], [59], [65], [66], [80], [91-4].

With a positive electrode below the flame the ionic wind would cause a recirculation of the combustion products and suppress the gas flow, allowing greater flowrates of fuel to be burnt. Two works of particular interest are Calcote and Berman [59] and Bowser and Weinberg [45] who measured an increase in the pressure inside a burner when a field was applied. Indicating that an aerodynamic force (the ionic wind) was suppressing the upwards gas flow.

With transverse fields or a negative electrode below the flame it has also been shown that the ionic wind can cause air entrainment which would enhance combustion of a rich flame [25], [33]. In both of these electrode configurations the flame becomes less stable at lower field strengths, while stabilising at higher field strengths [38], [58], [60].

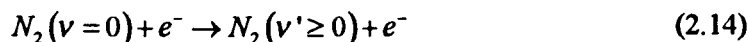
There have, however, been suggestions that DC fields can cause chemical changes. This could be due to several things

1. The excitation of N_2 (see equations(2.14), (2.15) and (2.16) below).
2. Electrons being pulled into the pre combustion zone and decomposing the fuel [27] (as with plasmas, see Section 2.4.2, below)
3. HCO^+ and H_3O^+ being pulled back towards the negative electrode (below the burner) where they dissociatively recombine creating radicals in the preheat zone which are normally deficient (such as OH^{\cdot}), therefore increasing the overall combustion rate [39], [40].

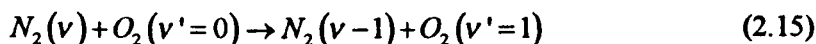
2.4.2 AC and Pulsed Fields

There is a great deal of contradicting reports with AC and pulsed fields. However, the ionic wind cannot cause the effects at these frequencies. As previously mentioned (section 2.2.1) it takes longer to establish the ionic wind than the electrodes are activated for frequencies over 50Hz. Therefore the modifications to flames due to pulsed and AC power supplies must be due to some form of chemical change occurring in the flame rather than aerodynamic effects caused by the ionic wind.

Modelling work by Bradley and Ibrahim [48], [49], and experiments by Gulyaev *et al* [64], shows how N₂ becomes excited at higher field strengths by free electrons. They showed that 90% of the energy transferred from electrons is gained by N₂ at fields strengths above 20 Vcm⁻¹Torr⁻¹. Independently, Tewari and Wilson [76] experimentally found that increases in burning velocity in an electric field occurred only when N₂ was present. The same effect did not occur when the air was replaced with a mixture of Ar and fuel. These results led to Shebeko [95] to suggest that N₂ was being excited by the field in the form;



The excited N₂ then transfer their oscillatory energy to O₂



The excitation of O₂ increases the reaction rate of



The pace of many combustion reactions is set by this elementary reaction [70] page 3. There have been several other papers that have also observed the effect with N₂ and not with other gasses, see references [64] and [75]. It also has been numerically shown [50] that alteration of this reaction is in the correct order of magnitude to explain the flame speed increases shown experimentally. Further support to this theory is given by Gulyaev *et al* [96] where the concentration of negative ions in the flame front is shown to decrease in the presence of N₂ but not when it is replaced with Ar.

It has also been suggested that electron attachment to OH and H₂O speeds up combustion [97], using data from [67]. There is not any other work to support this theory and it remains unproved.

Several authors [44], [47], [57] found an increase in electron movement (characterised by greater luminosity in the flame) in electric fields and Bradley and Ibrahim [49] showed that both AC and DC fields were able to alter the energy levels of electrons³. Jagers and Von Engel [26] also explained their results by increased electron excitation. These results seem to support the theory of Shebeko [95].

Several authors still attribute the effects to ionic wind effects theory [24], [36], [38], [45], [58], [59], [65], [66], [76], [80], [91-4]. However, the major problem with this is that it takes a finite time to set up. This has been found to be in the order of about 5ms [39] (14ms Kono [44]). For some of the high frequency electric fields applied there have been significant changes to combustion with pulses durations much shorter than the time required to establish an ionic wind (for example 1-10MHz [26]). It would therefore seem logical to expect some chemical change to be occurring.

There has also been measurement of the species involved in combustion and how quickly they appear. For example Starikovskii [50] measured the C₂, CH⁺ and OH. It was found that C₂ and CH⁺ appeared earlier in combustion when a field was applied, showing increased combustion rates. Also, OH started to appear in the plasma discharge region, showing fuel breakdown by the plasma/pulsed field [90].

The evidence therefore suggests that chemical changes of combustion are the primary source of the flame modifications observed in AC and pulsed fields.

³ The electron however had to be in the presence of several neutral species or the electron was pulled out of the field by the first pulse of the AC field. They also discovered that electron energy increased when the ratio of number of collisions to electrical field frequency increased (until this value reached 10).

2.4.3 Plasmas and Coronas

Plasma is the total breakdown of gas between two electrodes. A corona is the localised breakdown of the gas surrounding a single sharp electrode. There have been several studies [38], [39], [50], [55], [90] showing plasmas and coronas increasing burning velocities and enabling leaner burning flames. This could be due to a combination of factors, as plasmas have been shown to cause several effects.

1. Coronas have been shown to cause localised heating of the flames' gases [38]. This will increase the reaction rates close to the corona.
2. Coronas produce additional charged species [6]. These are at high energy levels and can either excite surrounding species or lead to secondary ionisation. The products of this secondary ionisation may lead to further effects as they are moved or excited by the electric field produced by the plasma.
3. Plasmas and coronas can be used to decompose fuels prior to combustion which has been shown to dramatically increase the reaction rate [50], [90].
4. The electric field produced by the plasma may be able to alter the reaction rates [50], [55], [90], as with AC and pulsed fields described above.
5. Slow pulses (of several milliseconds) can cause aerodynamic modifications to the flame [39], causing it to become wrinkled.

There is a need for further work in this area to establish which of the above effects dominate. It is likely that there is a combination of the above effects occurring but currently it is not possible to deduce which effects are the most significant.

2.5 Modelling

There has been extensive work to model the chemistry of a flame [61], [62]. However, in the standard mechanism there are no ionic species included (for example GRI Mech 3 [63]). There have been several authors who have attempted to include ionic reactions, see Pedersen [14] and Pedersen and Brown [15] for a good example of the mechanism used.

Others have tried to use this and other similar mechanisms to predict the effects of the field on a flame, particularly the ionic wind [24], [50], [98-100]. The most recent results from Hu *et al* [24] show a remarkably good correlation to experimental data. This is however, only for DC fields. There is currently no good model for AC or pulsed fields.

Modelling of the electric field is possible with programs such as Maxwell [101] and Finite Element Modelling Magnetics (FEMM) [102]. There has also been research into the movement and mixing of magnetic particles with biological cells as a method of preferential selection of specific cells [103]. Currently no-one has used such modelling programs to model the field produced by different electrode geometries and orientations. See Section 2.6 and Chapter 3 for more details on this. Measurement of the Electric field directly is also very difficult as the sensor (usually made from metal) distorts the field [104]. Optical sensors provide a more accurate method to measure the field. However, these optical sensors are temperature dependant. The presence of a flame may prevent the sensor providing reliable results but it has not been tested at such high temperatures [104].

2.6 Type/orientation of electrodes

In current literature the setup is not consistent. This makes comparison of the results very difficult. There are several types of electrodes used in several different orientations (see Table 2.1). Many of the effects are attributed to the aerodynamic effects caused by the ionic wind [21], [24], [36], [38], [45], [58], [59], [65], [66], [80], [91-4]. The orientation of the electrodes is therefore very significant as the direction of the wind is dependant on

the orientation of the electrodes. Also, if the field is not uniform then the ionic wind will not be produced uniformly across the field. This effect could be used to magnify the effect in certain areas once the effects are properly understood. However, the diversity of apparatus tends to make understanding this topic more difficult as the results cannot be compared.

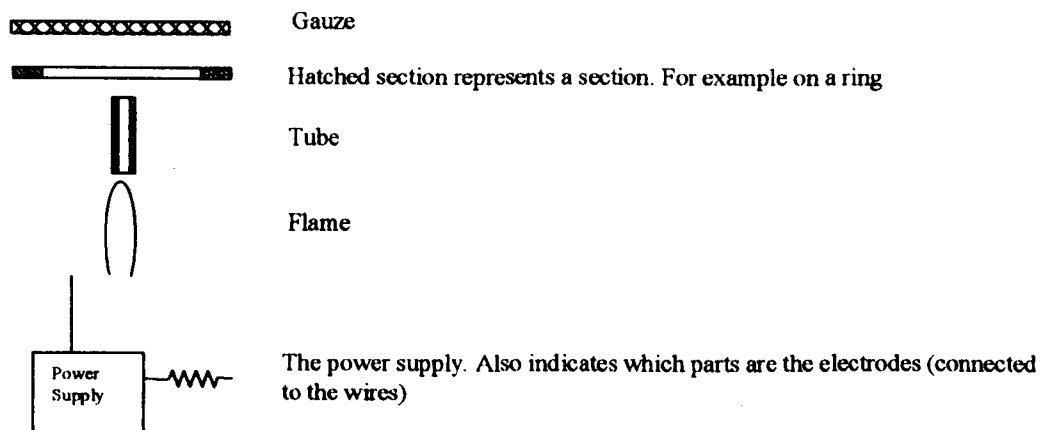
Work to predict what the electric field looks like and how the electrode geometry changes the type of field produced is contained in Lawton and Weinberg [7, P480] and [25] Fialkov [12, P508], Kono *et al* [57], Sher *et al* [91] and Gulyaev *et al* [96]. However, this work is relatively old, and modern modelling programs such as Maxwell [101] and FEMM [102] can offer a greater insight into how the field looks. There have even been suggestions that the shape and positioning of the lower electrode in a field parallel to a vertical burner does not greatly effect the field [59], [66]. However this is in conflict to the research conducted in other disciplines [101], [102], [105], [106]. The most frequently discussed criterion for electrode selection is the “coupling” between the flame and the field [12], [39–41]. This is when the saturation current is reached (mentioned previously in Section 2.3.4). Researchers have assumed that better coupling between the flame and field exists when the voltage required to reach the saturation current is reduced. However, there are many effects which could make this unreliable, such as the use of AC fields where the frequency may cause oscillations of smaller amplitude than the electrode separation, or recombination within the flame caused by excitation of the charged species by the field.

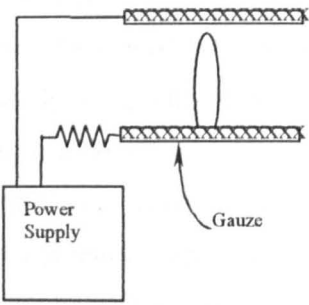
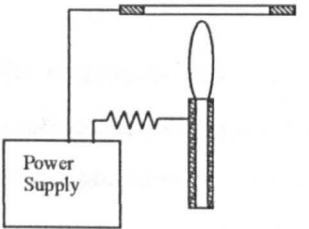
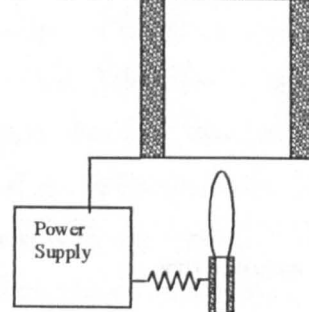
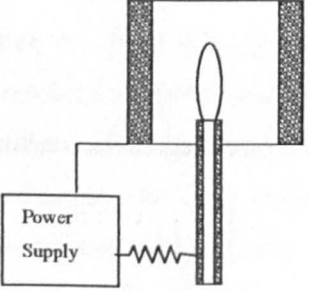
Exact predictions of the field are very complex, as Lawton and Weinberg [7] state, because the flame also effects the field which is in turn modifying the flame. To model this requires a combination of computation fluid dynamics (CFD), chemical schematic modelling that includes accurate ion reactions and a field modelling program. Currently a full schematic for ionic reactions is not currently available, however, there has been extensive work conducted to try and create a full model by Pedersen [14], Pedersen and Brown [15], Hu *et al* [24], [100] Yuan *et al* [35], Saito *et al* [77] Jones *et al* [98] and Smook *et al* [99] (also see Section 2.5). Models combining both CFD and chemical

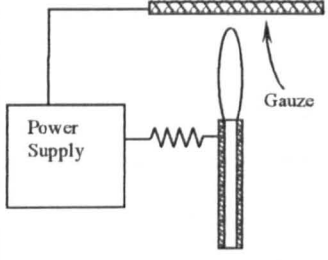
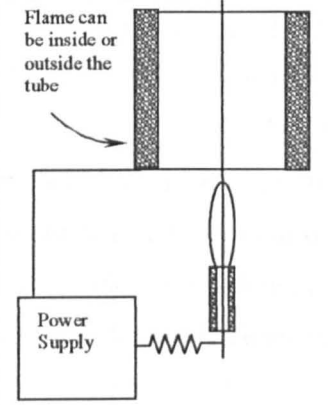
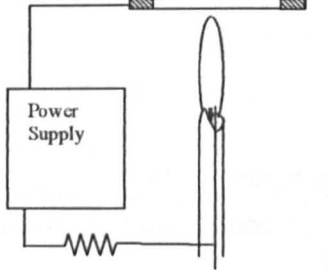
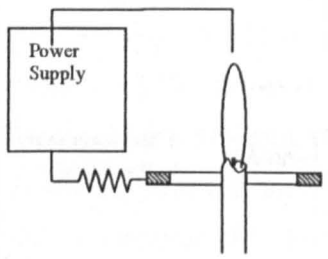
structure are possible but complex and not currently sophisticated enough to cope with the inclusion of ionic species. There has also been no attempt to try and couple a CFD program with an electric field modelling program. This makes modelling with current technology impossible. However, modelling of the electric field without the flame is possible. In fact this is a relatively well understood area. There have been several textbooks written in the area, for example “An Introduction to Applied Electromagnetism” by Christopoulos [105]. There are several programs written to model electric fields for use with modelling Antennae (high frequencies) motors or circuitry, for example, Maxwell [101] and FEMM [102]. See the results of this in Chapter 3.

In some of the papers, particularly the older ones the type and orientation of the electrodes is not even stated so the conclusions drawn could be very unreliable. Below is a table to show the reader the scale of the problem and demonstrate the wide variety of experimental apparatus used (see Table 2.1);

Key



	Apparatus	Ref
1.		[24]
2.		[13] [39] [41] [51] [59] [58] [66] [67] [94] [107]
3.		Solid Tube [39] [44] [55] [57] [64]
4.		Mesh Tube [51] [52] [75]

5.		[39] [42] [67] [89] [108] [109]
6.		[21] [33] [90] [93] [110]
7.		[13]
8.		[13]

9.		[35] [91] [111] [112]
10.		[36]
11.		[26] [97]
12.		[33]
13.		[50]
14.		[85]
15.		[38]
16.		[50] [53]
17.		[42] [57] [65] [83] [108] [109] [113]
18.		[50]

Table 2.1 The experimental set up used in the literature and the researchers that have used them

Christopoulos [105] predicts that the most uniform field would be produced by types of electrode similar to 1, 6, 11 and 17 in Table 2.1. Currently, when understanding the effects of an electric field it would seem most logical to attempt to use as uniform a field as possible to eliminate the field strength as a variable throughout the flame.

The electrode geometry is not the only consideration. The aerodynamic alterations need to be kept to a minimum to try and identify the effects of an electric field alone. For example, set up 1 in Table 2.1 would be expected to produce an even electric field, but the aerodynamic effect on the flame both up and downstream will be significant. The mesh below the flame may also entrain additional air which will prevent the air fuel ratio from being accurately calculated.

Aerodynamically the best set up is one in micro gravity where the flame can be one dimensional and the field can be made parallel with it (number 9). This enables the aerodynamic effects to be more easily observed. This has been done by Carleton and Weinberg [111]. However, these tests are very expensive to perform. The aerodynamic effects are further discussed in Chapter 3.

There are several methods used in the literature to produce an electric field. There are 3 ways to produce a field in the same direction (see Figure 2.19);

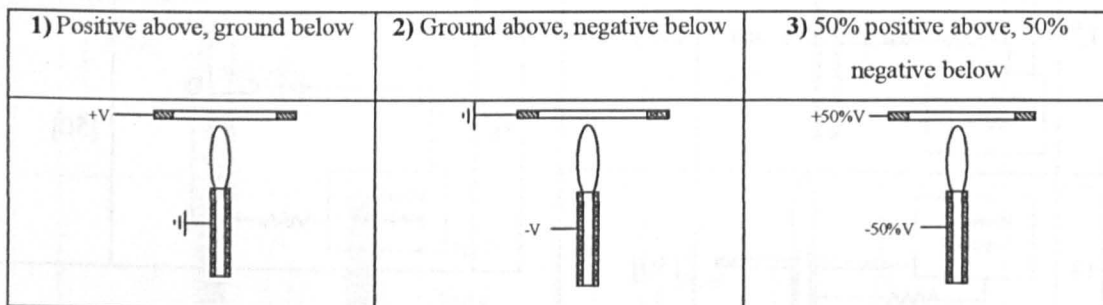


Figure 2.19 the 3 methods to produce the same field

Modelling of a field suggests that both methods produce the same field [101], [102]. This is consistent with the experimental data [41]. Further work needs to be conducted to create as uniform a field as possible, whilst minimising aerodynamic effects that the electrodes may cause.

2.7 Scope of the work

Currently the literature is made up of many different types of electrodes used in different orientations. The only work to directly discuss electrodes can be found in Lawton and Weinberg [7], [25]. There has been no modelling work done to try and assess what the field looks like and how different geometries could be used to manipulate the field or how a uniform field could be generated. There needs to be further work in this area to ensure that any future work is consistent.

There is still debate as to whether AC and pulsed fields can modify the combustion speed although there is gathering evidence that they can [26], [50], [54], [55], [90]. This is a highly important area to investigate further as it could be of great practical use. It is also unclear how they effect combustion (chemical changes or aerodynamic).

Pulsed fields have not been widely used in this area, although they have been used elsewhere [56]. If combustion can be controlled by AC fields the use of pulses may allow greater flexibility to excite ions and give an even greater range of modifications possible to flames. The effect of a pulsed field on a flame needs to be further investigated as well as discovering the pulse width and frequency which causes the greatest effect.

This study therefore intends to do the following:

1. Model the electric field for different geometries and asses the best set up to produce an even field strength to aid understanding of how the field modifies the flame.
2. Establish the effect of a DC field on various equivalence ratios
3. Use high speed cameras and particle imaging velocimetry (PIV) to determine if the ionic wind is causing the observed effects for DC, AC and Pulsed fields.
4. Measure the effect of varying the pulse width on the magnitude of the flame speed increase.
5. Measure the effect of the field frequency on the increase of flame speed using AC fields

Chapter 3 Electrostatic Field Modelling

3.1 Introduction

There have been many authors that have shown that an electric field has a strong influence on a flame (see Chapter 2 for a review of this work). The effect has also been shown to be dependant on the voltage, and therefore the field applied. Changing the voltage changes the field strength of a flame but so can the geometry. As previously mentioned in Section 2.6, there has been very little work done to predict the field generated by different electrode geometries. However, because the effect of a field on a flame is related to the field strength, and therefore the geometry, this is an important topic. The aim of this chapter is to try and predict the field produced by different experimental set ups. This work will also allow magnification of the effects observed by intensifying the field strength in specific areas using the electrode geometry. This will allow intensification of the affect on a flame. However, the aim of the present work is to understand the effects of a field on a flame not to intensify this affect. The results of the modelling will be used to decide which set up produces the most uniform field so that those electrode geometries can be used for the experiments in the rest of this thesis. The effects observed on the flame can then be more accurately associated with a given field strength.

Full modelling of the electric field with the flame in position is not possible with current technology. However, modelling of the electric field without the flame is possible. This can provide an insight into how the field might look with the flame present and enable the effects of the field to be better understood. Ideally the field should be uniform so that the effects caused will be independent of the field. This is particularly important in the areas of combustion (in this case, 40mm above the Bunsen mouth). Changes to the field outside of the combustion region are not important as they will not have such a significant effect on the flame (the ions are produced in the combustion region and recombine shortly afterwards, giving the field nothing to move after this). Earlier research [60] showed that an transverse electric field could extinguish a flame when a ceramic Bunsen was used but

not when a metal Bunsen was used. It became apparent that the field was effected by the materials used in the combustion area. Research from other areas showed that the geometry also changes the field [105]. Therefore this study will use “Maxwell” produced by Ansoft [101] (and compare the results with FEMM [102]) to examine the field distribution for different geometries and materials, and how the flame may alter this. The differences between the set ups used by previous researchers can be seen in Section 2.5 and in Table 3.3. The results of the modelling can be seen in the remaining sections of this chapter. The final set up has been chosen as a result of this modelling.

3.2 Settings used for modelling

3.2.1 Theory

The modelling program computes the static electric field arising from potential differences and charge distributions. To do this it relies on solving the first of Maxwell’s equations; Gauss’ law. Gauss’ law can be stated in several ways but it is the differential form that the modelling program uses. Gauss’ law states that the electric flux through a closed surface is proportional to the charged contained within that surface (3.1). This can be derived into the standard differential form for Gauss Law;

$$\nabla \bullet D = \rho \quad (3.1)$$

where;

- $\rho(x, y)$ is the charge density
- ∇ is the del operator. This expresses the divergence. So the divergence of the

vector $v(x, y, z) = v_x \mathbf{i} + v_y \mathbf{j} + v_z \mathbf{k}$ is; $div \vec{v} = \frac{\delta v_x}{\delta x} + \frac{\delta v_y}{\delta y} + \frac{\delta v_z}{\delta z} = \nabla \bullet v$

- $D(x, y)$ is the electric flux density and can also be written;

$$D = \epsilon, \epsilon_0 E \quad (3.2)$$

This gives;

$$\nabla \bullet (\epsilon, \epsilon_0 E(x, y)) = \rho \quad (3.3)$$

where

- ϵ_r is the relative permittivity. This is set in the modelling process
- ϵ_0 is the permittivity of free space, $8.854 \times 10^{-12} \text{ Fm}^{-1}$ (Farads per metre)

In a static field the electric field strength is the divergence of the potential so that

$$E = -\nabla\phi \quad (3.4)$$

This gives;

$$\nabla \cdot (\epsilon_r \epsilon_0 \nabla \phi(x, y)) = -\rho \quad (3.5)$$

where;

- $\phi(x, y)$ is the electric potential

The program solves (3.5) for the potential ($\phi(x, y)$). It then automatically computes the electric field and flux density using the equations (3.2) and (3.4).

3.2.2 Model, meshing and materials

The program relies on a finite element method. The area is split into a triangular mesh with a node at each vertex. The static electric field is calculated at each node. The results are then fed back into equation (3.5) and the new field calculated (iterative procedure). The difference between the input and the output is calculated. This shows the error at each vertex. In areas of high error the mesh is refined, according to user specifications until a preset percentage error value is reached. In the case of these models the mesh is refined by 15% and the percentage error was set to be below 1%. Convergence times varied greatly for different models. Those where coronas were formed (had sharp edges) such as number 8, 10 and 14 (from Table 2.1) could take up to 2 days (48 hours) to converge. However, more uniform fields such as number 1 took as little as 5 minutes to converge. A typical convergence can be seen in Figure 3.1 below;

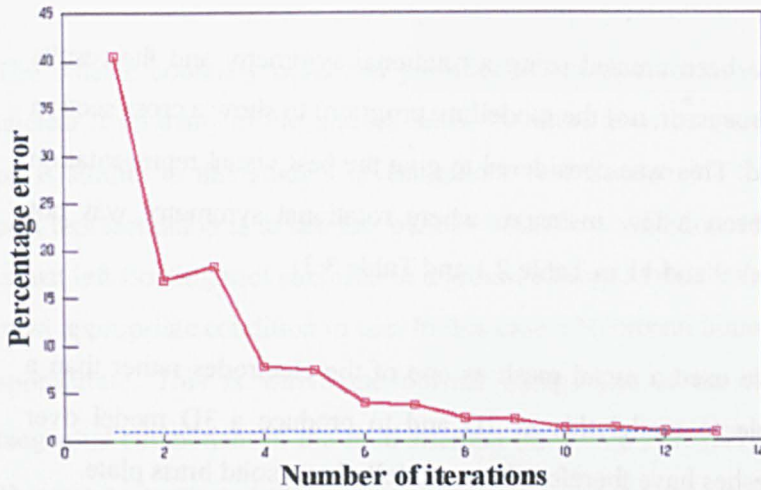


Figure 3.1 Percentage error against number of iterations

The following settings were used to try to make the results comparable to each other. All the electrodes are a distance of 60mm apart, and have a potential of +10kV facing 0V (ground). Unless stated the upper electrode is the one at high voltage (also know as EHT for Extremely High Tension). This is not the voltage used by many of the researchers. The main reason for conducting this modelling was to compare the types of field produced by different geometries to identify the best type for this study. To include the different voltages and distances would make the results very difficult to compare, so, as far as possible the voltages and distances between electrodes have been kept the same.

Material	Relative permittivity (Eps)	Conductivity (siemens/metre)	Situations used
Air	1.0006	0	Background
Brass	1	1.5×10^7	Electrodes
Ceramic insulator	1	10^{-15}	Burners when it is not used as an electrode
Salt water	81	4	Labelled flames
De ionised water	81	0.0002	Labelled flames

Table 3.1 Materials used

Virtually all the models have been created using a rotational symmetry and the results mirrored (using a graphical processor, not the modelling program) to show a cross section through the centre of the field. This was considered to give the best visual representation of the model. There have been a few instances where rotational symmetry was not suitable to use (set up numbers 9 and 11 in Table 2.1 and Table 3.3).

Some of the researchers have used a metal mesh as one of the electrodes rather than a solid plate. It is not possible to model this in 2D and to produce a 3D model over complicates the problem. Meshes have therefore been modelled as a solid brass plate.

3.2.3 Boundary Conditions

The voltages were applied to the electrodes using a sheet source applied to the outside of the conductor (either 0V or 10,000V). It was chosen to apply the boundary in this manor so that the voltages did not interfere with the rotational symmetry boundary condition (or the outer boundary) when they overlapped. It is also a good representation of the theory that the modelling program is based on. This requires that the model is in equilibrium. Gauss' law states that the charge in a combustor rests on the surface when in equilibrium so that is can be as far apart as possible. It also states that because charge is free to move in a conductor then if the conductor is in equilibrium then there cannot be a field in the conductor and the flux entering/leaving a conductor must be at 90° or the charge would experience an unbalanced force and move (meaning it is not in equilibrium).

The findings are presented below. The same scale has been used in all the models. Dark red indicates strong field, dark blue indicates no field.

The outside boundary of the model was set a significant distance away from the areas of interest to try an eliminate interference with the solution. This boundary was then set as a balloon boundary. This means that the voltage is assumed to be at ground level at an infinite distance away. This is a good representation of the experimental case used in this study, where the apparatus was enclosed in an earthed cage.

The outside boundary condition provides the most inconsistent part of the model. It is unclear from many of the sources in the literature how the experiment is set up. If the set up is similar to this study's investigations (see Section 4.2 for further details) then the best representation is to use this balloon boundary condition. However, if the experiment is just left floating (not enclosed in a grounded cage) then the balloon boundary is not the most appropriate condition to use. In this case a Neumann boundary condition is the most appropriate. This is where the normal component of the flux ($D = -\epsilon \nabla \phi$) and the tangential component of the field strength ($E = -\nabla \phi$) crossing the boundary is constant. This can be expressed as;

$$E_{t1} = E_{t2} \quad (3.6)$$

or

$$D_{n1} = D_{n2} + \rho_s \quad (3.7)$$

where,

E_t is the tangential component of the field strength

D_n is the normal component of the flux density

ρ is the surface charge density

Theoretically there should be no additional sources other than those modelled by the two electrodes. However, in reality there will be additional sources such as a Faraday cage or other grounded equipment in the lab. It was therefore decided to model the results using a balloon boundary where earth is set an infinite distance away from the model. The results between the two boundaries are quite different (see Figure 3.2 and Figure 3.3).

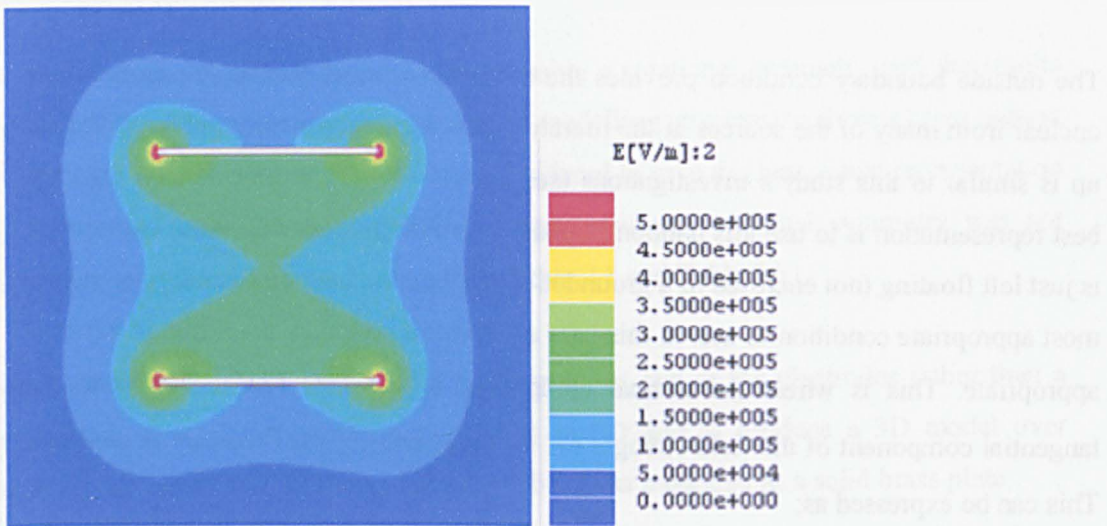


Figure 3.2 Neumann boundary

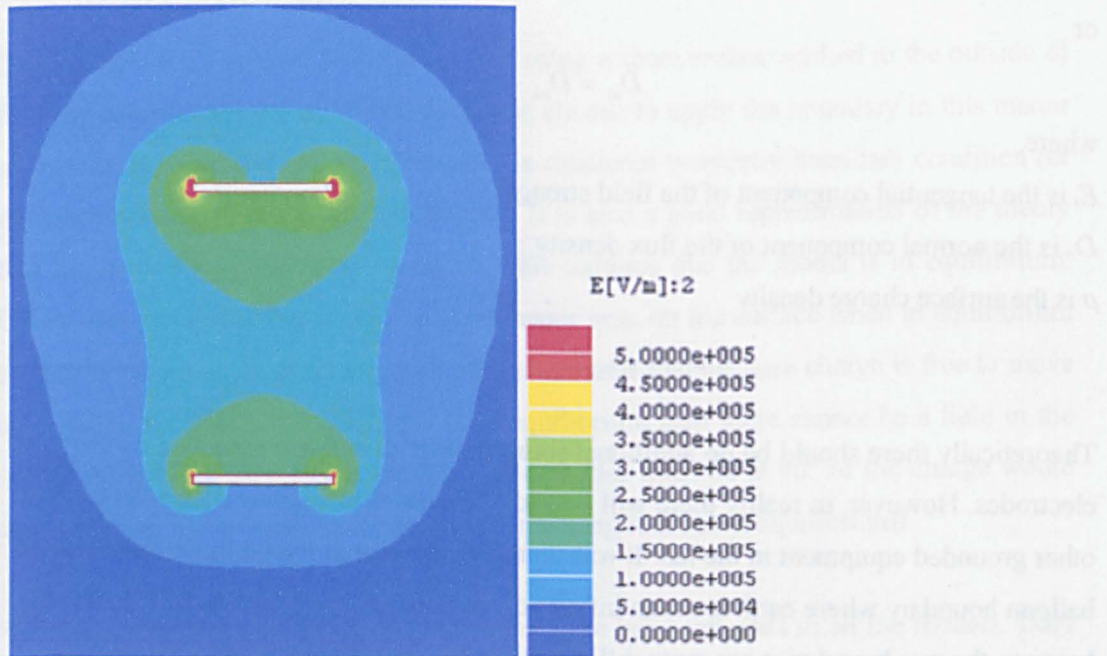


Figure 3.3 Balloon boundary

Figure 3.2 shows an even distribution between the two plates. This is due to there only being a potential difference between these two plates and no other conductors. Figure 3.3 shows the field is skewed towards the charged plate. This is results from there being a potential between the charged plate and the grounded plate, as well as the charged plate

and the boundary. As the boundary is slightly closer to the top plate then the potential is drawn above this plate.

There were some practical problems with using the balloon boundaries where an electrode met the balloon boundary. The program did not model a continuation of the electrode. This caused some unusual results outside the interrogation area (see Figure 3.4 below, circled area). This was set a long way away from the area of interest and it is assumed that these small inconsistencies did not effect the area of interest. The inconsistency was also outside the boundary. There was no way to eliminate these problems without making a much larger mesh that would have taken a significantly longer time to solve. Also making the boundary larger did not significantly alter the solution.

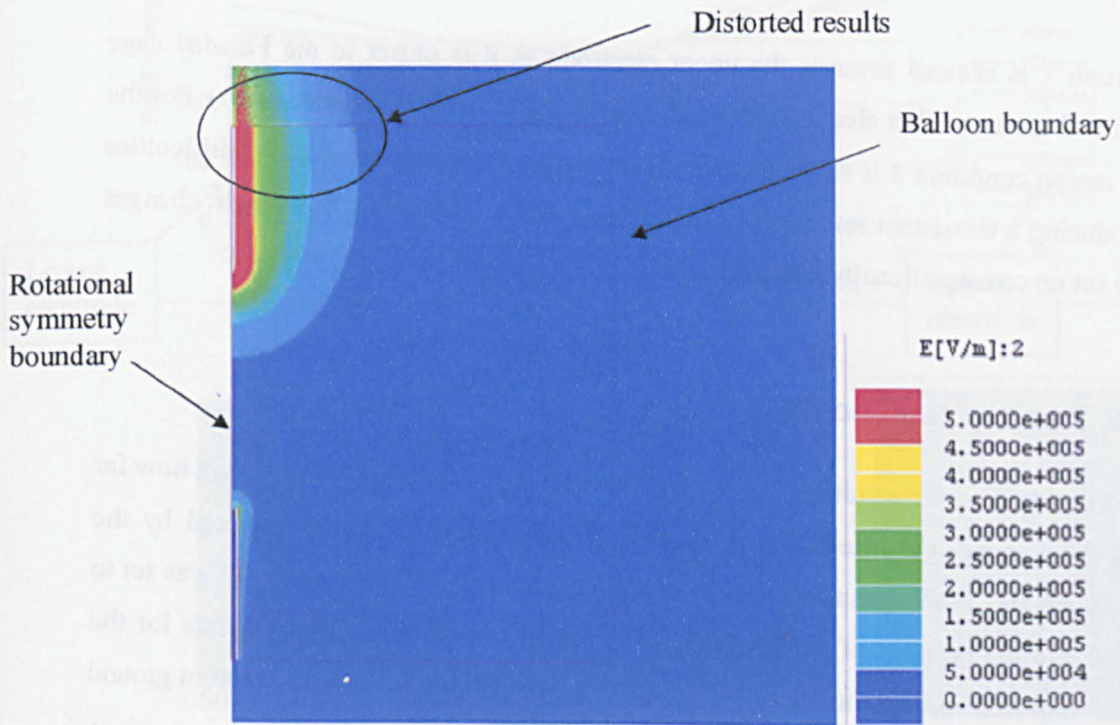


Figure 3.4 View showing inconsistencies on outside boundary

3.2.4 Field orientation

There are 3 ways to produce the same field if the conductor is isolated from all other potentials (this is the same as using a Neumann boundary). The set up and the type of field produced are listed in Table 3.2 below;

Condition	Top Plate (kV)	Bottom Plate (kV)	Balloon Boundary	Neumann Boundary
1.	+10kV	0kV	Figure 3.3	Figure 3.2
2.	+5kV	-5kV	Figure 3.2	Figure 3.2
3.	0kV	-10kV	Upside down Figure 3.3	Figure 3.2

Table 3.2 Field type and distribution of the field

Condition 1 is skewed towards the upper electrode as it is closer to the Faraday cage which will act as another electrode (even though this is an infinite distance away). For the same reason condition 3 is skewed to the lower electrode. This highlights the difficulties in producing a consistent set up for practical experiments and shows how slight changes to the set up can significantly alter the field.

3.2.5 Faraday cage position

The differences in the results mentioned above leads to the problem of assessing how far away the Faraday cage needs to be to prevent it effecting the field produced by the electrodes. This problem has been studied using Maxwell [101]. The boundary was set to ground and the position of the boundary from the electrodes varied. The results for the variation of field strength along a line in the centre of the plates (from the bottom ground electrode to the top positive EHT electrode) are plotted in

Figure 3.5. The colour of each line on the graph is the same colour as the border of the picture showing an image of the field plot.

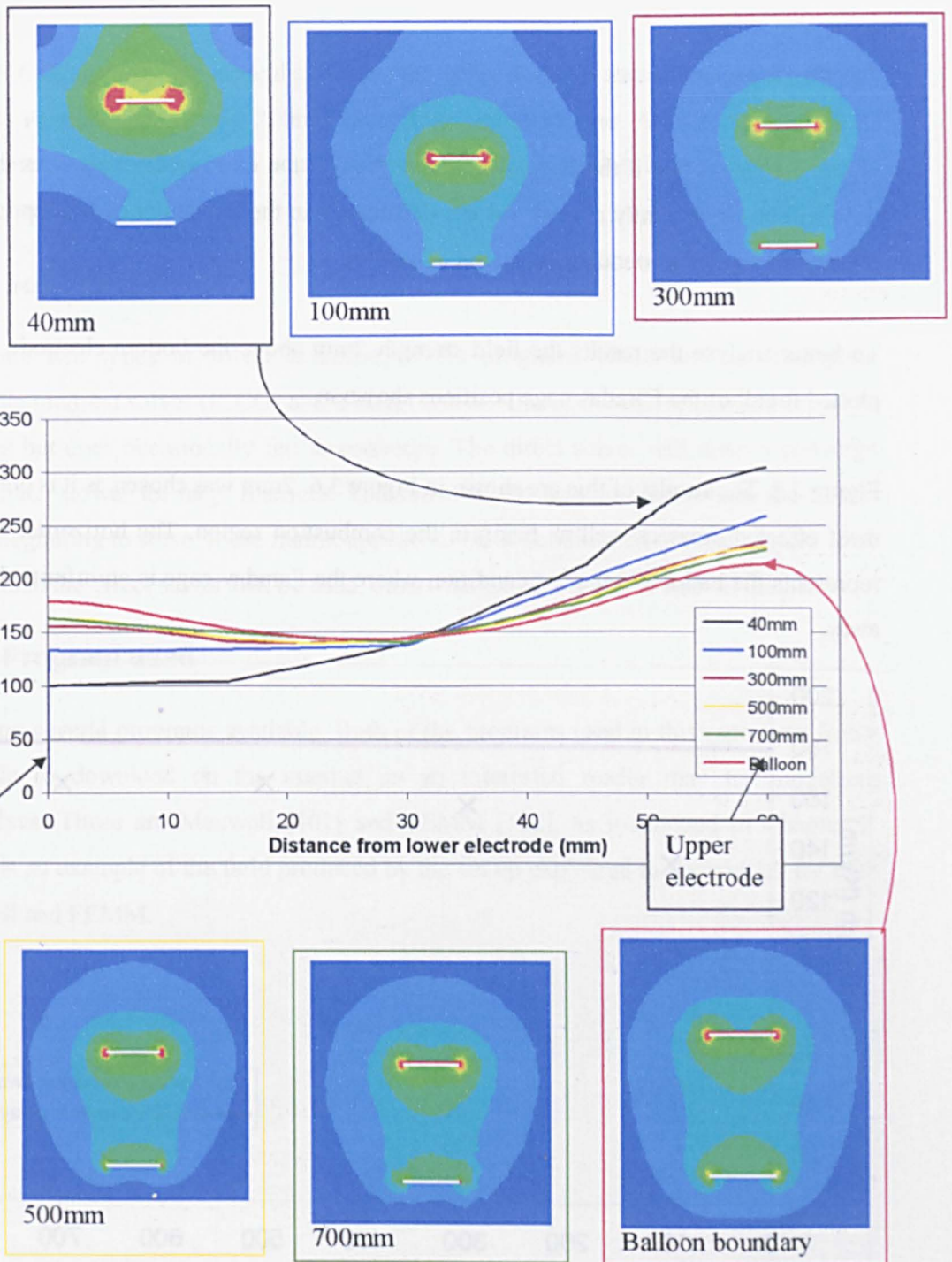


Figure 3.5 Graph to show the effect of altering the distance between the Faraday cage and the electrodes

Figure 3.5 shows that if the Faraday cage (earthed) is too close to the electrodes then the field will be significantly altered. All the simulations in the remainder of this report show the perfect case of a boundary that is set at infinity.

To better analyse the results the field strength 2mm above the bottom electrode can be plotted for all of the Faraday cage positions shown in

Figure 3.5. The results of this are shown in Figure 3.6. 2mm was chosen as it is one of the most effected areas as well as being in the combustion region. The horizontal red line represents the balloon boundary condition where the Faraday cage is an infinite distance away.

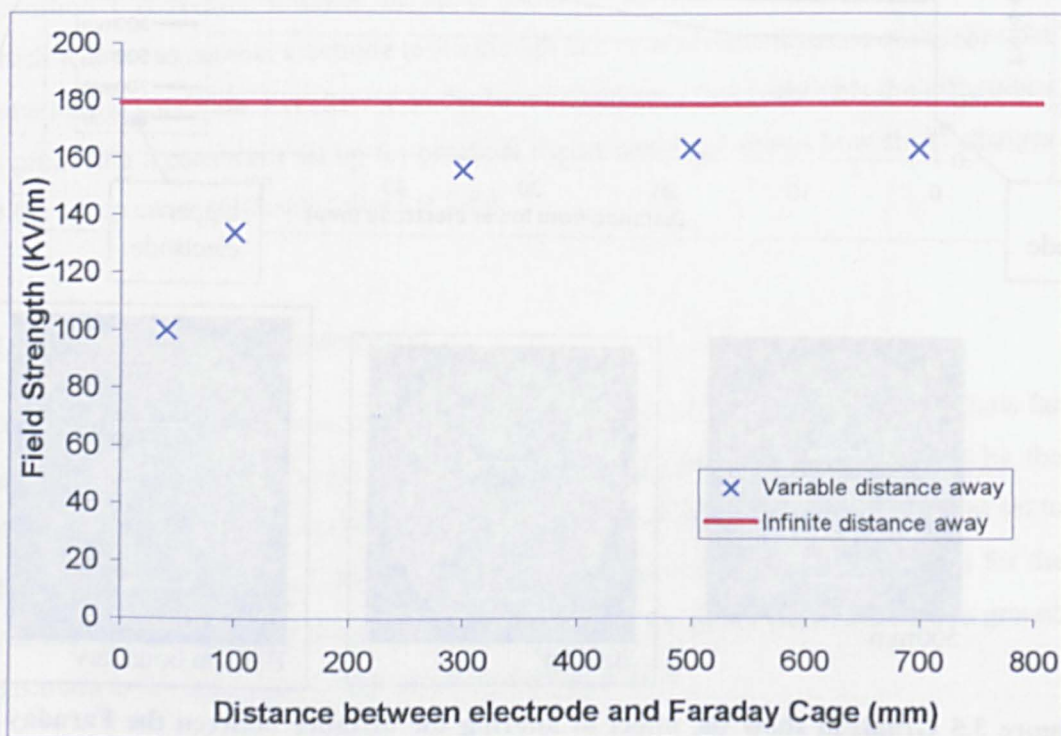


Figure 3.6 Graph to show the effect on the field strength (2mm above the bottom electrode) by altering the distance between Faraday cage and apparatus

Figure 3.6 shows that for practical situations the effect does not seem to be greatly altered once the Faraday cage is over 300mm away from the electrodes. All the experiments in this report have therefore been conducted in a Faraday cage that is over 300mm away from the apparatus.

3.2.6 Solver used

There are two types of solver available in the program. These are an incomplete conjugate gradient solver (ICCG) and a direct solver. The ICCG solver is faster for large matrices but does occasionally fail to converge. The direct solver will always converge but is much slower for large matrices. The software can be setup to evaluate the matrix before beginning to solve. If the matrix appears to be ill conditioned or small (under 1500 nodes) then the direct solver will be used, otherwise the ICCG solver will be used.

3.2.7 Program used

There are several programs available. Both of the programs used in this report are freely available to download on the internet so an interested reader may try modelling themselves. These are Maxwell [101] and FEMM [102], as mentioned in Chapter 2. Below is an example of the field produced by the set up explained in Section 3.2 for both Maxwell and FEMM.

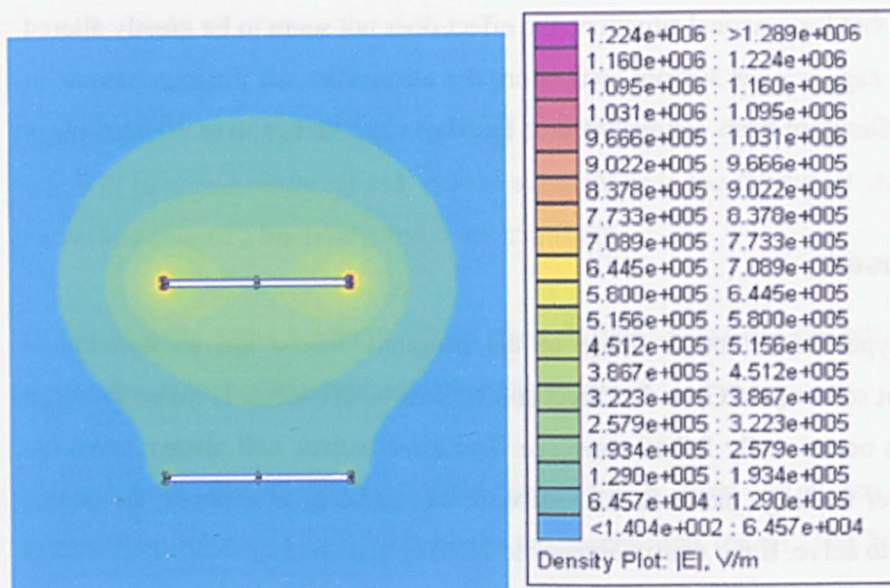


Figure 3.7 Field produced by FEMM balloon boundary

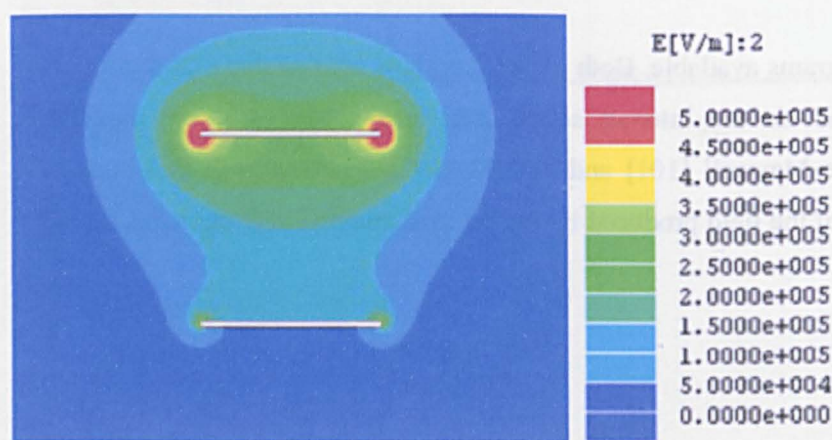


Figure 3.8 Field produced by Maxwell with a balloon boundary

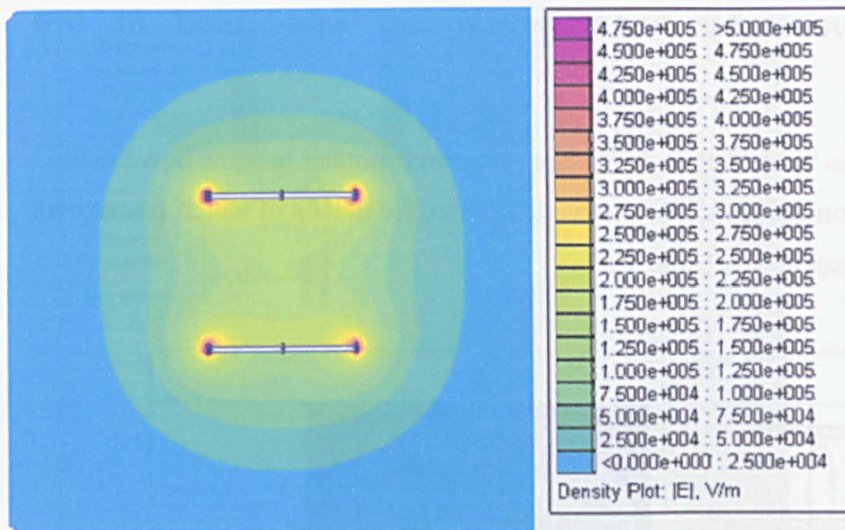


Figure 3.9 Field Produced by FEMM with a Neumann boundary

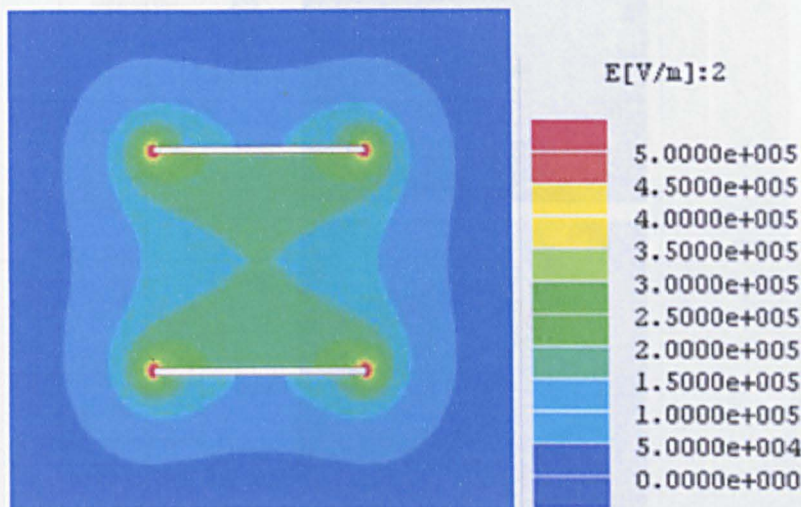
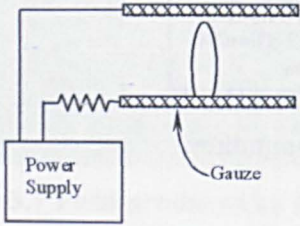
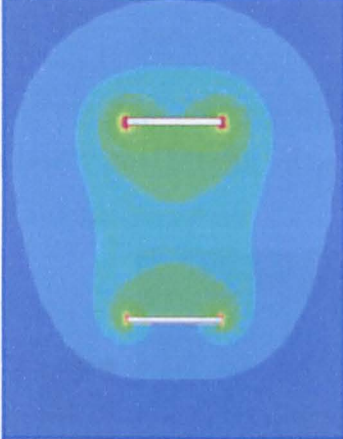
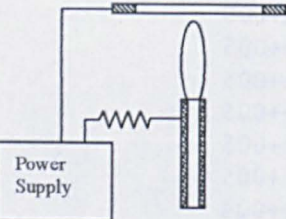
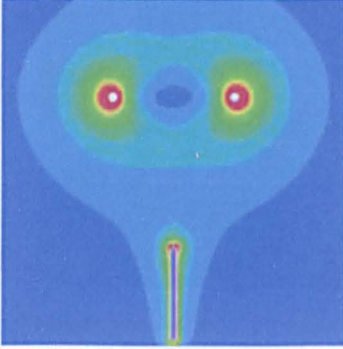


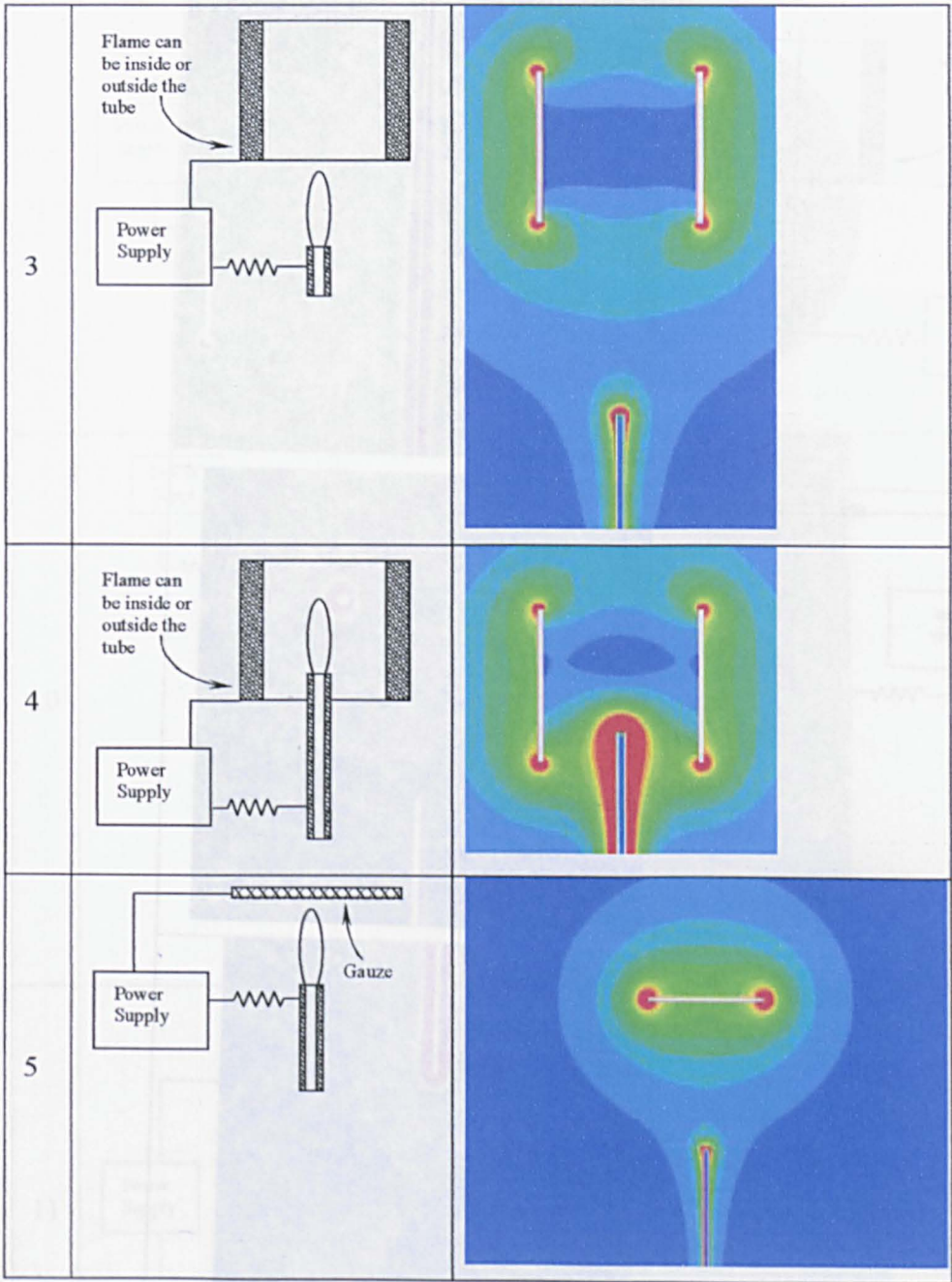
Figure 3.10 Field Produced by Maxwell with a Neumann boundary

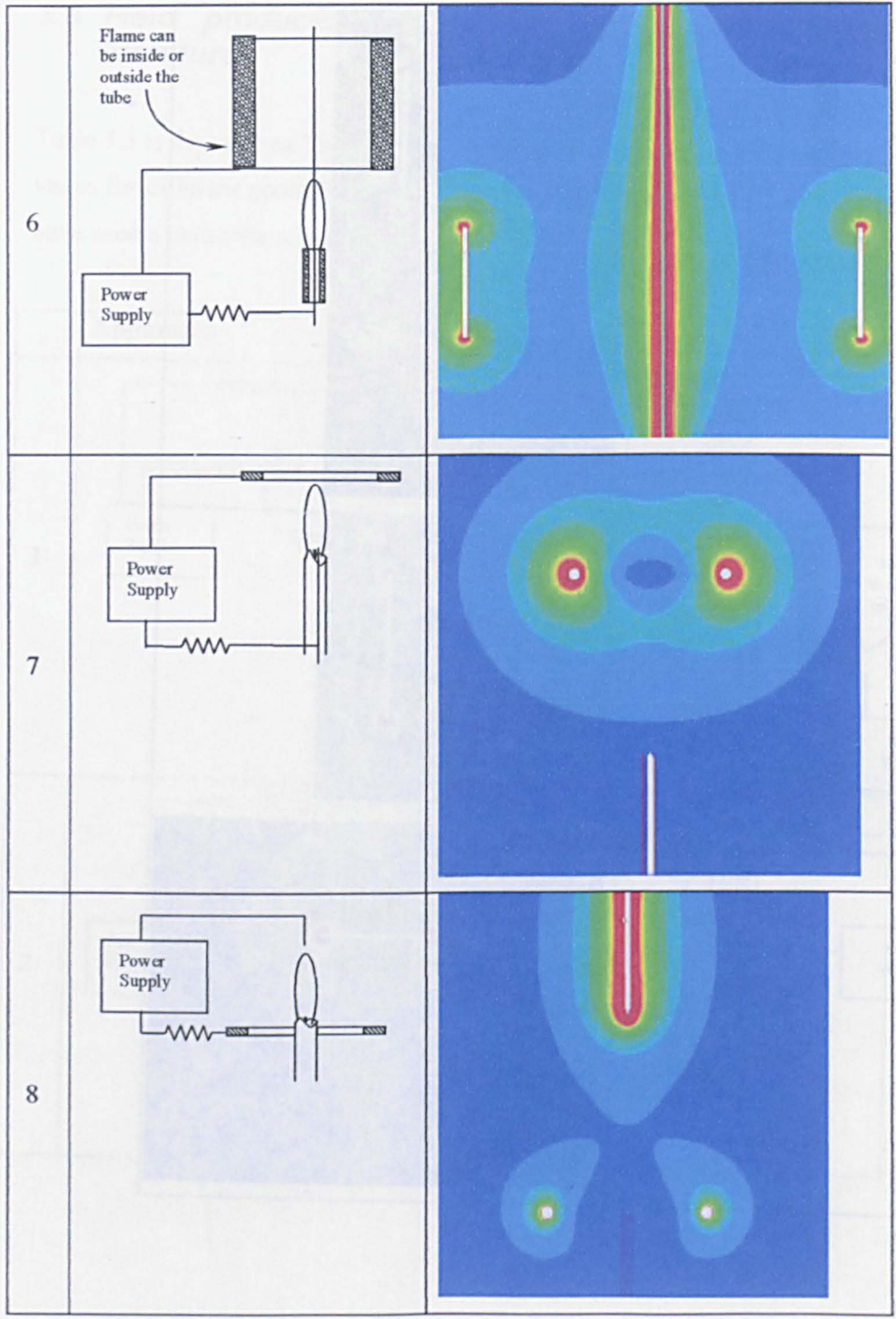
As you can see clearly from Figure 3.7, Figure 3.8, Figure 3.9 and Figure 3.10 both FEMM and Maxwell produce very similar results. Therefore only Maxwell will be used to produce the rest of the results in this report.

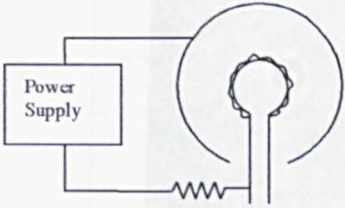
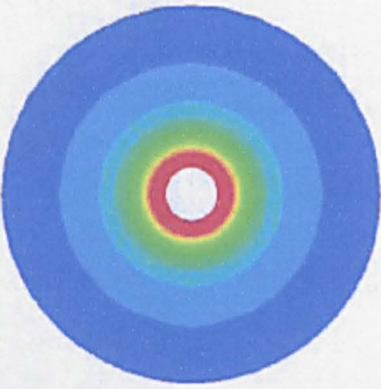
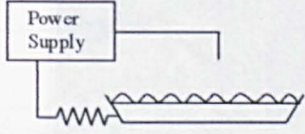
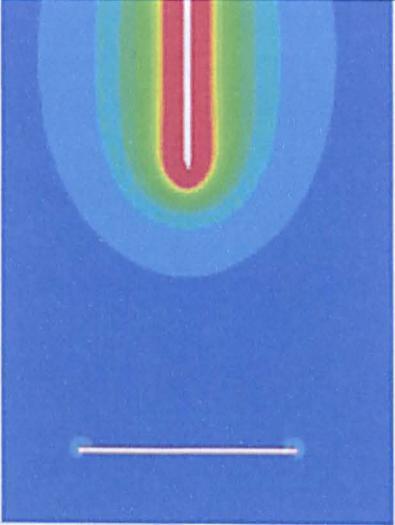
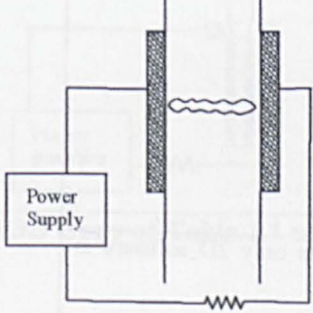
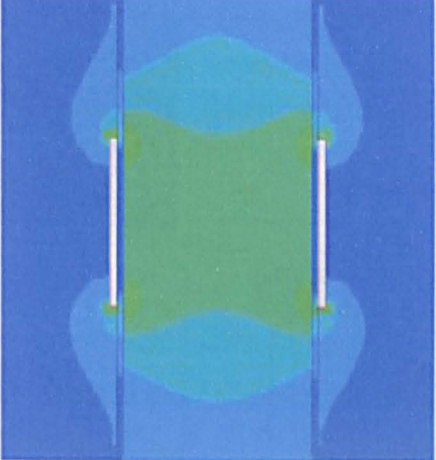
3.3 Field produced by experimental set ups used in the literature

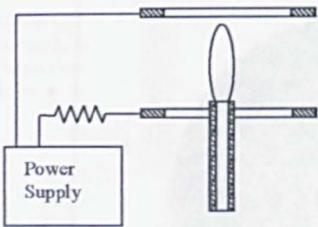
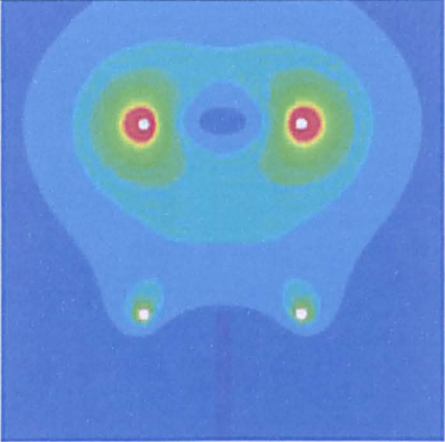
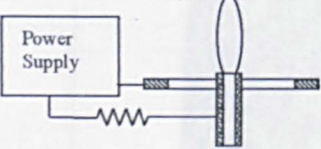
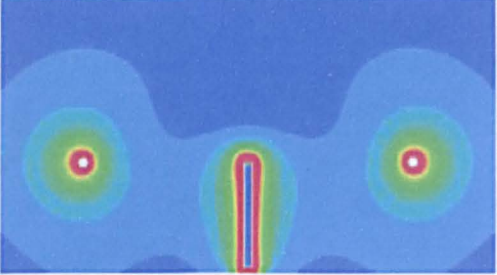
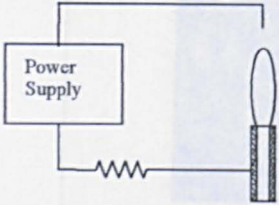
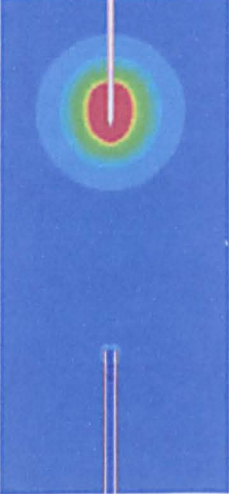
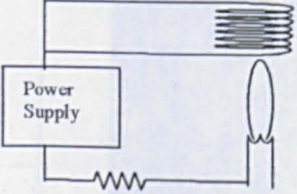
Table 3.3 is the same as Table 2.1, with the same reference number to show how the field varies for different geometries used in the literature. For the details of which researchers have used a particular set up see Table 2.1.

	Apparatus	Model
1	 <p>Power Supply</p> <p>Gauze</p>	
2	 <p>Power Supply</p>	





9		
10		
11		

12		
13		
14		
15		<p>Not possible to model as only 2D software is available</p>

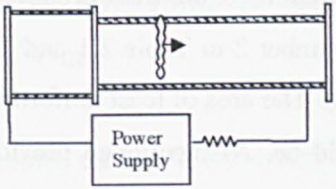
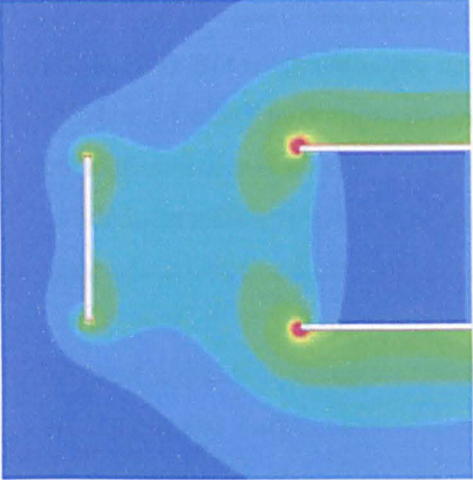
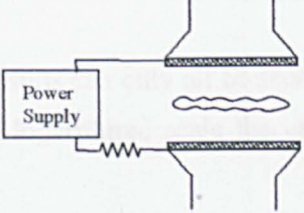
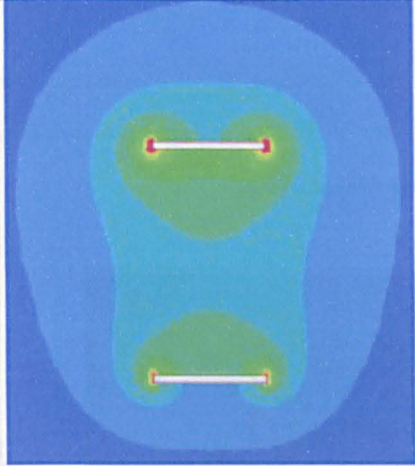
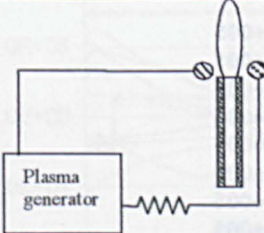
16		
17		
18		<p>This cannot easily be modelled as the field is created by the arc between the electrodes as well as from the electrodes themselves. The voltage is also AC and while this can be modelled it is not easily viewed.</p>

Table 3.3 Copy of Table 2.1 with model of field shown

The results above show that there are several field generation methods that provide an even field with little variation (1, 16, 17). Most notably there are several fields that do not produce a field at all in the flame region (numbers 7, 8, 10 and 14). Consequently, the results from these tests may therefore not provide reliable results.

Perhaps the most important thing to show from the simulations is the field produced by the most popular experimental set up (Figure 3.11 and number 2 in Table 2.1 and Table 3.3) is highly non uniform (see Table 3.3 and Figure 3.12). The area of least uniformity is actually around the burner mouth where the flame would be. As mentioned previously this is very undesirable as the effects of the electric field cannot be estimated if the electric field strength is unknown or even varying over the flame.

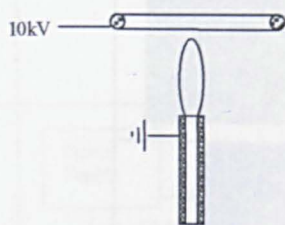


Figure 3.11 Experimental set up

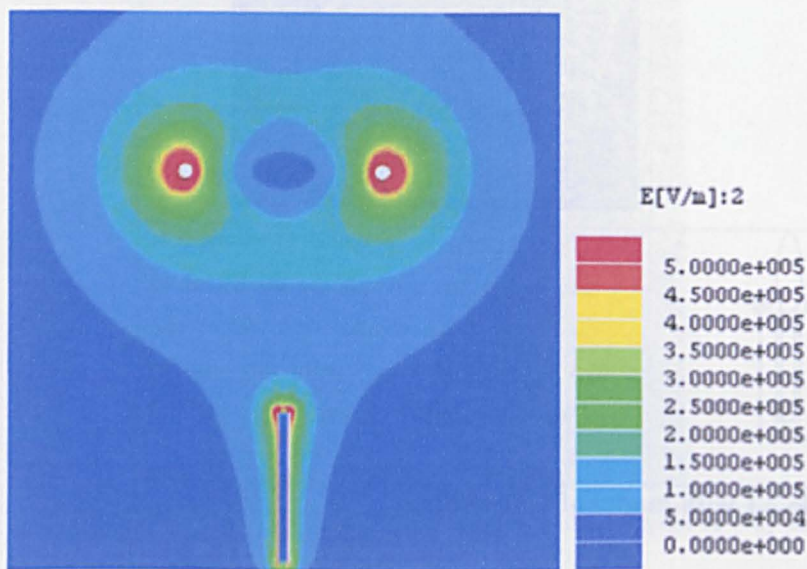


Figure 3.12 Model of Bunsen (earth) and ring (10kV positive) apparatus

The variation of this field is even greater than indicated on the model above, as the red region represents all regions above 5×10^5 V/m to remain consistent with the other models

represented here. However, the maximum (at the corner of the Bunsen) is actually $7.89 \times 10^6 \text{ V/m}$.

The results can be more easily compared if the field strength is plotted against the distance from the Bunsen exit (Figure 3.13). All the results are plotted along a vertical line from the Bunsen mouth to the upper electrode at 60mm, along the axis of symmetry. Only number 6 cannot be plotted in this way as there is a wire acting as the ground electrode along the axis of symmetry. The most uniform fields should appear as a flat horizontal line of the highest possible field strength. Large variations as mentioned previously are undesirable in this case.

The results can only all be seen together on a logarithmic scale as Figure 3.13 shows. On a non logarithmic scale the other apparatus does not even show on the bottom of the graph.

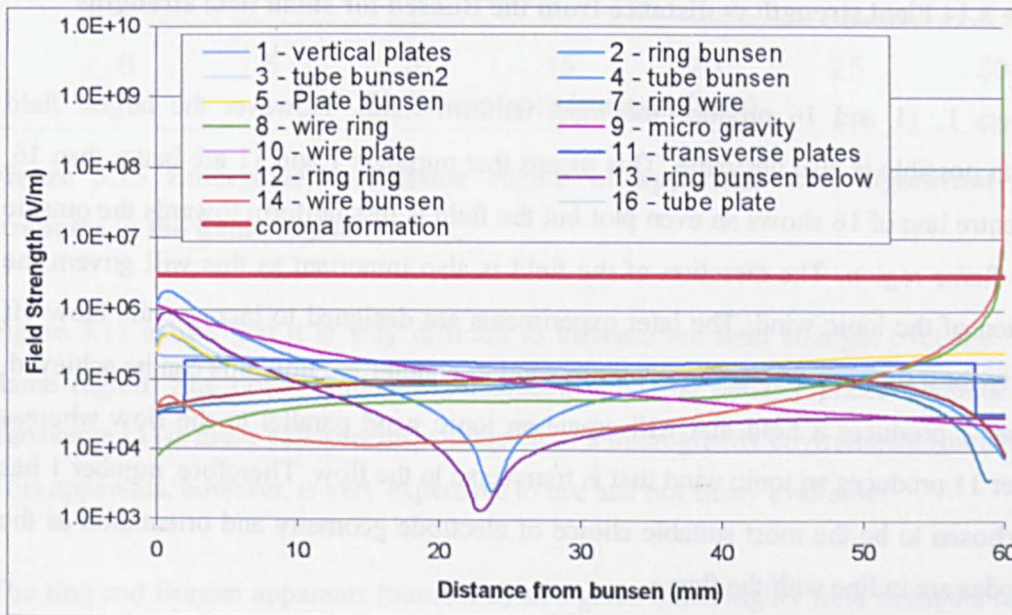


Figure 3.13 Plot of field strength against distance from the burner mouth for all apparatus

The thick red line in Figure 3.13 indicates the value at which air begins to ionise, forming a corona. Apparatus numbers 448 and 14 are well above this limit and numbers 4 and 9

are close but just below the limit. The most uniform fields are produced by those with lower maximum field strengths. These have therefore been plotted on a non logarithmic scale below (Figure 3.14).

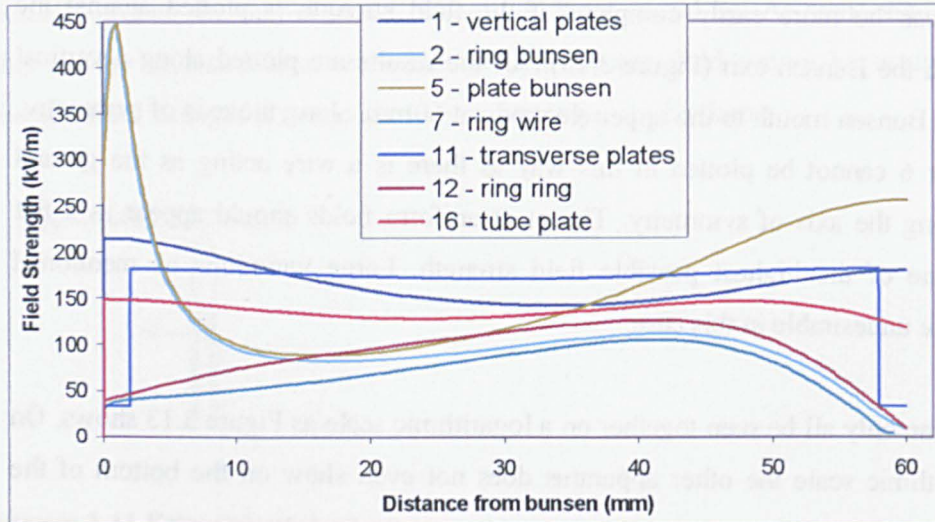


Figure 3.14 Field strength vs distance from the Bunsen for small field strengths

Numbers 1, 11 and 16 produce the most uniform fields. However the largest field strength possible is also desirable. This means that numbers 1 and 11 are better than 16. The centre line of 16 shows an even plot but the field is less uniform towards the outside of the flame region. The direction of the field is also important as this will govern the direction of the ionic wind. The later experiments are designed to increase the blow off velocity for a flame and by using the ionic wind to counter the flow this can be achieved. Number 1 produces a field that will create an ionic wind parallel to the flow whereas number 11 produces an ionic wind that is transverse to the flow. Therefore, number 1 has been chosen to be the most suitable choice of electrode geometry and orientation as the electrodes are in line with the flame.

The figures above also indicate how the choice of geometry can increase the maximum field strength by over 6 orders of magnitude from the estimated average field strength (shown approximately by numbers 1, 11 and 16). This maximum in the flame region could create a much greater ionic wind effect. The problem is that this ionic wind will

significantly move the flame and may pull it out of the region where the effect is greatest. The results are however very useful for those using AC or pulsed fields where the ionic wind is not significant. The effects observed in these fields could be greatly multiplied by choosing an electrode that concentrates the field into the flame region. This can be considered to be the first 30mm from the Bunsen mouth for the majority of the flames considered in the experiments performed in Chapter 3 and Chapter 4.

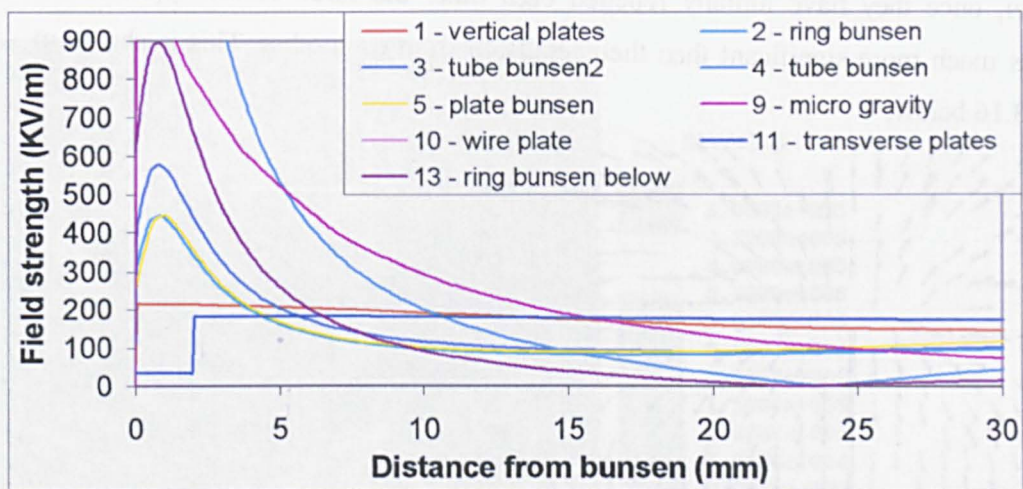


Figure 3.15 Enlargement of flame region of apparatus with significant field strengths in the flame region

Figure 3.15 shows that it is very difficult to increase the field strength over the entire flame region. The only significant enhancement on the parallel plates (vertical 1 or transverse 11) is those experiments conducted in a microgravity environment (number 9). This apparatus, however, is very expensive to use and not easily available.

The ring and Bunsen apparatus (number 2) also gives much higher field strengths for the first 10mm but then drops below the more uniform fields and even reaches 0 at 25mm above the Bunsen. The presence of the flame may however increase this region.

3.4 Ionic wind direction

The direction of the field can be plotted, showing the direction of the force exerted on chemi ions by the field, giving additional acceleration in that direction. This will not be the exact movement of the ions as the repulsion of the like charged ions when they are first created will be much greater than any applied field due to their close proximity. However, once they have initially repelled each other the force of the applied field becomes much more significant than their repulsion from each other. This is shown in Figure 3.16 below;

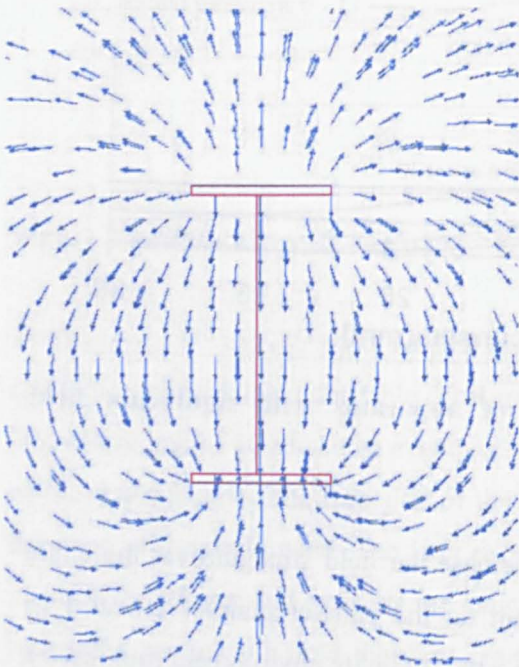


Figure 3.16 Plot of direction of field for number 1 (vertical plates)

The size of the arrows in Figure 3.16 are not scaled, only directional. In this case the ionic wind will flow from the upper electrode to the lower electrode in a straight path. The presence of the flame is likely to change this but this will be discussed further in Section 3.8.

3.5 Effect of the upper electrode

There was some speculation in the literature [59], [66] as to whether the geometry of the upper electrode made much difference to the field set up. It was found experimentally that it did not cause any measurable difference to the flame modifications caused. The same model was used as in Figure 3.12 and Figure 3.17 but with the upper electrode as a plate rather than as a ring.

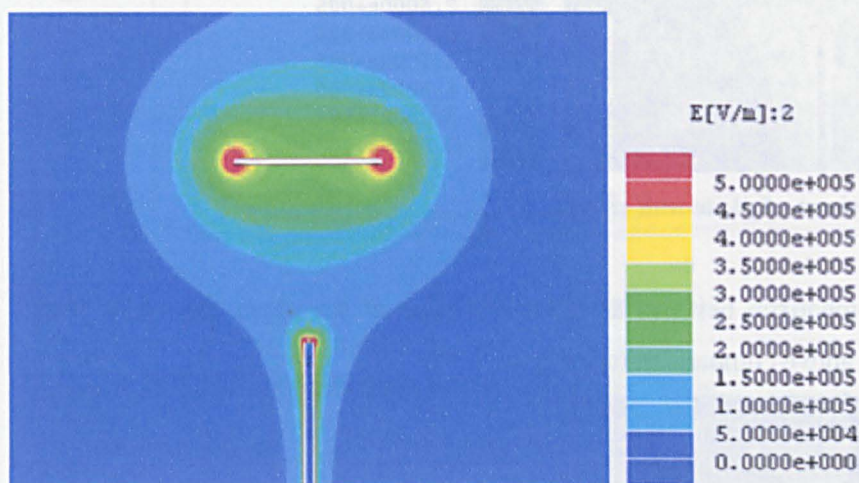


Figure 3.17 10kV positive applied to plate (top) and Bunsen grounded

The comparison of results can be seen below in Figure 3.18. The results show similar trends near to the Bunsen mouth but the plate produces a more uniform field at the top. This change near to the upper electrode is unlikely to effect the experimental results significantly as the flame would tend to be positioned below this area. With the plate the maximum field strength is lower ($4.58 \times 10^6 \text{V/m}$ with plate and $7.89 \times 10^6 \text{V/m}$ with a ring).

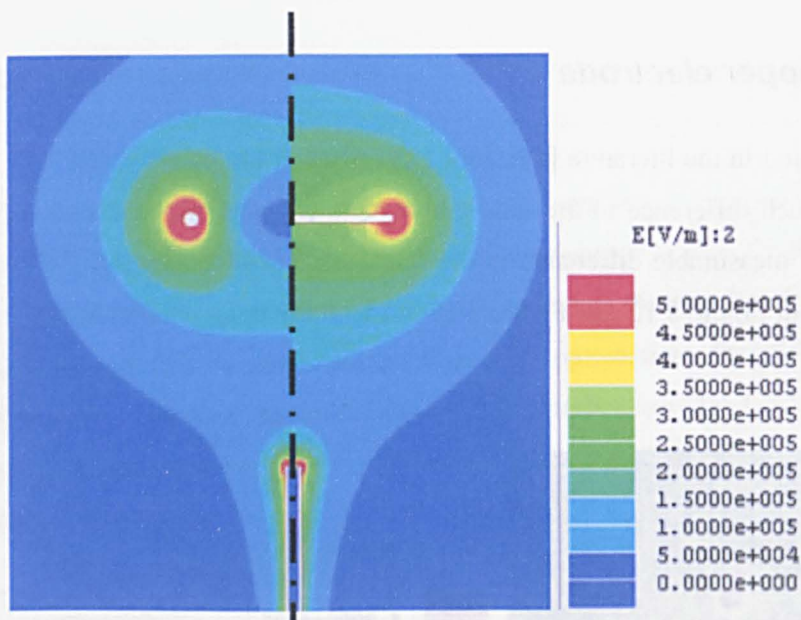


Figure 3.18 Comparison of plate and ring

The results for a comparison between a tube and a plate as the upper electrodes show similar results to the above comparison (see Figure 3.19).

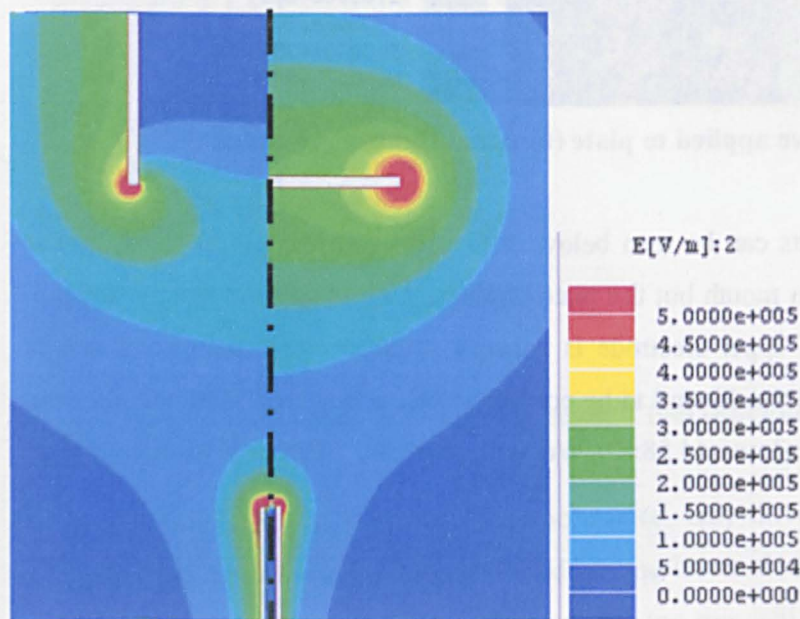


Figure 3.19 Comparison of tube and plate

As before the lower section near the Bunsen is very similar. However, in the vicinity of the upper electrode the field between the two sets of apparatus is very different. The

results from this do show a slight expansion of the higher field strength region close to the Bunsen mouth. These results can be plotted on a graph to show the field strength along the centre line of the model (Figure 3.20).

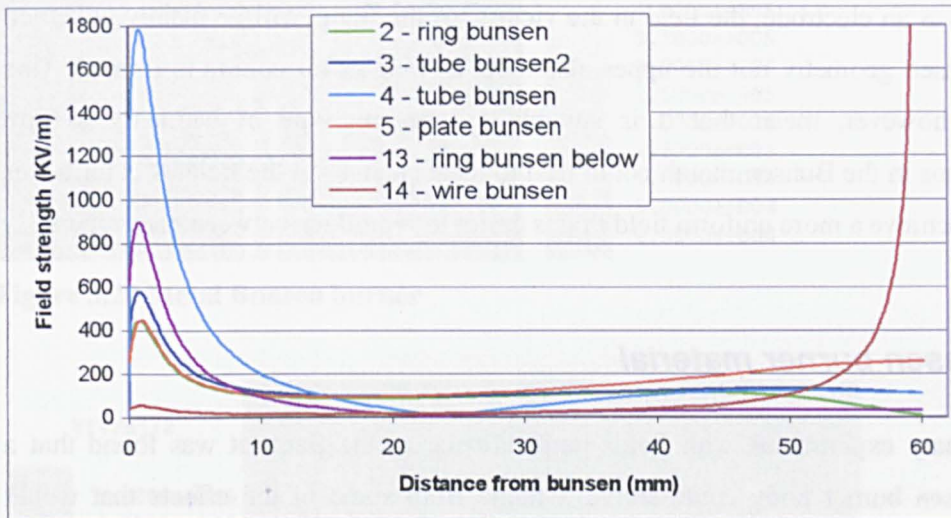


Figure 3.20 Effect of variations to the upper electrode

The experimental data tested a ring (number 2) and a mesh (number 5) as the upper electrodes. The modelling results (Figure 3.20) show that these two experimental apparatus produce almost identical fields.

The large peak of number 14 has been ignored for this discussion as a corona will be formed in this region. The experimental data also did not include the effect of coronas [59], [66].

The largest peak (number 4) was also not included in the experimental data. Although Figure 3.20 shows that the peak voltage varies by an order of magnitude this is only in the first 5 to 10mm. The presence of the flame will also change this meaning there is no way to plot this as the flame covers a significant part of the plotted axis.

In conclusion, the modelling correlates with the experimental results. The field in the combustion region is not significantly effected by different types of upper electrode but mainly by the lower electrode. This is logical as the major factor in the local production of a field is the geometry of the electrode nearest to it. In the case of a metal Bunsen being used as an electrode, the field in the vicinity of the flame will be mainly governed by the Bunsen geometry not the upper electrode, as long as no corona is formed. This does not, however, mean that it is suitable to use any type of geometry as any imperfections in the Bunsen mouth could lead to local changes in the field. It is far better to try and achieve a more uniform field that is easier to reproduce between researchers.

3.6 Bunsen burner material

In preliminary experiments with fields perpendicular to the flame it was found that a metal Bunsen burner body could shield a flame from some of the effects that would otherwise be observed. Figure 3.21 is a model of a transverse field with a non-metallic Bunsen. In Figure 3.22 and Figure 3.23 the significant change to the field can be observed with a metal Bunsen instead of a ceramic one.

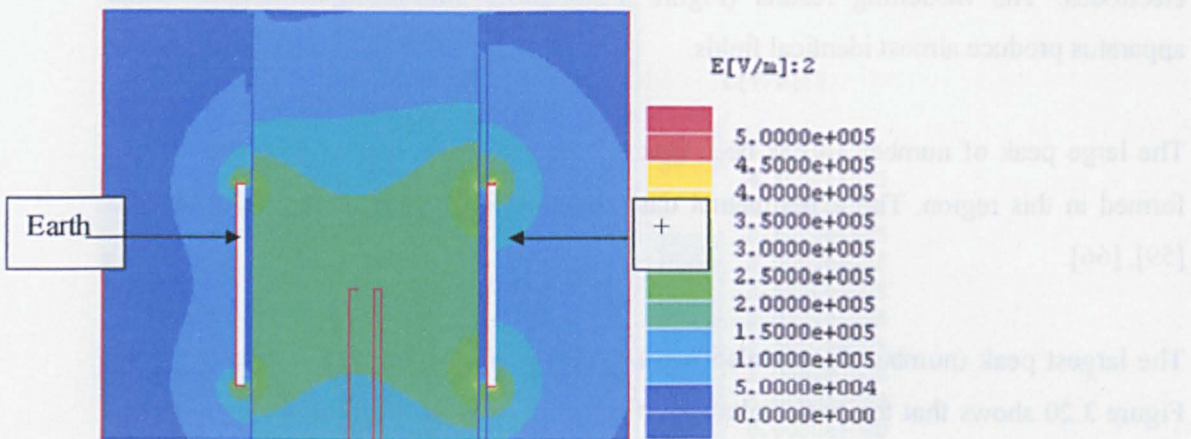


Figure 3.21 Ceramic Bunsen burner

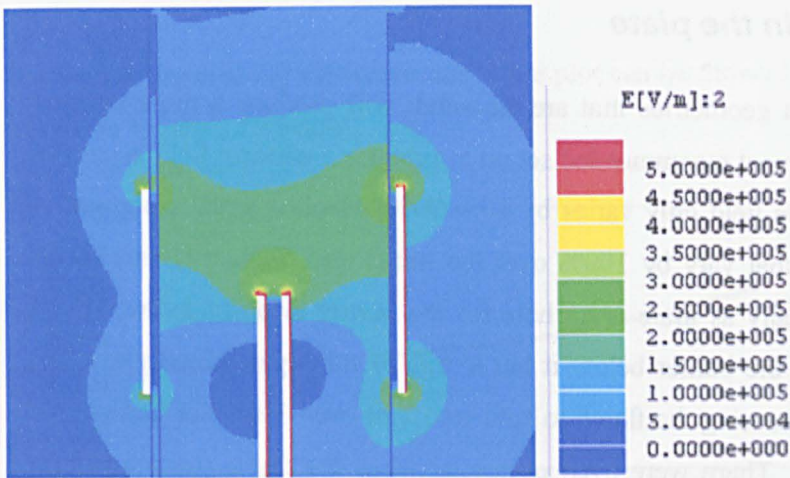


Figure 3.22 Metal Bunsen burner

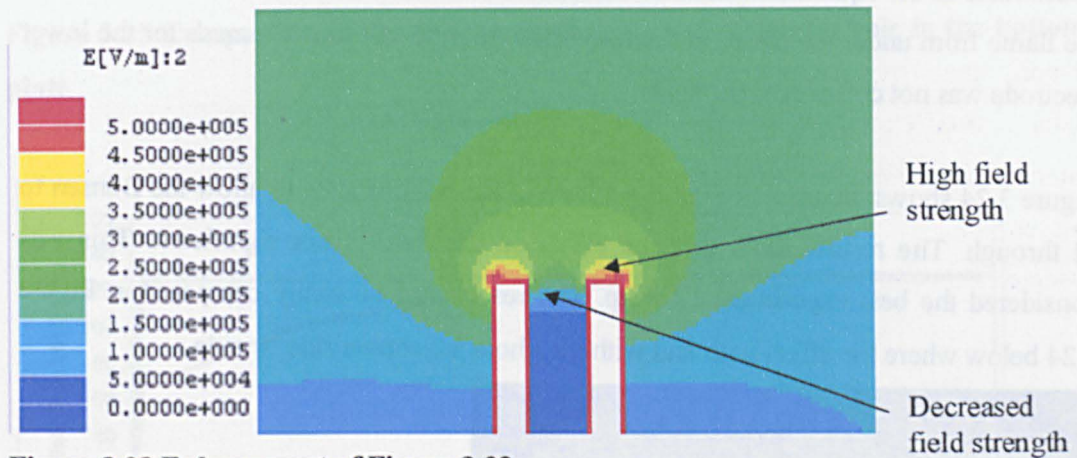


Figure 3.23 Enlargement of Figure 3.22

The metal Bunsen created a high field strength spike from the sharp corners. It also shields the incoming gasses from the field around the burner mouth. This seems consistent with the experimental data. It was attempted to extinguish the flame but extinction was not possible (even at very high field strengths) as the flame decreased in size until it was only present at the very tip of the Bunsen. At this point the flame was shielded from the field, as shown above. It was decided from the experimental work and from the modelling shown above to use a ceramic Bunsen so that minimal interference of the field was caused.

3.7 Cutting a hole in the plate

It would be expected that geometries that are smoother will produce a more uniform field. In the literature the most recommended set up to produce a uniform field is parallel plates (see number 1). The field only varies by 10 – 20%, which is small compared to many of the other fields that vary by 100% over the flame area. However, this set up could not be used practically as there is no hole for the burner to protrude through. A mesh could be used with the burner below it but it was found experimentally that this disturbed the flow, often causing the flame to split into 2 or even 3 smaller flames as it passed through the mesh. There were even occasions when the flame jumped off the burner and settled on the mesh. While this provided a stable flame it was considered undesirable as the equivalence ratio could not be calculated as extra air was entrained into the flame from under the mesh. For aerodynamic reasons the use of a mesh for the lower electrode was not considered suitable.

Figure 3.24 shows the effect of cutting a hole in the bottom plate to allow the Bunsen to fit through. The results show that the effect on the field is not significant. This was considered the best experimental set up. The results can be easily compared in Figure 3.24 below where the effect with and without a hole are shown side by side.

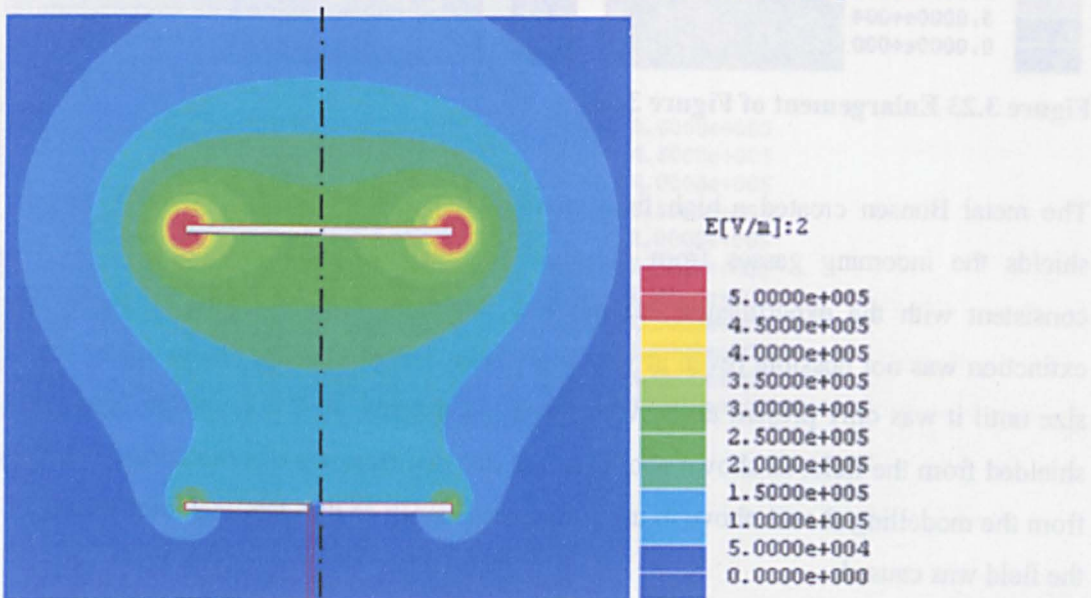


Figure 3.24 Comparison of bottom plates with (left) and without (right) a hole cut in

The field strength along the centre line of the plot can be shown for both results. This can be seen in Figure 3.25 below.

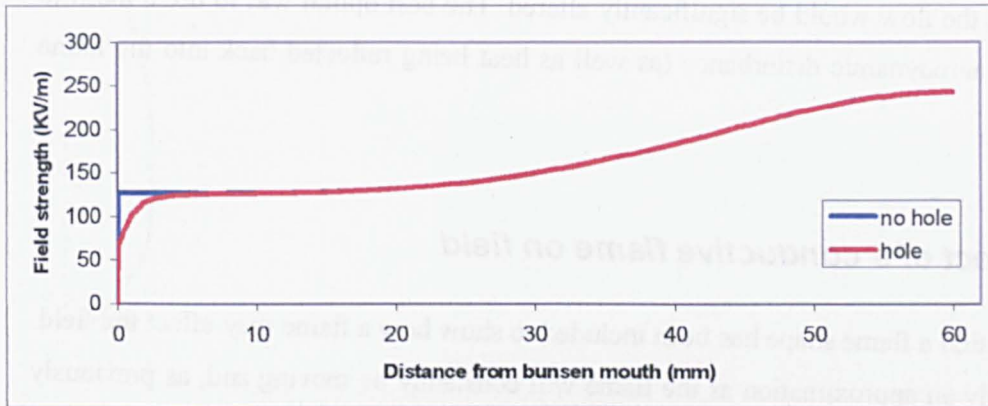


Figure 3.25 Comparison of the field strength with and without a hole in the bottom plate

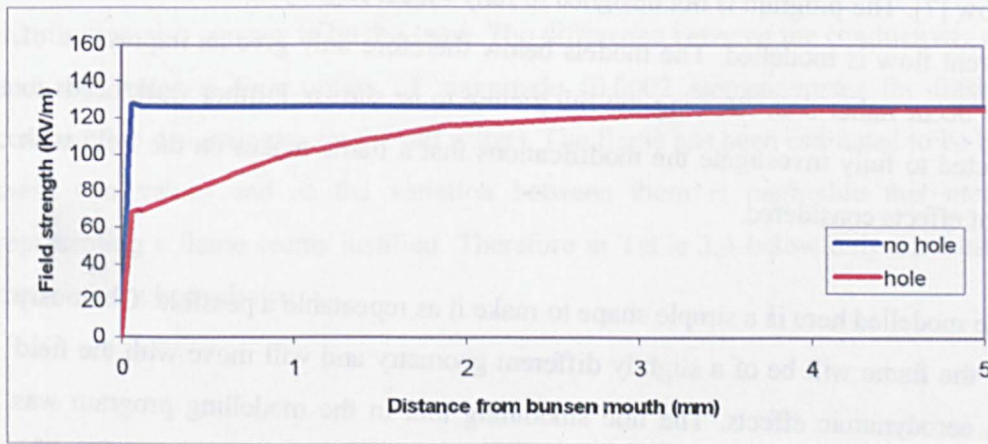


Figure 3.26 Enlargement of Figure 3.25

The results from Figure 3.25 and Figure 3.26 show that the effect on the field strength is only significant in the first 1-2mm above the Bunsen. As explained in Chapter 4 the flame may be lifted by 1mm from the Bunsen for the experiments. Therefore cutting a hole in the bottom plate to allow the Bunsen to protrude does not significantly alter the field characteristics.

Aerodynamically the bottom plate being made of a solid sheet will have an effect as additional air cannot be entrained from directly below. However, this effect should be small. The greater effect is from the electrode above the flame. If this was made from a solid sheet the flow would be significantly altered. The best option was to use a mesh to avoid this aerodynamic disturbance (as well as heat being reflected back into the flame region).

3.8 Effect of a conductive flame on field

In this section a flame shape has been included to show how a flame may effect the field. This is only an approximation as the flame will constantly be moving and, as previously mentioned, the software is not currently available to model the moving flame and field at the same time. Salt water (conductive) with ions (Na^+ and OH^-) conducts electricity in a similar way to a flame where the charged positive ions and free electrons simulate a current flow [7]. The program is not designed to fully model slightly conductive materials as no current flow is modelled. The models below therefore only give an impression of what may occur rather than allowing the full picture to be shown. Further work needs to be conducted to fully investigate the modifications that a flame makes on the field with the current effects considered.

The flame modelled here is a simple shape to make it as repeatable a possible. Obviously in reality the flame will be of a slightly different geometry and will move with the field and with aerodynamic effects. The line smoothing tool in the modelling program was used to smooth around the following coordinates as shown below (see Figure 3.27). The base of the flame was positioned 1 mm away from the Bunsen mouth.

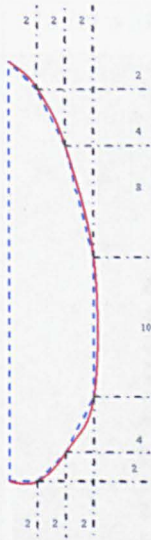


Figure 3.27 Flame geometry (dimensions in mm)

Both fresh water and salt water estimates have been used but the results are identical (see Figure 3.28). The maximum in both models is also the same ($1.53 \times 10^7 \text{V/m}$). The distribution also appears to be the same. The difference between the conductivity of fresh and salt water is four orders of magnitude (0.0002 siemens/meter for fresh water compared to 4 siemens/meter for salt water). The flame has been estimated to be between these two values and as the variation between them is negligible this method of representing a flame seems justified. Therefore in Table 3.4 below only the fresh water models have been shown.

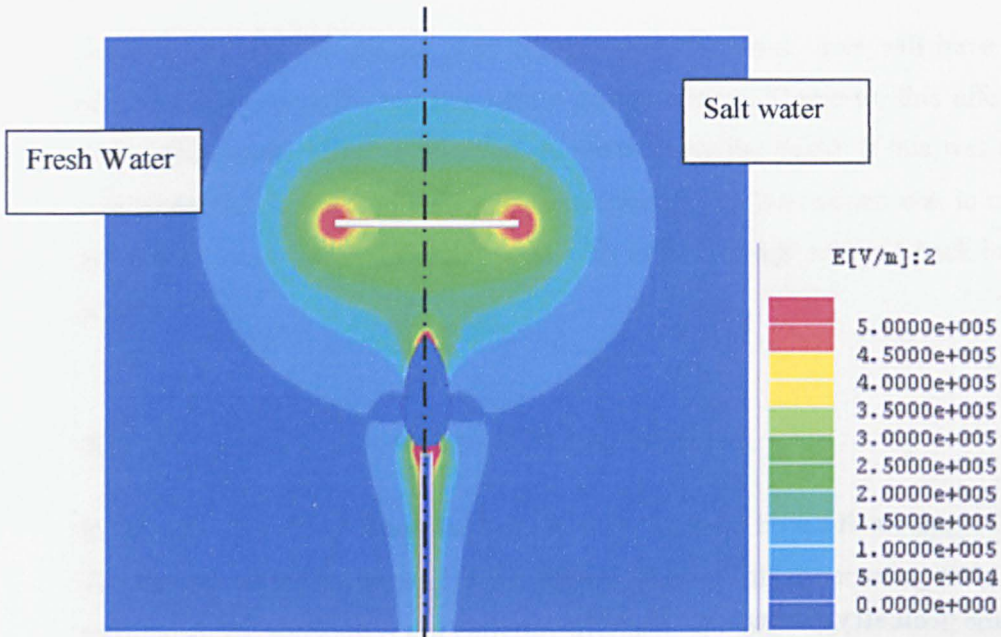
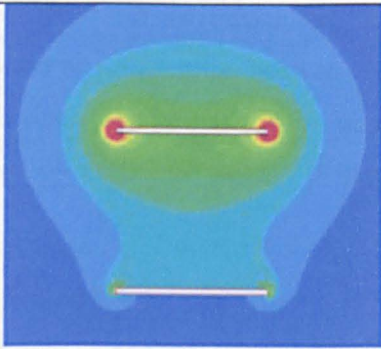
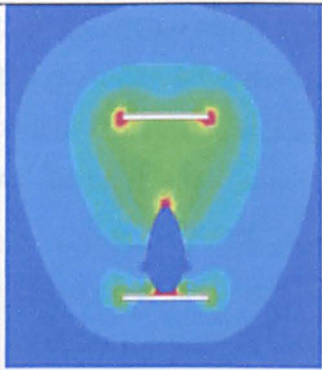
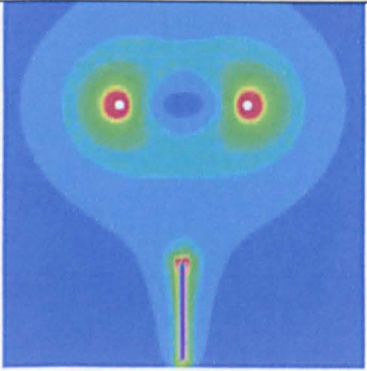
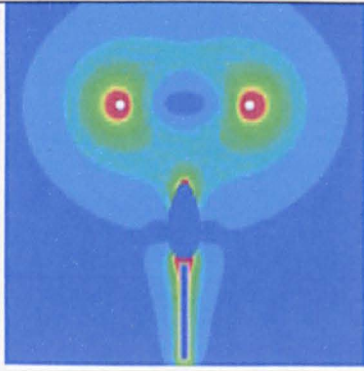
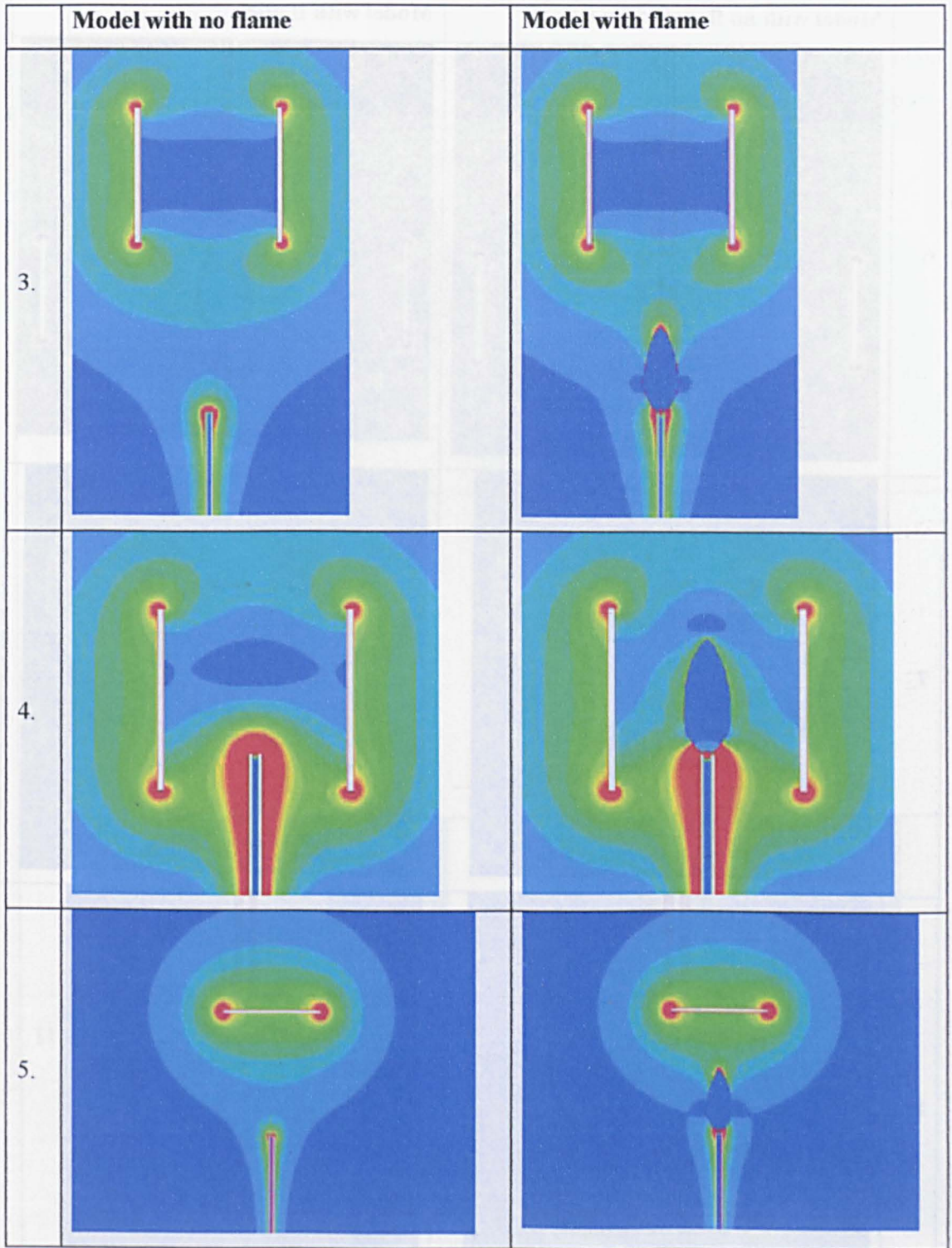
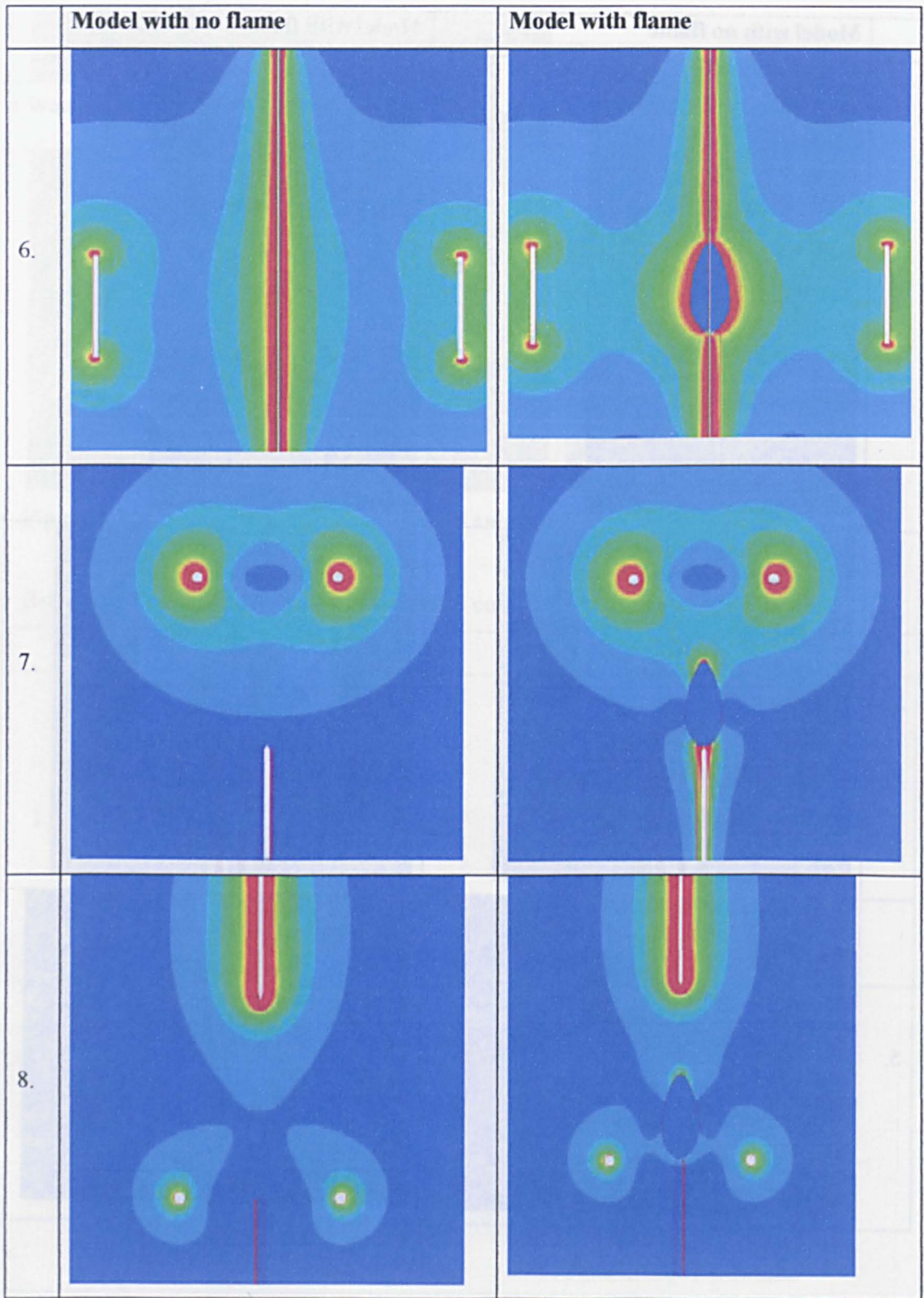


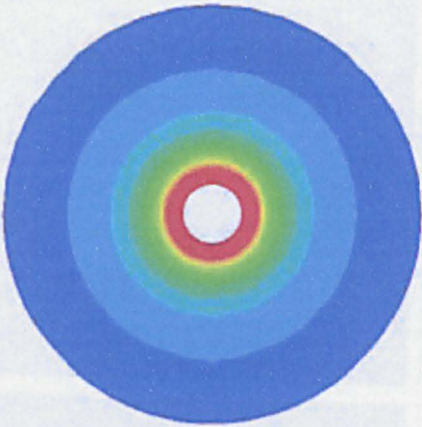
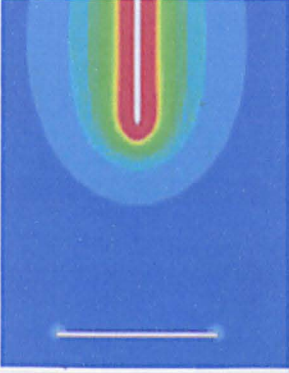
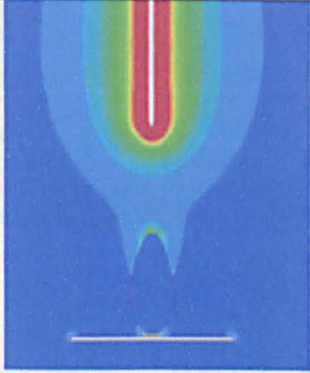
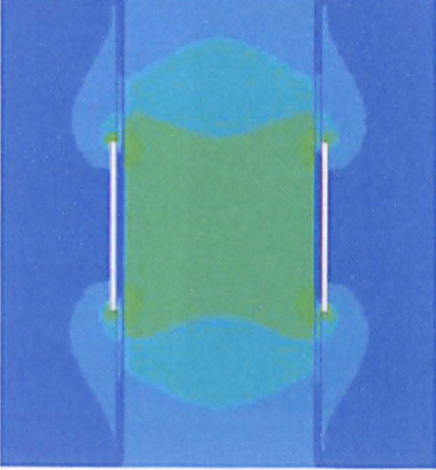
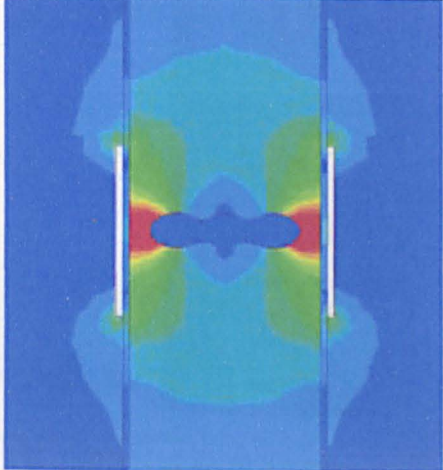
Figure 3.28 Comparison of fresh water and salt water used to simulate a flame

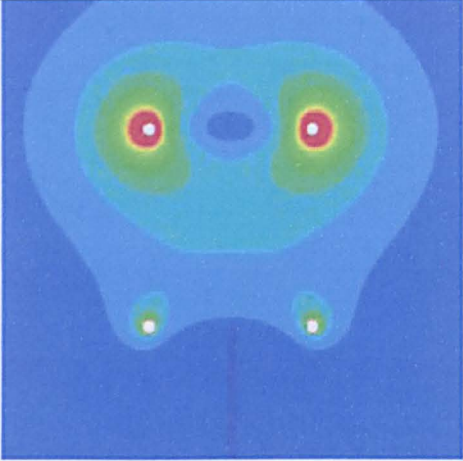
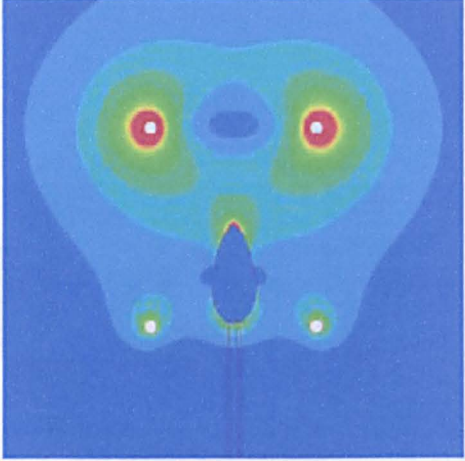
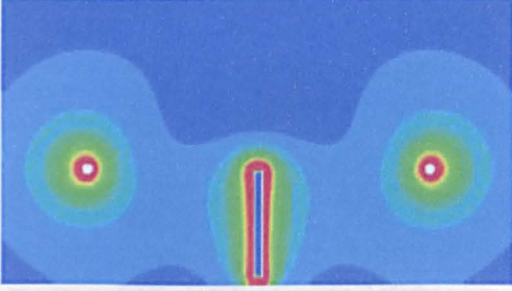
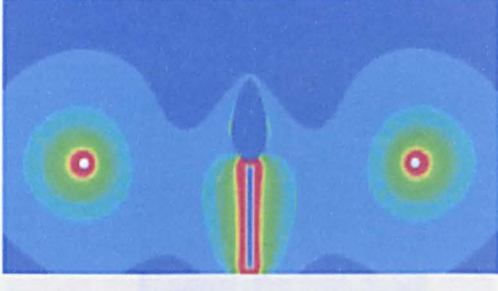

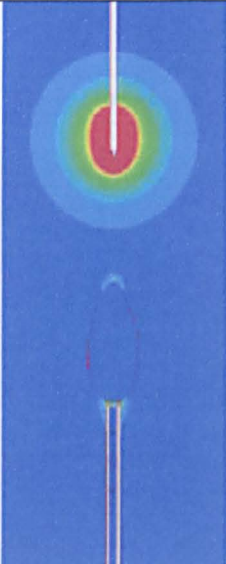
Below, Table 3.4 shows the effect of adding a conductive flame to the model.

	Model with no flame	Model with flame
1.		
2.		





	Model with no flame	Model with flame
9.		<p>Not possible to model this type of flame as the geometry of the flame is unknown</p>
10.		
11.		

	Model with no flame	Model with flame
12.		
13.		
14.		
15.	Not possible to model as only 2D software is available in this case	

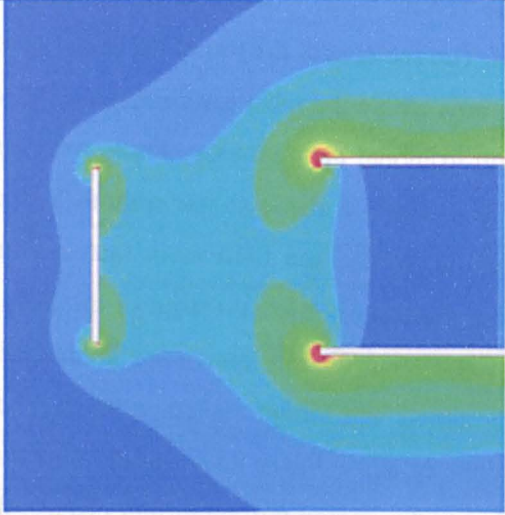
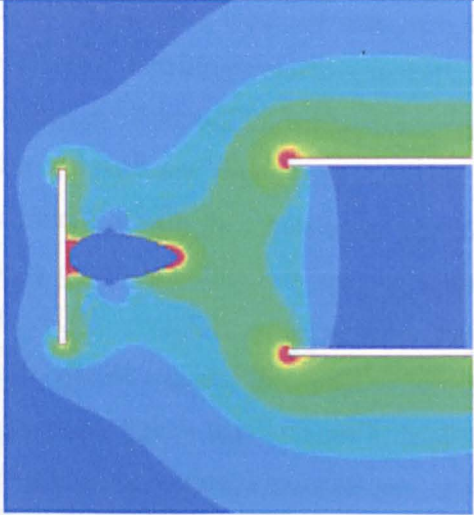
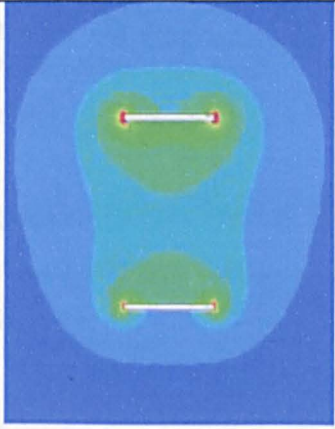
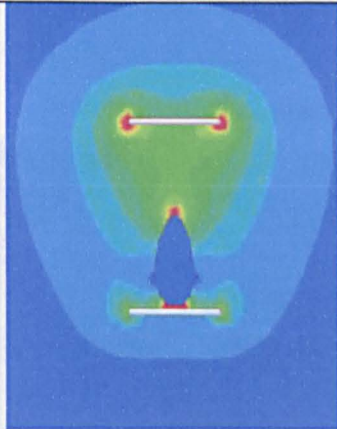
	Model with no flame	Model with flame
16.		
17.		
18.	<p>This cannot easily be modelled as the field is created by the arc between the electrodes as well as from the electrodes themselves. The voltage is also AC and while this can be modelled it is not easily viewed.</p>	

Table 3.4 Copy of Table 2.1 and Table 3.3 but with the flame estimated

It is important to note that the above simulations are only a first approximation as the field and flame will effect each other. Also the model does not allow for current flow.

In Section 3.3 it was shown that parallel plates produced the most uniform field. Figure 3.29 compares the field with no flame to the results when a flame is modelled. The overall change is less significant than expected. The red area at the top of the flame is the most unreliable part of the model as this is the area where the most aerodynamic changes are likely to occur and it was therefore difficult to model the geometry. There were also problems associated with drawing this area, as creating a flame shape without a sharp pointed top was difficult. The sharp edge then magnifies the field more than a flame would be expected to. However, it is likely that there is an intensification of the field in this region. This will create a locally strong ionic wind directly above the flame which will lead to recirculation of hot combustion products and longer residence times. These affects can be used to reduce pollutant emissions or allow faster flow rates to be passed through the burner. The affect on the ionic wind in this region will be further discussed in Section 6.3.6, where the ionic wind model prediction is compared with the velocities measured experimentally in the flame.

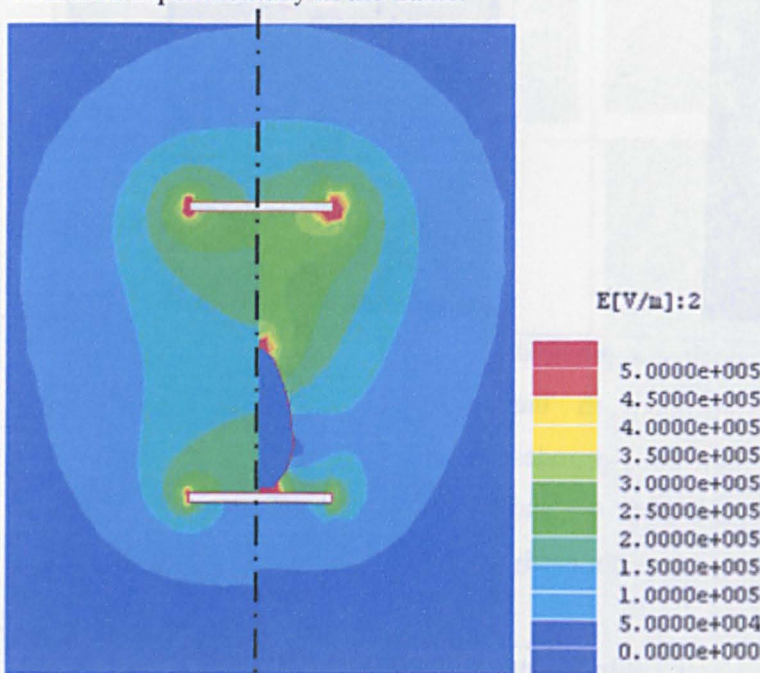


Figure 3.29 Comparison between flame and no flame with parallel vertical plates

The plot of the field strengths along the centreline of the plates shows the area of greatest variation between the results.

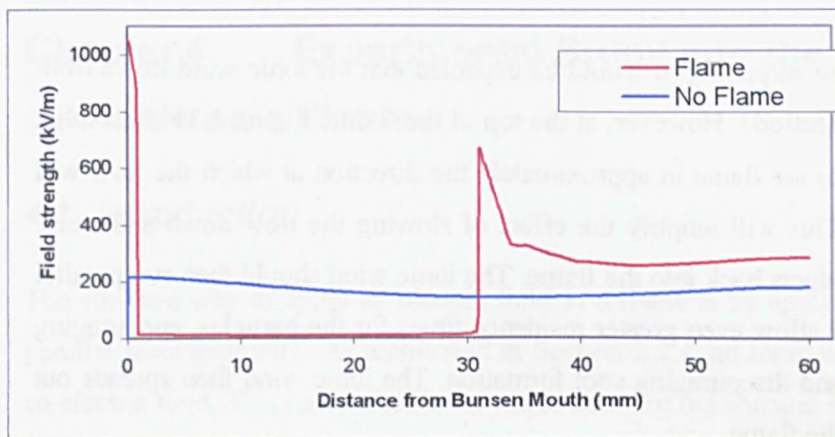


Figure 3.30 Comparison of vertical plates with and without a flame

Figure 3.30 shows the amplification of the field by the tip of the flame. The field and any ionic wind created should be strongest in this region. The high field strength at the Bunsen mouth should not be so significant due to there being few ions near the base of the flame.

The direction of the field can be plotted to show the direction of any ionic wind that might be created (see Figure 3.31) if the larger ions are positive and the negative ions are free electrons.

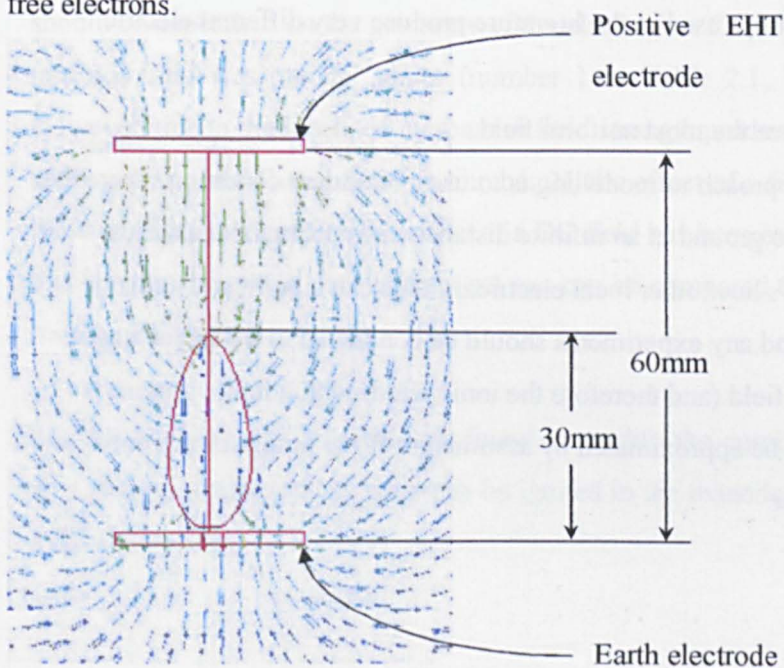


Figure 3.31 Direction of field plot

The results from this are surprising. It would be expected that the ionic wind flows from the top to the bottom electrode. However, at the top of the flame, Figure 3.31 shows that the ionic wind flow into the flame in approximately the direction at which the flow will be leaving the flame. This will amplify the effect of slowing the flow down and cause recirculation of hot products back into the flame. The ionic wind should then run parallel to the flame which will allow even greater residence times for the particles, encouraging complete combustion and discouraging soot formation. The ionic wind then spreads out at the base away from the flame.

These results have been tested by the use of Particle Image Velocimetry (PIV) in Chapter 6 and the results are further discussed there.

3.9 Conclusions

In this chapter it has been shown that;

- Modelling with the flame is not completely possible
- Modelling without the flame is possible
- The experimental set ups used in the literature produce very different electric fields
- Parallel plates produce the most uniform field
- The most realistic approach to modelling is to use a boundary condition where the field strength is set to ground at an infinite distance away from the apparatus
- Practically this shows how other local electrical fields can significantly change the field produced and any experiments should be conducted in a Faraday cage
- The direction of the field (and therefore the ionic wind) with a flame present is complex and cannot be approximated by assuming it flows straight from one electrode to the other

Chapter 4 Experimental Study into the Effect of a DC Fields on a Flame

4.1 Introduction

The simplest way to apply an electric field to a flame is by applying a DC voltage to a parallel plate geometry. As mentioned in Section 2.2.1, an ionic wind can be created by an electric field. This ionic wind is the major cause of the changes observed in a flame by a DC or low frequency ($\geq 50\text{Hz}$) field (Section 2.4). The ions are attracted towards the negative electrode (in this case the earth electrode is negative as the high voltage is positive). If this is the case then the results should show a strong difference with the electrodes in different orientations. The aim of this section is to show the effect of a DC field and how this effect is caused by an ionic wind, not chemical changes to the combustion process.

In Chapter 3 it was shown that the geometry of the electrodes had a strong effect on the field produced. Because the field has an effect on the flame, the strength of that effect should be dependant on the geometry of the electrodes. The set up that produced the most uniform field was parallel plates (number 1 in Table 2.1, Table 3.3 and Table 3.4). However, due to the localised increase in field strength produced by other configurations, such as a ring and Bunsen (set up number 2), the effect of a field should be increased for these configurations. Once the effect of a DC field has been established in the first part of this chapter the results for different set ups can be compared to experimentally prove the results of Chapter 3.

The application of a DC field was found to modify the combustion limits. This chapter also studies whether the mixture can be ignited in the extended flammability limits when a field is applied.

4.2 Experimental set up

4.2.1 Apparatus

Several configurations were adopted. These are 1, 2 and 6 from Table 2.1, Table 3.3 and Table 3.4 (see Figure 4.1). Set up number 1, was modified to minimise the aerodynamic disturbance to the normal flow pattern while maintaining the most uniform field possible. The model in Chapter 3 shows two parallel plates. However, the use of a solid plate above and below the flame would significantly alter the aerodynamics of the flame. The use of gauzes would minimise this but the field produced by the gauzes would be altered. It was considered best to use a plate below the flame with a hole cut in the centre (modelling showed that this had little effect in the field pattern) and a gauze above (where the aerodynamics are most effected by a plate).

The use of these different set ups allowed comparisons between the aerodynamic affects and the electrical affects. These can be seen below in Figure 4.1. However the most important one, as mentioned previously is number 1 as this produces the most uniform field. The electrodes are connected to the power supply (as shown in Figure 4.1) but the orientation (which electrode is positive and which is ground) is changed between the results and is indicated with the results.

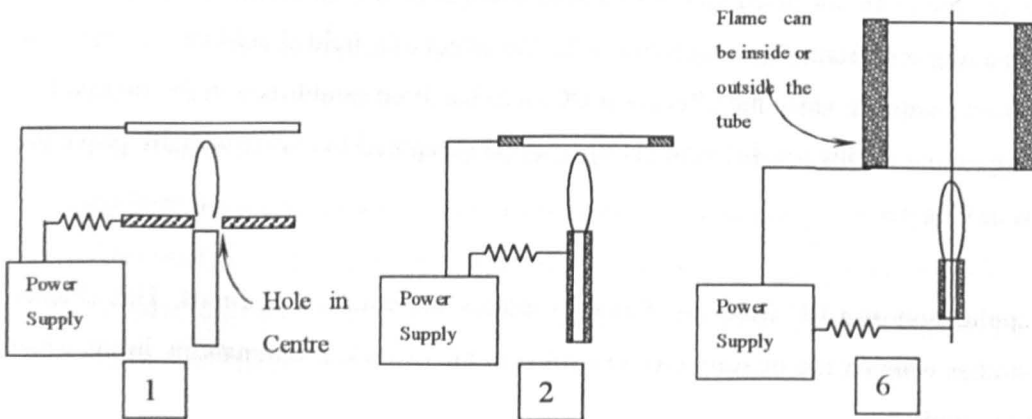


Figure 4.1 Set ups used

The flame was also subjected to a transverse field using parallel plates. This set up is similar to number 11, but the flame was not enclosed in a tube and was stabilised on a burner, shown in Figure 4.2.

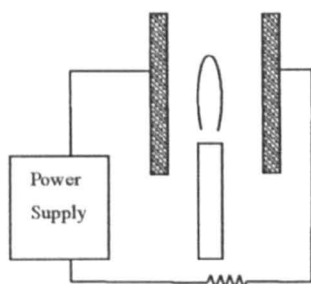


Figure 4.2 Transverse plates

The Bunsen burner body was made from perspex and the tube was made from a variety of ceramic pipes (see Figure 4.5). Metal tubes could not be used (see Chapter 3 and particularly Section 3.6 for the reasons for this). The availability of ceramic tubing is very limited, therefore the sizes and materials used could not be easily varied. The vast majority were glass but there were two tubes made from an unidentified ceramic. The wall thicknesses of all the tubes were comparable and considering the relationship of the results to the literature (see Section 4.3) it was considered that the small changes in wall thickness between different tubes did not effect the results significantly.

Each tube used was mounted into a M12 nylon bolt (Figure 4.3) which screwed into the body of the Bunsen (Figure 4.4). This allowed the tubes to be changed easily. Each tube was imbedded into the bolt by 20mm and there was 100mm protruding from the bolt. It was ensured that the tube fitted very tightly into the bolt ensuring friction would hold it in place. This tight fit, along with the seat for the tube at the base of the hole (see Figure 4.3) provided sufficient seal to stop gas leaks (tested by applying a leak detecting liquid). The bottom of the bolt was drilled out to match the internal diameter of the tube. A fibre washer was inserted between the bolt and the Bunsen body to prevent gas leaks. A picture of the assembled Bunsen can be seen below (Figure 4.5)

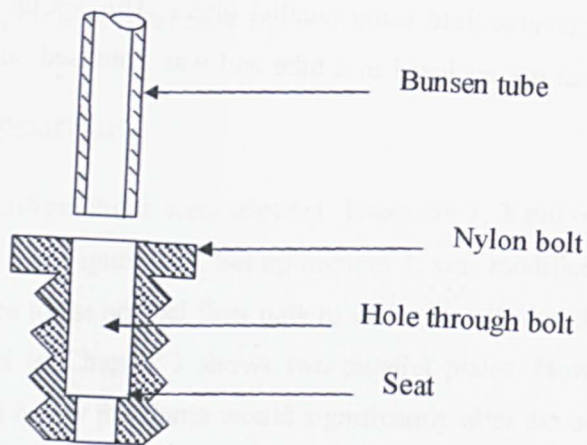


Figure 4.3 Cross section through nylon bolt

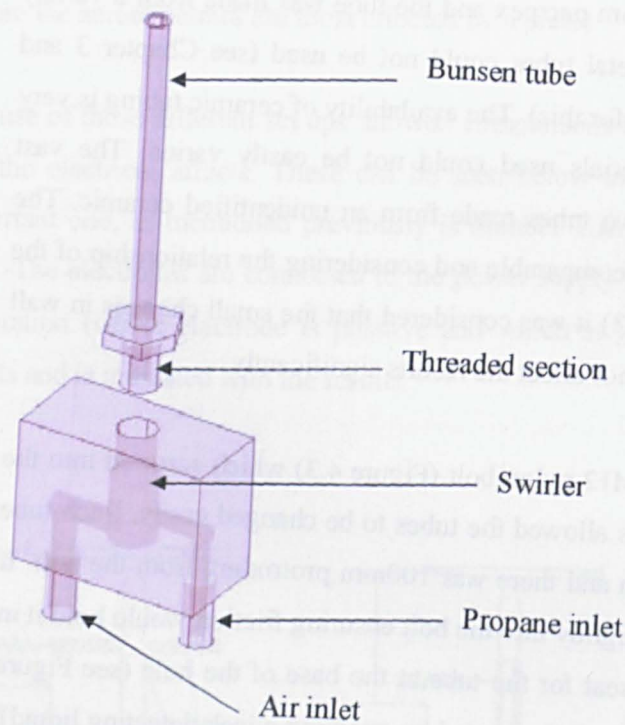
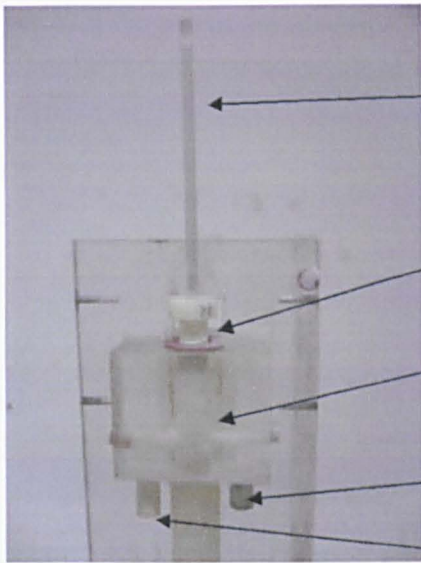


Figure 4.4 The Bunsen burner



Bunsen tube

Threaded section

Swirler

Propane inlet

Air inlet

4.2.2 Figure 4.5 Picture of the Bunsen assembled

4.2.3 Mixer

The air and fuel needed to be fully mixed at the Bunsen mouth ensuring that an even flame could be created. Partial mixing could result in an unsymmetrical flame with rich and lean pockets through its cross section. This could change the effect of the electric field through the flame. The temperature distribution will also be effected as would the burning characteristics. In a flame where modifications caused by electric fields are to be observed these fluctuations are undesirable and could distort analysis of the electric field affects. It is therefore advantageous to have full mixing of the fuel and air. This was achieved by the use of a swirler (see Figure 4.4, Figure 4.6 and Figure 4.7).

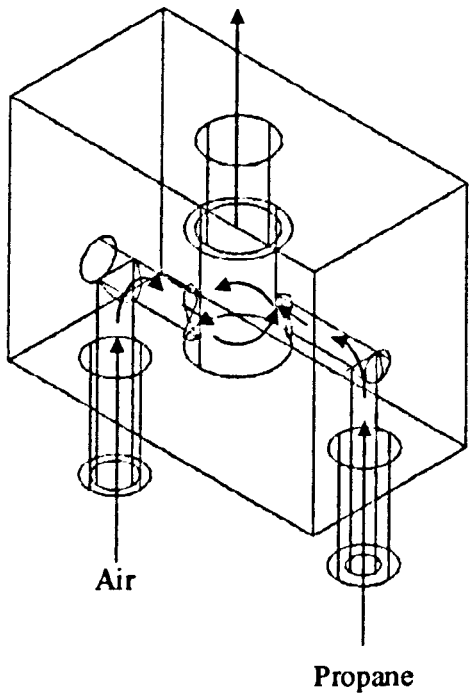


Figure 4.6 Bunsen swirler

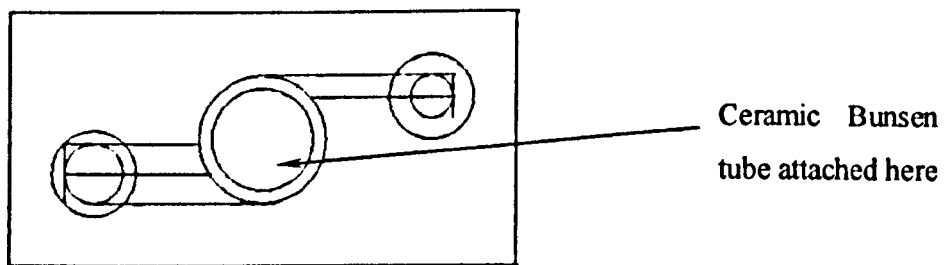


Figure 4.7 Plan view of swirler

It was considered that the swirler fully mixed the air and fuel. This could be seen when a titanium dioxide seed was applied through the air inlet (for more details of this technique see Chapter 6). Once the seed was applied a laser sheet was shone at 90° to the camera creating a 2D profile through the flame. The seed appeared evenly distributed from the Bunsen exit. The results of this can be seen in Figure 4.8. The cone shape of the flame can be seen, as well as the even seeding (white particles) inside the flame. There appear to be no clusters of the seed or areas without any seed, indicating there are no pockets of

unmixed gas. A 3D picture of the flow can be seen in Figure 4.9 which shows there is no swirl at the exit of the Bunsen.

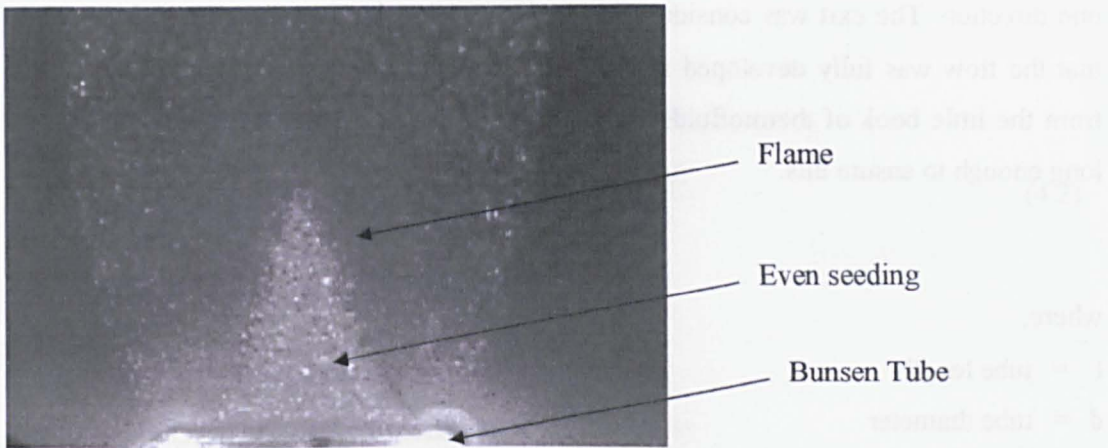


Figure 4.8 Even distribution through cross section

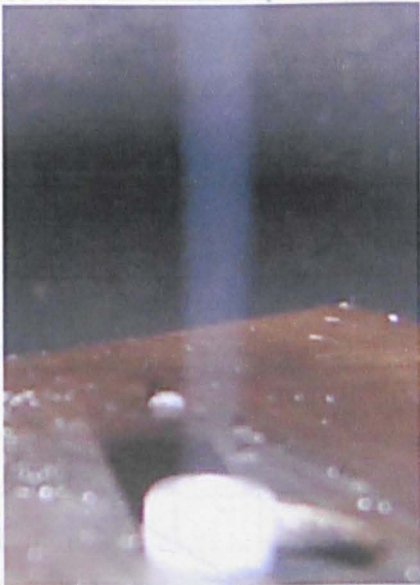


Figure 4.9 Picture of the seed from the Bunsen (not to the same scale as previous picture)

The swirler causes a large disturbance to the flow. It was important to prevent this turbulence reaching the burner mouth as the burning characteristics of a turbulent flame are different to a laminar flame. The air entrainment is different and the temperature profile will vary for different turbulence levels. Both of these effects are difficult to

quantify and it was therefore considered best to use a laminar flame where it could be ensured that the air entrainment was constant and the thermal transport of the gas was in one direction. The exit was considered to be undisturbed by the mixer by making sure that the flow was fully developed at the tube exit. The following equation (4.1), taken from the little book of thermofluids [115], was used to ensure that the pipe length was long enough to ensure this.

$$\frac{l}{d} \geq 10 \quad (4.1)$$

where,

l = tube length

d = tube diameter

This was proved to occur when particle image velocimetry was applied to the flame (see Chapter 6). This procedure calculates the velocity profile through a 2D section of a gas. As is clear from the picture below (Figure 4.10) the gas is flowing vertically upwards without any sign of turbulence. The slightly uneven velocities at the very bottom of the picture (marked Bunsen mouth) are due to distortion of the calculations by the light reflecting from the Bunsen tube.

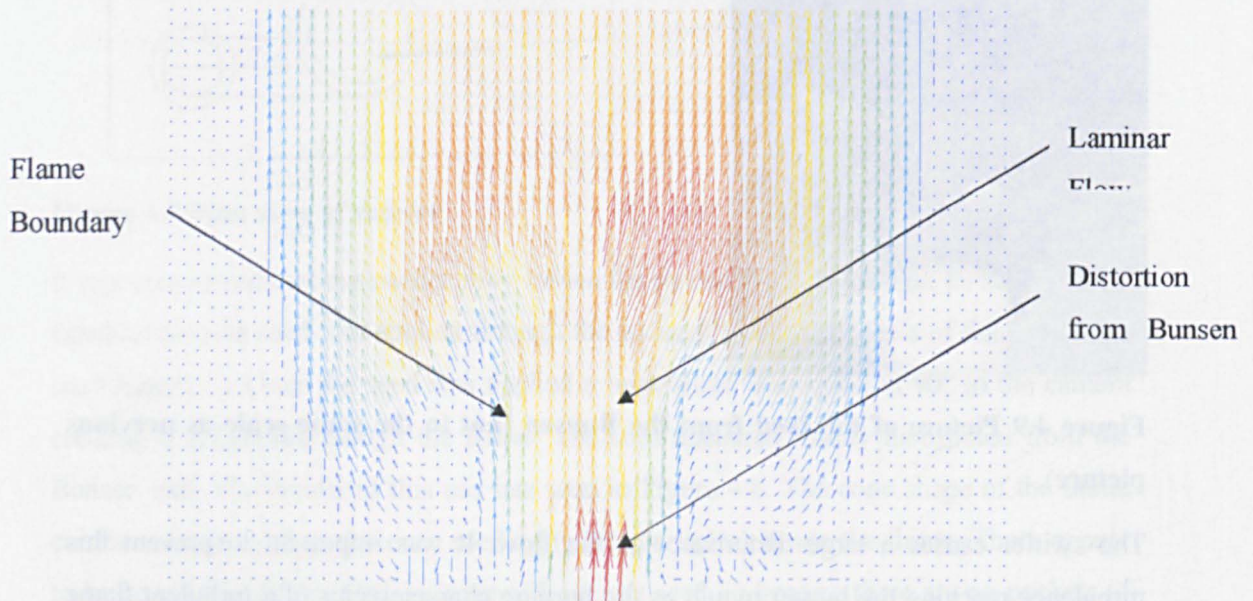


Figure 4.10 PIV image of the flame without a field applied

The flow is considered to be laminar if Reynolds number is below 2300 [116] page 41. Reynolds number can be calculated from equation (4.2).

$$\text{Reynolds number} = \frac{\rho u L}{\mu} \quad (4.2)$$

where,

ρ = Density

u = Velocity

L = Characteristic length (pipe diameter it typically used)

μ = Dynamic fluid viscosity

To give an estimate of the Reynolds numbers for the experiments conducted the values for air can be used (instead of the mixture of fuel and air). This is realistic as the majority of the gas is air with a small proportion of fuel (by mass this ranged from about 7 times more air than fuel, for rich flames, to 40 times more air than fuel, for lean flames). The density of air is 1.28Kg/m³ and the dynamic fluid viscosity is 1.73x10⁻⁵kg/ms, both from Rogers and Mayhew [114] page 16. The following data (Table 4.1) shows the maximum and minimum velocities in the results.

Characteristic length (pipe diameter) (mm)	Velocity (m/s)	Reynolds number
4.9	0.4	145
1.8	6	800

Table 4.1 Reynolds numbers for maximum and minimum settings

4.2.4 Mass flow rate

To try and eliminate thermal effects the mass flow rate was kept as constant as possible. This effect is caused due to higher mass flows absorbing greater heat energy from the flame, making extinction more difficult. It was assumed that the different heating coefficients between fuel and air were negligible due to the much higher proportion of air

to fuel. Practically this means that the velocity at the exit of the Bunsen cannot be altered by simply changing the air flow. Different Bunsen tubes were used with a variety of internal diameters to increase or decrease the velocity, while keeping the mass flow constant. The tubes were attached to the rest of the Bunsen via a screwed thread at the top of the swirler, as mentioned previously.

4.2.5 Measurement

The flow of fuel and air was controlled by a needle valve and measured by in line rotameters. The high voltage (also known as Extremely High Tension, EHT) was provided by a Glassman MK25P3 power supply. The maximum voltage of this power supply was 25kV and the maximum current was 3mA. The voltage was controlled by a remote control device (for safety) and the voltage measured using a high voltage voltmeter connected in parallel with the plates. The accuracy of the voltmeter was verified using a Testek TT-HVP15 HF 1000:1 probe, connected to a Tektronics oscilloscope. The configuration can be seen in Figure 4.11. All the equipment was enclosed in a Faraday cage for safety and to ensure that there was no electrical interference. The reasons for this and the difference to the field without a Faraday cage have been explained in Section 3.2.3.

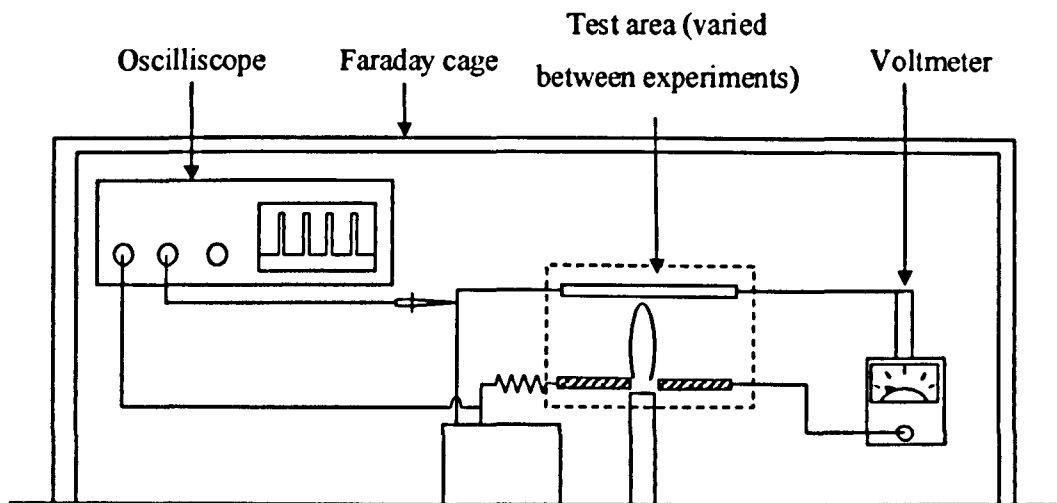


Figure 4.11 Experimental set up

4.2.6 Procedure

The procedure was conducted as follows:

1. Set the air and fuel flow rates
2. Light the Bunsen burner
3. Slowly reduce the fuel flow until extinction
4. Ensure that the final mass flow rate is within 10% of the desired value (10mg/s or 20mg/s)
5. If the flow rate is not within 10% of the desired value then repeat from stage 1 with different air flow
6. Repeat with 5kV and then with 10kV applied voltage

Ignition Tests

7. Once an acceptable reading was taken (within the mass flow constraints), it was attempted to reignite the gas/air mixture with a flame ignition source
8. If no ignition was possible then the fuel flow was increased until ignition could be achieved

In reality it can be very difficult to observe the blow off point of the flame (when it was extinguished) and read the scale on the rotameter at the point where extinction occurs. The final results presented below are the result of several attempts. This set of data was considered to be the most reliable as two people took the results. One person watched the rotameters and decreased the flow rate of fuel with the needle valve. The other watched the flame and indicated when it was extinguished to the person reading the rotameter. This enabled an accurate reading to be taken on the rotameter. The needle valve was turned down very gradually at this point to make the reading as accurate as possible. Three readings were taken at each point and the average plotted on the graphs in the following section.

4.3 Results of applying a DC field

The results without any field need to be presented first, as the blow off trend can then be compared. These results can be seen below in Figure 4.12. The diagram in the top right corner of the graph indicates the experimental set up used and the polarity of the electrodes.

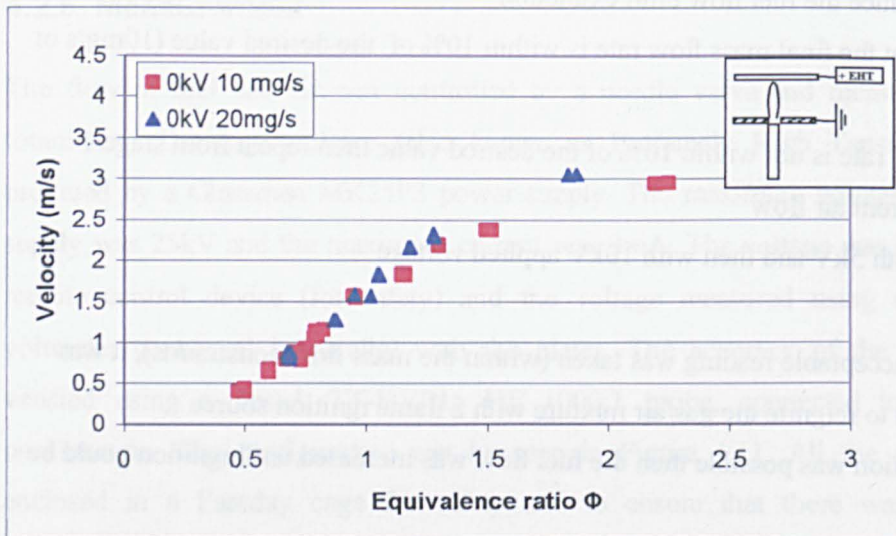


Figure 4.12 Blow off velocity against equivalence ratio for no applied voltage

On the graph above the results have been separated by mass flow rate; 10mg/s is represented by red squares and 20mg/s by dark blue triangles.

Figure 4.12 shows that the results for 10mg/s and 20 mg/s appear to follow the same trend. A logarithmic fit seems to produce the best trend line based on both 10 and 20mg/s. This can be seen in Figure 4.13. The equation of the best fit line is;

$$y = 1.9972\ln(x) + 1.6498.$$

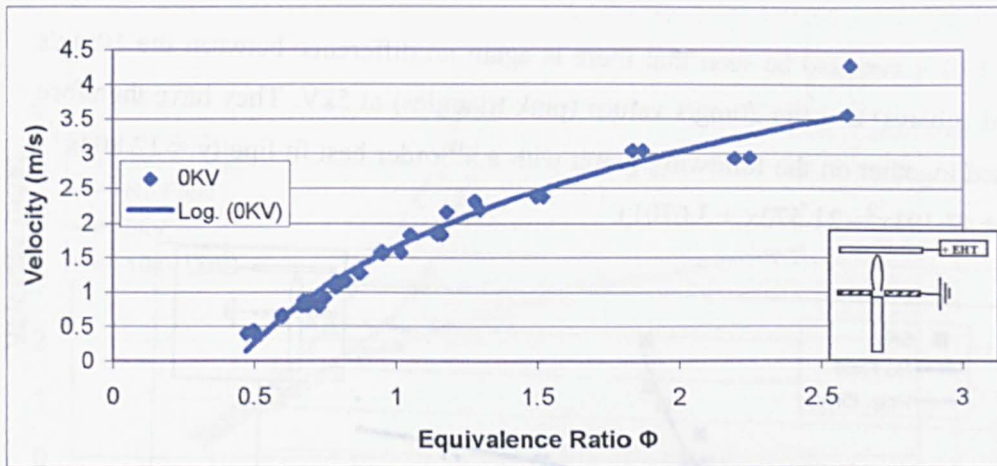


Figure 4.13 Best fit trend line for all mass flowrates

The results do follow the literature for no field (see Griffiths and Barnard [90]). The comparison to the literature and further discussion can be found in Section 4.7.

In the following graph (Figure 4.14) these results have been extended by the application of 5kV potential to the electrodes (60mm apart). The no field values have been plotted as small dots along with the trend line.

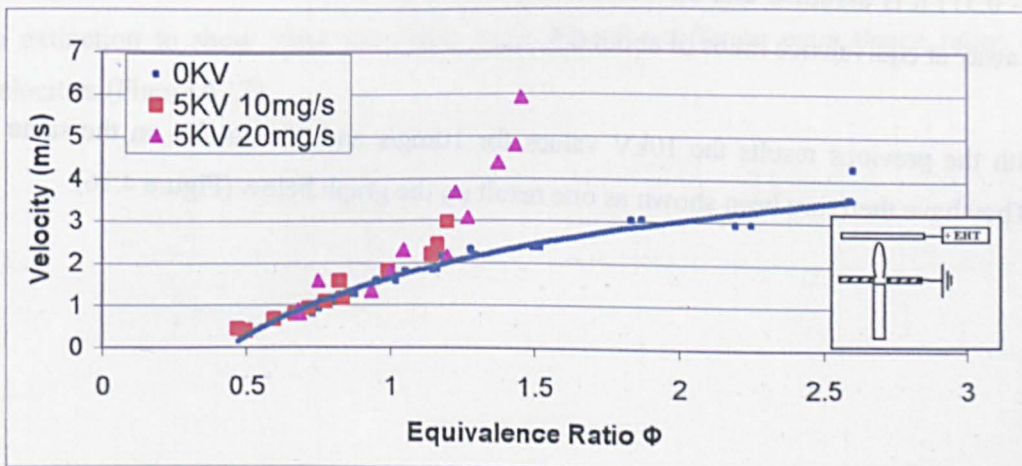


Figure 4.14 The effect of an electric field

The 5kV electric field shows a large increase in the blow off velocity with rich flames, compared to the blow off velocity with no field. There does not seem to be a discernable difference for very lean flames.

In Figure 4.14 it can also be seen that there is again no difference between the 10mg/s values (red squares) and the 20mg/s values (pink triangles) at 5kV. They have therefore been plotted together on the following graph with a 4th order best fit line ($y = 12.804x^4 - 40.247x^3 + 47.191x^2 - 21.572x + 3.6701$).

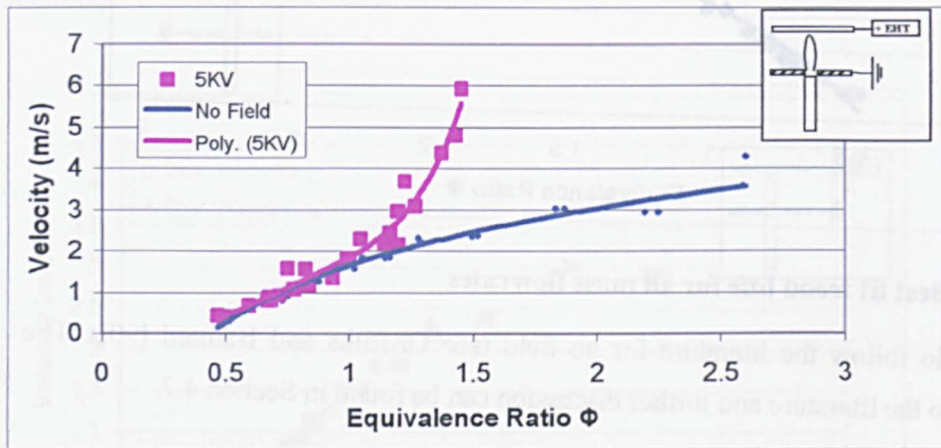


Figure 4.15 Best fit for 5kV applied voltage

This best fit line provides a good fit at higher equivalence ratios but for very lean flames (0.49 - 0.51) it is assumed that the line follows the no field values, rather than begin to curve away at equivalence ratios of about 0.5.

As with the previous results the 10kV values for 10mg/s and 20mg/s fall on the same line. They have therefore been shown as one result on the graph below (Figure 4.16).

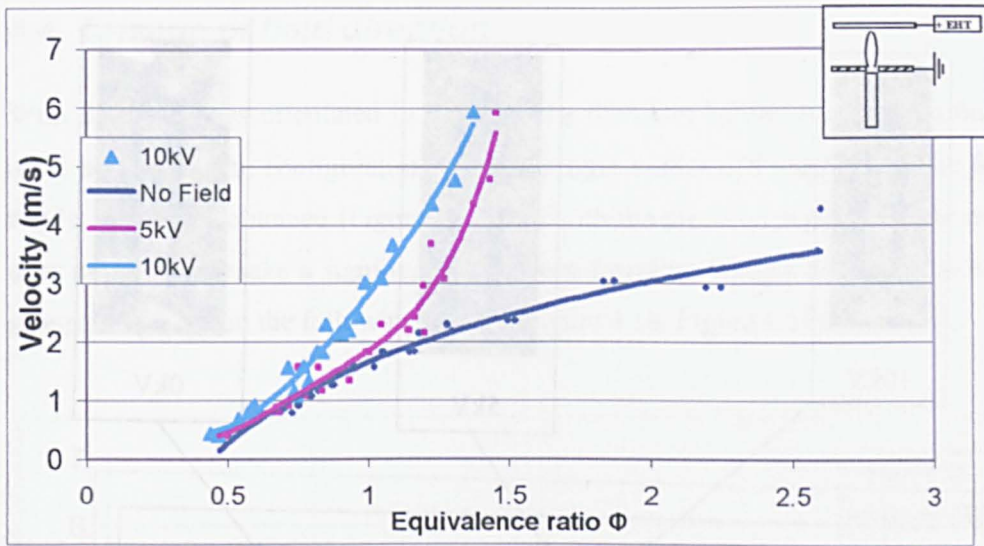


Figure 4.16 10kV best fit included

The results for 10kV show an even greater increase in the blow off velocity than the 5kV applied field. It also shows an increase in blow off velocities for lean flames as well as for rich flames, although the rich improvement is still much greater.

A diagram of the blow off velocities can be seen below, along with pictures taken at close to extinction to show what the flame looks like for different equivalence ratios and velocities (Figure 4.17).



Figure 4.17 Best fit with factors of velocity relative to blow off velocity

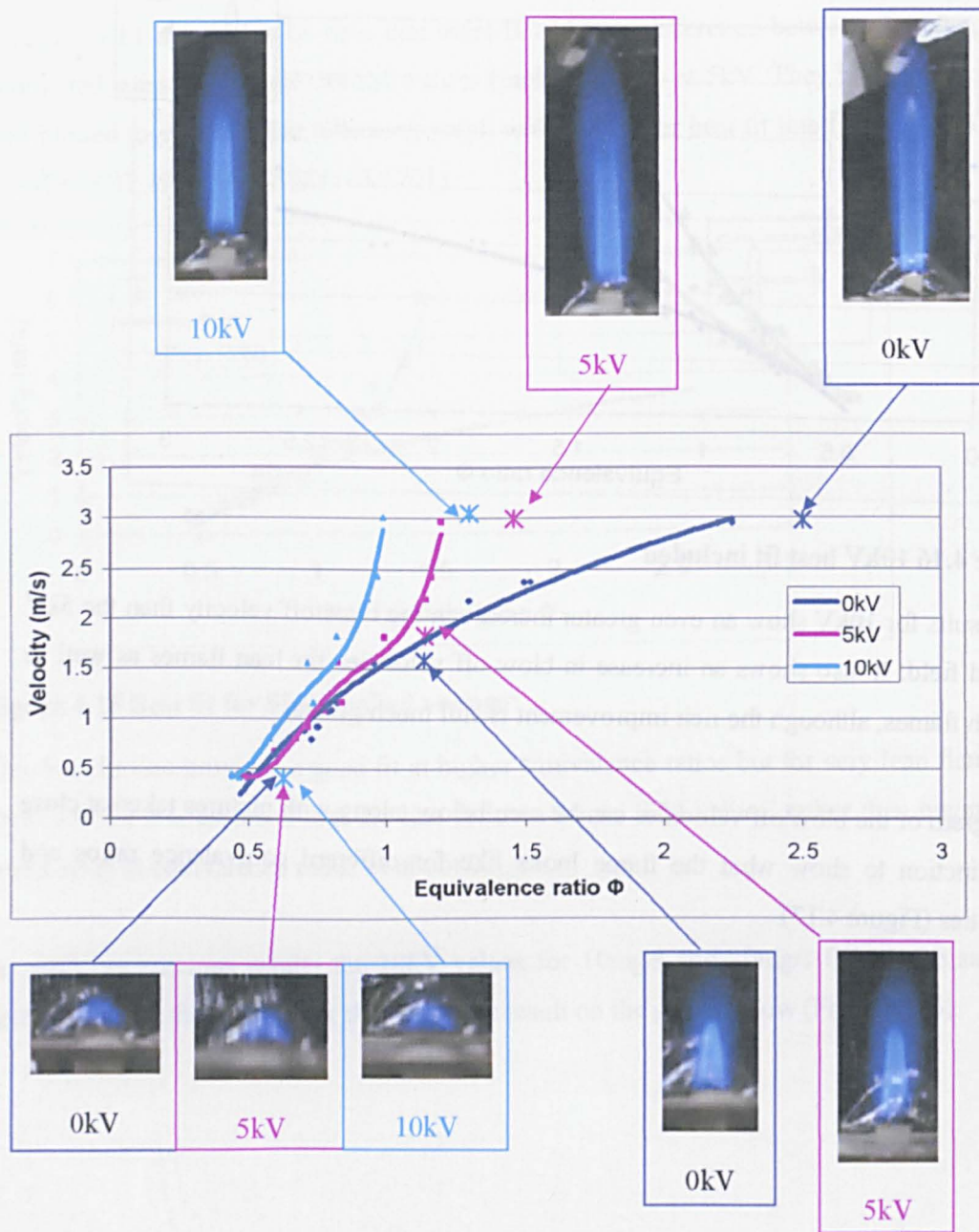


Figure 4.17 Best fit with photos at various velocities and equivalence ratios

4.4 Change of field direction

With the electrodes orientated in the opposite direction (positive below the burner and earth above, see the configuration in the top right corner of Figure 4.18), the following results have been obtained (Figure 4.18). As with the previous experiment the mass flow does not seem to make a significant difference therefore 10mg/s and 20 mg/s have been grouped together on the following graphs (Figure 4.18, Figure 4.19).

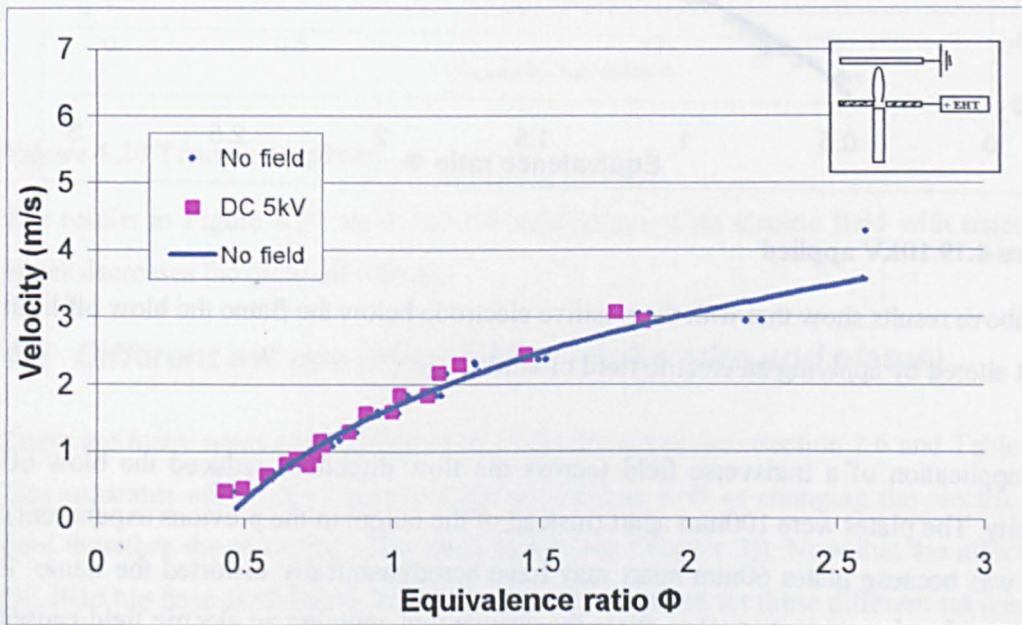


Figure 4.18 5kV applied voltage

The results for 5kV do not show a significant difference on the no field blow off velocity.

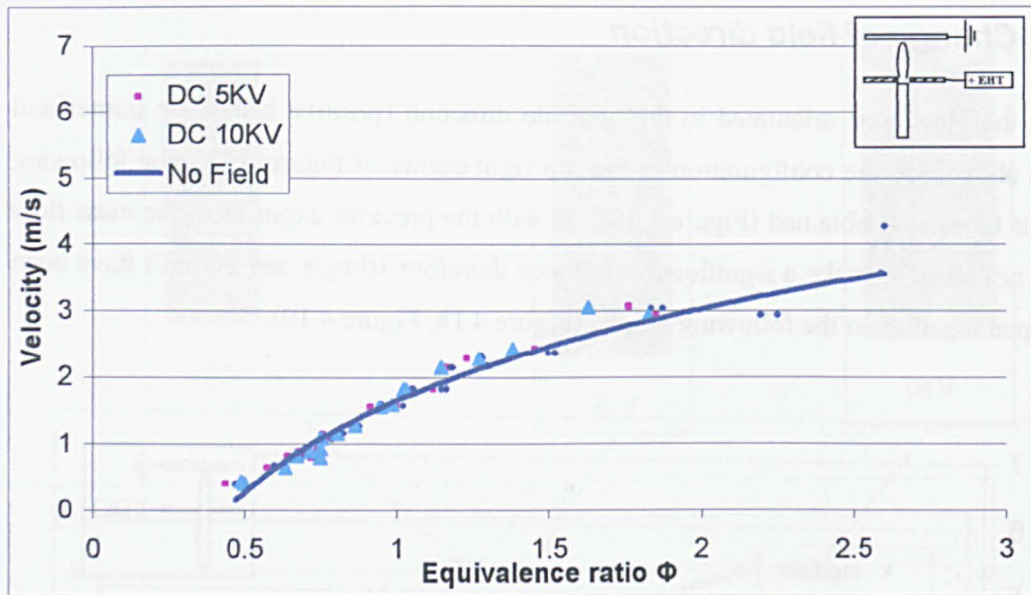


Figure 4.19 10kV applied

The above results show that with the positive electrode below the flame the blow off limit is not altered by applying an electric field of 10kV.

The application of a transverse field (across the flow direction) reduced the blow off velocity. The plates were 100mm apart (instead of the 60mm in the previous experiment). This was because plates 60mm apart may have aerodynamically distorted the flame. It was considered more important to show the change that applying an electric field caused rather than ensure that exactly the same field strength was applied. It was therefore necessary to apply larger voltages to achieve similar field strengths.

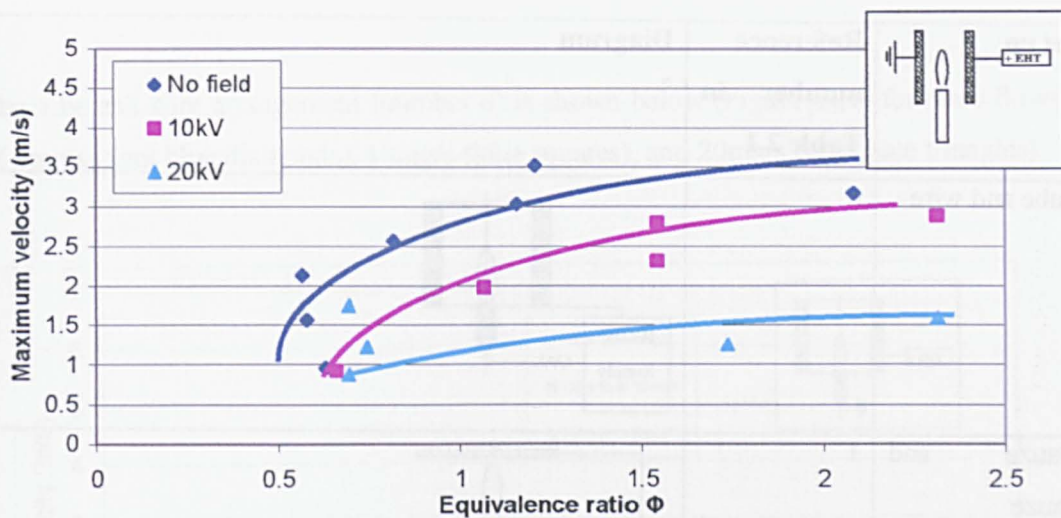


Figure 4.20 Transverse plates

The results in Figure 4.20 show that the application of an electric field with transverse plates decreases the blow off velocity.

4.5 Different set ups (ring Bunsen, tube wire and plates)

There are many types of apparatus used in the literature (see Section 2.6 and Table 2.1). The apparatus effects the flame aerodynamically as well as changing the electric field (and therefore the electrical affect on a flame (see Chapter 3)). Now that the affect of a DC field has been established, the results can be compared for these different set ups.

The apparatus was set up with the electrodes 60mm apart (except for the tube and wire; where the tube was 60mm diameter, giving a 30mm separation but half of the voltage was applied this was due to practicalities of the available space). The set ups measured were;

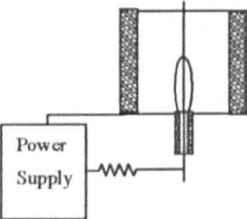
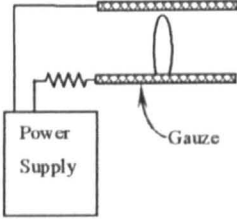
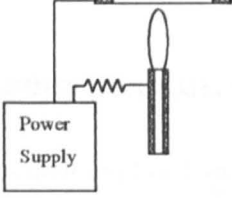
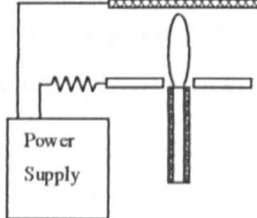
Set up	Reference number in Table 2.1	Diagram
Tube and wire	6	
Gauze and gauze	1	
Ring and Bunsen	2	
Gauze and plate		

Table 4.2 Apparatus used

The procedure was the same as that described in Section 4.2.

4.5.1 Aerodynamic effect

When no field is applied the changes due to the apparatus can be seen. The results have been included individually for each apparatus.

The tube and wire arrangement (number 6) is shown below (Figure 4.21) for mass flows of 5mg/s (dark blue diamonds), 10mg/s (blue squares), and 20mg/s (light blue triangles).

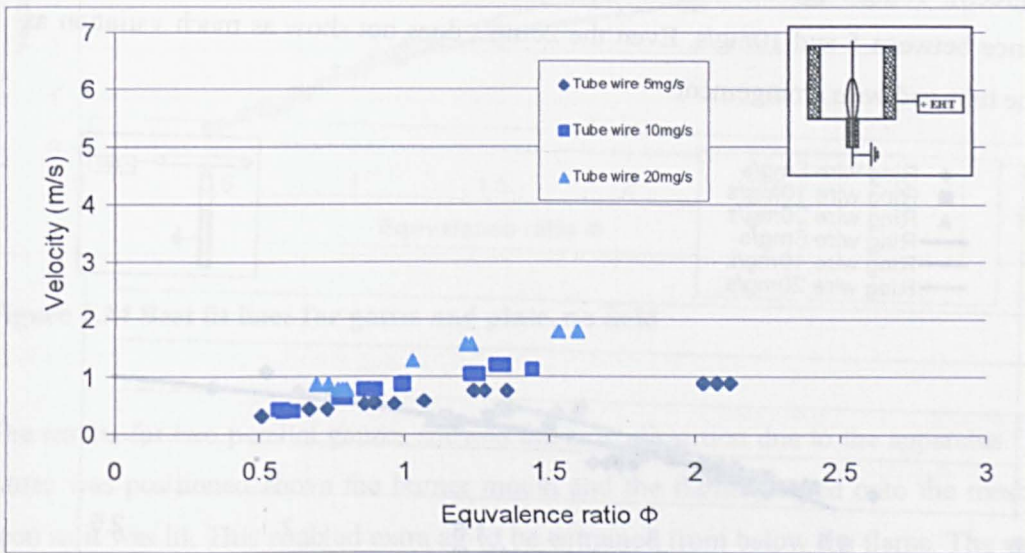


Figure 4.21 Tube and wire no field

The results show that the mass flow does make a difference for this experimental set up. Logarithmic best fit lines have been applied below.

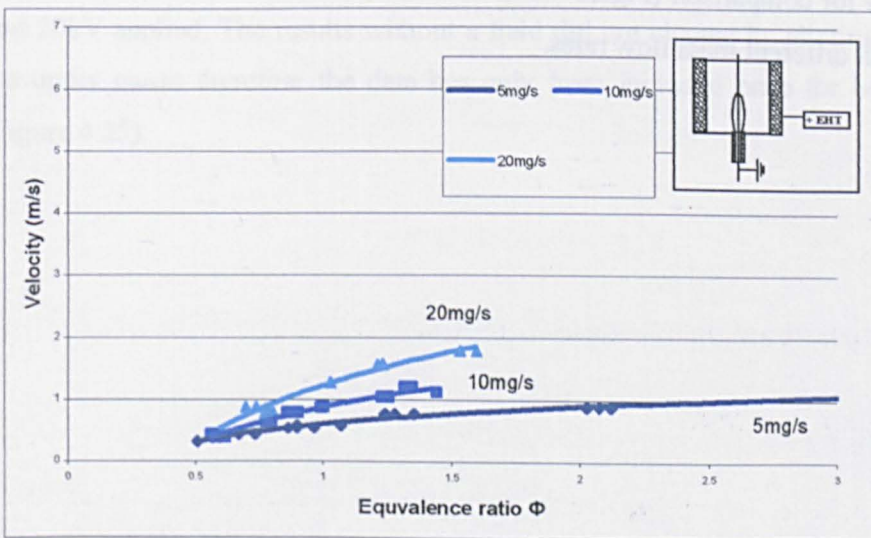


Figure 4.22 Best fit lines for tube and wire, no field

The results show that there is a strong dependence on mass flow rate for this arrangement.

The ring and Bunsen arrangement (number 2) is shown below (Figure 4.23) for 5mg/s (dark green), 10mg/s (green) and 20mg/s (light green). There seems to be very little difference between 5 and 10mg/s. Even the 20mg/s does not show as much variation as with the tube and wire arrangement.

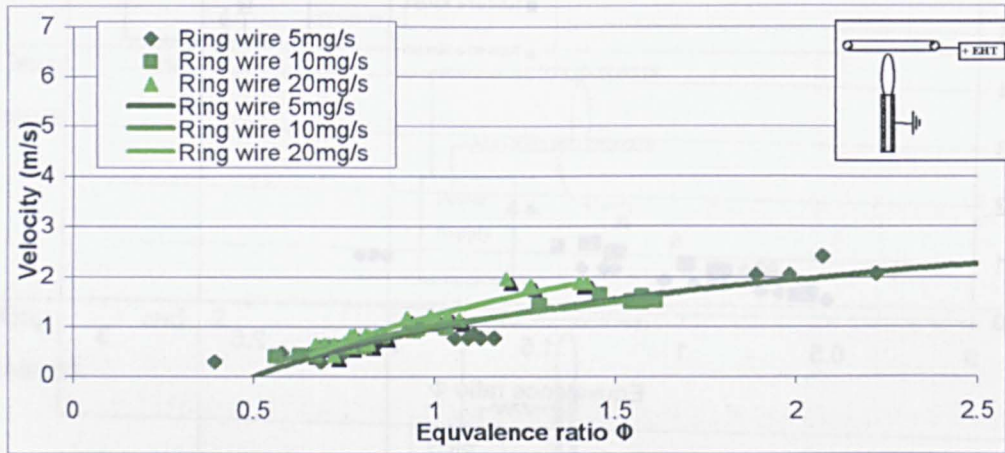


Figure 4.23 Best fit lines for ring and Bunsen, no field

The results for a gauze and plate have already been presented (Section 4.3 and 4.4). They are presented here for comparison (Figure 4.24). As already mentioned the results do not seem to differ with different mass flow rates.

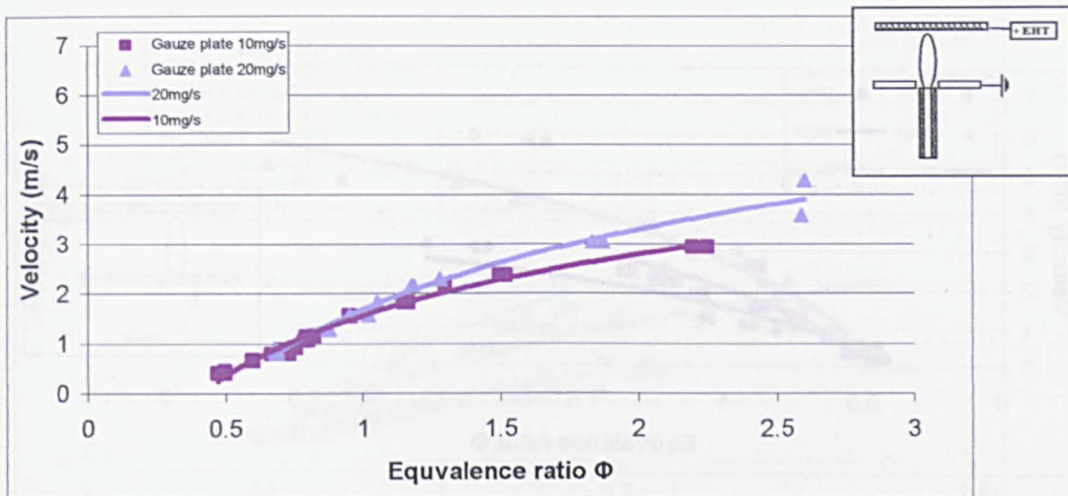


Figure 4.24 Best fit lines for gauze and plate, no field

The results for two parallel gauzes showed the most distortion due to the apparatus. The gauze was positioned above the burner mouth and the flame jumped onto the mesh as soon as it was lit. This enabled extra air to be entrained from below the flame. The mesh also slowed the flow down and spread it out, enabling faster flow rates to be sustained. While this was interesting experimentally, it does not provide a practical way to stabilize flames for industrial burners as the gauze is burnt away by the flame. Later experiments show results for a 60mm gap with 5 and 10 kV applied as well as a 120mm Gap with 10 and 20kV applied. The results without a field did not change by altering the position of the upper gauze therefore the data has only been included once for both experiments (Figure 4.25).

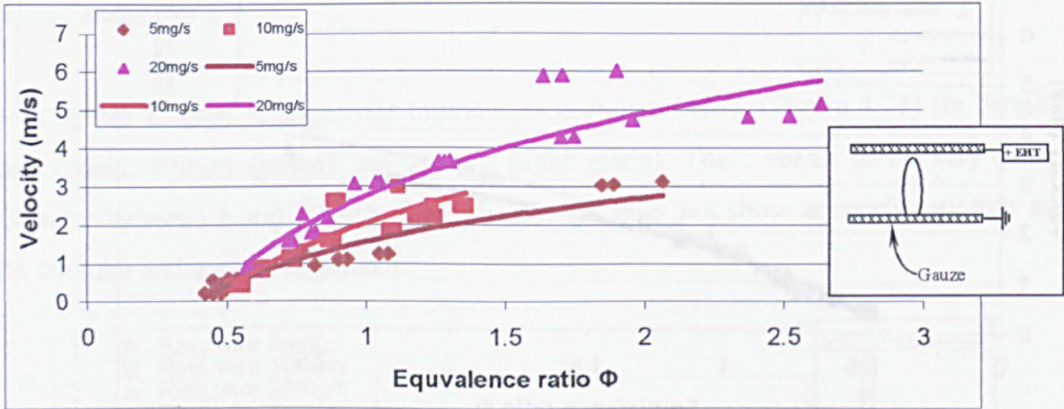


Figure 4.25 Best fit for parallel gauze, no field

The graph below compares the results for all the experiments at 5mg/s. The plate and gauze results are not included as they were not conducted at 5mg/s due to the limitations of the rotameter.

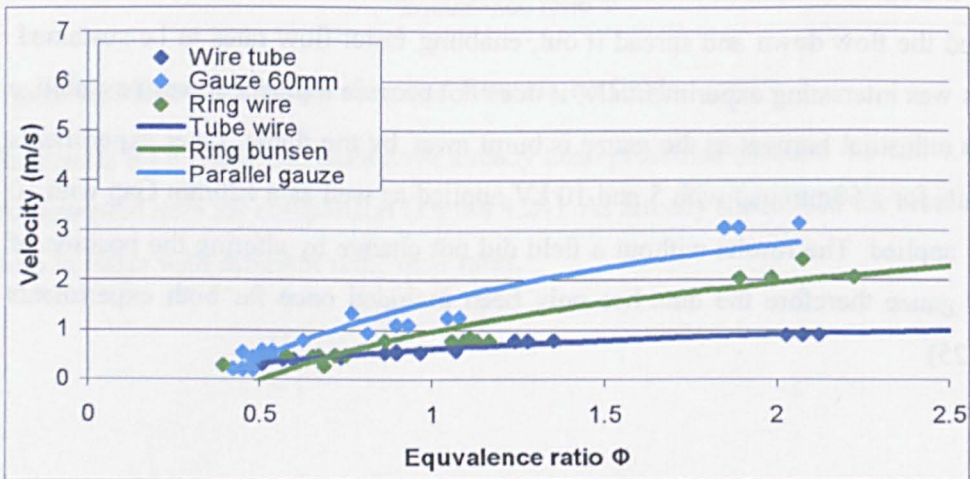


Figure 4.26 Comparison of the results at 5mg/s

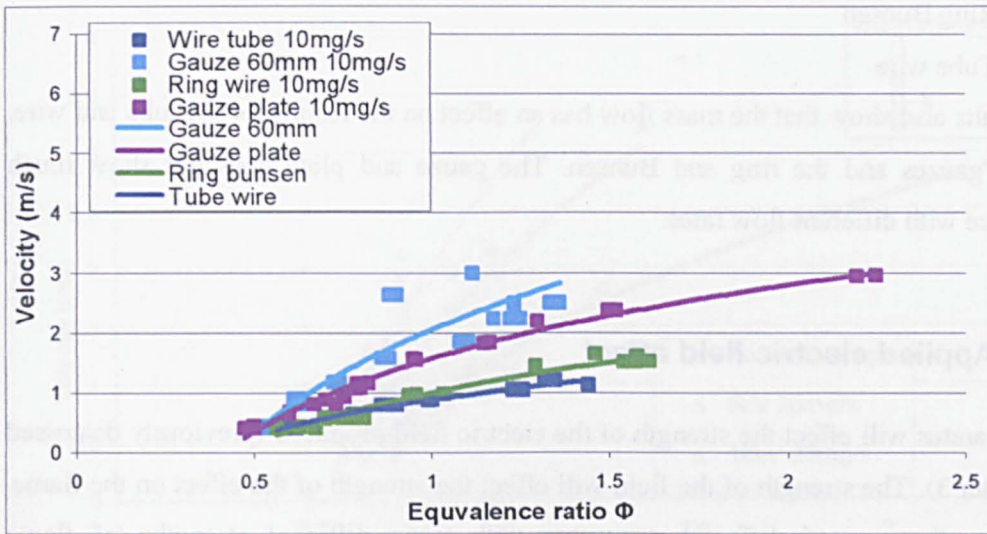


Figure 4.27 Comparison of the results at 10mg/s

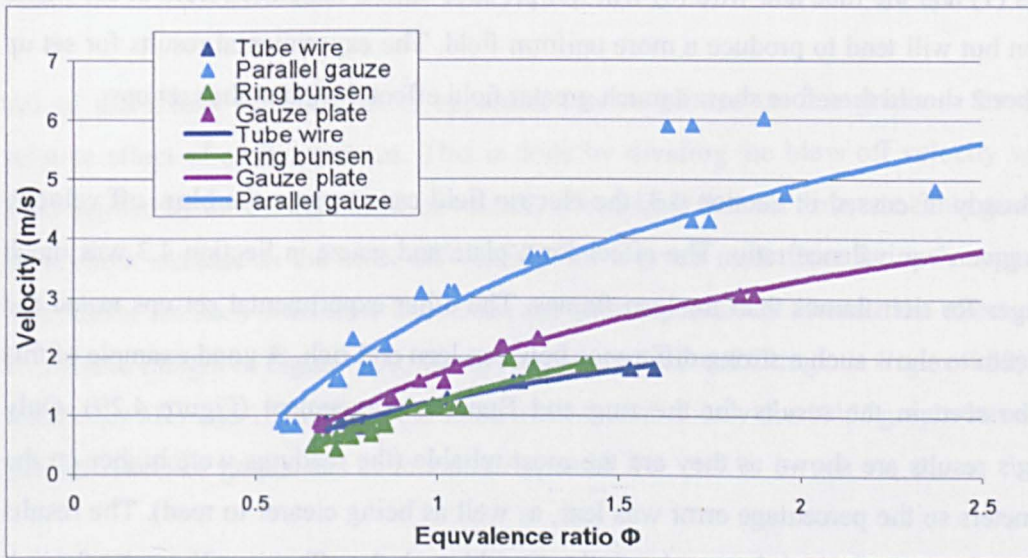


Figure 4.28 Comparison of the results at 20mg/s

All the results show the same trend. From highest to lowest blow off the results are in the order of;

1. Parallel gauze
2. Gauze plate

3. Ring Bunsen

4. Tube wire

The results also show that the mass flow has an effect on the results for the tube and wire, parallel gauzes and the ring and Bunsen. The gauze and plate does not show much difference with different flow rates.

4.5.2 Applied electric field effect

The apparatus will effect the strength of the electric field produced (previously discussed in Chapter 3). The strength of the field will effect the strength of the effect on the flame. Therefore the use of different apparatus will cause different strengths of flame modification. The strongest fields will be applied in the area surrounding the flame by the apparatus arrangements such as the ring and Bunsen (2). Whereas setups such as parallel plates (1) and the tube and wire (6) will not produce such a magnified field in the flame region but will tend to produce a more uniform field. The experimental results for set up number 2 should therefore show a much greater field effect then the other set ups.

As already discussed in Section 4.3, the electric field can increase the blow off velocity for a given equivalence ratio. The effect for a plate and gauze in Section 4.3 was much stronger for rich flames than for lean flames. The other experimental set ups tested did not seem to show such a strong difference between lean and rich. A good example of this can be seen in the results for the ring and Bunsen arrangement (Figure 4.29). Only 20mg/s results are shown as they are the most reliable (the readings were higher on the rotameters so the percentage error was less, as well as being clearer to read). The results show an increase for both lean and rich flames (although the effect is still greater for rich than lean).

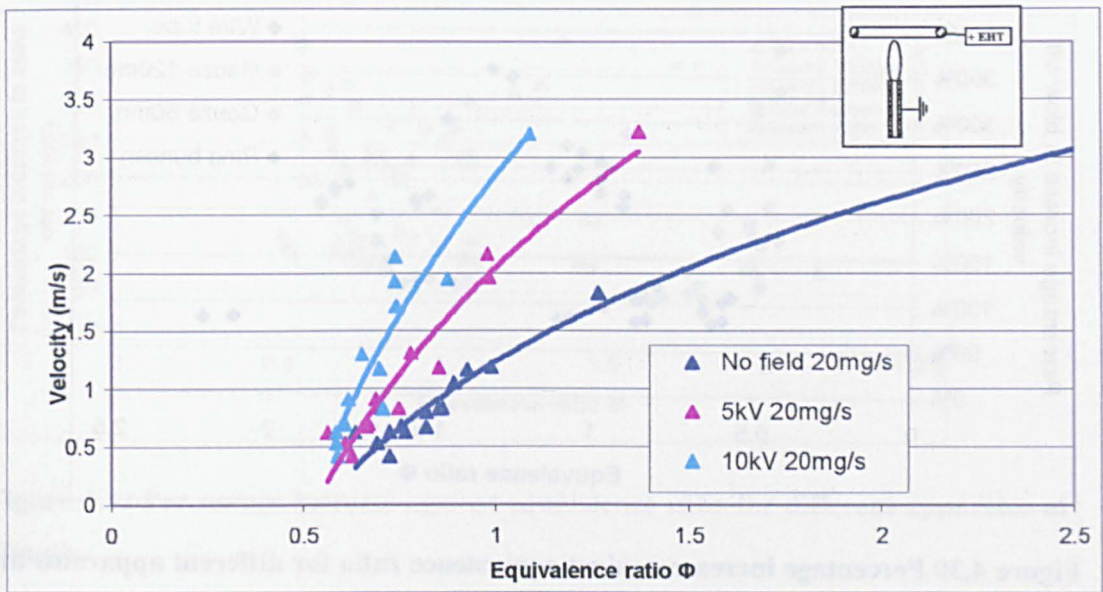


Figure 4.29 Ring and Bunsen, 20mg/s, effect of applied field

All of the results for each set of apparatus can be plotted on one graph to show the relative effect of each apparatus. This is done by dividing the blow off velocity with a field applied by the no field blow off velocity (trend line) for that flow rate. This gives the percentage increase in the blow off velocity for a given mass flow for each apparatus. The results for each mass flow have been shown independently to make the effect easier to observe (5mg/s in Figure 4.30, 10mg/s in Figure 4.31 and 20mg/s in Figure 4.32). The results for 5Kv and 10kV show the same trend therefore only the 10kV graphs have been plotted. The 5kV graphs can be found in Appendix 2.

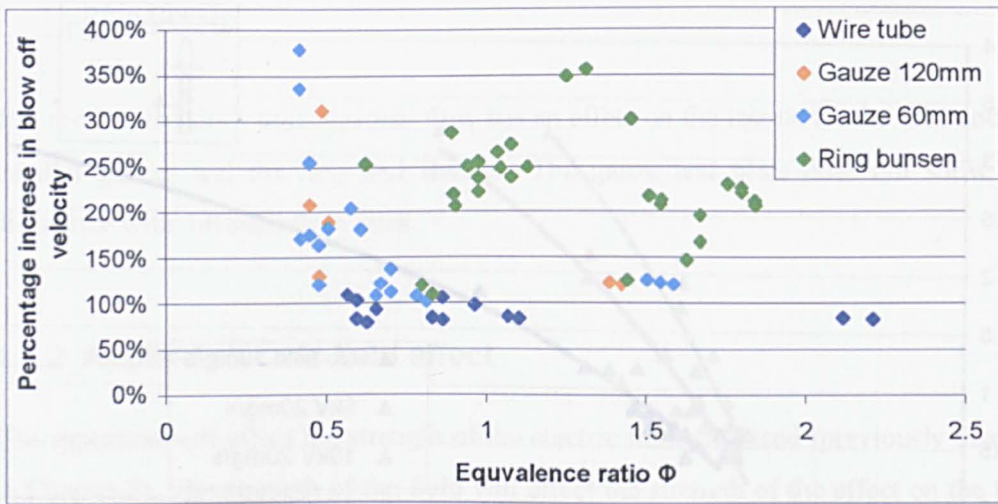


Figure 4.30 Percentage increase against equivalence ratio for different apparatus at 5mg/s

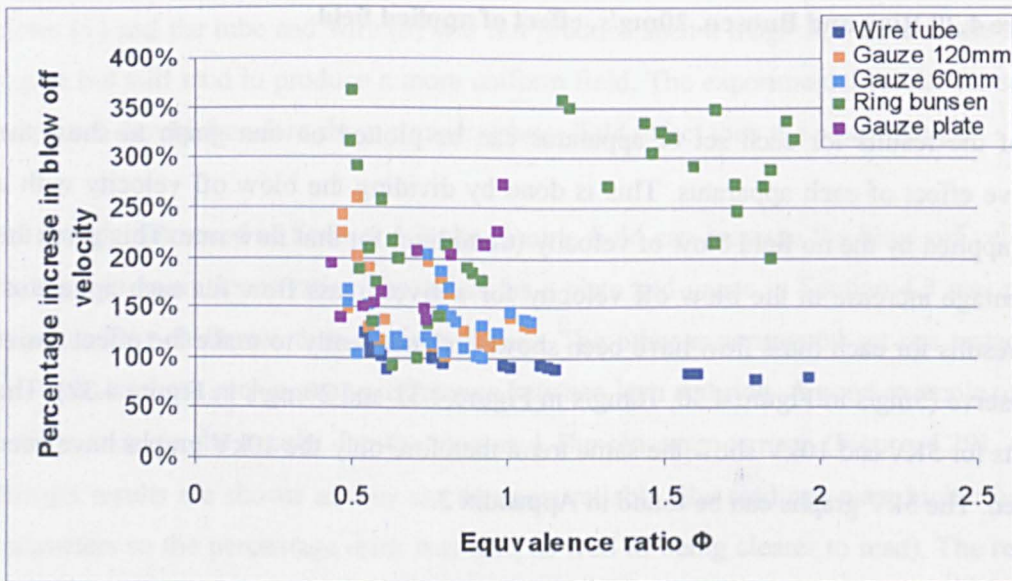


Figure 4.31 percentage increase against equivalence ratio for different apparatus at 10mg/s

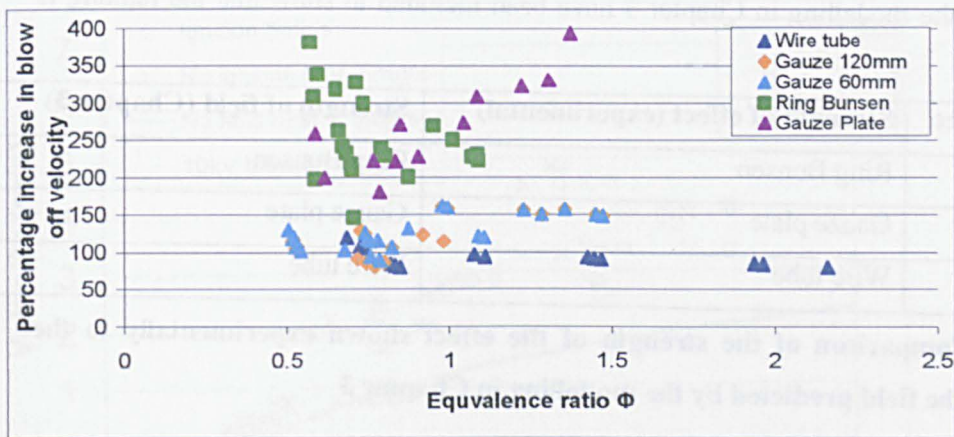


Figure 4.32 Percentage increase against equivalence ratio for different apparatus at 20mg/s

With no field applied the parallel gauzes produced the greatest increase in the blow off velocity of the gases. However, when a field is applied the field distortion mixed with the aerodynamic disturbance does not produce such a large increase in the blow off velocity of the flame (see Figure 4.30-Figure 4.32). As previously mentioned, when the field was applied to the gauzes it caused the flame to jump above the upper gauze or split into smaller flames on the lower gauze. The results do, however, show that there is negligible modification to the blow off limit when twice the field is applied over double the distance for a uniform field. This is consistent with the literature [105].

Figure 4.30-Figure 4.32 all show that the gauze and plate produces a diagonal line with a positive gradient. This is due to the increase in blow off velocity being greater for rich flames than for lean as previously mentioned. Similar trends (greater increase for rich flames than for lean) can also be seen for the other experimental set ups but they are not as pronounced.

The difference of greatest interest is that the effect on the blow off limit is different for different electrode geometries, even though the same potential is applied and the distance between them is the same (except for the 120mm gauze, as previously discussed). The results have been ranked below in Table 4.3. Also the results of the field strength

predicted by the modelling in Chapter 3 have been included to show that the ranking is the same.

Rank of effect	Strength of effect (experimental)	Strength of field (Chapter 3)
1	Ring Bunsen	Ring Bunsen
2	Gauze plate	Gauze plate
4	Wire tube	Wire tube

Table 4.3 Comparison of the strength of the effect shown experimentally to the strength of the field predicted by the modelling in Chapter 3

The results show how strong the effect of changing the apparatus (and therefore the field produced) is on the blow off limits of a flame. It also indicates that the modelling is good enough for comparisons between results. However, further work needs to be done to validate the models by measuring the field strengths produced experimentally. This is further discussed in section 7.1.

4.6 Ignition tests

The final test was to try and reignite the fuel and air mixture beyond the normal blow off limits using the electric field (using the procedure described in Section 4.2.6). A flame ignition source was used. Spark igniters were considered but they require metal electrodes in the unburnt gas region. This region is directly next to the high voltage plates and would cause breakdown and make it impossible to produce a field.

On the graphs below (Figure 4.33Figure 4.35) the blue circle corresponds to an ignition and a red cross corresponds to a non ignition. Only the two closest points have been shown. The best fit lines from the previous section have been added to show how it corresponds to the blow off points with and without a field. Each graph is separated by mass flow. Only the ring and Bunsen results have been shown as they are typical of all the apparatus. The same trend is found for 5kV and 10kV so only the 10kV results have been shown (the 5kV results can be found in Appendix 2).

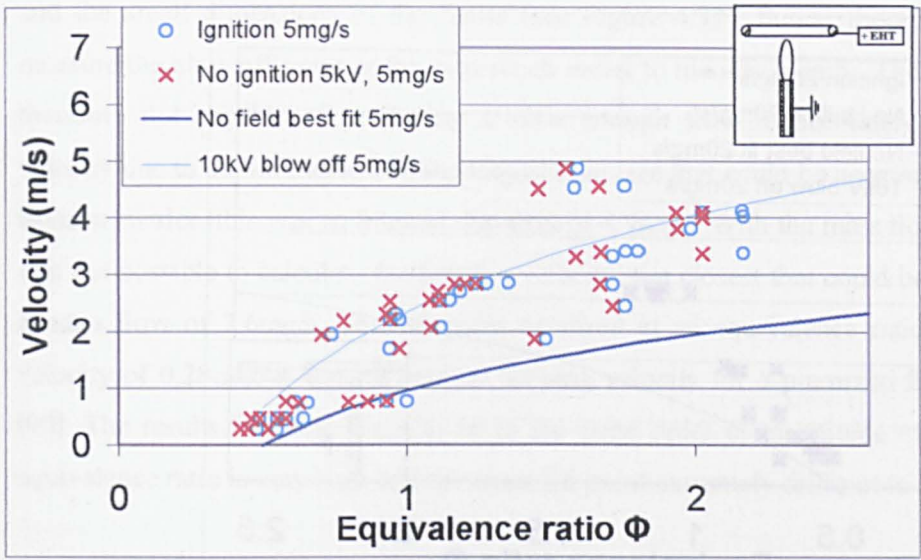


Figure 4.33 Ignition points for 10kV, 5mg/s

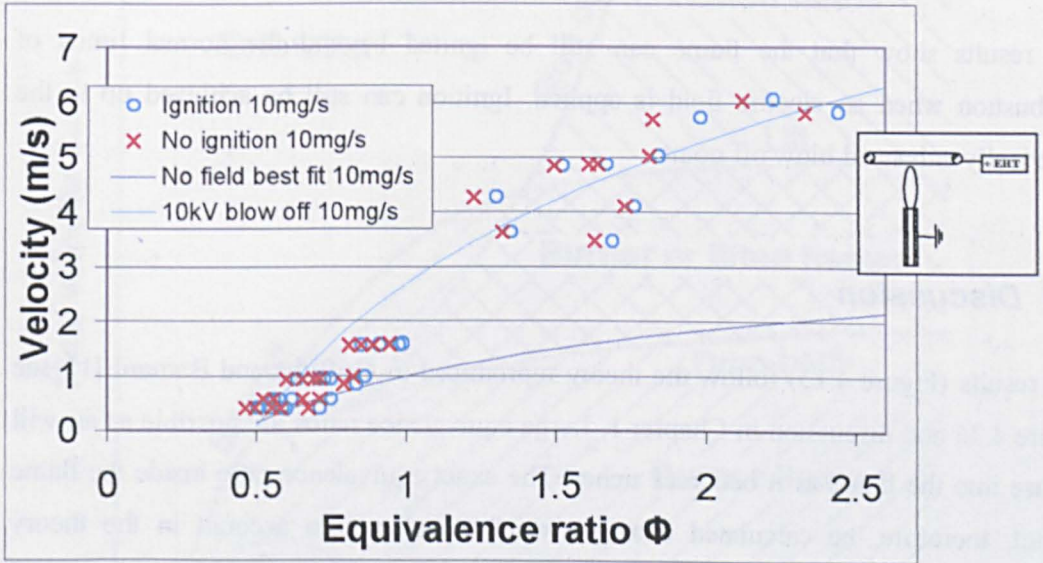


Figure 4.34 Ignition points 10kV, 10mg/s

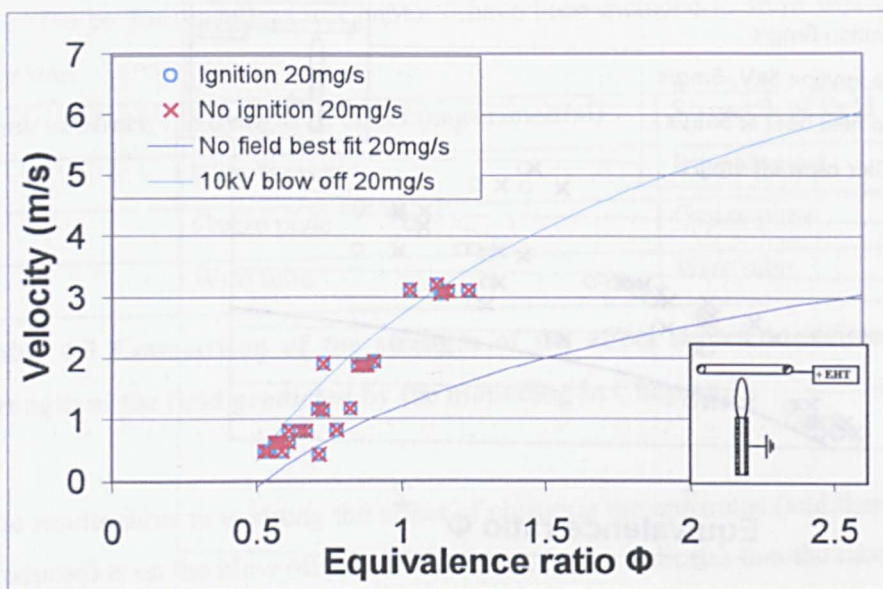


Figure 4.35 Ignition points for 10kV, 20mg/s

The results show that the flame can still be ignited beyond the normal limits of combustion when an electric field is applied. Ignition can still be achieved up to the electrically enhanced blow off point.

4.7 Discussion

The results (Figure 4.13) follow the theory reproduced in Griffiths and Barnard [1], see Figure 4.36 and discussion in Chapter 1. Large equivalence ratios are possible as air will diffuse into the flame as it becomes richer. The exact equivalence ratio inside the flame cannot, therefore, be calculated exactly (which is taken into account in the theory reproduced in Griffiths and Barnard). The values plotted are the equivalence ratios at the burner mouth (ie the air and fuel put through the Bunsen). The results plotted in this report should therefore look the same as the results from Griffiths and Barnard [1], even though the x axis is labelled differently. They also report that the flame will blow off from a lifted flame following a similar trend to the lifted flame line shown below. The lift point of the flame was very difficult to accurately establish due to the small lift height

and the small dimensions of the flame (see Figure 4.37). It was therefore decided to measure the blow off point as this was much easier to identify clearly. The apparatus was therefore not capable of producing a slow enough flow to accurately show the lift velocity due to the limitations on the largest tube size that could be accommodated by the Bunsen swirler (this was an internal diameter of 4.9mm). With the mass flow of 10mg/s it was not possible to calculate the burning velocity; the closest that could be achieved was a mass flow of 7.6mg/s. The lift point occurred at an equivalence ratio of 9.5 and a velocity of 0.28m/s. A typical laminar burning velocity for a premixed flame is 0.4m/s [90]. The results therefore seem to be in the same order of magnitude even though the equivalence ratio is very high and the exact lift point extremely difficult to identify.

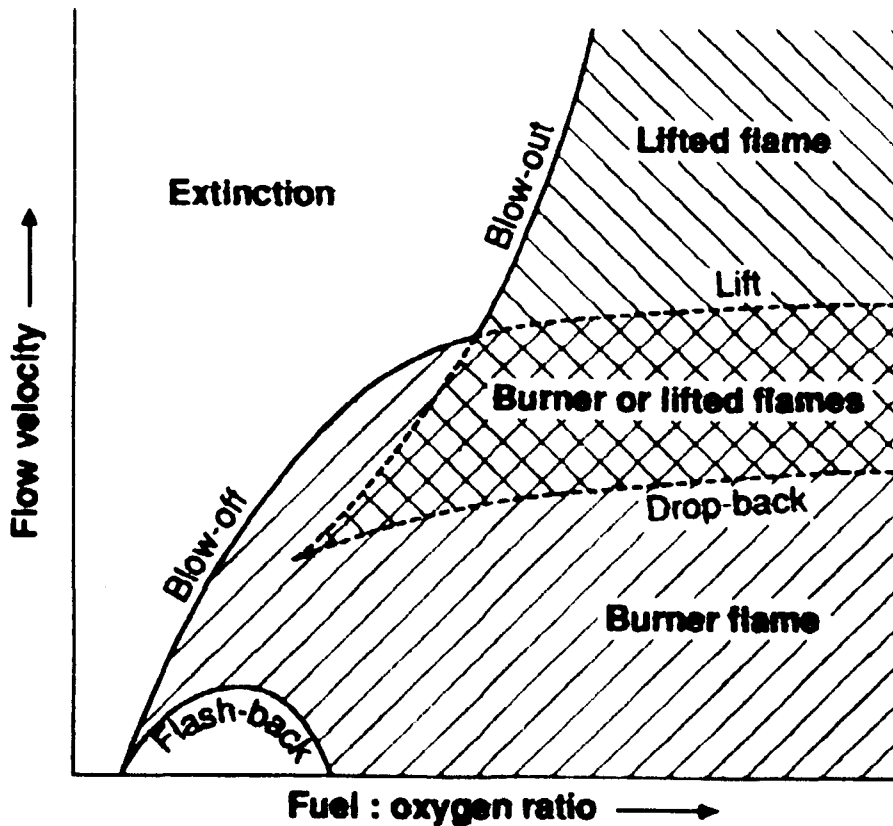


Figure 4.36 Taken from Griffiths and Barnard [1]

The same procedure conducted in the presence of an electric field produces an increase in the blow off velocity. This increase is small for lean flames (equivalence ratios below 1) and much larger for rich flames (equivalence ratios over 1). This is probably caused by the increased number of ions present in a rich flame. In Section 2.1 it was shown that ions are produced by a chemical reaction (2.1), which is dependant on the carbon present in the combustion process. Lean flames, by definition are deficient in fuel, so there will be little carbon present. However, in rich flames, where O_2 is deficient there is an abundance of carbon. Hence the results prove to be stronger for rich flames than for lean flames as more carbon is present and therefore more sources for the production of ions.

Practically, the lift off point was very difficult to establish. This was due to the flame being small and therefore the amount that the flame lifted being very small (see Figure 4.37). In Figure 4.37 the photograph of the lifted and attached flames has been enlarged at the Bunsen mouth to show the lift of the flame. The points plotted on all the above graphs are the blow off line. This can be from either an attached flame for low equivalence ratios (when the flame does not lift before blow off) or a lifted flame for higher equivalence ratios (when the flame lifts before blow off).

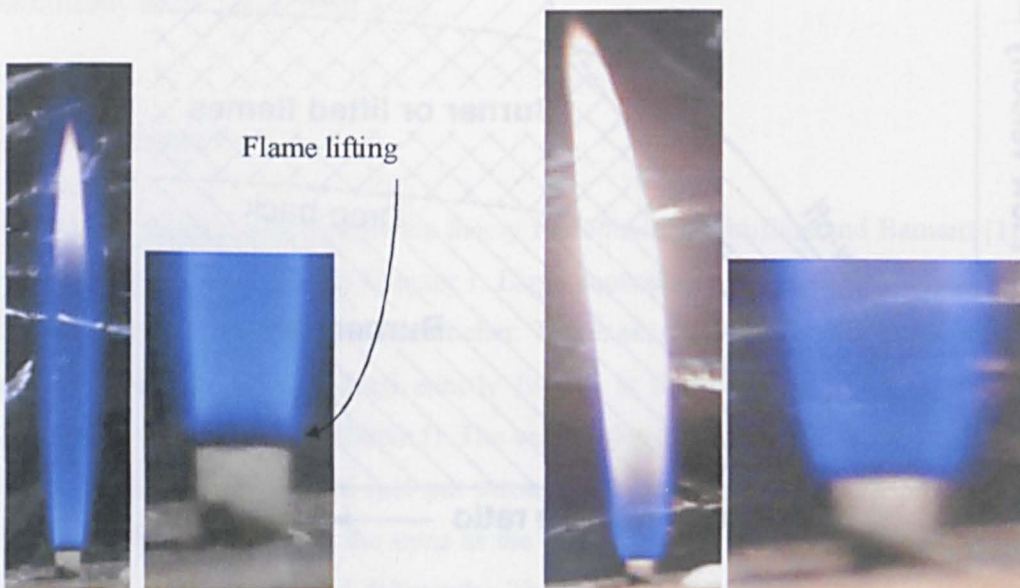


Figure 4.37 Lifted (left) and attached (right) flames

The results for an applied field seem to follow the blow off line from a lifted flame in the literature. However, the experimental procedure was the same for an applied field as for no field and a difference was still found between applying a field and not applying a field. It is therefore considered that the line recorded with the positive electrode below the burner is still the lift line and not the blow off line.

Further weight is given to this argument when the results from applying a field in the opposite direction are analysed. The results (Figure 4.18, 5kV applied and Figure 4.19, 10kV applied) do not differ from those without a voltage. This shows that the blow off velocity is not altered by applying a DC electric field with a positive electrode below the flame. Therefore the effect must be a change in the lift point of the flame caused by applying a field, not experimental error or measurement of the blow off point rather than the lifting point.

By comparing Figure 4.17 (positive above the flame) with Figure 4.19 (positive below the flame) it can be seen that the electric field only increases the lift/blow off velocity when the positive electrode is above the burner. The results cannot, therefore, be easily explained by chemical changes caused directly by excitation of charged particles in the flame. If the changes were caused by chemical excitation then the direction of the field should not be significant and the increase in blow off velocity observed in Figure 4.19 should be the same as those in Figure 4.16. This assumes that the electric field gives the charged particles energy which could increase their reaction rates. The direction of their movement should not be as significant as the amount of energy imparted. If the cause of the modifications were chemical excitation then there should still be an increase for both field directions.

The results are, however, easily explained by ionic wind effects. The ionic wind will blow from the positive electrode to the negative. In the case of Figure 4.17 it will hinder the upwards propagation of the flame and slow its velocity. This is consistent with the literature. An increase in the pressure inside a Bunsen tube was measured when a field was applied [45], [59], indicating this downwards force created by the ionic wind. The

increase in blow off velocity (as mentioned previously) will be greater for rich flames than for lean flames due to more ions being present in rich flames (more ions means a stronger ionic wind). This conclusion is further reinforced by looking at the results of a transverse field. The ionic wind is pulling perpendicular to the flame. Therefore the burning velocity becomes the resultant of the ionic wind and the flow velocity (see Figure 4.38). Hence, the flow velocity at which combustion can be sustained is reduced.

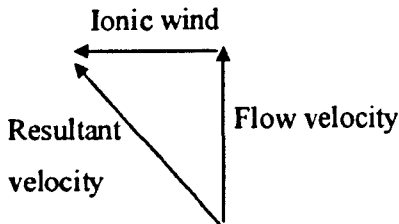


Figure 4.38 Vector diagram for transverse electric field effect

Now that the reader is familiar with the effect of an applied electric field the experimental results of using different apparatus can be compared with the modelling results from Chapter 3. In Chapter 3 it was predicted that certain experimental set ups would produce different electric fields. In particular the electric field in the region of the flame could be amplified by the geometry used. In summary, set ups such as parallel plates (number 1) would produce a uniform field, while set ups such as a ring and Bunsen (number 2) would cause amplification around the Bunsen mouth. If the field was stronger then the ionic wind that will also become stronger. The effects of a DC field have already been attributed to the ionic wind so any increase in the ionic wind strength will have a significant effect on the change in blow off velocity that the field causes.

In Figure 4.27, Figure 4.28 and Figure 4.29 it can be clearly seen that the greatest increase in blow off velocity is created by the ring and Bunsen set up. This corresponds with the conclusions of Chapter 3 as this set up produces the most amplification of the field in the flame region.

It has been illustrated that it is possible to enable a flame to burn outside the normal blow off velocity using an electrical field (Figure 4.16). It has also been shown (Figure 4.33, Figure 4.34 and Figure 4.35) that it is still possible to ignite the flame in this region beyond normal combustion. The ignition source did contain ions and the ignition of a flame without ions present has not been assessed. The practicalities of creating a spark inside a high voltage field without disrupting the field or causing the field electrodes to breakdown to the spark electrodes are beyond the scope of this work. This experiment was intended to simulate a much larger combustor where it was assumed that there would be ions present during ignition (hence the use of a flame ignition source).

4.8 Conclusions

In this chapter it has been shown that;

- Applying a field increases the apparent blow off limits of a flame
- The increase only occurs for configurations where the positive electrode is above the burner
- Apparatus that produce locally stronger fields in the flame region cause a greater increase in blow off velocity than those that produce a weaker field
- The flame can still be ignited by an ignition source outside of the normal combustion region when a field is applied

Chapter 5 Effect of Pulsed Fields

5.1 Introduction and apparatus

The apparatus is set up as described in Section 4.2, using parallel plates as the electrodes. The power supply, however, is a Bournlea model 2780 high voltage pulse generator. This power supply requires a low voltage pulse input which was supplied by a data pulse signal generator. The 2780 unit produces a high voltage pulse up to a maximum voltage of 5kV and a frequency of 5kHz. The minimum pulse width was 500ns. The pulses are produced relative to earth and when the pulse is not active the electrodes return to earth as can be seen in Figure 5.1. The pulse was measured using a Testek TT-HVP15 HF 1000:1 probe, connected to a Tektronics oscilloscope. The pulse width can also be called the “on time”, referring to the time that the electrodes are charged.

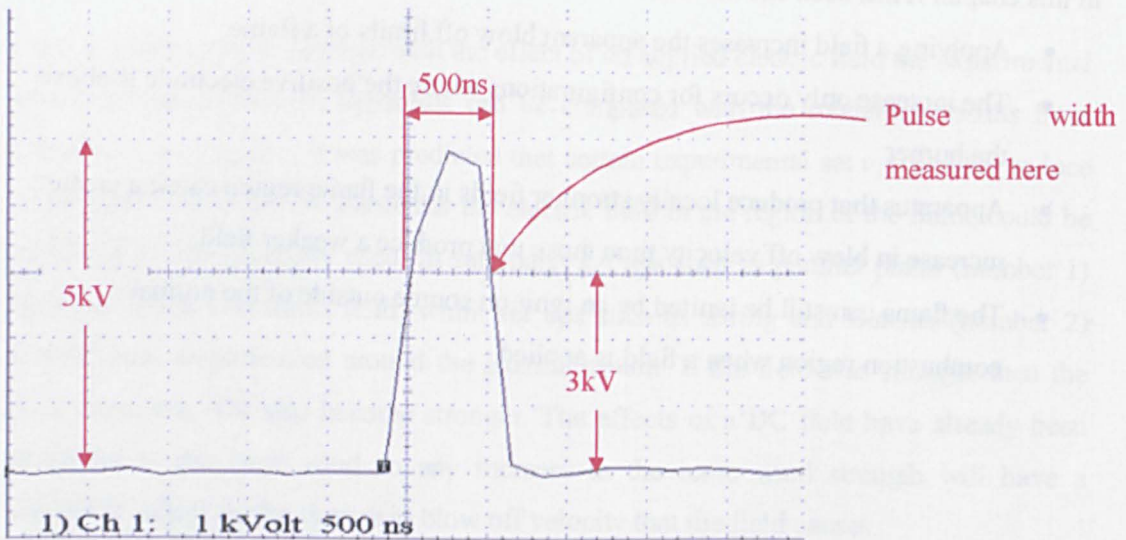


Figure 5.1 Wave form at 5kHz, 500ns pulse width (scale = 1kV by 500ns)

The rise and fall time was 200ns, therefore the waveform for virtually all the results can be considered to be square except for the very fast pulses where the waveform was slightly distorted. In this case the time period was measured from when the voltage reached 3kV to when the voltage dropped below 3kV. The waveform can be seen in

Figure 5.1 and Figure 5.2 below for the fastest (shortest) pulse (500ns) at 5kHz. Each vertical division is 1kV and each horizontal division is 500ns in Figure 5.1. The pulse width and frequency will be stated in the title of each picture along with the x against y division size for all waveform pictures.

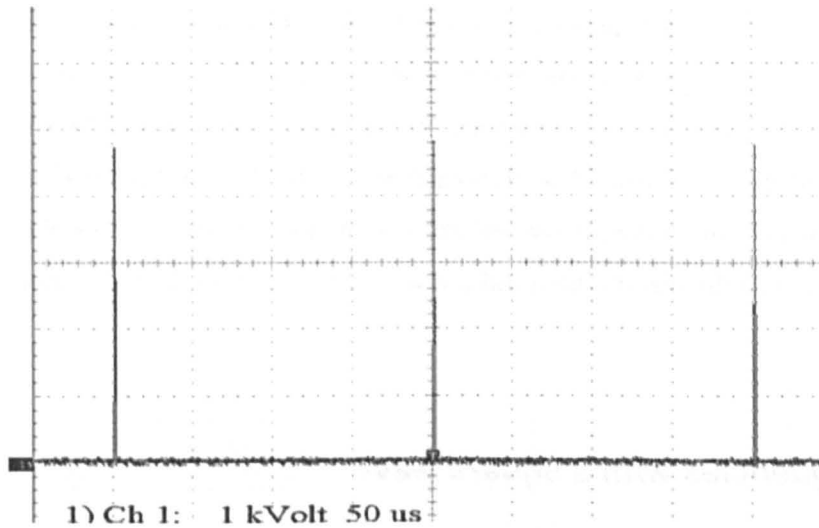


Figure 5.2 Wave form at 5kHz, 500ns pulse width (scale = 1kV by 50 μ s)

The procedure is almost identical to the previous experiments. The desired voltage, pulse width and frequency were set on the power supply. The air flow was set and the fuel flow reduced until blow off occurred. The mass flow was calculated and if it was not within 10% of 10mg/s or 20mg/s (two sets of data) then the air flow was altered and the experiment repeated until the mass flow was within 10% of the desired value.

There are several variables that effect the flame; frequency, pulse width, equivalence ratio and geometry of the electrodes (shape, orientation and polarity). Each of these has an important effect that needs to be understood. The effect of each of these will therefore be shown individually, beginning with the frequency effect. The results show the broadest view in the same format as the previous experiment (equivalence ratio vs velocity). The pulse width can then be examined in reference to these results. The geometry of the plates has already been discussed previously (all of Chapter 3 and

Section 4.5). Consequently, in this set of experiments only the plate facing gauze has been used. However, the results have been repeated for both polarities.

The equivalence ratio was limited by the apparatus. As the flame gets richer it needs to spread to absorb O_2 from the surroundings. The flame provides an easier breakdown path than air and so very rich and enlarged flames caused electrical breakdown. This trips out the power supply due to the large current. The lower limit was the flashback region (this can be seen on Figure 4.36). The blow off of flames leaner than those measured in the experiments below could not be measured as flashback inside the Bunsen burner tube occurred. The point at which this occurred was measured (although not included on the graphs) and it was found that the electric field did not have any effect on the value that this occurred at.

5.2 Effect of frequencies with a square wave

5.2.1 Results

The effect of frequency is examined first. A square wave of various frequencies has been applied to the flame, using the procedure described above. The square wave has equal "on" and "off" times and can be seen for 5kHz in Figure 5.3 below.

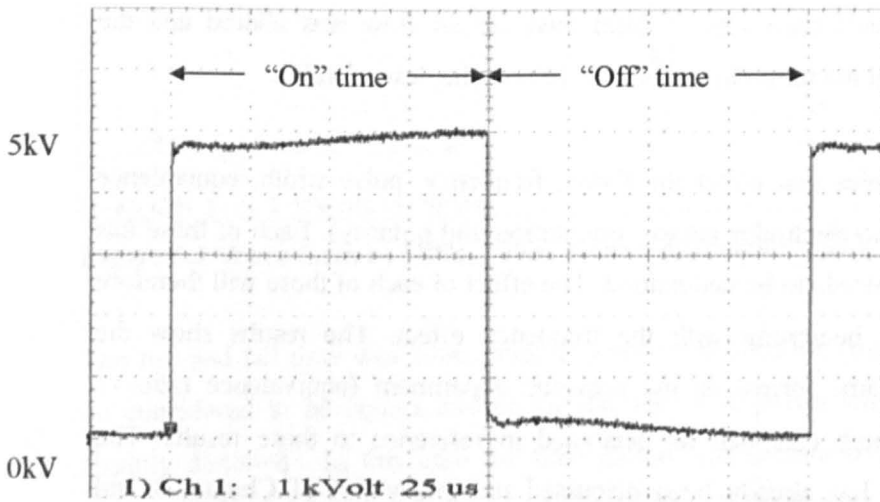


Figure 5.3 Wave form at 5kHz, 0.1ms pulse width (scale = 1kV by 25 μ s)

As in the previous section, the diagram in the top right of the graph indicates the set up used for each graph and the polarity of the field. The choice of apparatus was discussed in Chapter 3 and sections 4.2 and 4.5 and will therefore not be repeated here. In this case it is the gauze (earth) above the flame and a plate (positive) below it. The previous results (no field and DC) have also been shown on the graph for reference (4.3, Figure 4.18). It was shown that the DC voltage with the positive electrode below did not have a significant effect on the blow off velocity, which can also be seen below (Figure 5.4). A logarithmic best fit has been applied to the results to show the trend. Each of the results plotted in Figure 4.18 are an average of 3 readings taken.

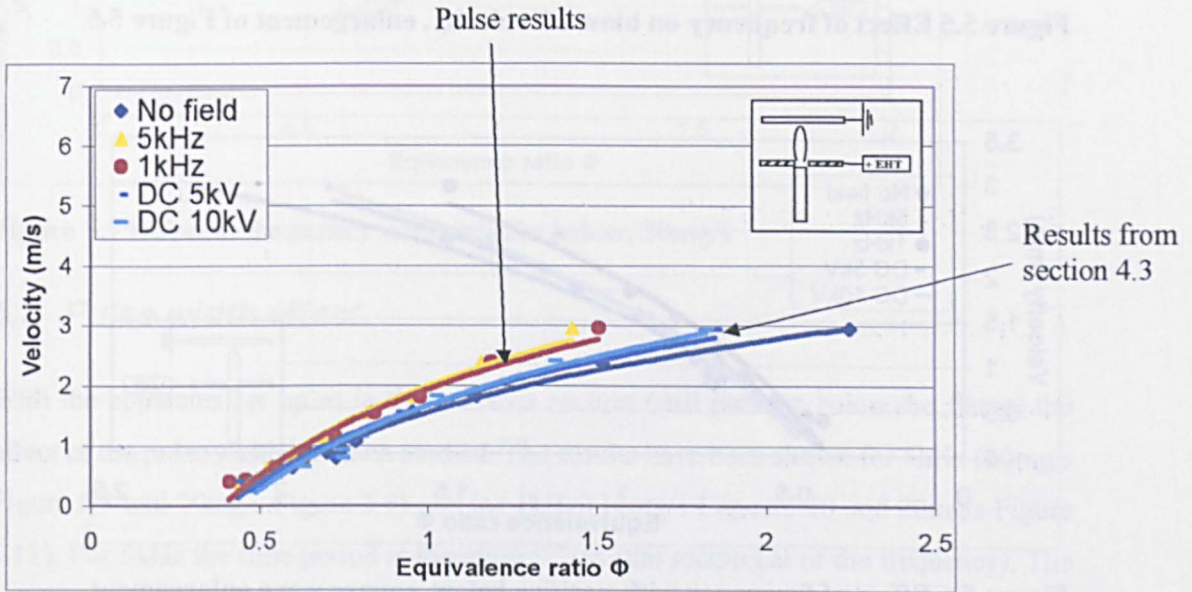


Figure 5.4 Effect of frequency with positive below 10mg/s square wave

The above graph has been drawn on the same scale all the previous results have been plotted on (0-7m/s on the y axis). This is too large for these results so an enlargement has been included below. The trend without the logarithmic fit can be seen more clearly (Figure 5.5, and with logarithmic fit Figure 5.6)

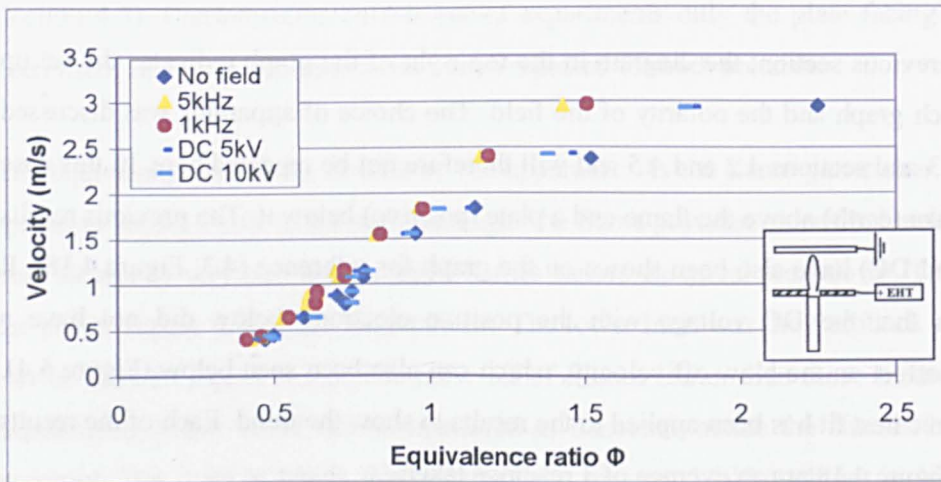


Figure 5.5 Effect of frequency on blow off velocity, enlargement of Figure 5.5

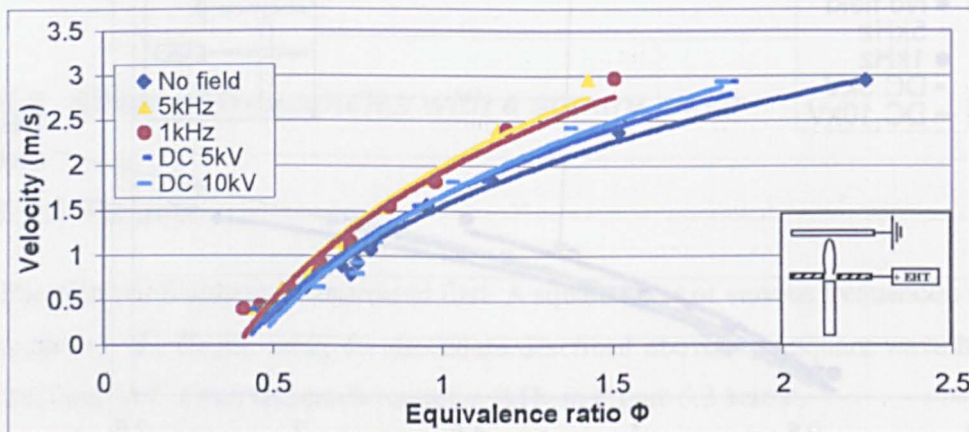


Figure 5.6 Effect of frequency with positive below, square wave enlargement

The graph above shows how the effect of a pulsed field is greater than the DC field (Section 4.4 showed that DC voltage in this orientation has negligible effect). A DC field in this orientation increases the blow off velocity by approximately 6%. However a 5kHz pulsed field can increase it by 35% (both figures calculated from the best fit lines at an equivalence ratio of 0.7, the increase for a rich flame at an equivalence ratio of 1.3 is 3% and 30% for DC and 5kHz respectively). It also shows that the higher the frequency the greater the effect on blow off velocity. Further experiments (see 5.4) have shown that the

increase in blow off velocity becomes larger for higher frequencies within the experimental range of the equipment (16Hz to 5kHz).

The experiment was also repeated for 20mg/s. The results show the same trend (Figure 5.7).

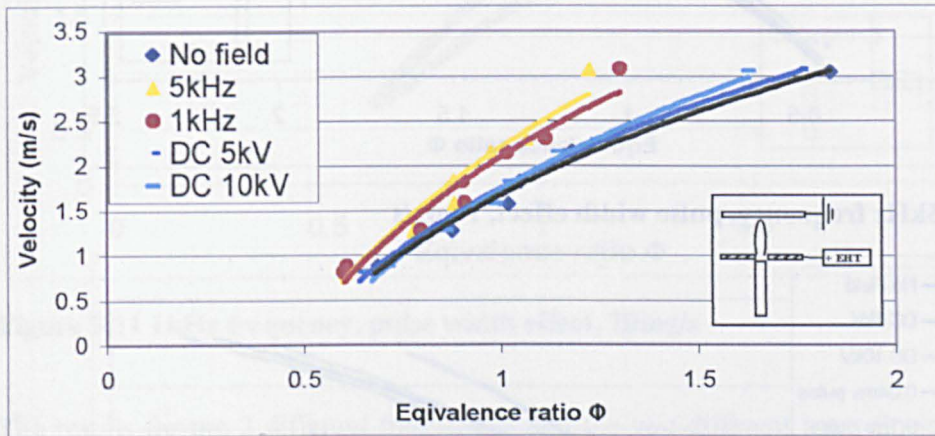


Figure 5.7 Effect of frequency with positive below, 20mg/s

5.3 Pulse width effect

With the apparatus set up as in the previous section (still positive below the flame) the effect of the pulse width has been studied. The results have been shown for 5kHz (10mg/s Figure 5.8 and 20mg/s Figure 5.9) and for 1kHz (10mg/s Figure 5.10 and 20mg/s Figure 5.11). For 5kHz the time period is therefore 0.2ms (the reciprocal of the frequency). The results (Figure 5.8 and Figure 5.9) show a pulse at 0.04ms, 0.1ms and 0.16ms. These correspond to pulses with a percentage “on time” of 20%, 50% and 80% respectively. A square wave would have a percentage “on time” of 50%. The results for 1kHz show the same percentage “on times” of 20%, 50% and 80% (0.2ms, 0.5ms and 0.8ms respectively).

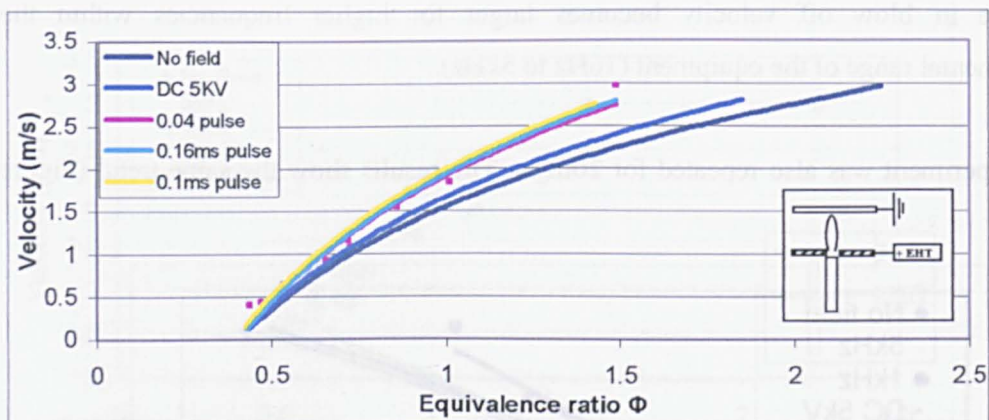


Figure 5.8 5kHz frequency, pulse width effect, 10mg/s

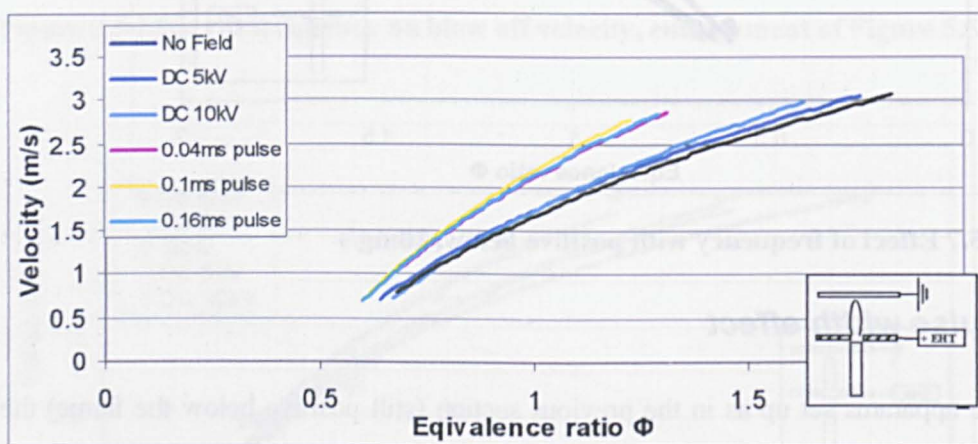


Figure 5.9 5kHz frequency, pulse width effect, 20mg/s

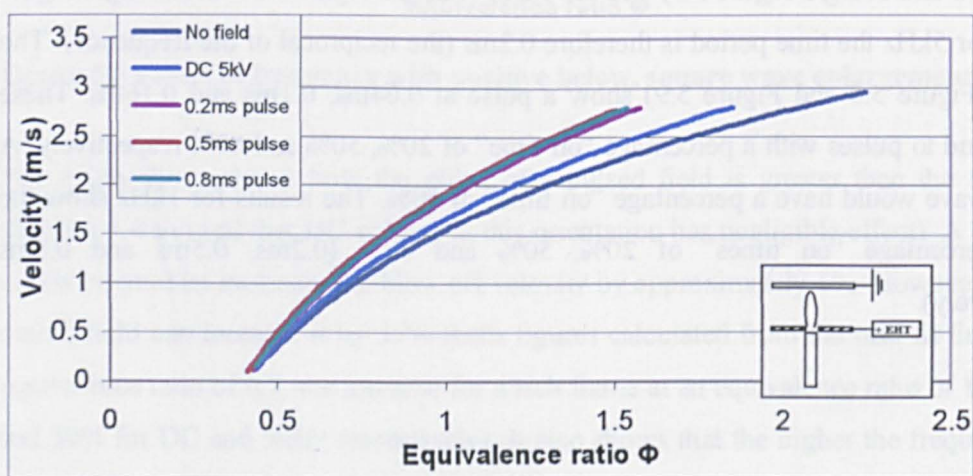


Figure 5.10 1kHz frequency, pulse width effect, 10mg/s

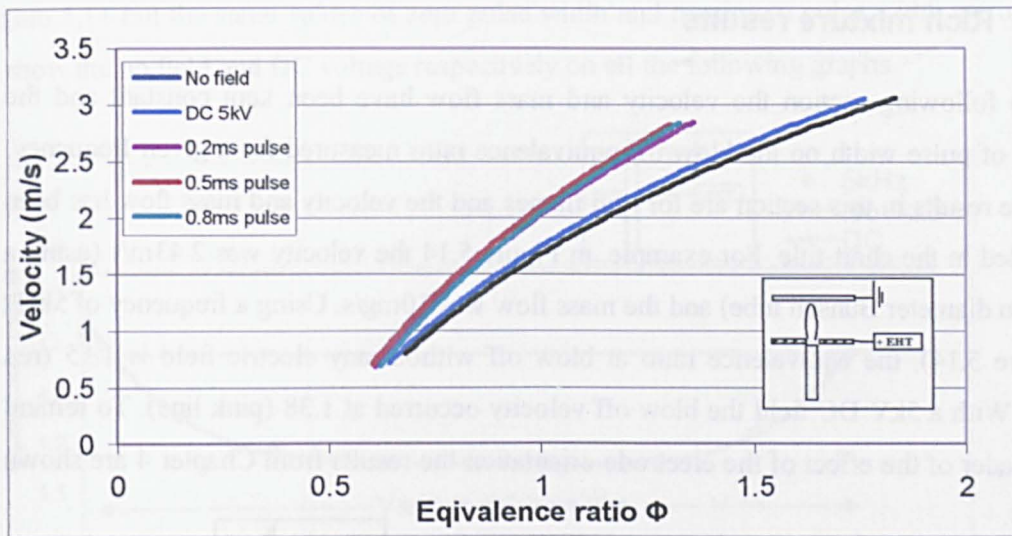


Figure 5.11 1kHz frequency, pulse width effect, 20mg/s

The results for the 2 different frequencies and the two different mass flows show very similar results. This being that the best percentage “on time” is 50% or a square wave and the worst is 20%, with the 80% value falling between. The results are also very close together. To illustrate the effect described above the 1kHz pulse at 20mg/s has been enlarged to show the difference between 20, 50 and 80% “on times” (Figure 5.12).

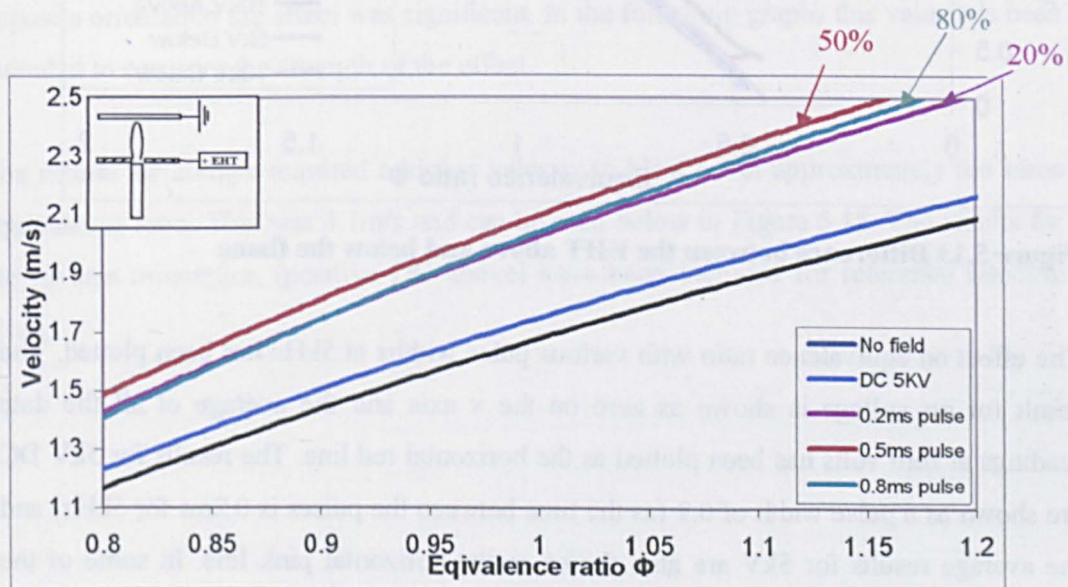


Figure 5.12 Enlargement of Figure 5.11

5.3.1 Rich mixture results

In the following section the velocity and mass flow have been kept constant and the effect of pulse width on the blow off equivalence ratio measured for a given frequency. All the results in this section are for rich flames and the velocity and mass flow has been included in the chart title. For example, in Figure 5.14 the velocity was 2.43m/s (using a 2.0mm diameter Bunsen tube) and the mass flow was 10mg/s. Using a frequency of 5kHz (Figure 5.14), the equivalence ratio at blow off without any electric field is 1.55 (red line). With a 5kV DC field the blow off velocity occurred at 1.38 (pink line). To remind the reader of the effect of the electrode orientation the results from Chapter 4 are shown below.

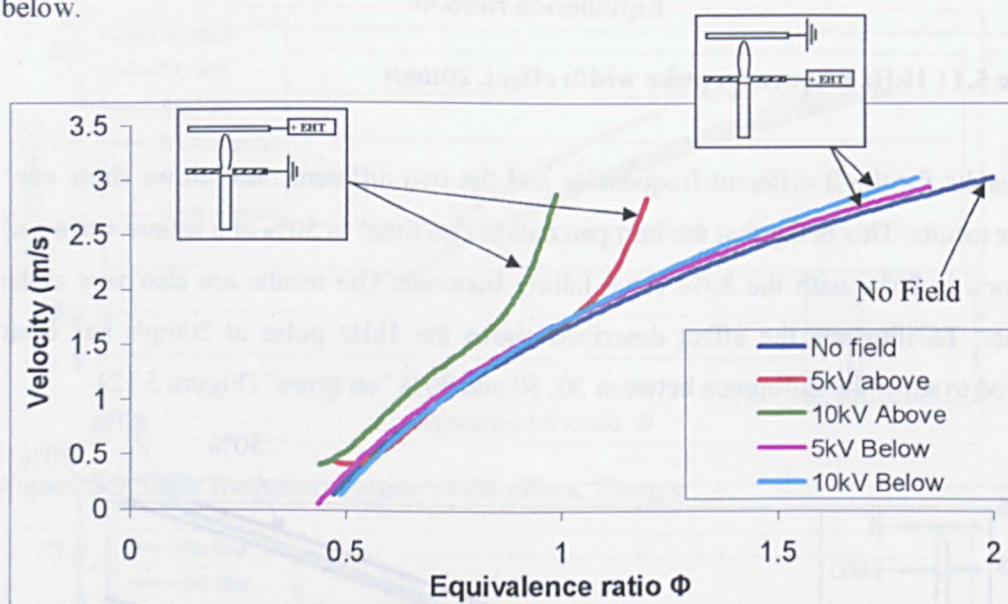


Figure 5.13 Difference between the EHT above and below the flame

The effect on equivalence ratio with various pulse widths at 5kHz has been plotted. The result for no voltage is shown as zero on the x axis and the average of all the data readings at zero volts has been plotted as the horizontal red line. The results for 5kV DC are shown as a pulse width of 0.2 (as the time between the pulses is 0.2ms for 5kHz) and the average results for 5kV are also shown as the horizontal pink line. In some of the graphs the 5kV results are also plotted for the reverse polarity (+5kV above and ground below), which is represented by a horizontal light blue line. Both of these are marked on

Figure 5.14 but the same values of zero pulse width and maximum pulse width are used to show the no field and DC voltage respectively on all the following graphs.

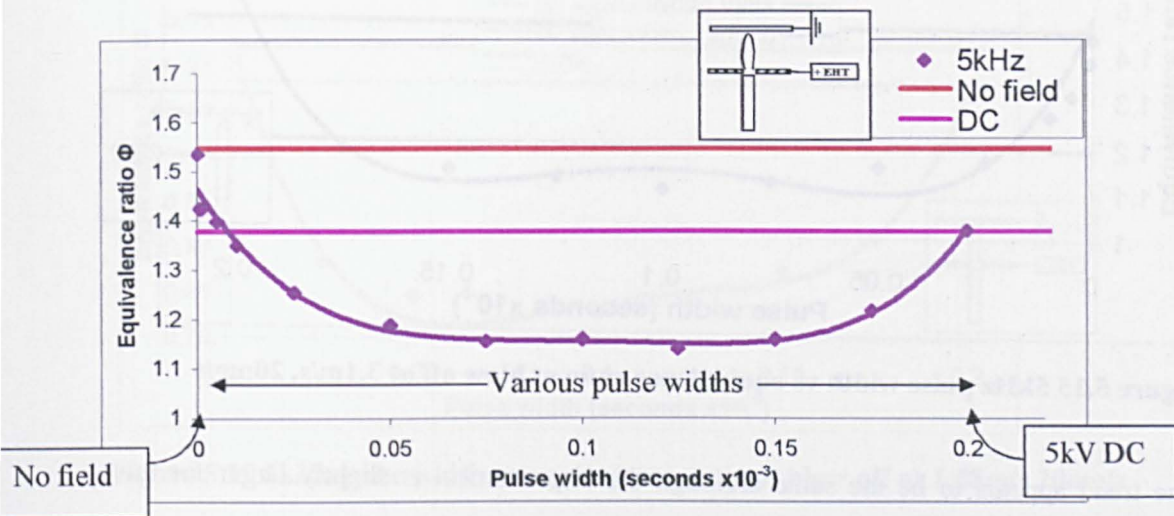


Figure 5.14 5kHz, pulse width vs equivalence ratio at blow off at 2.43m/s, 10mg/s

The best pulse width is between 0.05 and 0.15ms which means that the pulse is on for between 25% and 75% of the time. It was shown in Section 4.4 that the DC field in this orientation had very little effect on the flame. However with the electrodes in the opposite orientation the effect was significant. In the following graphs this value has been included to compare the strength of the effect.

The results for 20mg/s required a higher velocity to blow off at approximately the same equivalence ratio. This was 3.1m/s and can be seen below in Figure 5.15. The results for the reverse orientation (positive DC above) have been included for reference (electric blue).

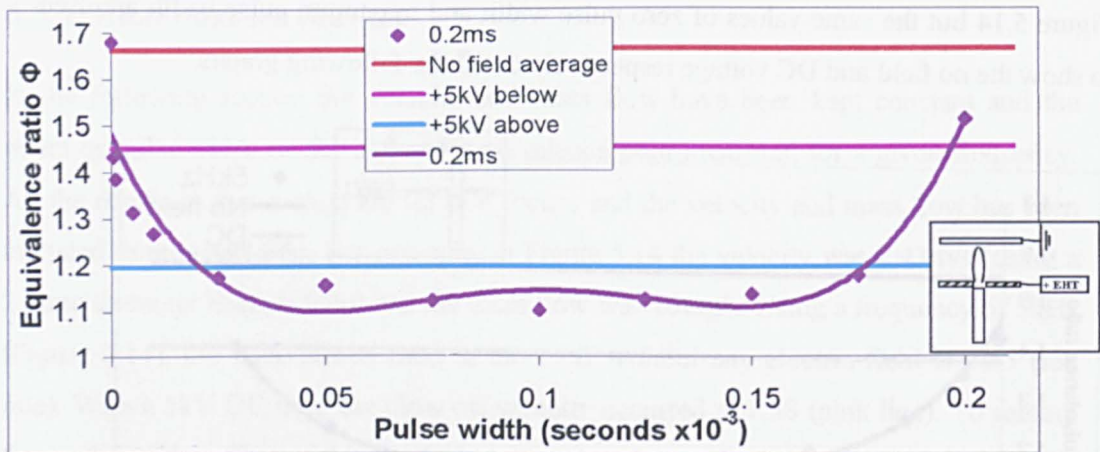


Figure 5.15 5kHz pulse width vs equivalence ratio at blow off at 3.1m/s, 20mg/s

The trend appears to be the same although the improvement is slightly larger for the higher flow rate (55% instead of 52% for 10mg/s).

5.3.2 Around stoichiometric mixture results

The same graphs can be plotted for an approximately stoichiometric flame. In this case the velocity was 1.55m/s and 1.58m/s for 10mg/s (Figure 5.16) and 20mg/s (Figure 5.17) respectively.

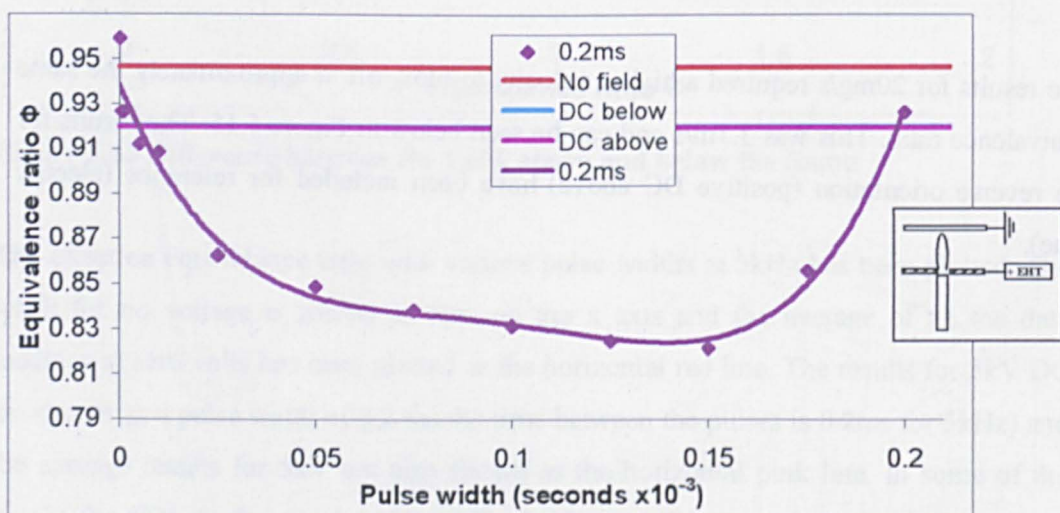


Figure 5.16 5kHz pulse width vs equivalence ratio at blow off at 1.55m/s 10mg/s

5.4 Effect of pulse frequency and pulse width

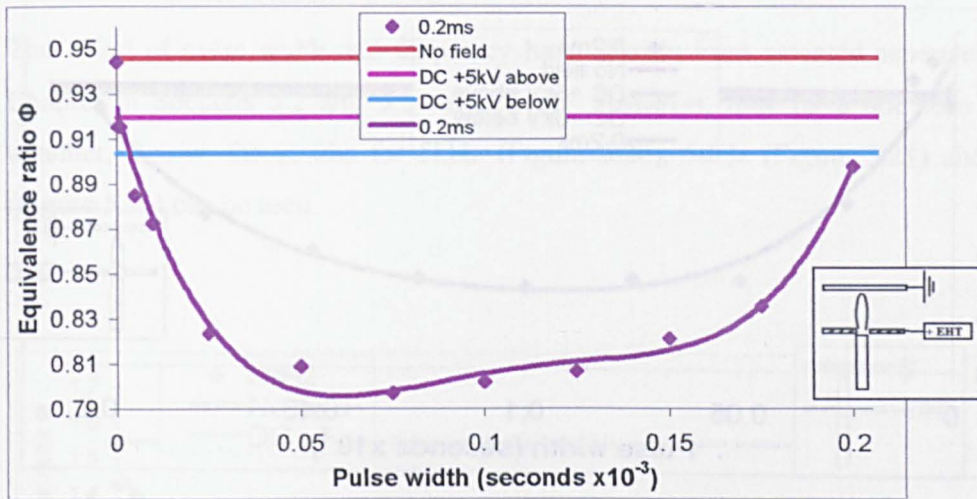


Figure 5.17 5kHz pulse width vs equivalence ratio at blow off at 1.58m/s 20mg/s

The results from Chapter 4 showed that a DC field only had a small effect on the blow off velocity for stoichiometric flames. In Figure 5.16 and Figure 5.17 this can be seen as the pink (positive below) and electric blue (positive above) lines. The effect compared with the no field blow off (red line) is very small. However the pulse at 5kHz has a much greater effect than the DC field for almost all pulse widths. Both the 10mg/s (Figure 5.16) and 20mg/s (Figure 5.17) show similar results, however the 10mg/s is skewed to the left (smaller pulse widths) and the 20mg/s to the right (larger pulse widths). The difference is within experimental error and it is assumed that they are the same. The effect also seems to be of the same magnitude for both mass flow rates.

5.3.3 Lean mixture results

The results from Chapter 4 showed that a DC field only had a small effect on the blow off velocity for lean flames. As previously mentioned, these results can be seen on the graphs (horizontal lines were no field; red line, +5kV above; electric blue, +5kV below; pink).

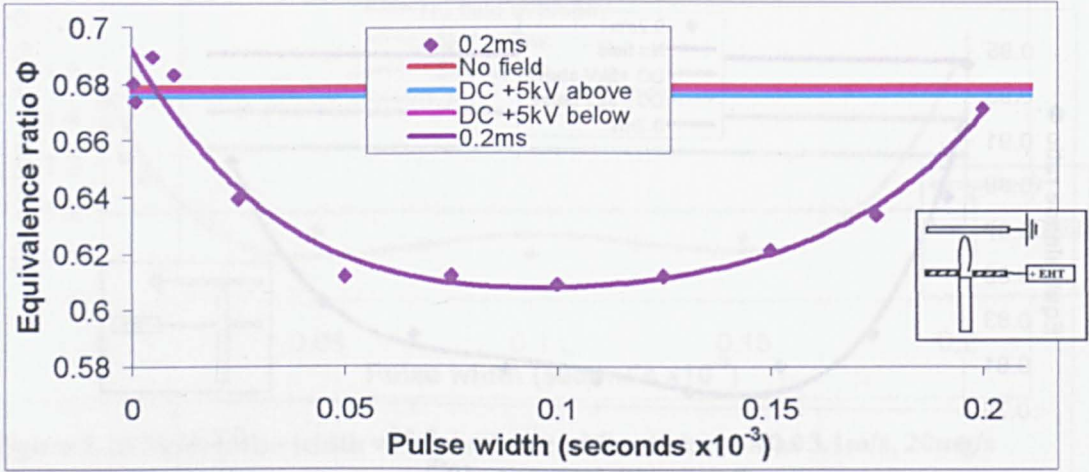


Figure 5.18 5kHz pulse width vs equivalence ratio at blow off at 0.88m/s 10mg/s

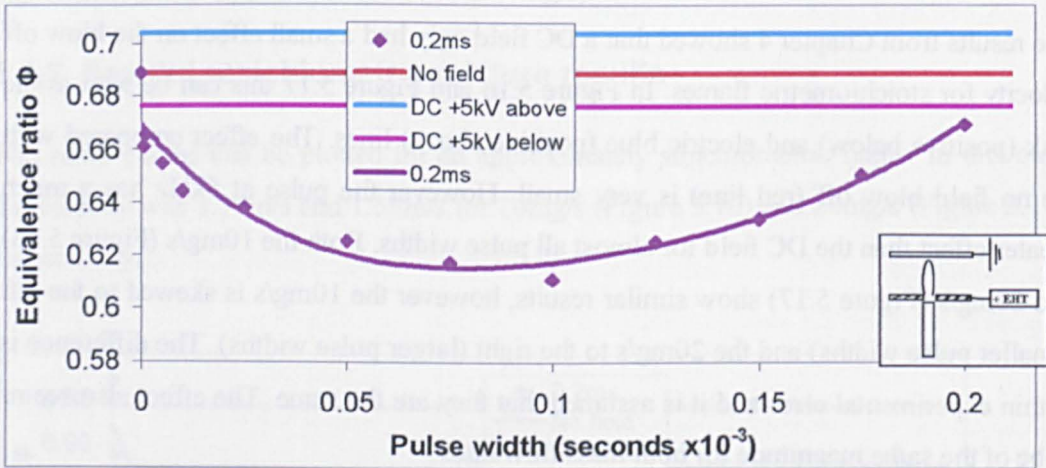


Figure 5.19 5kHz pulse width vs equivalence ratio at blow off at 0.89m/s 20mg/s

The results show a much larger decrease in the blow off equivalence ratio than for DC fields. The effect is the same for both 10mg/s and 20mg/s.

5.4 Effect of both frequency and pulse width

The effect of pulse width and frequency have already been assessed separately in this Chapter in Sections 5.2 and 5.3 respectively. However, they have not been assessed together. Below, the results for 5kHz (Figure 5.20), 50Hz (Figure 5.21) and 16.7Hz (Figure 5.22) can be seen.

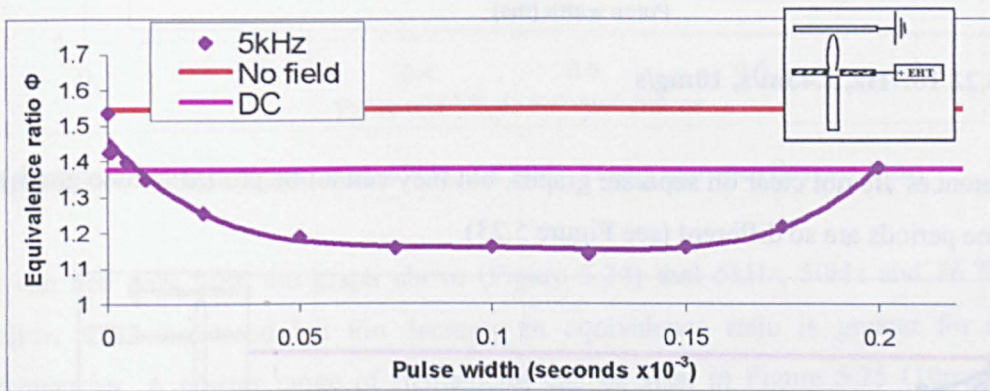


Figure 5.20 5kHz, at 2.43m/s, 10mg/s



Figure 5.21 50Hz, at 2.43m/s, 10mg/s

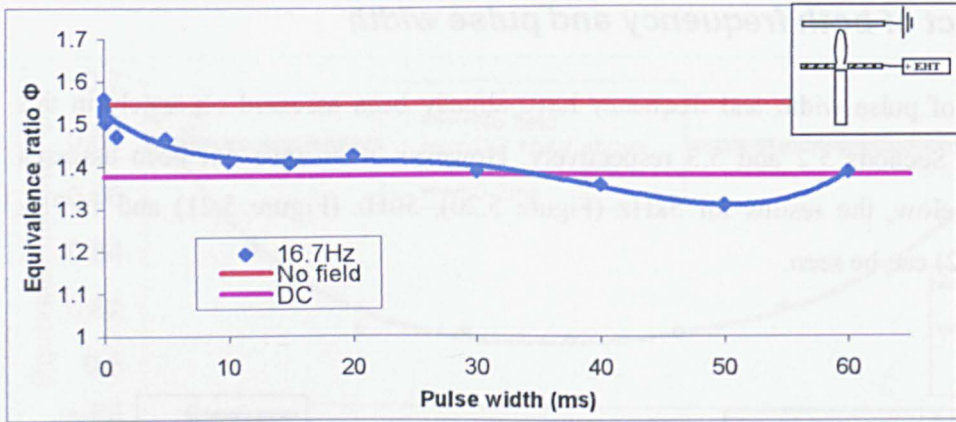


Figure 5.22 16.7Hz, 2.43m/s, 10mg/s

The differences are not clear on separate graphs, but they cannot be plotted on one graph as the time periods are so different (see Figure 5.23).

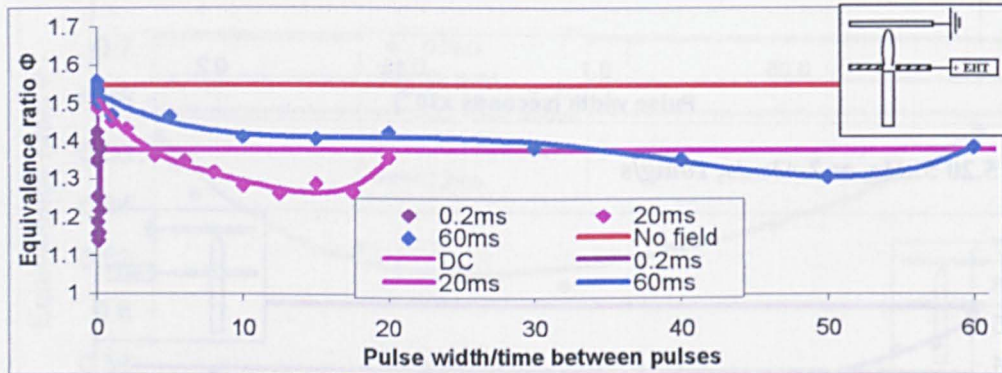


Figure 5.23 5kHz, 50Hz and 16.67Hz, 2.43m/s, 10mg/s

The solution to this problem is to use the formula shown below (5.1).

$$\frac{\text{Pulse width}}{\text{Time period}} = \text{Fraction "on time"} \quad (5.1)$$

where the time period is the time from the beginning of one pulse to the beginning of the next. This gives the fraction of time that the pulse is “on” for (see Figure 5.24). All the results therefore have a fraction “on time” of between 0 and 1, allowing all the different frequencies to be plotted onto one graph, as shown in Figure 5.24.

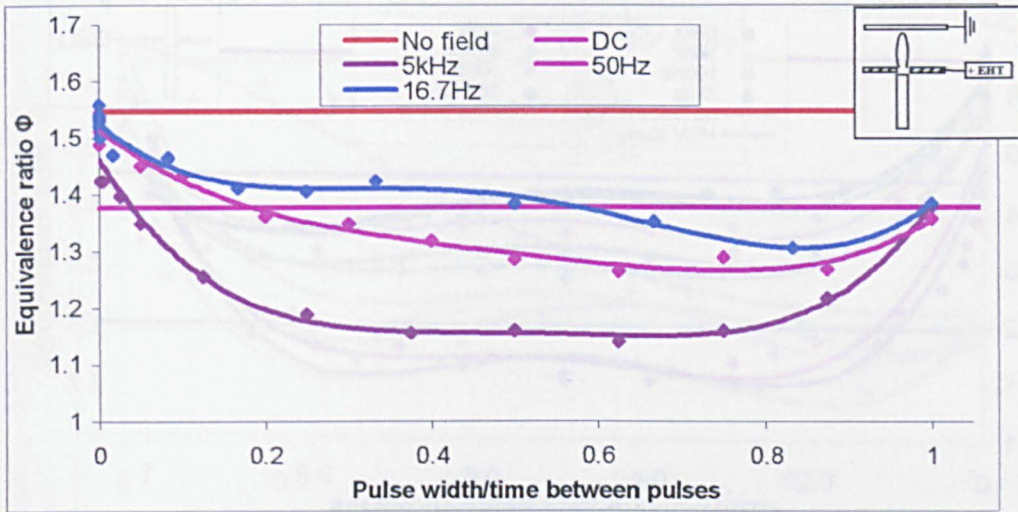


Figure 5.24 5kHz, 50Hz and 16.67Hz, 2.43m/s, 10mg/s proportion on time

It can be seen from the graph above (Figure 5.24) that 5kHz, 50Hz and 16.7Hz all follow the same trend but the decrease in equivalence ratio is greater for higher frequencies. A greater range of frequencies can be seen in Figure 5.25 (10mg/s) and Figure 5.26 (20mg/s) but the same pattern appears; the decrease in equivalence ratios is greater for higher frequencies and when the pulse is on for between 25% and 75% of the time.

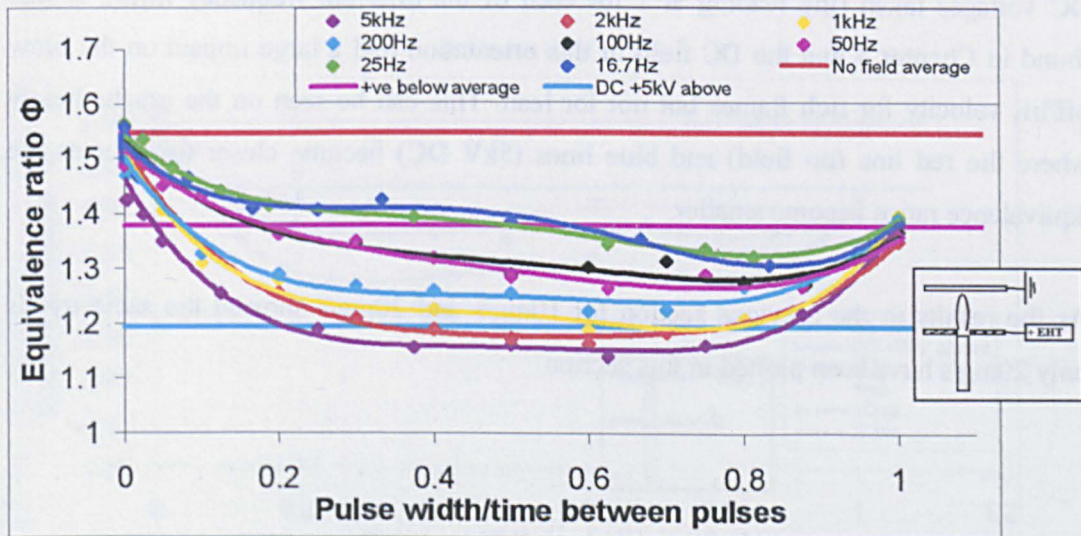


Figure 5.25 Range of frequencies 2.43m/s, 10mg/s proportion on time

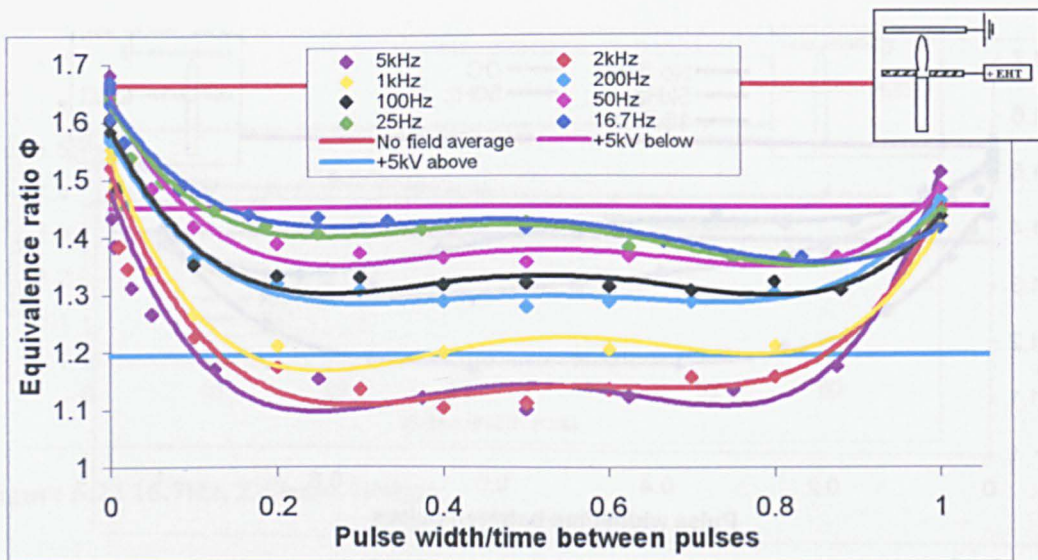


Figure 5.26 Range of frequencies 3.1m/s, 20mg/s percentage on time

5.5 Reverse polarity

The electrodes were reversed (+5kV above and earth below the flame) and the experiment repeated. The DC results for this orientation have been plotted on the graphs as a horizontal electric blue line. The DC line plotted is the average of all the finishing DC voltages taken (the reading at 1 for each of the different frequency lines). It was found in Chapter 4 that the DC field in this orientation had a large impact on the blow off/lift velocity for rich flames but not for lean. This can be seen on the graphs below where the red line (no field) and blue lines (5kV DC) become closer together as the equivalence ratios become smaller.

As the results in the previous section for 10mg/s and 20mg/s showed the same trends only 20mg/s have been plotted in this section.

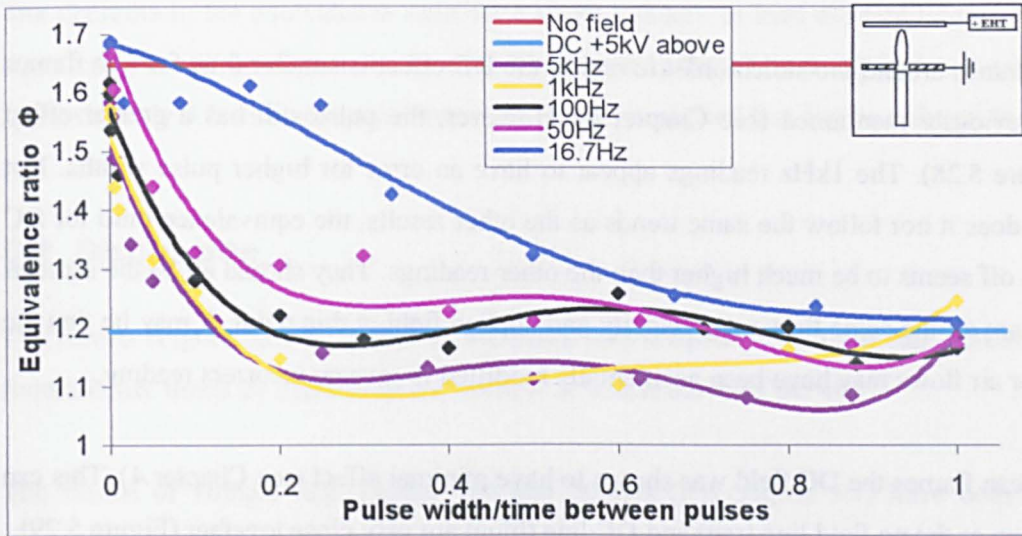


Figure 5.27 Rich flame 20mg/s velocity 3.1m/s

It was shown in Section 5.4 that the higher the frequency the greater the effect on the blow off equivalence ratio. The same is true for the reverse polarity. The effect is also strongest when the field is applied for between 25% and 75% of the time. The large difference that the DC voltage makes at rich flames can be clearly seen (from red to blue lines). The higher frequency pulses, however, have a stronger effect from an “on time” of 15%.

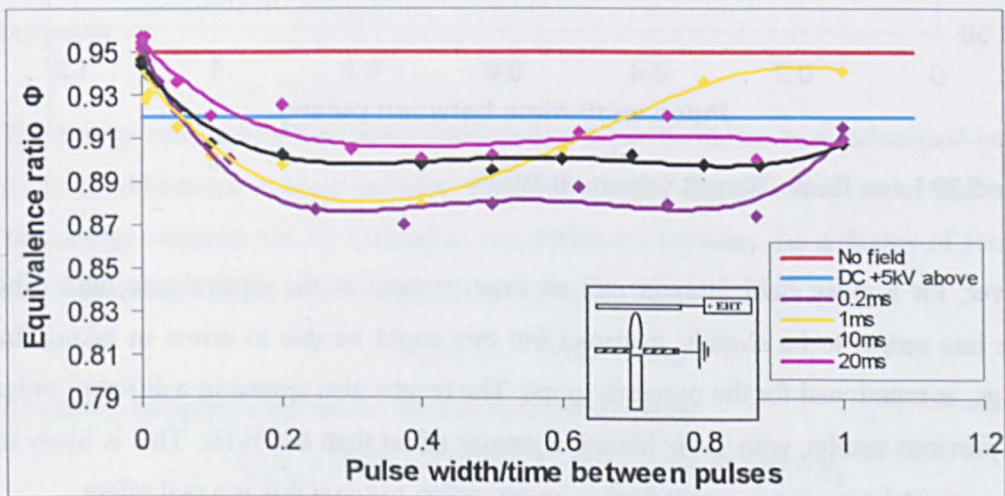


Figure 5.28 Stoichiometric flame 20mg/s velocity 1.59m/s

For flames around the stoichiometric region the DC effect is smaller than for rich flames as previously mentioned (see Chapter 4). However, the pulse still has a greater effect (Figure 5.28). The 1kHz readings appear to have an error for higher pulse widths. Not only does it not follow the same trends as the other results, the equivalence ratio for DC blow off seems to be much higher than the other readings. They should all be the same as they are all the same flow rate, velocity and applied field at this point. It may be that the gas or air flows may have been accidentally modified to give an incorrect reading.

For lean flames the DC field was shown to have minimal effect (see Chapter 4). This can be seen as the no field line (red) and DC line (blue) are very close together (Figure 5.29).

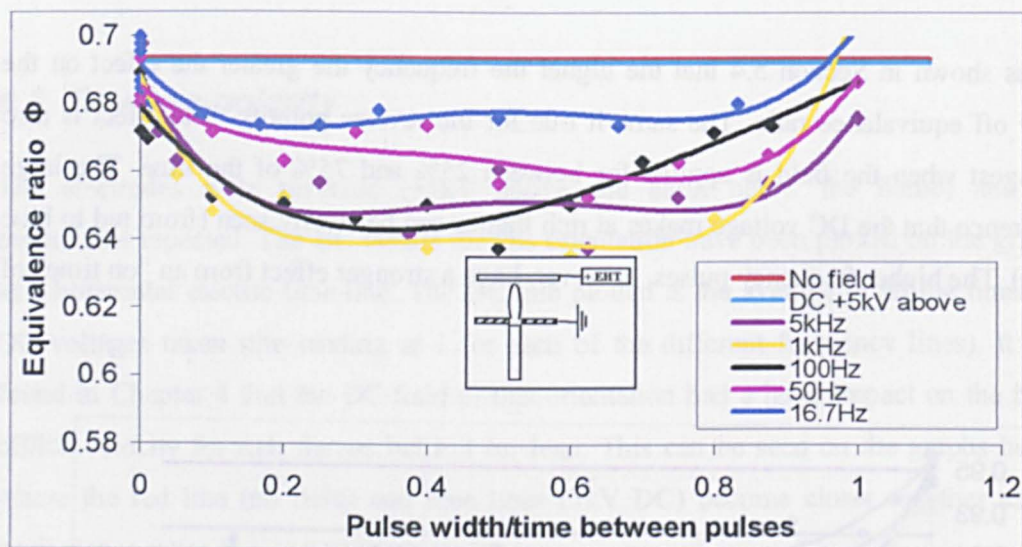


Figure 5.29 Lean flame 20mg/s velocity 0.89m/s

However, for a pulse field there is still an improvement in the equivalence ratio. The 100Hz line seems to be slightly incorrect but this could be due to errors in taking the readings, as mentioned for the previous graph. The results also appear in a different order to the previous results, with 1kHz having a greater effect than the 5kHz. This is likely to be experimental error but is worth further investigation to see if this is a real effect.

The decrease in the equivalence ratio for a given velocity in lean mixture flames, while significant, is still small; a velocity of 0.89m/s will blow off at an equivalence ratio of approximately 0.7 without a pulse but when a pulse is applied this can be reduced to 0.64.

5.6 Discussion

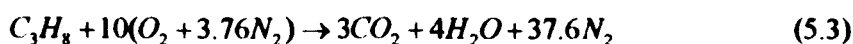
The results (Figure 5.6) show that an AC field with a square waveform can increase the flammability limits by increasing the velocity at which blow off occurs.

The results of 10mg/s (e.g. Figure 5.6) and 20mg/s (e.g. Figure 5.7) have both been plotted for the pulse experiments. They both show the same trend. However, exactly the same equivalence ratios have not been used due to the limitations on the tube sizes available and therefore the velocity that can be used. This means that the results cannot be directly compared on the same graph although the trend is the same. The experiment does not appear, therefore, to be dependant on the mass flow. However, although there is a significant difference between the mass flows (100%) in this experiment they are not on the same scale as many of the common flames used by industry (650MW [117]). The experiments were not designed to prove that the effects were completely independent of mass flow, only that it did not have a significant effect in the context of this experiment. It is worth investigating the effect on much larger flames, but this is beyond the scope of this work.

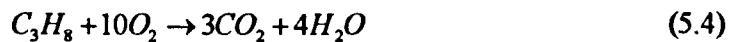
The energy released by the flames used in this experiment has been calculated below to show the difference in scale between these flames and those used by industrial burners. The energy released can be defined as the difference between the enthalpy of formation of the products and the reactants [116], as shown by equation (5.2).

$$H_{\text{combustion}} = H_{\text{prod}} - H_{\text{react}} \quad (5.2)$$

Assuming complete combustion the reaction can be given by



As mentioned previously this is not the exact reaction and there are many intermediate states. However, the total energy released is given by the difference between the formation energies of the starting molecules and the final molecules which reaction (5.3) represents. For the purposes of the energy calculation N_2 can be ignored as the energy it contains is the same for both the products and the reactants. So the equation (5.3) becomes;



Therefore equation (5.2) can be written as;

$$H_{\text{combustion}} = (3H_{CO_2} + 4H_{H_2O}) - (H_{C_3H_8}) \quad (5.5)$$

The energy of formation of all of the molecules is given below in Table 5.1.

Molecule	Enthalpy of formation
C_3H_8	-103,850
O_2	0 (Oxygen is an atom so there is no formation energy)
CO_2	-393,520
H_2O	(liquid) -241,820 (vapour) -285,830

Table 5.1 Formation energy for products and reactants

For the flames used in these experiments the energy stored in the water (making it a vapour not a liquid) is not recovered. Equation (5.5) can then be solved;

$$\begin{aligned} H_{\text{combustion}} &= (3(-393,520) + 4(-241,820)) - (1(-103,850)) \\ H_{\text{combustion}} &= -2,043,990 \text{ kJ / kmol} \end{aligned} \quad (5.6)$$

The molecular weight of propane is 44.097 [116]. Therefore the result in kJ/kg is

$$\begin{aligned} H_{\text{combustion}} &= \frac{-2,043,990}{44.097} \\ H_{\text{combustion}} &= 46352 \text{ kJ / kg} \end{aligned} \quad (5.7)$$

The fuel flow in the experiments is between 1.5mg/s and 0.15mg/s. This gives

$$\begin{aligned} \text{Max } 1.5 \times 10^{-6} \times 46352 &= 0.069 \text{ kJ / s} \\ \text{Min } 0.15 \times 10^{-6} \times 46352 &= 6.9 \times 10^{-3} \text{ kJ / s} \end{aligned} \quad (5.8)$$

Therefore the flames used in this experiment range from 6.9 to 69.5watts.

The effect of a high voltage pulse on a flame is much larger than for a DC field in both orientations of electrodes. The difference is larger for the first set up described (positive below and earth above, Figure 5.30), particularly as a DC field in this orientation was shown to have negligible effect in Chapter 4. This was true for all the frequencies used (although at 50Hz the effect was only equal to the DC rather than significantly exceeding it). The results were very frequency dependant. It is probably easiest to see this from Figure 5.25 and Figure 5.26. These graphs clearly show that the higher the frequency the greater the enhancement of the blow off velocity. This was true for rich, stoichiometric and lean flames for both mass flow rates.

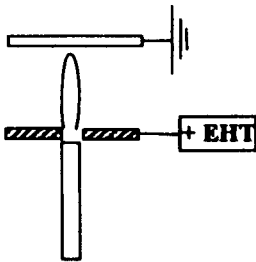


Figure 5.30 Positive EHT below

All the frequencies show that the best ratio of pulse width to the time between pulses is between 0.2 and 0.8 but peaking at approximately 0.5. The curve is very flat bottomed and the difference between the effect at 0.2 and 0.5 is small. Practically this could be very advantageous as the power consumption for a 0.2 (or 20% on time) pulse is much less than a 0.8 (or 80% on time) pulse. The improvement between 0.2 and 0.5 is small and probably not worth the extra energy consumption (0.5 takes 150% more than 0.2).

It is also very important to note that the effect seems to occur in both rich and lean flames. The effect does appear to be greater for rich flames than for lean flames, as in the experiments with DC field. Many of the modern burners work in the lean region (to ensure complete combustion and to try and keep the flame cooler to prevent NO_x). The

increases in the blow off limits in this region are therefore very useful as they could be used to stabilise lean flames, which are generally less stable than rich flames.

Unlike the DC results in Chapter 4, the results cannot easily be explained by the ionic wind. This is mainly because of the time it takes for the ionic wind to activate. Marcum and Ganguly [39] used a high speed camera to show the ionic wind effect on a flame when a pulse is applied. Figure 5.31 shows clearly the time period that the ionic wind takes to effect the flame; it is in the order of 6ms. The effect was still easily observable with pulses of less than 6ms, in fact it could still be seen with a pulse width of 500ns which is 12,000 times less than that required to cause ionic wind effects. This means that the effects cannot be due to the ionic wind for any pulse of less than 6ms or a square wave frequency of greater than 83Hz.

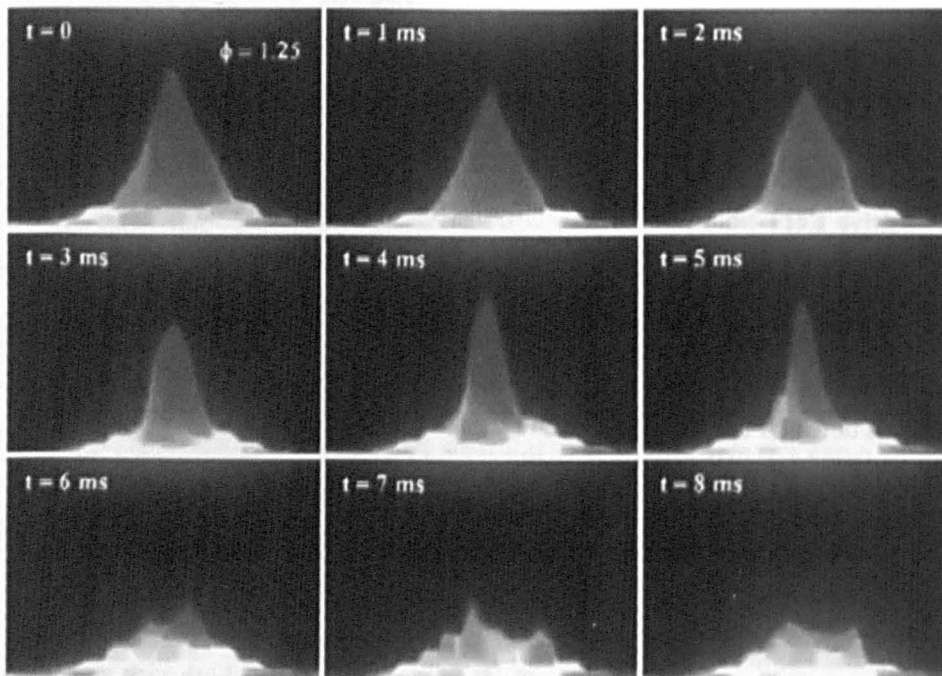


Figure 5.31 Ionic wind effect on a flame from Marcum and Ganguly [39]

The enhancement of the blow off velocity occurs for both orientations of electrodes (Figure 5.30 and Figure 5.33). However, the effect is stronger when the positive electrode is above and the earth below (Figure 5.33). It was shown in Section 2.1 that the major

ionic species were positive, while the negative species were free electrons. It has been suggested that the effects of AC fields could be due to an increase in the energy levels of electrons by the electric field [26]. When the positive electrode is above the flame the electrons would be pulled up, away from the reaction zone. Figure 5.32 shows that electrons are pulled out of the flame with frequencies of 10^6 Hz or less. This means that the electrode must be charged for 500ns to pull an electron out of the flame completely (assuming no collisions). For the frequencies used (5kHz and below) it is therefore probable that the electrons will be pulled out to the electrodes rather than being excited in the flame, unless they combine by secondary ionisation. However, ionic species and ions will not be pulled out of the flame by the frequencies used in this experiment, particularly when the reduction in speed due to collisions is taken into account. The amplitude of ionic species at 5kHz, according to Figure 5.32, is the width of the pyrolysis zone. The pyrolysis zone is within the flame and would cause the ions to be pulled back through the reaction zone, allowing more time for them to react fully. This may even allow reactions with other species that they would not normally be possible because they would not normally coexist in the same part of the flame. This is the method used by Marcum and Ganguly [39] and Wiseman et al [40] to describe the effects of an electric field on a flame. If this was the case then it would explain why the higher frequencies used in this experiment showed stronger effects as the amplitude was lower and fewer ionic species escaped to recombine at the electrodes. The description of [39] and [40] is mostly related to a DC field where it is assumed that OH is ionised and is pulled back into the preheat zone. There is a deficiency of OH in this region and the increase in the concentration of OH caused by the electric field therefore increases the reaction rate. The use of a pulse could also achieve this effect if its duration were long enough for OH to be moved the distance between the flame boundary and the preheat zone (as shown by Figure 4.30).

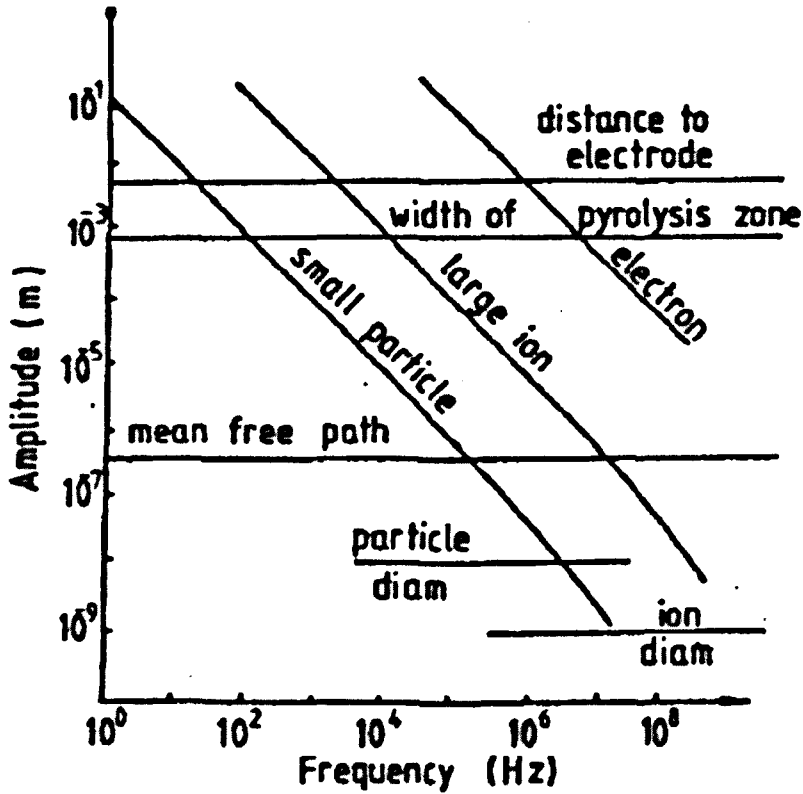
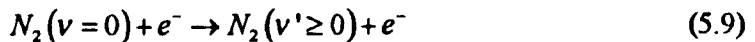


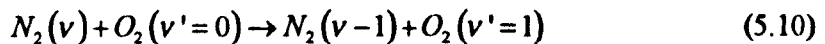
Figure 5.32 Copy of Figure 2.5. Taken from Weinberg [47]

It has also been suggested that nitrogen could be ionised by free electrons in the manor described below (from Shebeko [95]). This would allow electrons to cause the effects observed.

The field excites nitrogen particles



The excited N_2 then transfers their oscillatory energy to O_2



The excitation of O_2 increases the reaction rate of



The pace of many combustion reactions is set by this elementary reaction, page 3 [70]. There have been several other papers that have also observed the effect with N_2 and not

with other gasses [64], [75]. It also has been numerically shown that alteration of this reaction is in the correct order of magnitude to explain the flame speed increases shown experimentally [50]. Further support to this theory is given by Gulyaev et al [96] where the concentration of negative ions in the flame front is shown to decrease in the presence of N_2 but not when it is replaced with Ar.

The results of the tests conducted by Shebeko [95] were repeated by Gulyaev et al [64] with Ar used instead of N_2 and the effect of the electric field on a flame was greatly reduced. This has been further discussed in Section 2.4 and consequently will not be repeated again here. Further work is suggested to repeat the tests using a pulsed field with air replaced by an Ar/ O_2 atmosphere. This would identify the importance of N_2 for the use of pulsed fields as the tests were conducted for AC square wave forms.

This study has looked at the use of pulses as short as 500ns. However, the time between the pulses was comparatively long due to the limitations of the power supply. The effect was observable with these shorter pulse times but by the time the next pulse was applied there would have been several generations of species that would have been completely unaffected by a pulse, thus the average effect would be small. This is probably the reason why the effect is strongest when the pulse time is approximately 50% of the time between pulses (square wave). It would be expected, if the cause was due to larger ions or ionic species, that the effect would begin to decrease again as the frequency increases. This is due to the amplitude of the ions becoming smaller for higher frequencies. If the results were due to additional energy being given to the ions rather than their amplitude then the effect may not decrease as the frequency increases. Further work is needed to identify which effect is dominant.

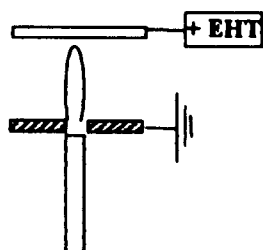


Figure 5.33 Positive EHT above

The difference between the rich and lean flames could be due to the direction the ions are pulled in compared to the flame. An image of the seed in the flame used in Chapter 6 shows the flame boundary clearly (Figure 5.34). The bright white seed at the base of the flame is before the reaction zone and the lighter seed is after the reaction (this is because some of the seed is burnt up in the reaction zone).

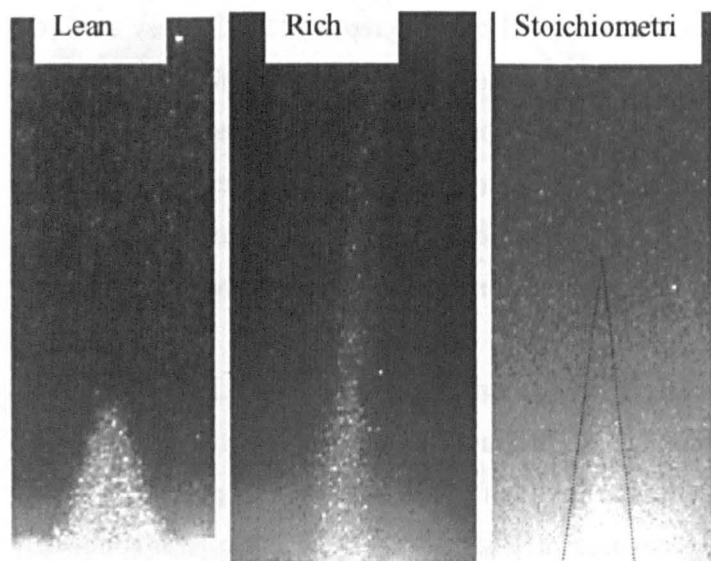


Figure 5.34 Comparison between lean, rich and stoichiometric flames

From Figure 5.34 it can be seen that the flames for the 3 different equivalence ratios are very different in size. The field however is in the same direction. This means that the field relative to the flame boundary is not the same for all of the results. For a rich flame the field will pull the ions much more parallel to the boundary but for a lean flame it will be much more perpendicular. This may have a significant difference and needs further work to clarify this. This could be conducted using the spherical burner used by Yuan et al [35] and Sher et al [91] (see number 9 in Table 2.1) as the field would always be perpendicular to the flame. The results could only be qualitatively compared due to the difficulties predicting the field strength with this orientation.

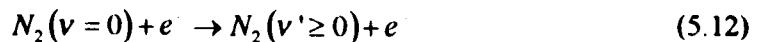
5.7 Conclusions

In this chapter it has been shown that:

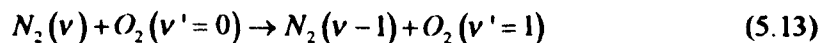
- A pulse field can increase the flammability limits of a propane flame by increasing the blow off/lift velocity
- The increase in blow off velocity is greater than the increase for a DC field
- There is an increase in flammability limits whether the positive electrode is above the flame or whether it is below the flame
- The effect is strongest when the plate below is earth and gauze above is positive
- The greatest increase in blow off/lift velocity occurs when the pulse is on for between 25% and 75% of the time
- The increase cannot be due to ionic wind effects as the pulses used are shorter than the time taken to create an ionic wind
- The effect must be due directly to chemical changes to the flame caused by excitation or greater mobility of ionic species
- The increase in flammability limits is greater for higher frequencies up to the limit of the equipment (5kHz)
- Further work needs to be conducted to discover the effect of increasing the pulse repetition frequency

Further work is required to show whether method of increasing the blow off limit is described by;

The field excites nitrogen particles



The excited N_2 then transfer their oscillatory energy to O_2



The excitation of O_2 increases the reaction rate of



or by ions being pulled into the preheat region and recombining to form OH directly.

Chapter 6 High Speed Camera Work

6.1 Particle image velocimetry (PIV)

Particle image velocimetry or PIV is a technique that gives the velocity map of a fluid in 2D. It is a powerful technique that allows a large amount of data to be processed very quickly. It relies on the simple formula of velocity being equal to distance divided by time. The movement of small particles carried in the fluid flow (known as seed) is measured between two frames taken by a high speed camera (so the time between frames is known).

The seed is illuminated by the use of a laser sheet to give a 2D view of the flow. A camera was mounted at 90° (as shown in Figure 6.1) and took two images.

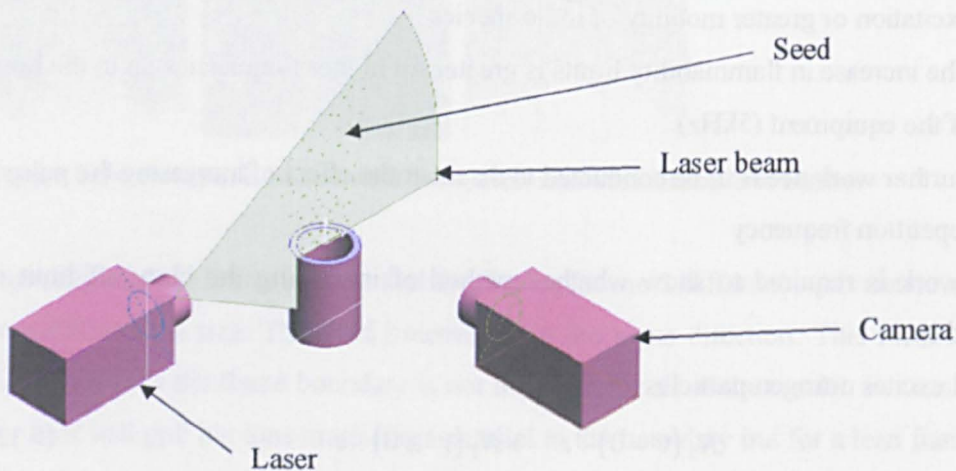


Figure 6.1 PIV set up

The laser sheet is pulsed and the timing coordinated with the camera, meaning that the exposure time and therefore brightness and sharpness of the particles can be manipulated (see Figure 6.2). The laser is so much brighter than the flame, only the particles illuminated from the laser are detected. This means that the laser can pulse at the end of

one frame and the beginning of the next. This allows a much shorter time between the images recorded than if the processing relied purely on the camera frame rate.

Time for one frame

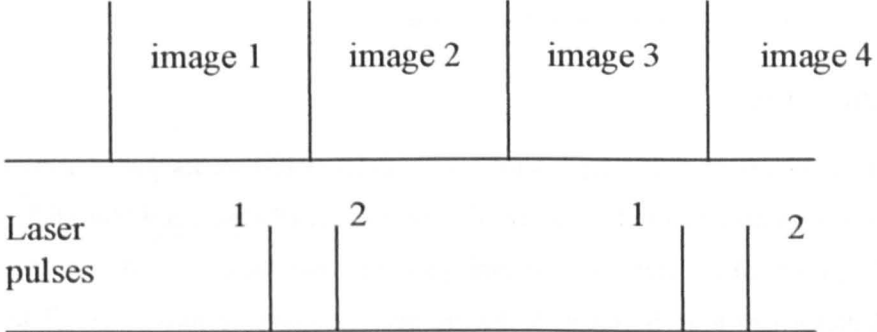


Figure 6.2 Comparison of laser pulse and frame time for camera

The two images recorded are black and white to allow easier processing (for an example see Figure 6.3).

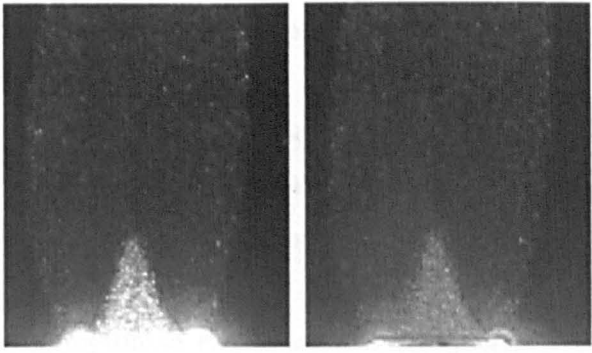


Figure 6.3 PIV images

Both of the images are split up into interrogation areas. The interrogation area is defined at the beginning of the processing by the user. The choice of interrogation area requires skilful choice. The interrogation area needs to be small enough so that it can be assumed that all the seed in a given interrogation area has the same velocity. However, it also needs to be large enough so that there are enough particles to calculate the average velocity of the interrogation area. The average velocity of all the seed in that interrogation area is found by correlating the pixel intensity with particle distances. To demonstrate this, a simplified one dimensional example can be used (Figure 6.4).

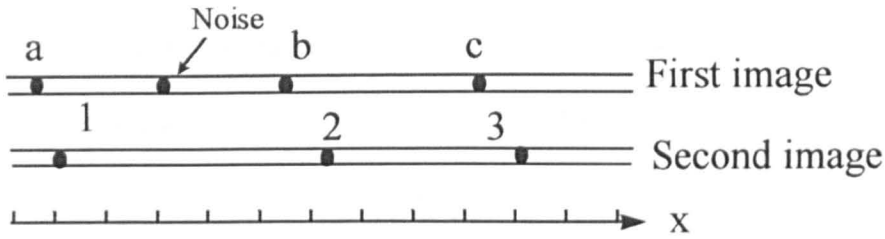


Figure 6.4 Simplified PIV

The results are made binary so that 1 represents a light patch and 0 a dark patch with no seed. Equation (6.1) can then be used. If the results for this are plotted (see Figure 6.5) a large spike will appear when there are several particles that have moved the same distance. This distance can then be taken to be the average distance moved by all the particles in that interrogation area and the velocity can be calculated.

$$R(\delta x) = \sum_{\delta x} I_1(x)I_2(x + \delta x) \quad (6.1)$$

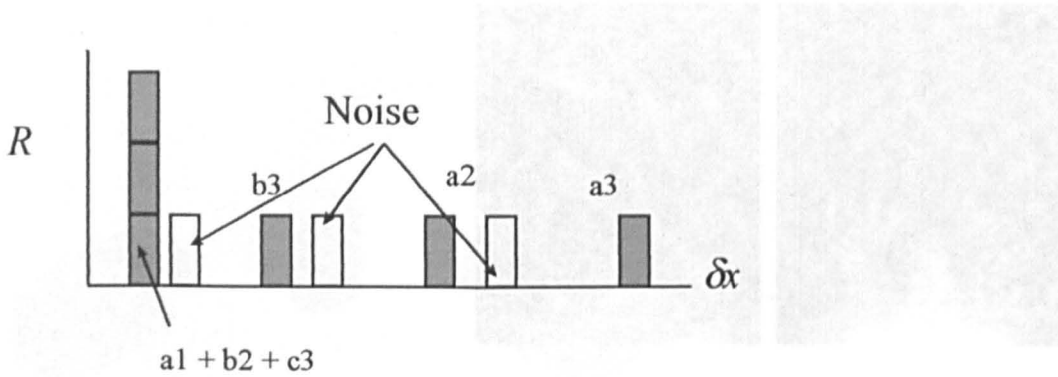


Figure 6.5 PIV calculation

As Figure 6.5 shows this also eliminates the noise. The same can be repeated for the y direction and a 3D graph can be plotted, similar to Figure 6.6, courtesy of La Vision [118].



Figure 6.6 Typical graph of particle movement from La Vision [118]

The peak can then clearly be identified and the average distance moved by the particles in that interrogation area found. The time between frames (laser pulses) is known and so the velocity can be calculated. This is then repeated for the remaining interrogation areas.

The time between the pulses can be varied for different applications. This time must be short enough to be able to identify the particle pairs but the greater the distance moved by the seed the more accurate the velocity calculation.

The resolution is dependant on the size of the interrogation area. Smaller areas give a higher resolution but require more seed. There needs to be several particles to pair within each interrogation area. Therefore the smaller the area the greater the seed density needs to be. There is a limit to the amount of seed that can be introduced into the fluid and this therefore ends up being the limiting factor.

The resolution can only be as good as one pixel as this is the method to make the data binary. However, if a Gaussian fit is applied to the data the resolution can be made greater than 1 pixel with good accuracy (see La Vision [118] and Dantec Dynamics [119] data sheets and website). Figure 6.7 shows how the distance moved (in pixels) can be

shown for an interrogation area. The Gaussian fit is then shown on top of the integer plot. This gives a resolution of greater than 1 pixel. The top image shows how allowing the image to become slightly unfocused blurs the image so a single seed is spread over several pixels, giving a stronger peak (the noise is comparatively less). The bottom image shows the larger effect of noise.

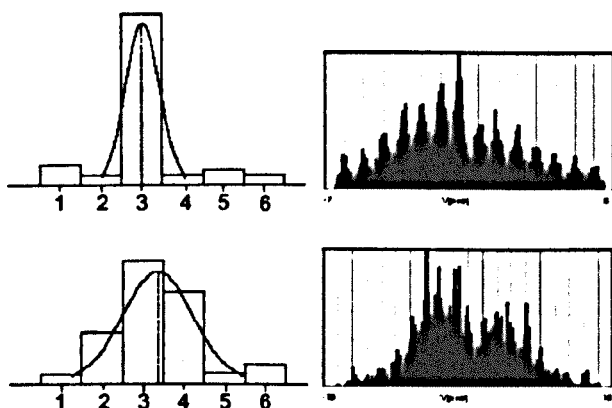


Figure 6.7 Gaussian fit of the binary data (top several pixel per particle, bottom one pixels per particle)

6.2 Seeding

6.2.1 Apparatus selection

As mentioned previously, seeding is the major factor in determining the size of the interrogation area and therefore the resolution possible in a particular situation. Seeding is also very difficult to achieve correctly. If there is not enough seed then the resolution will be too low, however, if there is too much seed then it can quench the flame or alter other burning characteristics. Introducing the seed into the air flow is also difficult. The flow rates in this experiment were small (10mg/s and 20mg/s). This means that getting the air flow to pick up seed particles is a problem. In order to achieve the correct seeding level in these experiments several types of apparatus were tested. These included a fluidised bed, liquid seeding and a variable flow rate seeding device.

The fluidised bed seeder consisted of a sealed container containing titanium dioxide powder. The air from the inlet was intended to create a fluidised bed and as it did so carry the titanium dioxide particles through the outlet to the flame. However, the small air flow could not carry the seed with it. More successful attempts were made when the titanium powder was dried before use. However, this only worked for one test and a fresh batch had to be purchased for each test.

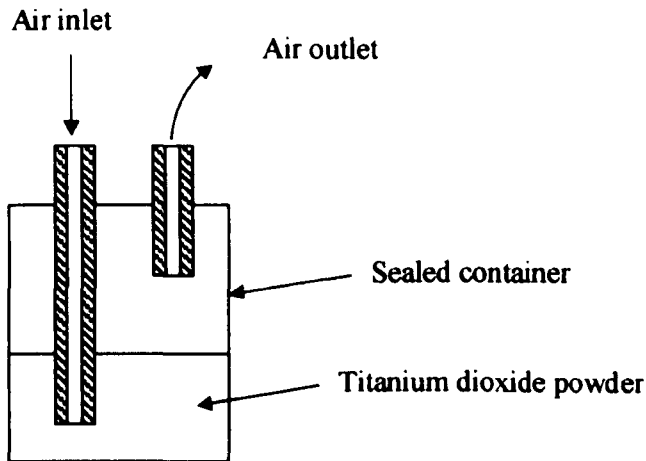
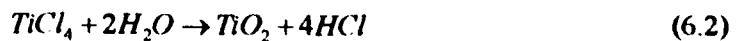
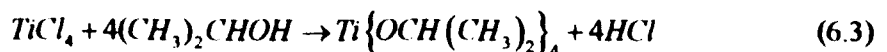


Figure 6.8 Fluidised bed seeding device

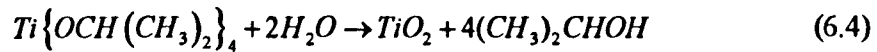
An alternative was found by the use of liquids that once exposed to water produced titanium dioxide. The two options available are titanium tetrachloride ($TiCl_4$) and titanium isopropoxide ($Ti\{OCH(CH_3)_2\}_4$). Titanium tetrachloride reacts with water as shown in equation (6.2);



This is unfavourable as when HCl is dissolved in water it forms hydrochloric acid which is dangerous. This makes handling of it difficult in laboratory conditions. Titanium isopropoxide is a derivative of titanium chloride with isopropanol as shown in reaction (6.3)



Titanium isopropoxide also reacts with water to form titanium dioxide, as shown in reaction (6.4);



The bi-product is propan-2-ol ((CH₃)₂CHOH). The experiments conducted previously used propane as the fuel. The propan-2-ol produced by the titanium isopropoxide will also combust and will provide a distortion to the results. Tests were conducted to see if the propan-2-ol altered the electrical effects of the flame, which can be seen below. The results of this will be discussed below.

However, there is a danger that if the flame flashes back into the swirler it may also be able to flashback into the seeding device due to the propan-2-ol present in the airline. In the worst case this may cause the seeding container to explode. To minimise danger from this, the seeding device was enclosed within a metal container. The holes for the fuel and air lines at the top were made large enough to vent any explosion safely away from anybody present. This would not normally be possible as the flame could not burn in either the pure propane or the air inletting the swirler. The flame would then just form at the exit of the propane inlet where it could be oxidised from the air entering the swirler.

The compressed air used in these experiments was damp enough to provide sufficient moisture to allow the reaction shown above. The titanium dioxide powder was also already airborne after formation which allowed the smaller flow rates to carry it into the flame. The set up can be seen below in Figure 6.9. The air inlet required a series of small holes at 90° to the main bore. This prevented large bubbles forming at the exit, which caused the flame to pulsate. The smaller holes allowed the air to flow through the liquid at a more constant rate by allowing a slight pressure to build up behind the exit.

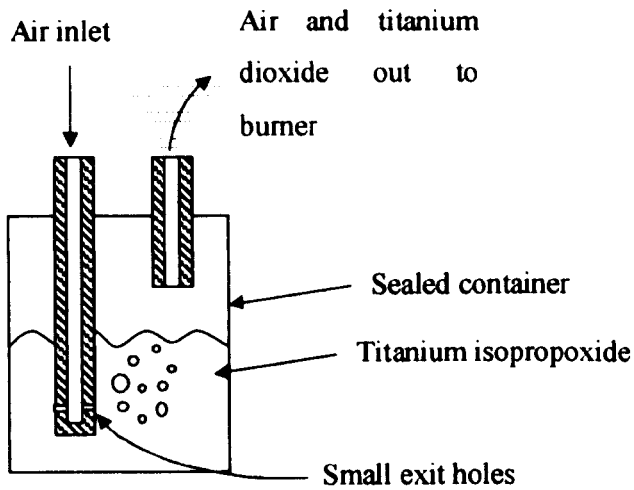


Figure 6.9 Seeding method

The difficulty with any seeding method is to achieve the correct amount of seed. Too little seed and the PIV will not be able to achieve an interrogation area small enough and too much and the seed may start to effect the flame (quenching it for example). To try and resolve this issue, the following set up was used (Figure 6.10).

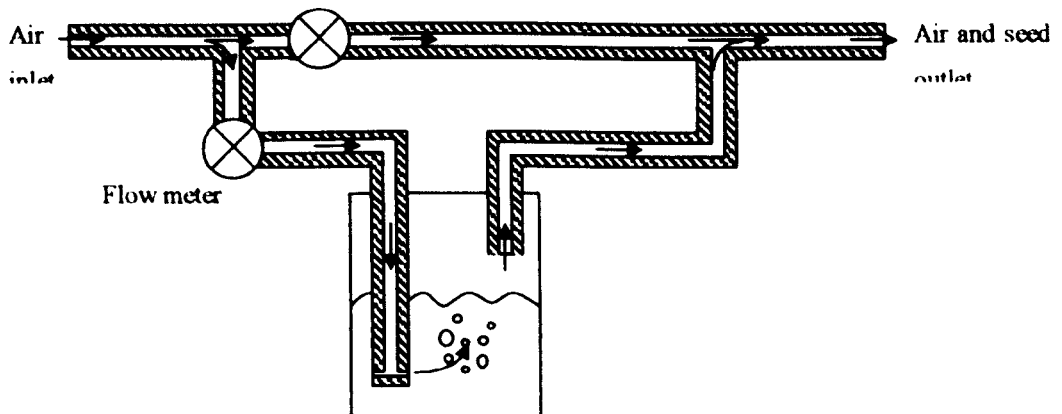


Figure 6.10 Variable air flow system

This system allowed the amount of air passing through the seed container to be varied, thus controlling the seeding rate. It was found, for the low flow rates used in this experiment, that all the air needed to be passed through the seeding device to generate sufficient seed. This meant that the variable air flow system was not required for the flow rates used in this report.

This procedure has not been widely documented and no research has been conducted to calculate the exact amount of propan-2-ol produced. This is extremely difficult to calculate due to the difficulties in predicting the amount of water vapour in the air inlet. This additional fuel will effect the equivalence ratio. However, the seeding is only being used to make the flow visible and the results shown in the previous sections do not use the results with the seeding method present. As an approximation it may be possible to assume an additional “imaginary” propane input from the titanium isopropoxide to account for the change in the equivalence ratio. This method for doing this is shown below. It is also possible that the propan-2-ol creates ions in different concentrations to those produced by propane alone. The titanium dioxide can also quench the flame if present in large enough quantities. The tests conducted in Chapter 4 have therefore been repeated with the seeding present to verify that there are no other significant effects of the small amount of propan-2-ol than to change the equivalence ratio.

Below the best fit lines of Chapter 4 have been plotted, along with the data taken with the seeding present for 10mg/s (Figure 6.11) and 20 mg/s (Figure 6.12).

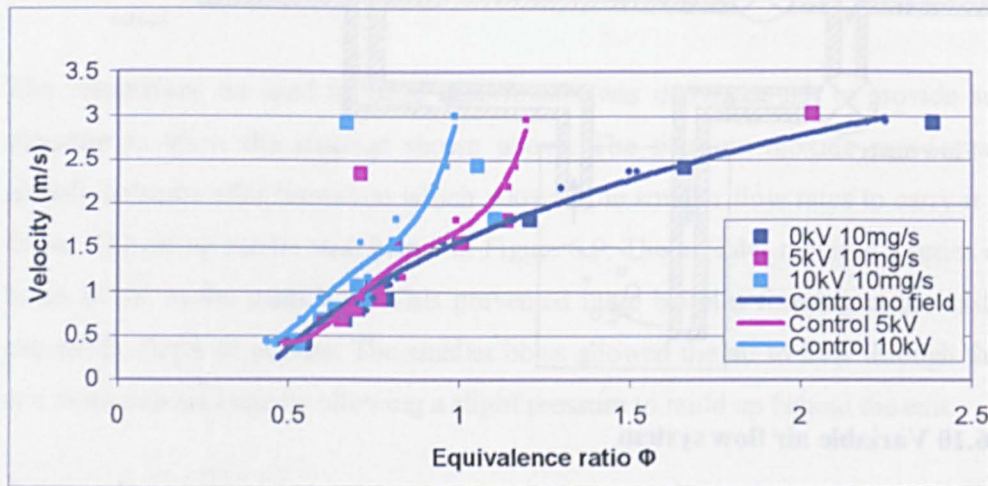


Figure 6.11 10mg/s titanium isopropoxide

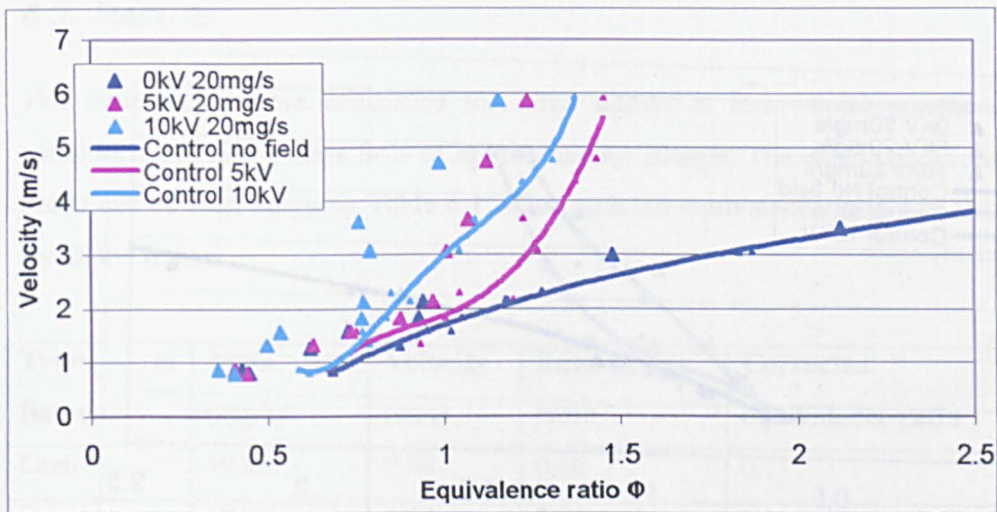


Figure 6.12 20mg/s titanium isopropoxide

Both Figure 6.11 and Figure 6.12 show that with the seeding present the data is shifted slightly to the left (the effect at low equivalence ratios is greater than at higher equivalence ratios). If a guess of the equivalent propane present is made to account for the propan-2-ol (1ml/s for the 10mg/s case and 1.5ml/s for the 20mg/s) data points follow the best fit lines from Chapter 4 very closely (see Figure 6.13 and Figure 6.14).

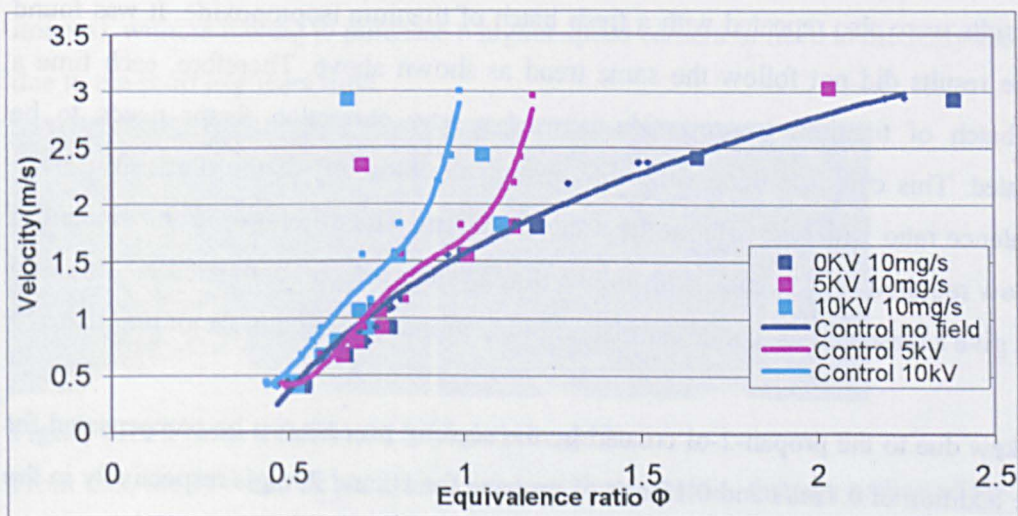


Figure 6.13 10mg/s with 1ml/s of additional fuel added

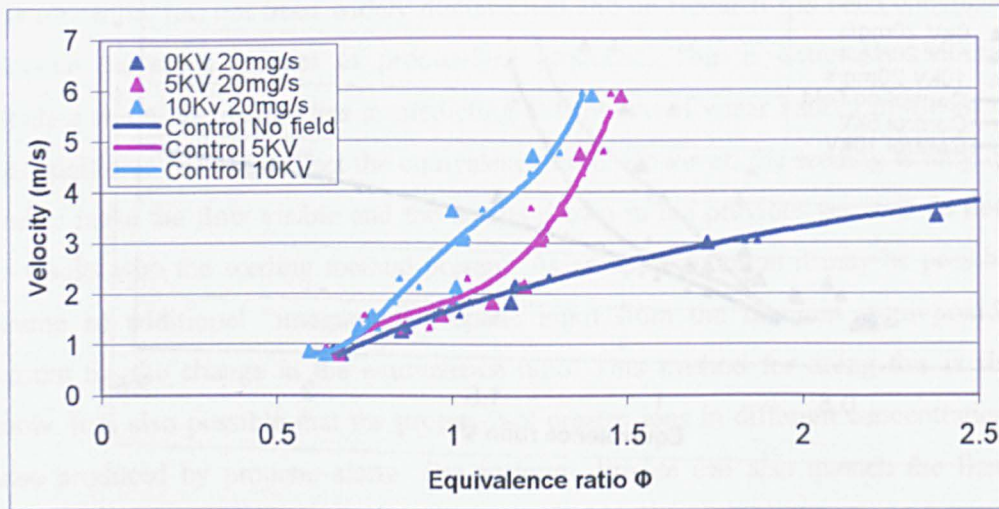


Figure 6.14 20ml/s with 0.15mg/s fuel added

The reason that a greater amount of propan-2-ol is produced by the 20mg/s case compared to the 10mg/s case is that the flow rate of air through the titanium isopropoxide is greater, therefore there is more water vapour to react with, producing a greater amount of propan-2-ol and titanium dioxide.

The results were also repeated with a fresh batch of titanium isopropoxide. It was found that the results did not follow the same trend as shown above. Therefore, each time a fresh batch of titanium isopropoxide is used a new correction factor needs to be calculated. This could be done simply by testing the blow off of the flame at a given equivalence ratio with and without the seeding present. The difference in the amount of fuel flow required at extinction with the seeding system present, compared to without it would give a reasonably accurate estimation of the propane correction factor required.

The skew due to the propan-2-ol created by the seeding process can be compensated for by the addition of 0.1ml/s and 0.15ml/s of propane for 10 and 20mg/s respectively in the calculations. This difference is not crucial as the PIV work only aims to show the results for a typical lean, stoichiometric and rich flame.

6.3 Results

The experiments were conducted for three flames at lean, stoichiometric and rich conditions. All had a mass flow of approximately 20mg/s. The exact conditions of each flame can be seen below in Table 6.1. The corrected equivalence ratio can also be seen for all the flames.

Type of flame	Mass flow (mg/s)	Velocity (m/s)	Equivalence ratio	Corrected equivalence ratio
Lean	19.83	0.88	0.46	0.71
Stoichiometric	19.97	1.58	0.86	1.1
Rich	20.43	3.12	1.64	1.88

Table 6.1 Conditions of the three flames used in the PIV work

The two images taken by the camera for zero applied field can be seen in Figure 6.15. The flame can be clearly identified (cone shape). The laser produces a pulse at the end of the first frame and another at the beginning of the second frame. In this way the images are recorded over a smaller time frame (for both the image itself and the time between the images), without having to purchase a higher speed camera or have to intensify the image due to the short exposure time.



Figure 6.15 Frame 1 (left) and 2 (right) image 7

From this, the PIV can be performed to show the velocities through a slice of the flame. The final example of this can be seen in Figure 6.16 below.

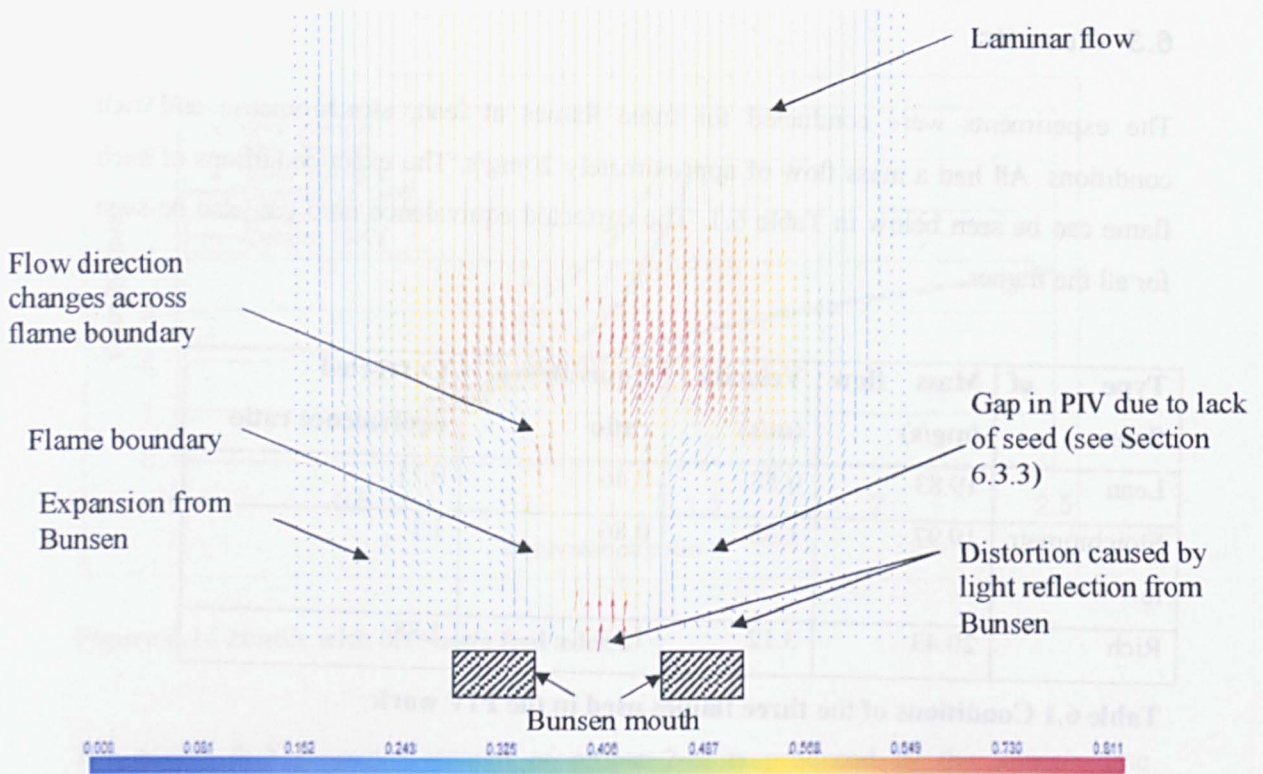


Figure 6.16 Average PIV

The scale of the arrows (colour) is shown below the PIV image. At the base of the PIV the gas flows in from the Bunsen (as indicated). The Bunsen caused light from the laser to reflect giving a false reading as shown (this is discussed further in Section 6.3.3 and can be seen in Figure 6.18). The gas expands out from the Bunsen mouth, particularly sharply at the flame boundary. Immediately beyond this there is a gap in the PIV. This is due to either the seed being burnt up in the flame front or its reflective properties being altered when it is hot. From the flame front the flow continues to expand until it reaches an even, laminar velocity.

The PIV shown above is the average of 100 processed “moving average” PIV images. The following Sections (6.3.1 and 6.3.2) show how the raw black and white images are processed to attain the average shown in Figure 6.16.

6.3.1 Adaptive correlation

From these two images the PIV can be developed as explained above. A technique called adaptive correlation has been employed to refine the interrogation area.

Adaptive correlation is a method that automatically selects the smallest interrogation area possible for the seed available. A large initial interrogation area is used. The results from this initial guess are used to form a new smaller interrogation area. This is repeated until the smallest interrogation area to produce realistic results is found.

The results for this can be seen in Figure 6.17. The results are colour and size coded meaning that faster velocities are large red arrows, while slower velocities are small blue arrows. From Figure 6.17 it can be seen that there are several vectors that appear to be incorrect as they are in different directions to the surrounding flow. This is often the case for PIV work and a technique called “moving average” has been employed to try and identify these outlying vectors and remove them (see Section 6.3.2 for more details).

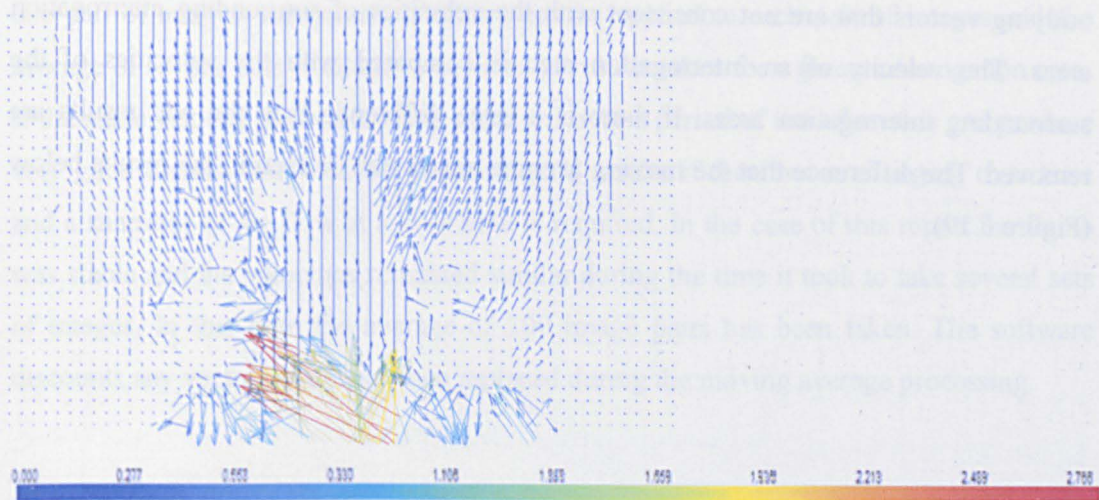


Figure 6.17 Adaptive correlation

The gap around the flame boundary, where the flow expands, is probably due to the flame reaction zone being here and the seed being consumed in the combustion process.

If the PIV results are shown on top of the image (Figure 6.18) then it can be seen that the gap is in and immediately after the reaction zone.

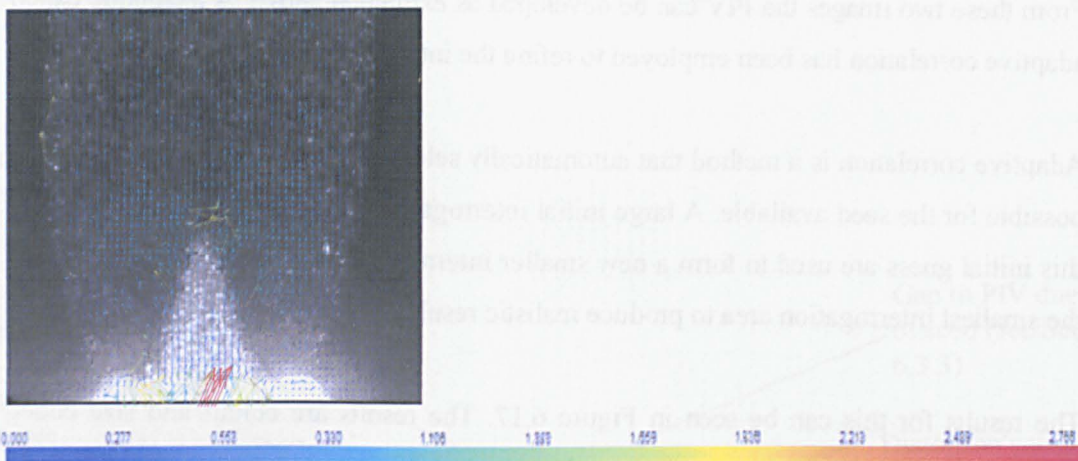


Figure 6.18 Adaptive correlation on top of image

6.3.2 Moving Average

This method uses the results from the adaptive correlation and tries to eliminate the outlying vectors that are not consistent with the velocities of surrounding interrogation areas. The velocity of an interrogation area is compared with the velocities of the surrounding interrogation areas. If there is a large difference then the odd results are removed. The difference that the moving average makes can be seen in the results below (Figure 6.19).

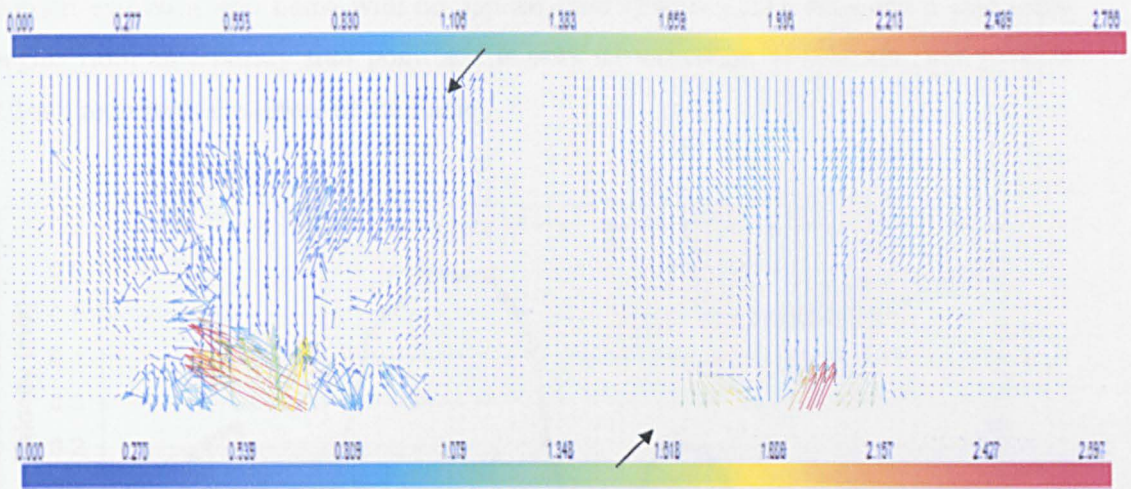


Figure 6.19 Adaptive correlation (left) and moving average (right)

As the results show the moving average removes the outlying vectors. However, this processing is only for one pair of images. The software can be set up to take more than one pair of images. Adaptive correlation can be applied to each pair of images and the average of several sets of adaptive correlation results taken for a given interrogation area. If the same velocity pattern is being observed over a period of time then this can produce very good results. This will not produce good results if the flow is changing over time and a snapshot of the flow at a give time is required. In the case of this report the flame was stable and the velocities remained similar during the time it took to take several sets of images. In this case the average of 100 image pairs has been taken. The software discounts any vectors that have been replaced during the moving average processing.

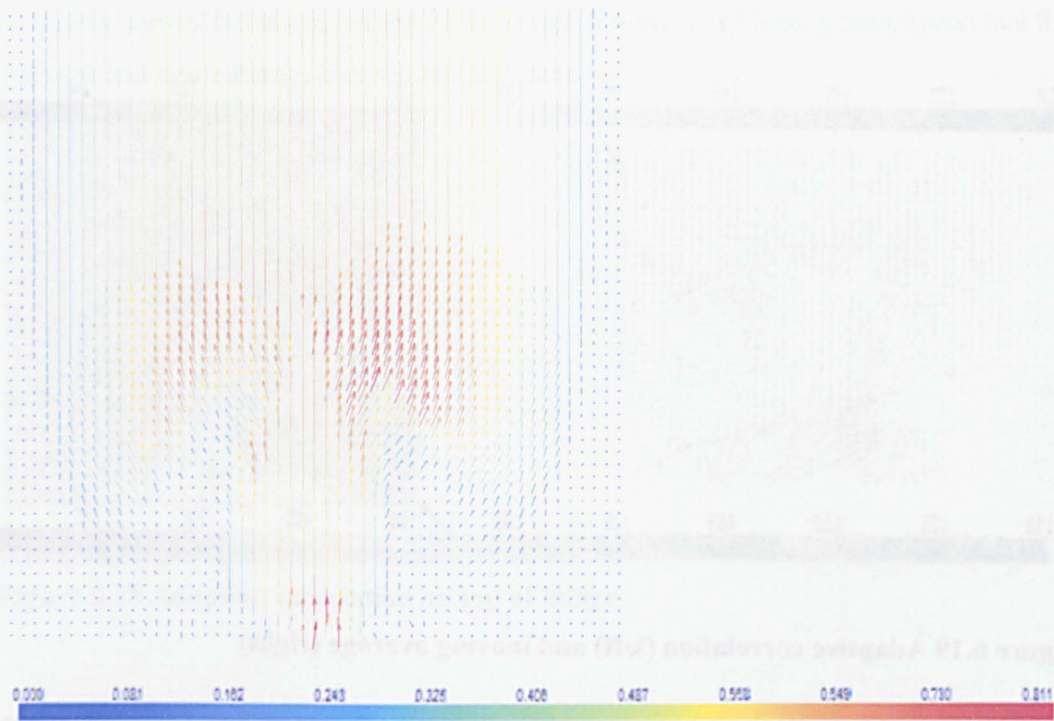


Figure 6.20 Average

The colours only show the difference in scale for each PIV, not the absolute velocity therefore the colours cannot be compared between PIV figures.

6.3.3 Velocity profile and regions of poor seeding

In order to compare the PIV to the experimental results of Chapter 4 and Chapter 5, the velocity of the flow at the Bunsen exit could be measured. It can be seen in Figure 6.18 that there is a region of high reflection from the Bunsen at the base of the image. The PIV in this area shows large velocities that do not seem realistic. However, the larger vectors at the base of the image can be explained by the reflection of the Bunsen tube distorting the PIV signal.

From the calculations performed in Chapter 4 and Chapter 5 the velocity at the exit was predicted to be 0.89m/s at a mass flow of 20mg/s. The velocity at the exit is not readable in the PIV due to the reflections from the burner, but just above the burner the velocity

was approximately 0.6m/s. This can be seen from the velocity profile 11mm from the Bunsen exit on a lean flame with no applied field (Figure 6.21). Note the x axis scale begins from an arbitrary start point and is only an indication of position. The peak at 2.3mm represents the centre of the flame.

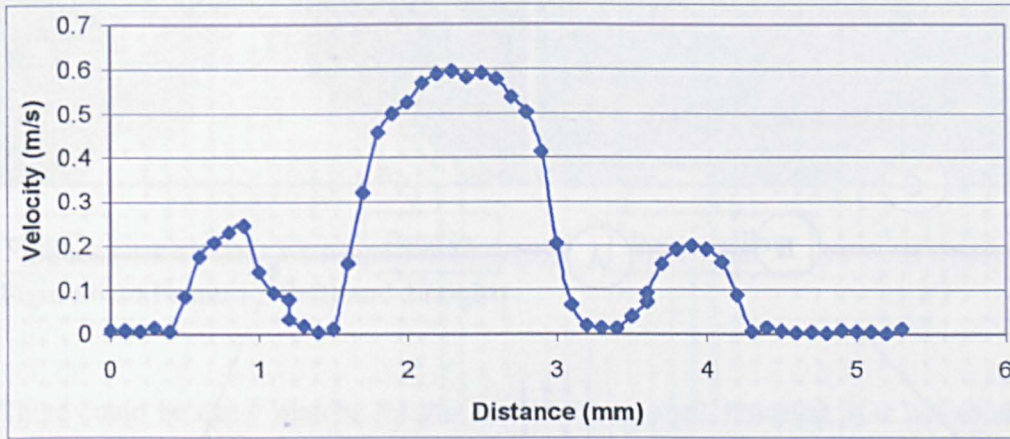


Figure 6.21 Velocity profile 11mm above Bunsen nozzle

In Figure 6.21 three peaks can be seen. This is due to a poor PIV signal in the regions between 0.8-1.8mm and 2.9-3.9mm. This can be seen from the average PIV in Figure 6.22 below, marked “B”.



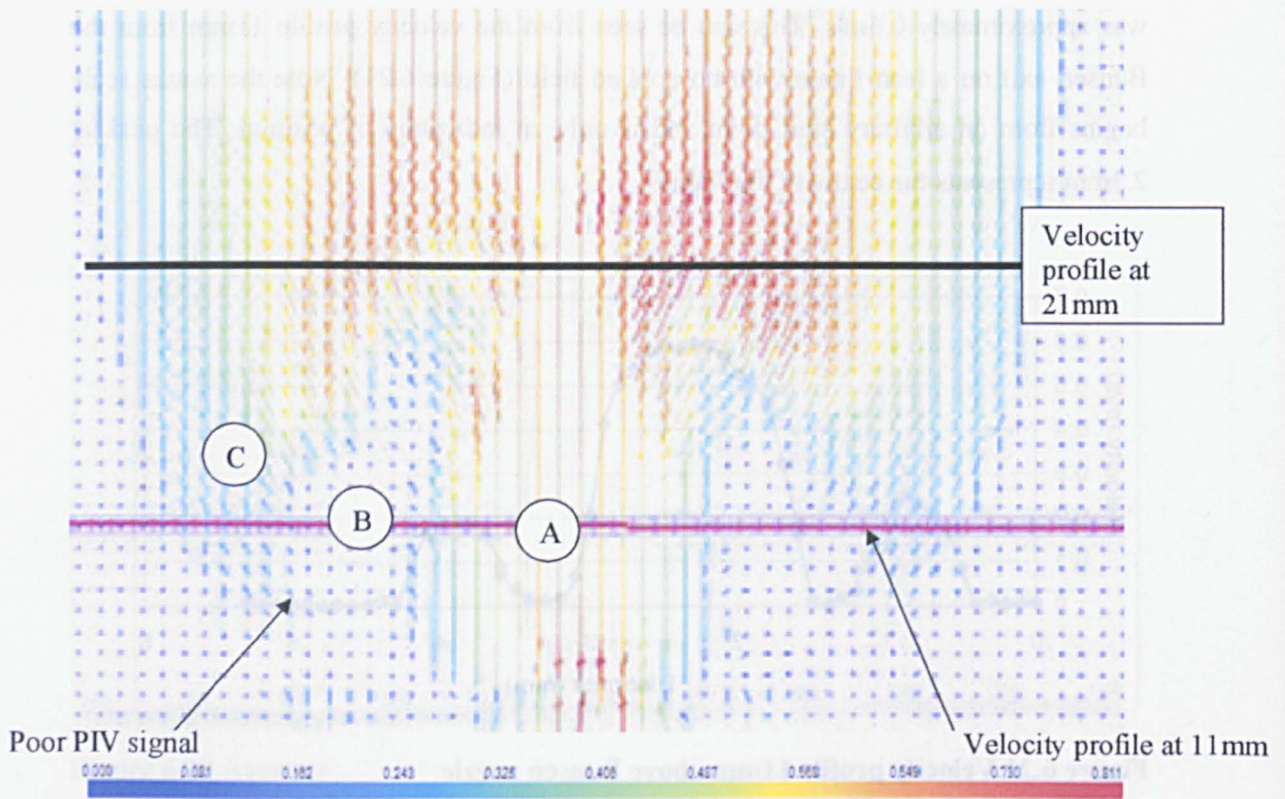


Figure 6.22 Average showing line analysed

In Figure 6.22 there is a region where there is no PIV (region “B”). This can be seen in Figure 6.23 as the area immediately surrounding the sides of the flame.

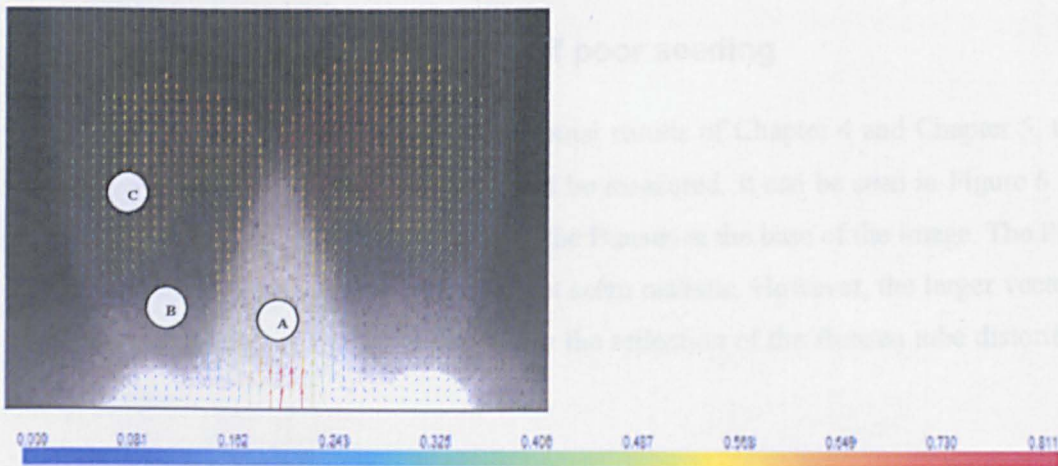


Figure 6.23 PIV superimposed on top of image

The reason for the lack of PIV in this region is due to a lack of seed (as Figure 6.24 shows). The region where there is no PIV signal seems to have very little seed present.

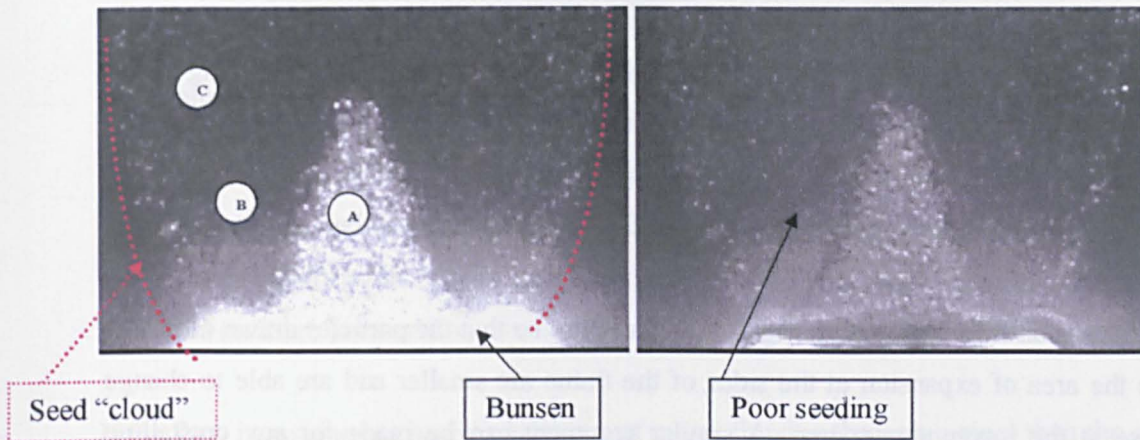


Figure 6.24 Frames 1 (left) and 2 (right)

There could be many reasons for this containing no seed, however, it is not so easy to explain why this seed reappears (region “C”). There are two possible explanations for why this is occurring;

1. Air entrainment (fresh air will not contain seed) and recirculation of flame gases which contain seed
2. Poor reflection from seed

Both of these explanations have problems. Air entrainment would seem like the obvious explanation. However, in order for the seed to reappear in region “C” there must be a recirculation of air from “A” over the top of region “B” into region “C”. If this was the case then the recirculation would be visible in the PIV, shown in Figure 6.22. The PIV vectors do not support this theory.

The other possibility is that the seed loses some of its refractive properties in this region. It has been shown that titanium dioxide experiences a phase change (from anatase to rutile) where it loses its refractive properties between 100 and 400°C [120], [121] and then turn back again as it cools. The problem with this argument is that it would be expected that this phase change occurs in all areas surrounding the flame. This does not happen as there is still sufficient seed at the top of the flame for the PIV to be calculated.

The region above the flame is also the hottest and it would be expected that the seed more readily changes phase in this region. It may be that a signal is still achieved because there is much more seed in this region as it is directly in the flow path. Figure 6.24 does support this argument as there does seem to be the same region of lower seeding above the flame as there is to the sides. There has also been suggestion that the phase change occurs in smaller particles at a lower temperature than for larger particles [120]; this may explain the results. The lighter, smaller particles are more likely to be drawn to the sides as they are easier to move and the larger particles will tend to flow straight upwards as the expansion flow is not as strong. It may therefore be that the particles drawn outwards into the area of expansion at the sides of the flame are smaller and are able to change phase at the lower temperature. A similar argument can be made for any crystalline changes to the seed. Smaller particles will change structure more readily than larger ones. These crystalline changes, which can be caused by temperature changes, also change the refractive properties of titanium dioxide [121].

Figure 6.24 also supports this argument as the seed “cloud” does not seem to be distorted by air entrainment in region “B”. The seed appears to expand out evenly from the Bunsen mouth, indicating that no significant air entrainment is occurring. If this is the case then the velocity profile should look more like Figure 6.25 than Figure 6.21.

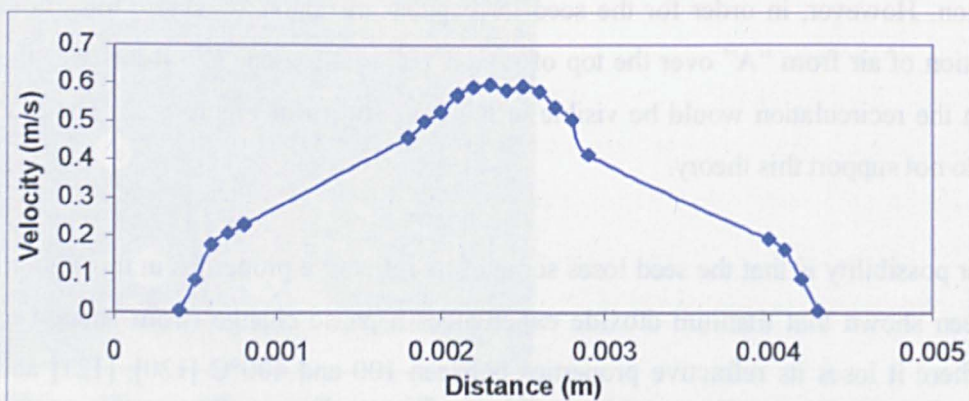


Figure 6.25 Estimated velocity profile for regions where seed is deficient, 11mm above Bunsen

Calculation of the flow rates from the velocity profile supports the second argument;

The volumetric flow rate (\dot{V}) is given by;

$$\dot{V} = vA \tag{6.5}$$

where,

v = velocity ($v = f(r)$)

A = Area (in three dimensions)

If the flow is assumed to be cylindrical (as if it was flowing through a pipe) then the area of a thin slice (width dr) can be given by

$$A = 2\pi r dr \tag{6.6}$$

As dr tends to 0 then the volumetric flow rate between the centreline (r_0) and the outside radius (r_d) can be given by;

$$\int_{r_0}^{r_d} f(r) \times 2\pi r dr \tag{6.7}$$

This can be solved by Simpson's rule (trapezium rule) for the two velocity profiles. The volumetric flow rate can be converted into the mass flow rate by multiplying it by the density. It is reasonable to assume that the density is that of air (the flame is lean and the flow rate of air is much greater than that of propane). The velocity profile from Figure 6.21 gives a mass flow of 12.2mg/s. The velocity profile shown in Figure 6.25 gives a mass flow of 19mg/s. The flow rate measured experimentally was 20mg/s. The lower mass flow rate could be easily accounted for by the underestimate of the velocity fit of Figure 6.25. Figure 6.26 shows that the profile slightly further from the Bunsen is much broader at the top and more curved, rather than the straight line estimated in Figure 6.25. The inclusion of the additional mass of propane would also increase the mass flow rate calculation.

The flow rate is further developed at 21mm above the Bunsen and is not effected by the loss of PIV. Additional air will have been entrained by this point. The calculated flow

rate for this profile is 27mg/s. This seems realistic when it is compared with the profile at 11 mm above the Bunsen (see Figure 6.26).

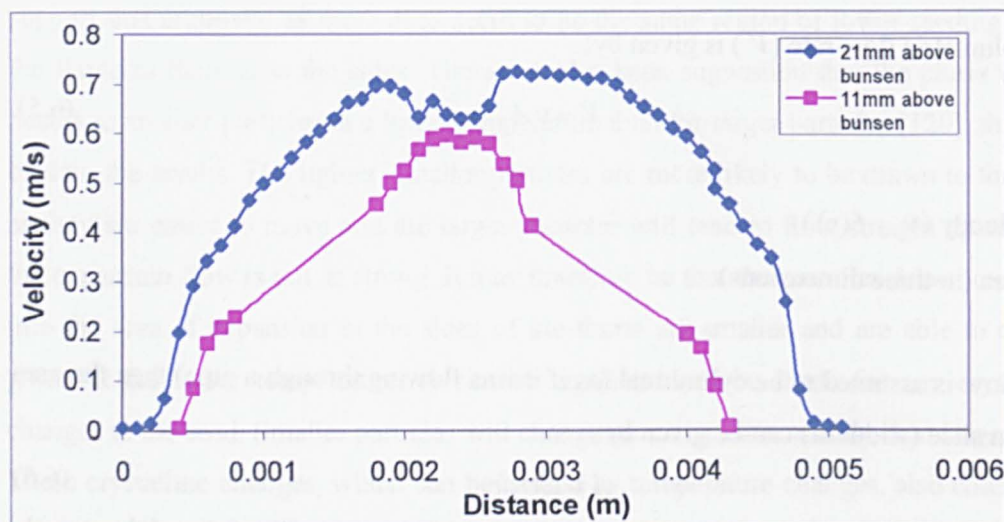


Figure 6.26 Comparison of the velocity profiles 11mm and 21mm above the Bunsen

It can be concluded that the likely cause for the reduction in seed is a drop in the refractive index of the titanium dioxide particles due to either a phase or crystalline structure change. However, further work is required to confirm this. The mass flow readings from the experimental data are also confirmed by the measurements taken from the PIV.

The results for rich flames showed even greater distortion due to this seeding problem (Figure 6.27). Stoichiometric flames were so distorted it was not even possible to generate any PIV in the flame region (Figure 6.28). This supports the phase change argument as the higher temperatures in stoichiometric flames will increase the amount of titanium dioxide which transforms from the anatase phase to the rutile phase, or the number of particles which change to their crystalline structure. The PIV for stoichiometric flames has therefore not been included in this report. However, the results can be found in Appendix 3, along with additional pictures of the results that have not been used.

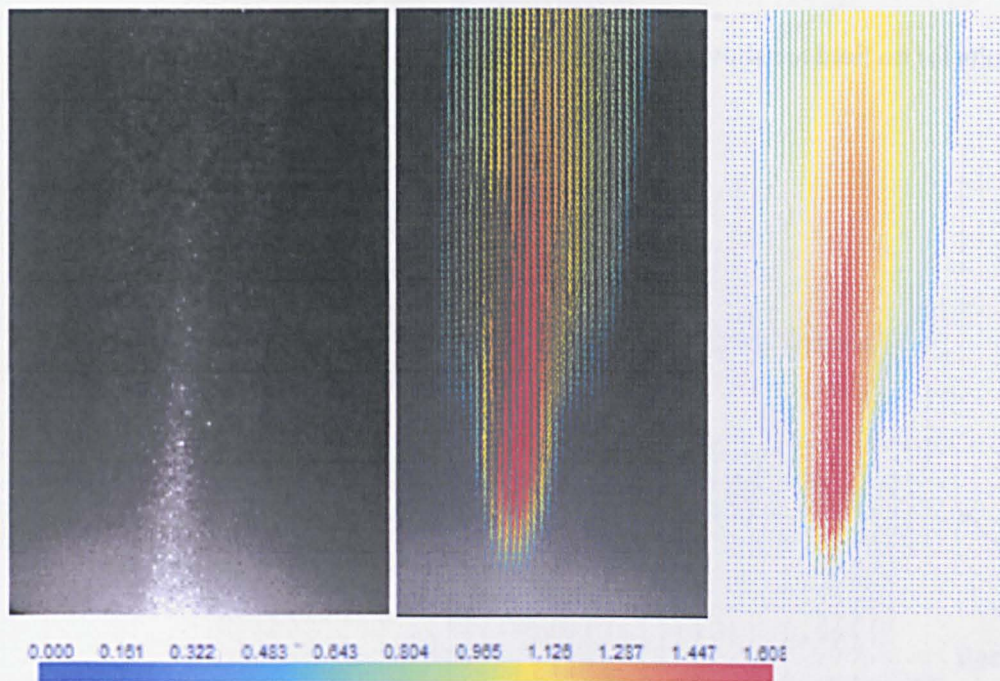


Figure 6.27 Rich flame image and average PIV

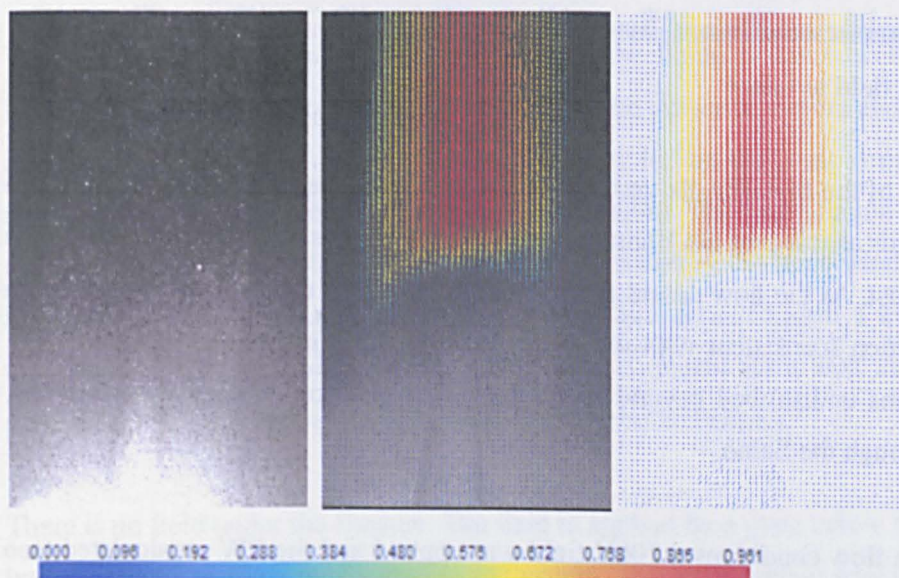


Figure 6.28 Stoichiometric flame, flame image (left), average PIV superimposed on top of image (centre) and PIV alone (right)

6.3.4 Comparison of PIV with and without an applied field

The results for no field are shown below (Figure 6.29).

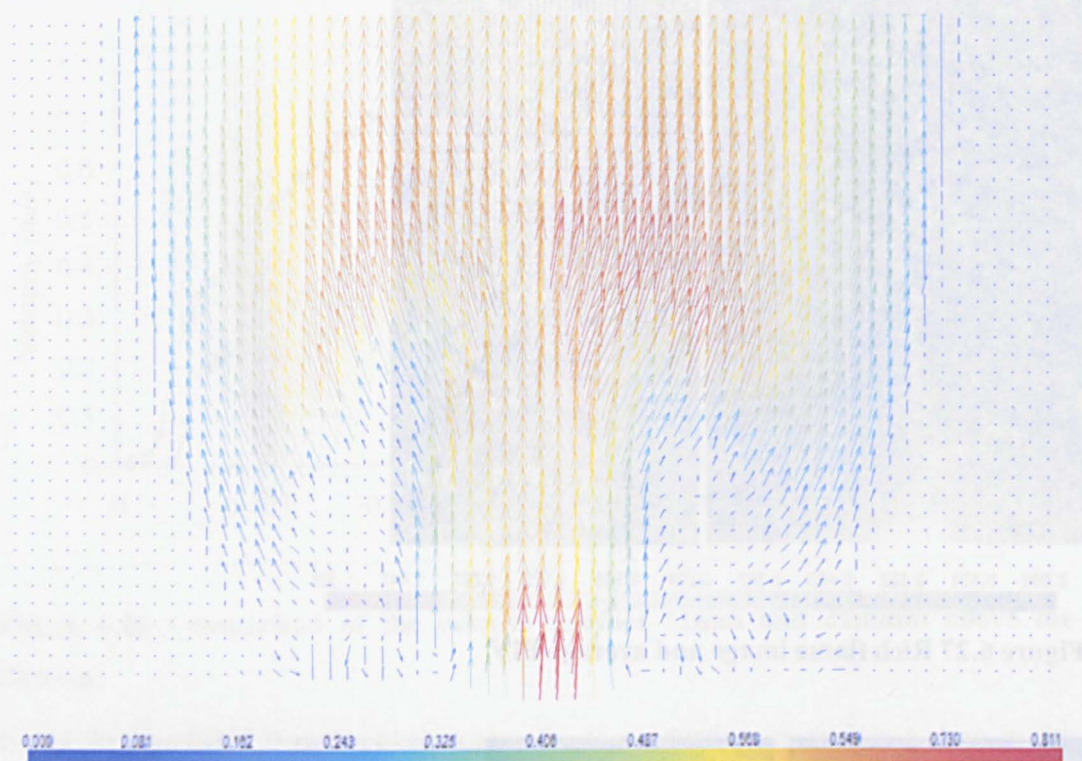


Figure 6.29 No field average

The main body of the flow travels vertically up from the Bunsen mouth but some of the flow also expands as it leaves the Bunsen. The premixed flow is lean, allowing this entire region to combust. As the flow passes through the boundary of the flame it experiences a change in direction (consistent with the theory presented in Griffiths and Bamard [1]). The flow remains undisturbed beyond this region. Laminar flow vertically is observed, after passing through the flame.

Under the same flow conditions a 10kV field was applied and the PIV recalculated (see Figure 6.30)

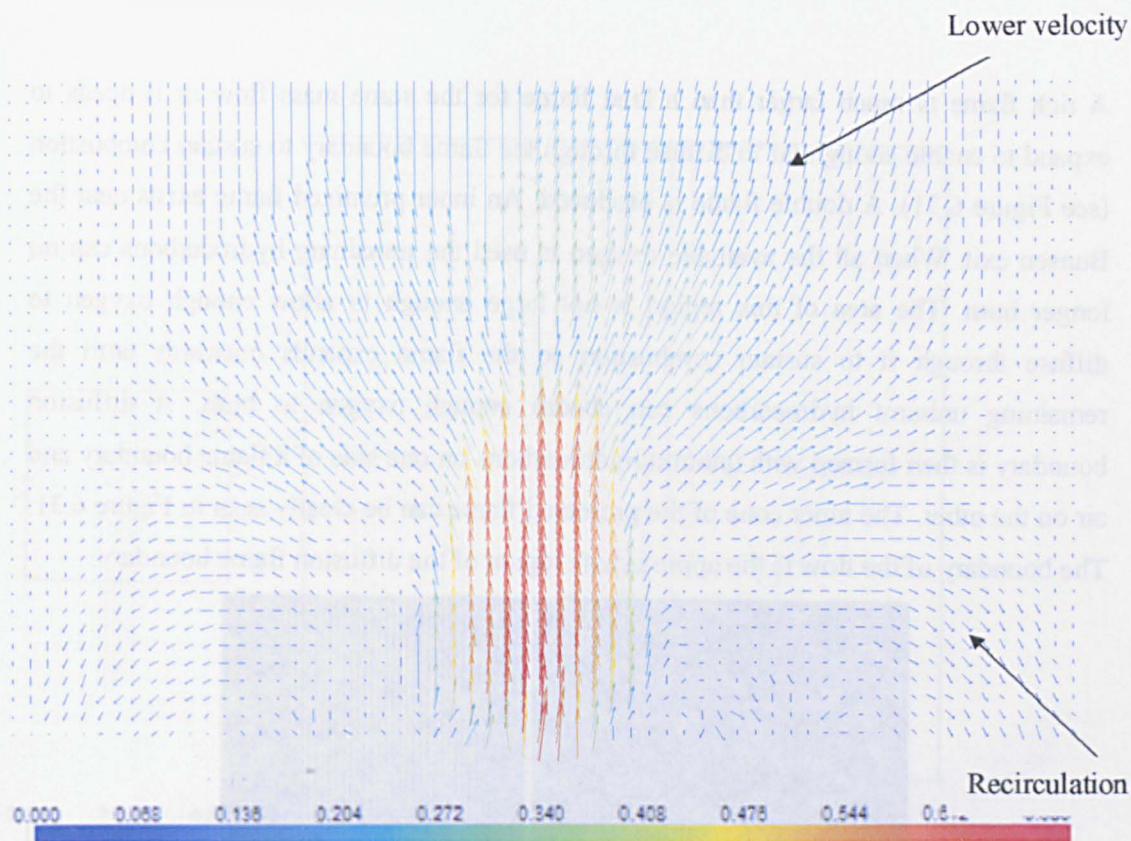


Figure 6.30 Average of 10kV lean

The velocity after the flow has passed through the flame is dramatically different for 10kV than for no field. For no field (Figure 6.29) the velocities before and after the flame are similar. For the 10kV (Figure 6.30) the velocity before the flame is much larger than after it (notice the difference in the colour distribution). The recirculation of the flow can also be seen in Figure 6.30 (10kV). This effect is caused by the ionic wind as described in Section 2.2.1. The increase in blow off velocity observed in Chapter 4 was explained by the effect of the ionic wind and the results above clearly show that the ionic wind is present and strongly resisting the upwards flow from the Bunsen.

There is no field under the Bunsen. The field is applied by a plate below the flame with a hole cut into it to allow the Bunsen to fit through. This may explain why the recirculation is stronger to the sides than to the middle.

A rich flame is much larger than a lean flame for the same mass flow as it needs to expand to enable enough air to diffuse through the flame boundary to sustain combustion (see Figure 6.31). A double flame is produced. An inner premixed flame exists near the Bunsen exit. When all the available oxygen is used the remaining hydrocarbons can no longer burn. The area of this region is not large enough to allow enough oxygen to diffuse through it to sustain combustion so the flame expands outwards until the remaining unburnt hydrocarbons can absorb enough oxygen to burn. A diffusion boundary is then formed with unburnt hydrocarbons on one side of a flame boundary and air on the other. The inner cone of the premixed flame can be clearly seen in Figure 6.31. The boundary of the flow is the approximate region of the diffusion flame boundary.

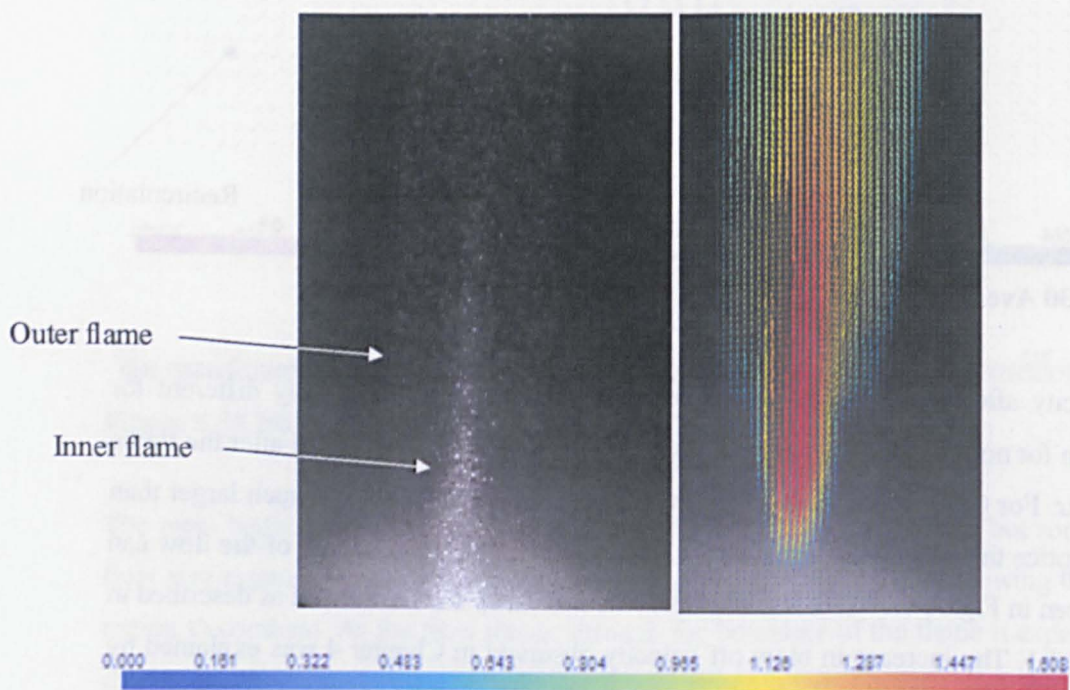


Figure 6.31 Rich flame image and average PIV

As mentioned previously the seed was either burnt up or became less refractive, preventing PIV to be measured at the base of the flame. There were also significant light reflections from either the plate below the flame (electrode) or the Bunsen to prevent the PIV being calculated at the Bunsen exit (this can be seen in Figure 6.31).

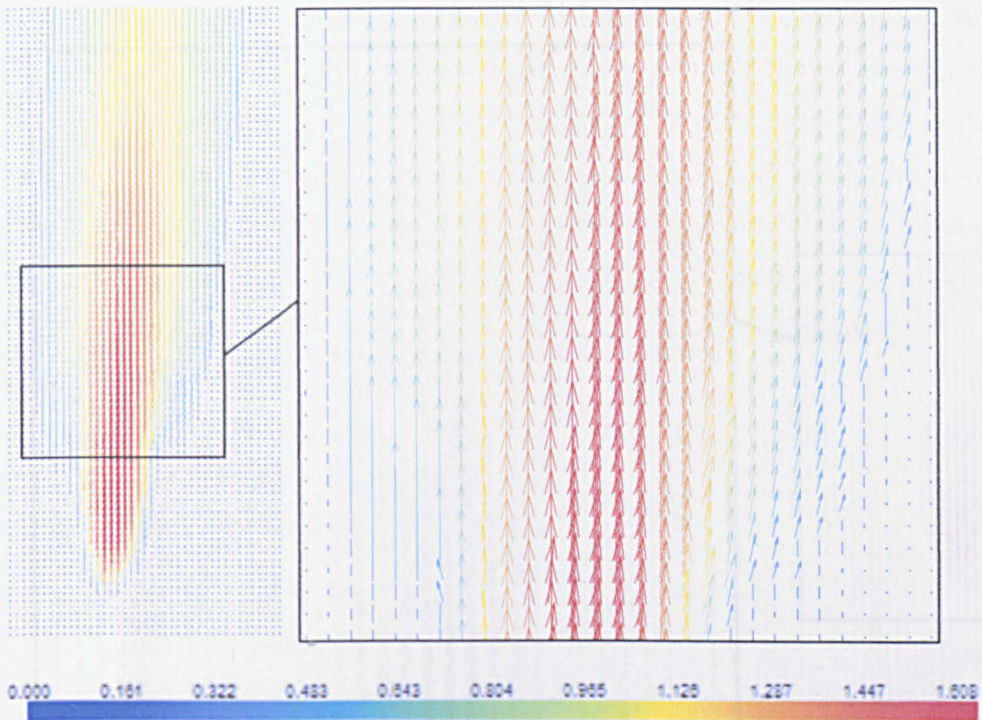


Figure 6.32 Rich flame, no applied field (expansion on right of area marked)

The results for 10kV can be seen below in Figure 6.33.

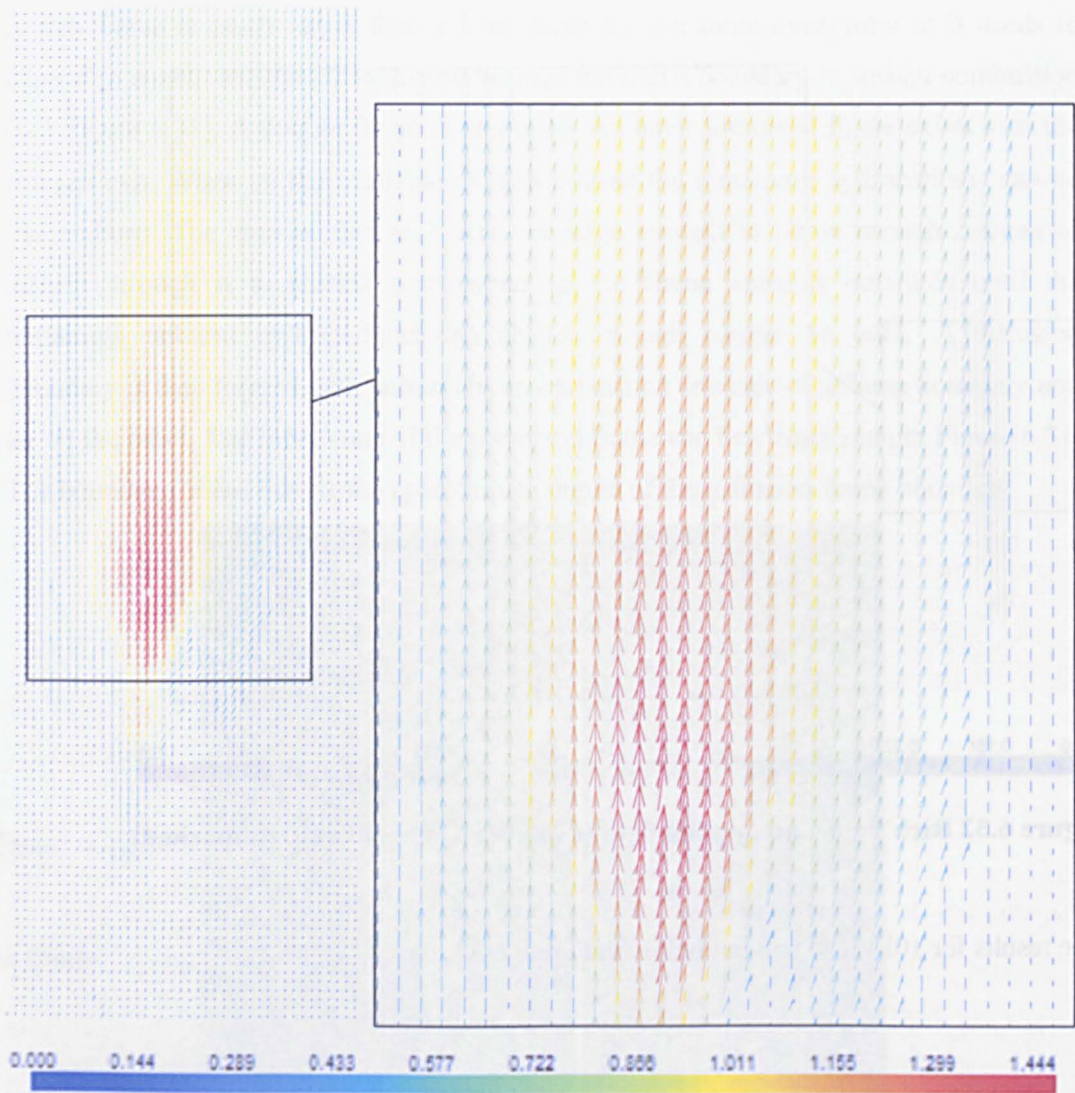


Figure 6.33 Rich flame 10kV applied field

The flow pattern does seem to be very similar. Due to the size of the rich flame the effect is spread over a much larger region. This makes comparisons of the PIV very difficult to see. However it can be seen that the velocity of the flame with an applied field is much less (maximum of 1.44m/s compared to 1.6m/s) and that less of the flow is at the maximum velocity. The flame also appears to widen slightly. This can be more easily seen when the two PIV are shown together (see Figure 6.34).

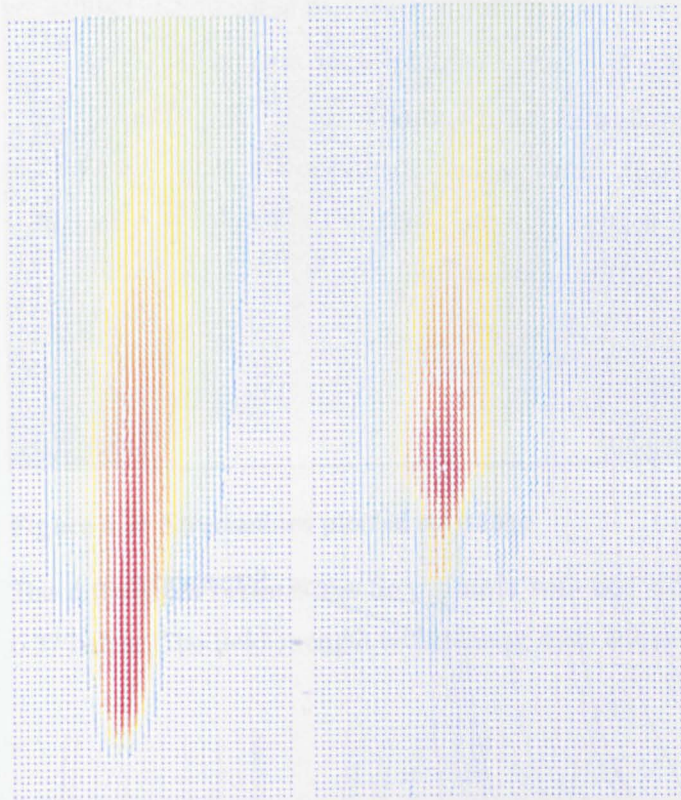


Figure 6.34 No field (left) compared to 10kV (right)

Less PIV seems possible on the 10kV sample. This could be due to higher temperatures causing more seed to burn up or reduce its refractive index. The results for the rich flame are more easily visualised by the use of streamlines, shown in Section 6.3.5.

6.3.5 Streamlines

A stream line represents a line that has no mass flow across it. The use of streamlines can show the difference between two flows visually. The formula for creating streamlines is based on the potential flow theory (an example of how they are formed can be found in Massy and Ward-Smith [122]). This theory assumes that the flow is inviscid, incompressible and 2-dimensional. For the flow rates used in the PIV analysed in this case the assumptions are reasonable;

- The flow can be considered to be inviscid as the viscous shear forces in the flow should be negligible compared to pressure and inertia forces as the flow is laminar
- The Mach number is low, so the flow can be considered incompressible.
- The flow is 2D (shown by particle tracking in Section 6.4).

The base of the PIV model is “seeded” with imaginary particles. The path of each of these particles is then traced through the PIV system. This can be seen by looking at a streamline map superimposed onto the PIV image (see Figure 6.35).

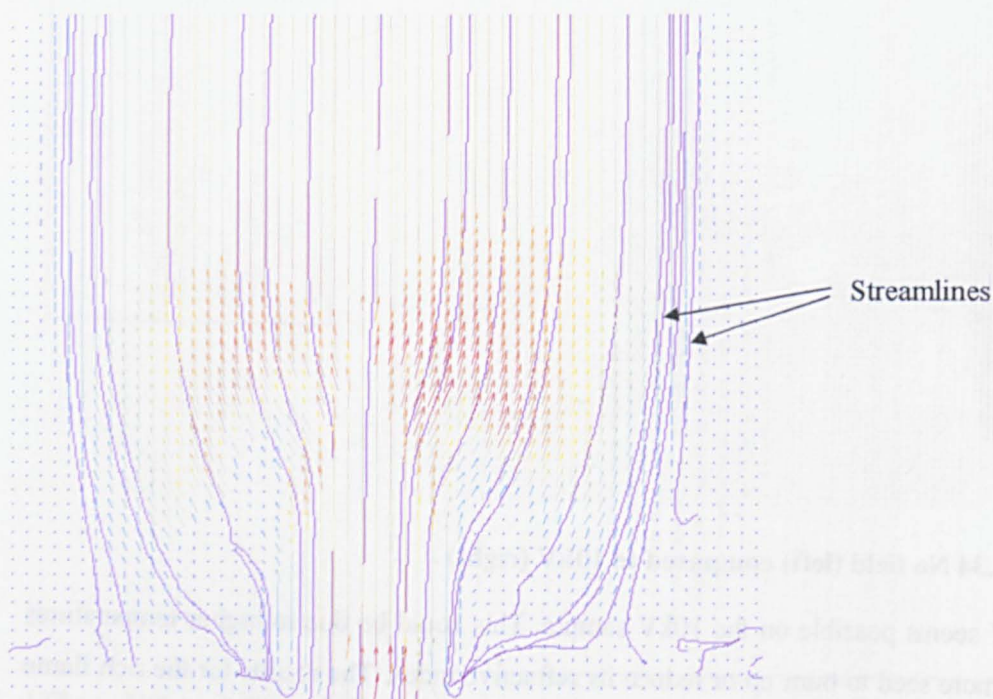


Figure 6.35 Streamline superimposed on top of PIV for a lean flame with no applied field

The results can also be shown on the image (Figure 6.36). The change in flow as it exits the flame can be seen very clearly.

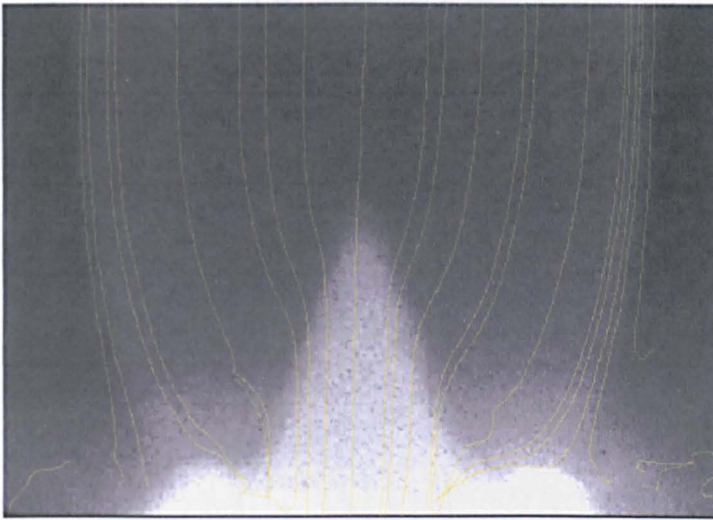


Figure 6.36 Streamlines plotted on image

The differences between the flow pattern with and without a field are shown in Figure 6.37 below. The field strength is increasing from left to right.



Figure 6.37 Streamlines no field, 5kV and 10kV

The widening of the flame is clearly seen. The recirculation of the flow on the outside of the flame is also visible in the 10kV streamline. The results clearly show that an aerodynamic force is acting on the flame. This aerodynamic force is enough to cause the changes that have been observed by DC fields shown in Chapter 4 and discussed in Section 2.4.

Although the results for rich flames are not as conclusive, the flame does appear to widen when a field is present (see Figure 6.38).



Figure 6.38 Comparison of rich flame no field, 5kV and 10kV (left to right)

6.3.6 Ionic wind

The vector maps with and without an applied field in Section 6.3.4 can be compared to show the ionic wind and how it is distributed through the flame. The vector map for the no field case has been subtracted from the applied voltage case for a lean flame and for a rich flame.

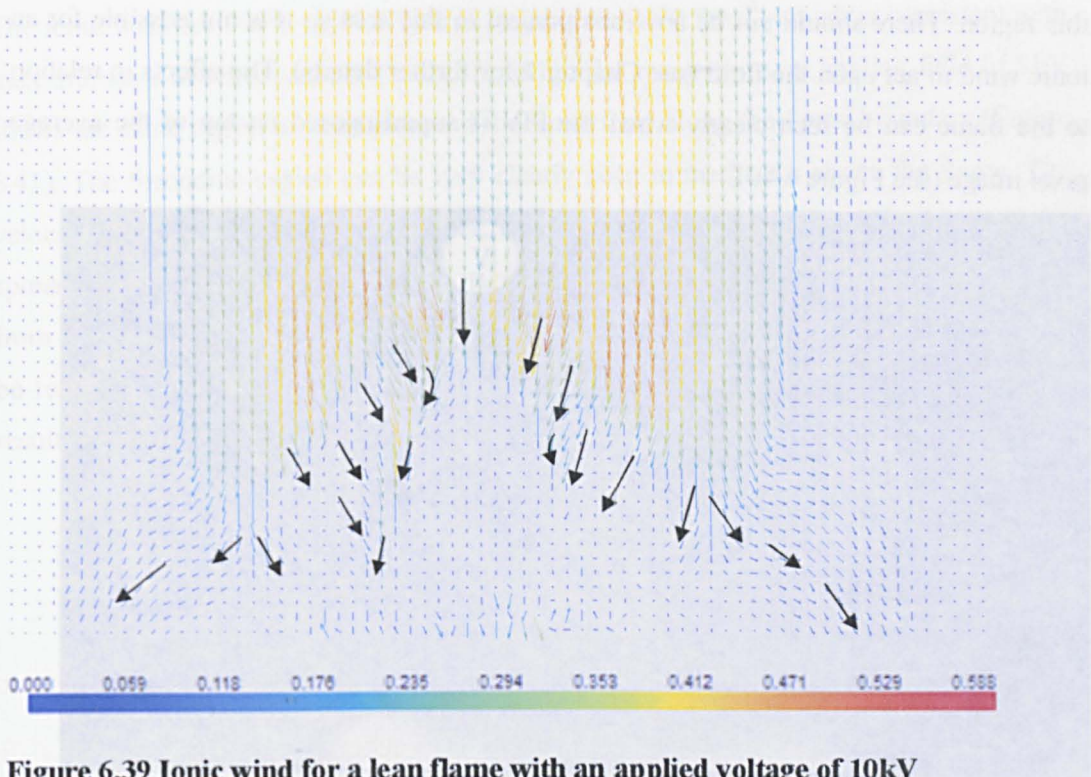


Figure 6.39 Ionic wind for a lean flame with an applied voltage of 10kV

The flame again shows the areas of missing seed. The black arrows have been superimposed on a larger scale to show the estimated position of the ionic wind, particularly in the region where the seeding is sparse. There is a strong downwards velocity just above the flame region. The ionic wind appears to counter the flow velocity directly rather than simply being pulled towards the electrode (at the base). This is unexpected as it would seem logical that the ionic wind is directed towards the electrode which is causing it, not counter to the flow. The counter flow velocity then begins to run perpendicular to the flame front. There are areas where this is not clear to see as this is also the area where the seeding is sparse and very little PIV has been obtainable. As the ionic wind reaches the base of the flame it spreads out. This could be due to the presence of the solid plate below the flame which prevents the downwards force from propagating. To the top of the image there is an evenly distributed downwards velocity. This is probably caused by the reduction in the downstream velocity of the flow due to the ionic wind effects surrounding the flame, rather than the presence of the ionic wind itself in

this region. There should not be any ions present in this area so it is not possible for an ionic wind to act upon the fluid (see Chapter 2 for further details). The effects in relation to the flame can be seen clearly when the PIV is superimposed on top of the average pixel image (see Figure 6.40).

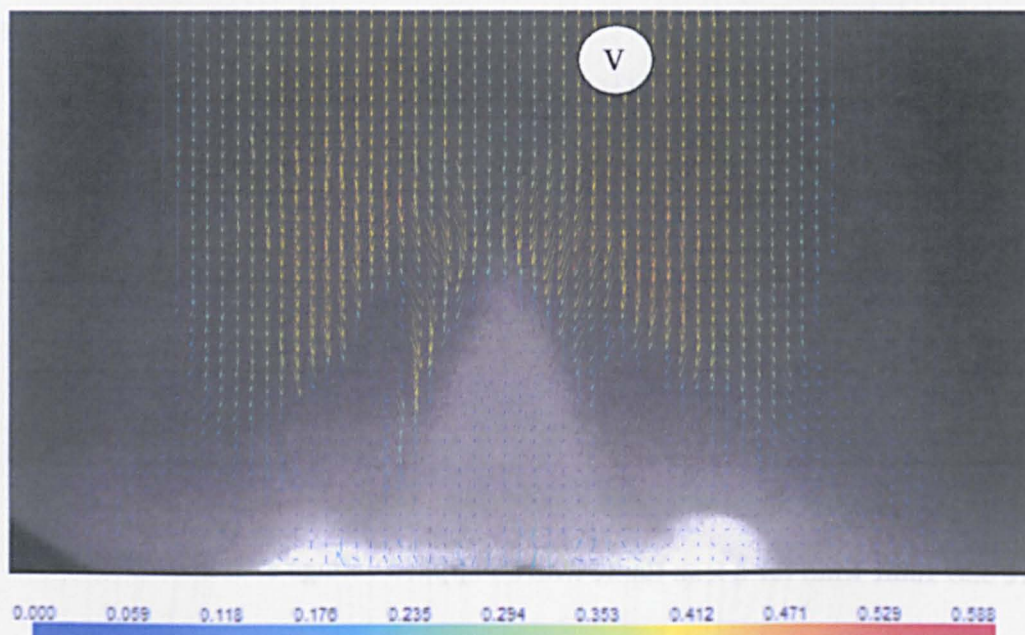


Figure 6.40 Ionic wind in a 10kV lean flame

As mentioned above the areas of uniform velocity above the flame (marked region “V”) are purely a result of the ionic wind effects caused surrounding the flame and are not the ionic wind itself. The most interesting point to note is that the ionic wind does not form inside the premixed cone. The ionic wind forms after the premixed zone. It acts vertically down towards until it reaches the flame front where it runs along the flame boundary. This means that the ionic wind is being created predominantly by the movement of the downstream ions. From other work these ions have been measured to be almost entirely H_3O^+ (see Section 2.1 for further details). This means that the ionic wind will be made up of the hot post combustion products and could be used to recirculate them to enhance complete combustion or to aid soot oxidation. This is also supported by the most abundant ion found in flames being H_3O^+ which is found in the later combustion region.

The ionic wind for 10kV applied field is in the order of 0.5ms^{-1} , which is consistent with measurements of other authors [21], [37], [41]. The result from an applied field of 5kV shows the same region of formation and the same flow along the flame boundary (Figure 6.41). The formation region can be very clearly seen immediately above the flame. The velocity seems to be of the same order, at approximately 0.5 to 0.6ms^{-1} . However the spread at the base of the flame is not visible. This could be due to a lower pressure effect from the ionic wind as the field is weaker. The vectors at the Bunsen exit are not likely to be real as this is in the region where the light reflections from the Bunsen distort the results (as mentioned in Section 6.3.3).

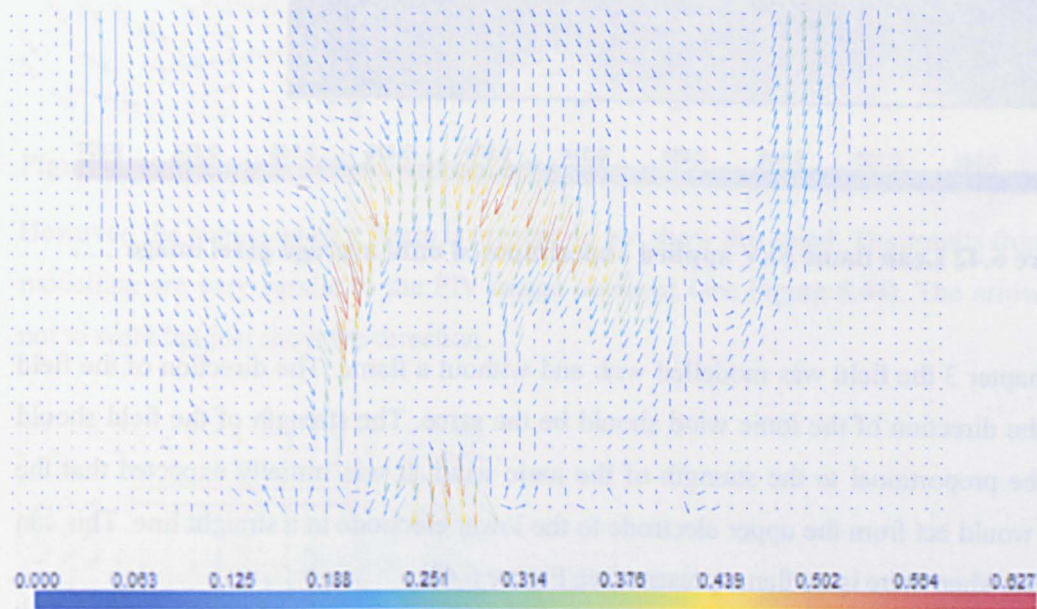


Figure 6.41 Lean flame 5kV applied

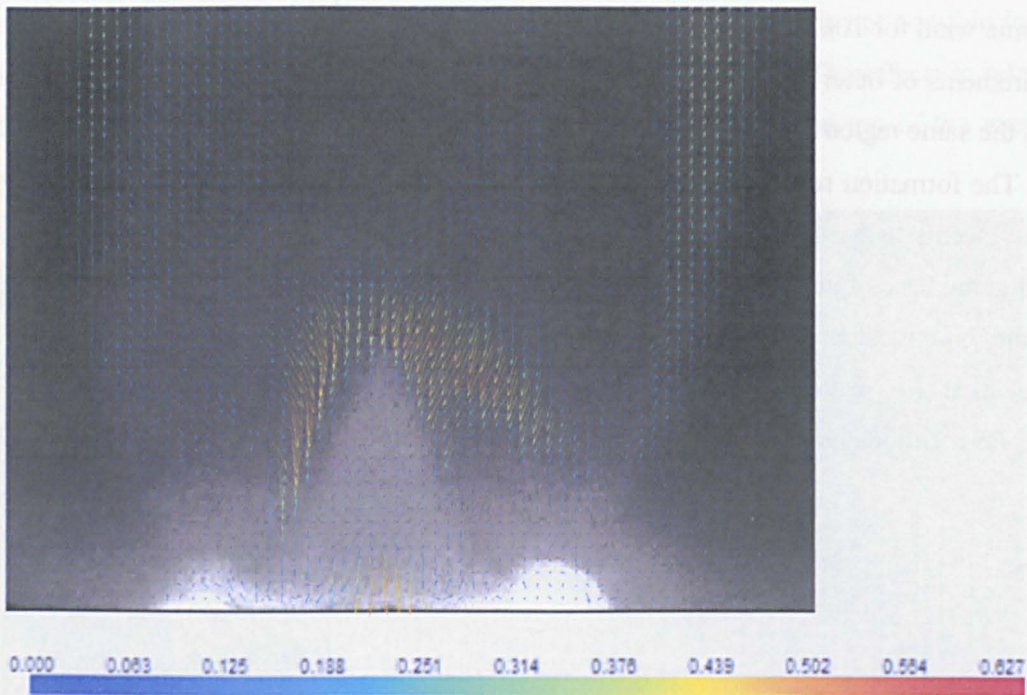


Figure 6.42 Lean flame 5kV applied superimposed onto average pixel image

In Chapter 3 the field was modelled with and without a flame. The direction of the field and the direction of the ionic wind should be the same. The strength of the field should also be proportional to the strength of the ionic wind. It was initially expected that the field would act from the upper electrode to the lower electrode in a straight line. This can be seen when there is no flame present (see Figure 6.43).

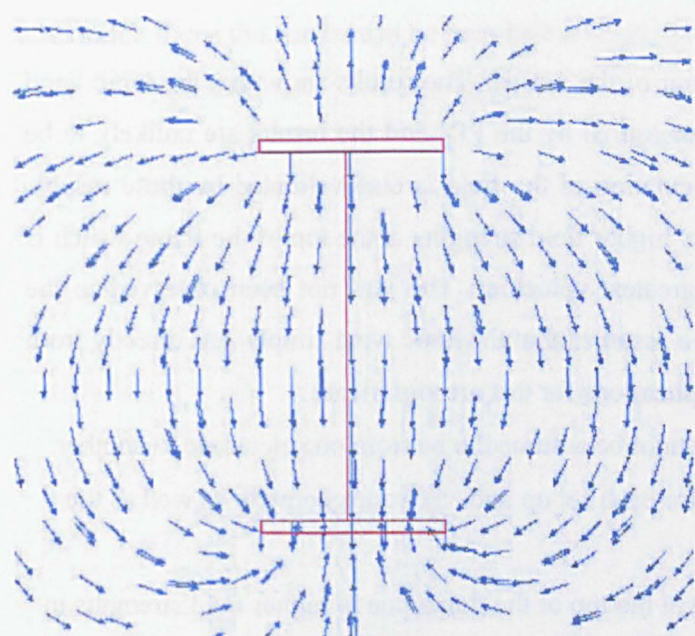


Figure 6.43 Direction of field without a flame

However, the results when a flame is present do not show this trend. The results from this modelling are very similar to the PIV image obtained (see Figure 6.44). The arrows are not to scale but just show the direction.

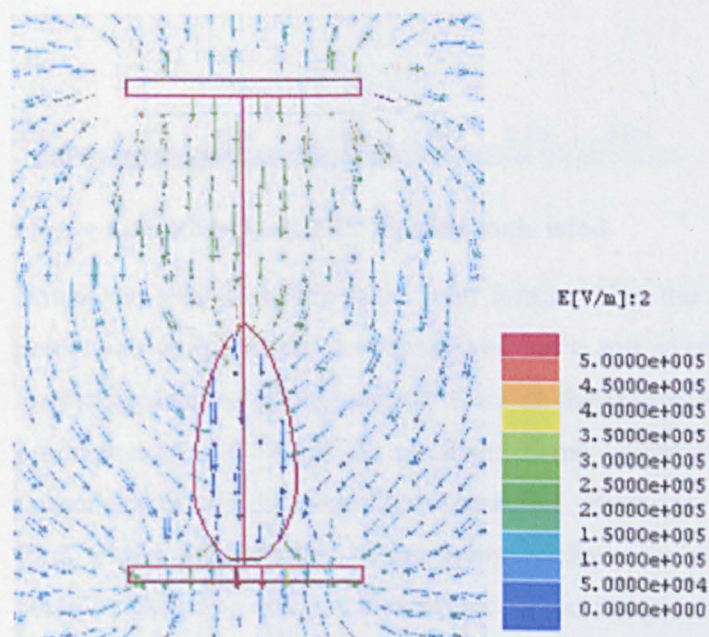
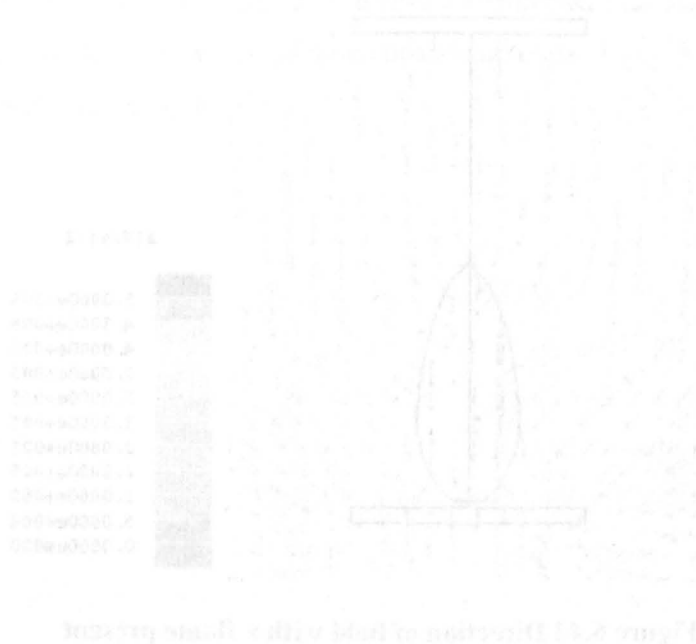


Figure 6.44 Direction of field with a flame present

The colour chart refers to the colour of the arrows. The results show that the ionic wind should be acting in the direction measured by the PIV and the results are unlikely to be due to calculation errors. The calculation of the field is also validated by these results. The results of the model also show higher field strengths at the top of the flame which is also where the PIV showed the greatest velocities. This has not been observed in the literature and all other authors have assumed that the ionic wind simply acts directly from one electrode to the other. The implications for this are significant.

- The ionic wind direction cannot be assumed to be from one electrode to another.
- The ionic wind will differ for each set up and electrode geometry as well as the flame geometry
- The ionic wind is strongest at the top of the flame due to higher field strengths in this region
- The type of ionic wind shown in the above figures will greatly enhance the residence times, allowing more complete combustion
- This type of ionic wind will also increase the recirculation of hot combustion products which should heat the incoming gasses and therefore increase the reaction rate



With a rich flame the results can be seen below (Figure 6.45).

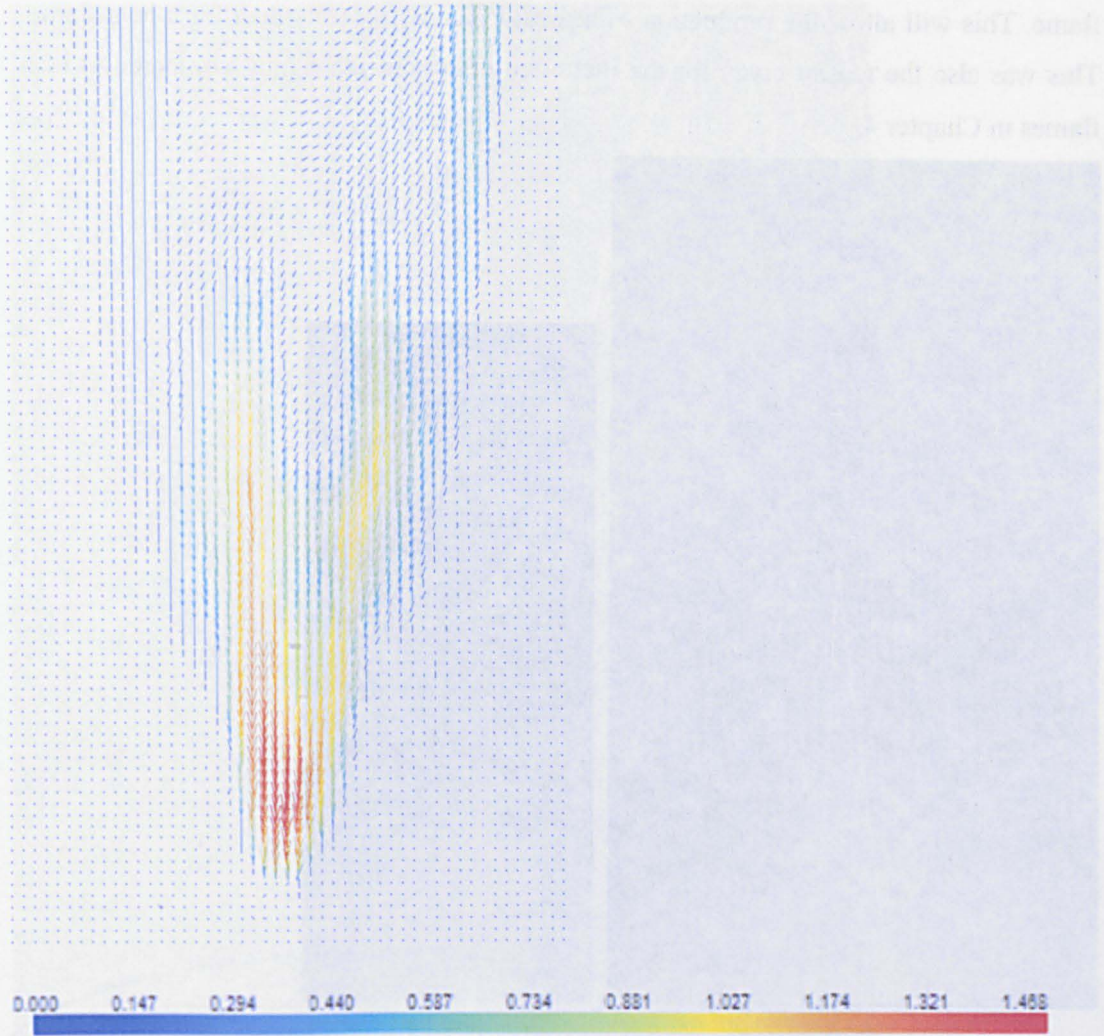


Figure 6.45 Rich flame 5kV applied ionic wind

Unlike the lean flame the ionic wind forms within the flame boundary. There are two parts to a rich flame, the inner premixed flame and an outer diffusion flame. The reason for the appearance of the ionic wind within the diffusion flame can be explained by the production of H_3O^+ from the premixed flame, which will allow the ionic wind to be formed inside the diffusion flame boundary. However, the ionic wind also appears to form within the boundary of the premixed flame as well as the diffusion flame. This could be occurring due to the increased carbon content of the fuel. The formation of ions is dependant on the carbon content of the fluid (see Section 2.1 for details of this). In the

rich premixed flame there will be a much higher proportion of carbon than in a lean flame. This will allow the production of a greater number of ions than for a lean flame. This was also the reason given for the increased effect on rich flames compared to lean flames in Chapter 4.

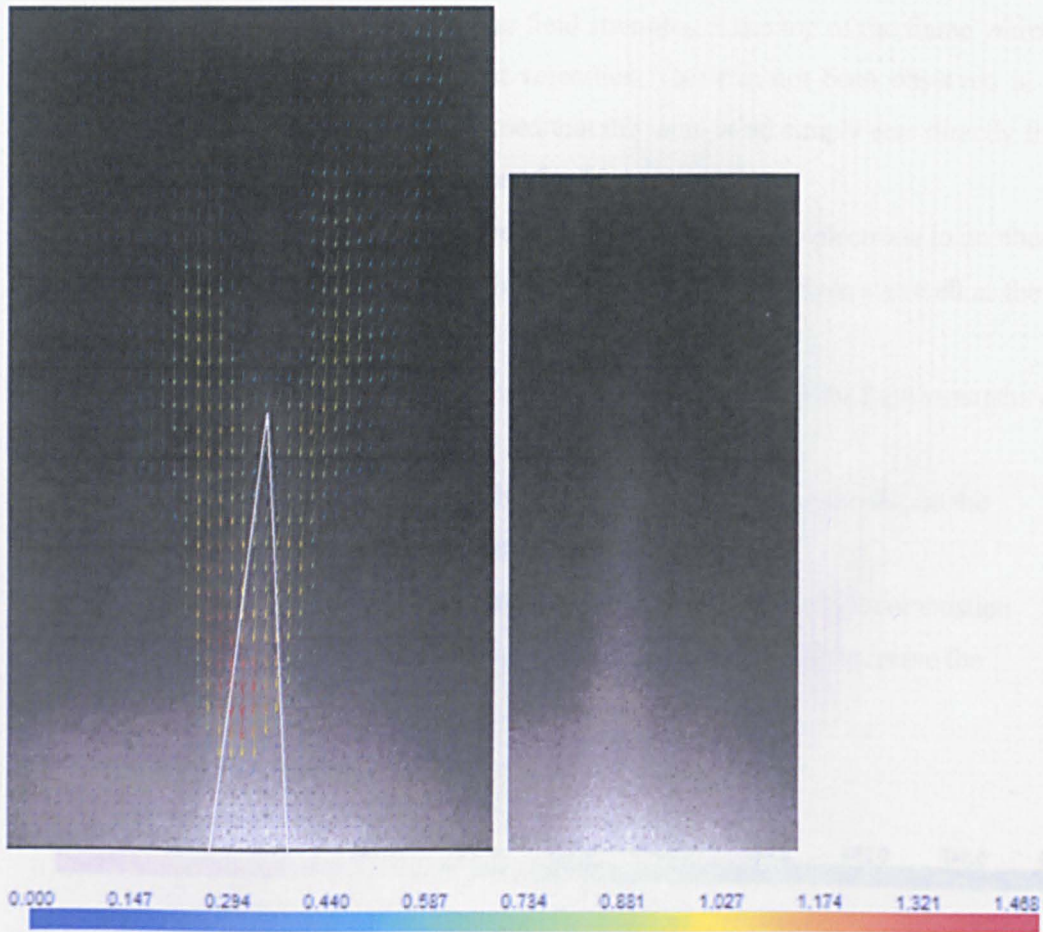


Figure 6.46 Rich flame 5kV applied superimposed on top of average pixel image

The results for 10kV applied to the same rich flame show a similar result (Figure 6.47).

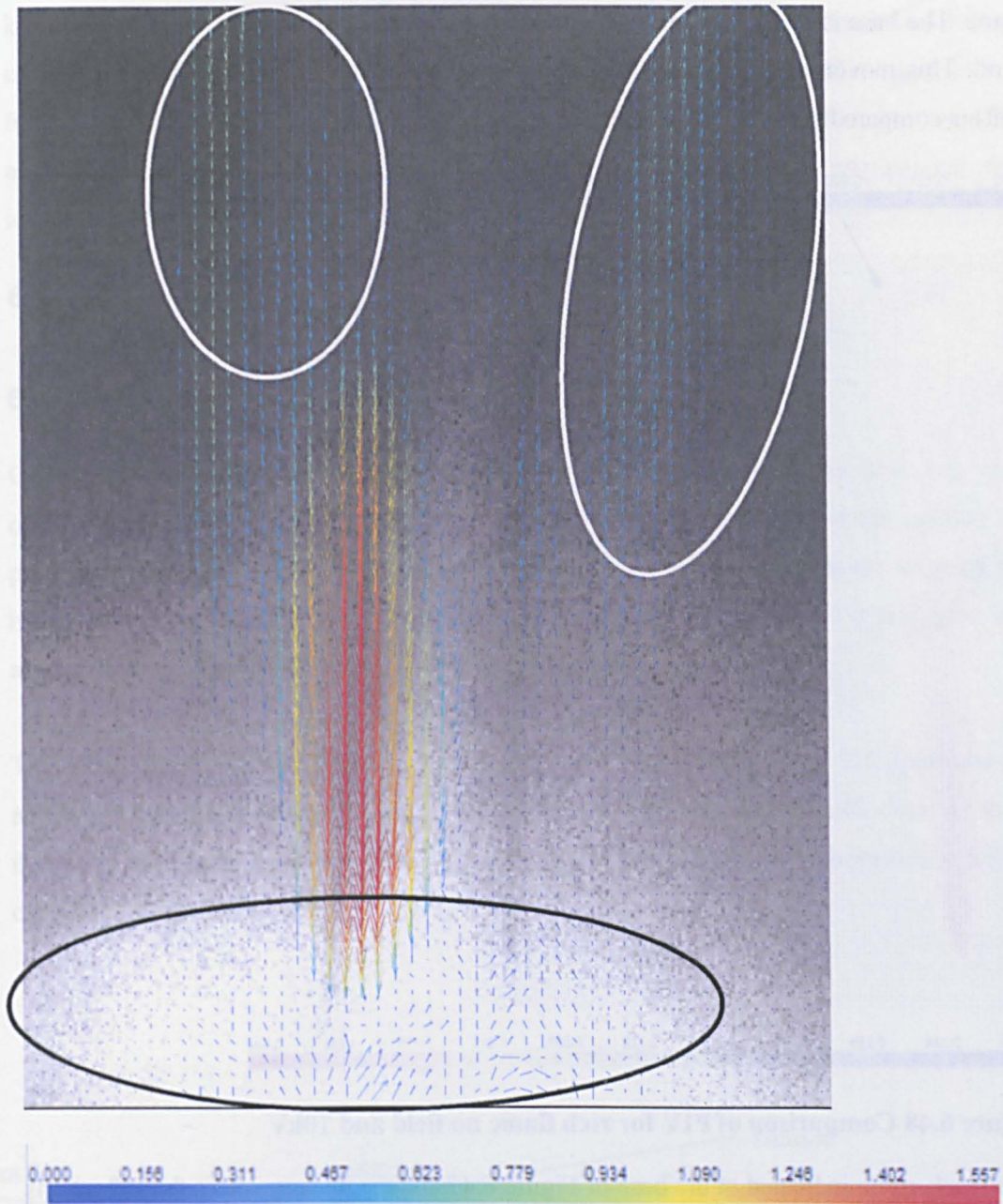


Figure 6.47 Rich flame 10kV applied with no field subtracted superimposed on top of average pixel image

The areas of the PIV marked are unreliable. The two white areas at the top of the image show a region where the flame has been influenced by an external aerodynamic force.

This could have been a draft from an open door or movement of a person close to the flame. The base is much less effected and has been considered suitable to show the ionic wind. This movement to the right can be seen below in Figure 6.48 where the no field (left) is compared to the applied field of 10kV (right).

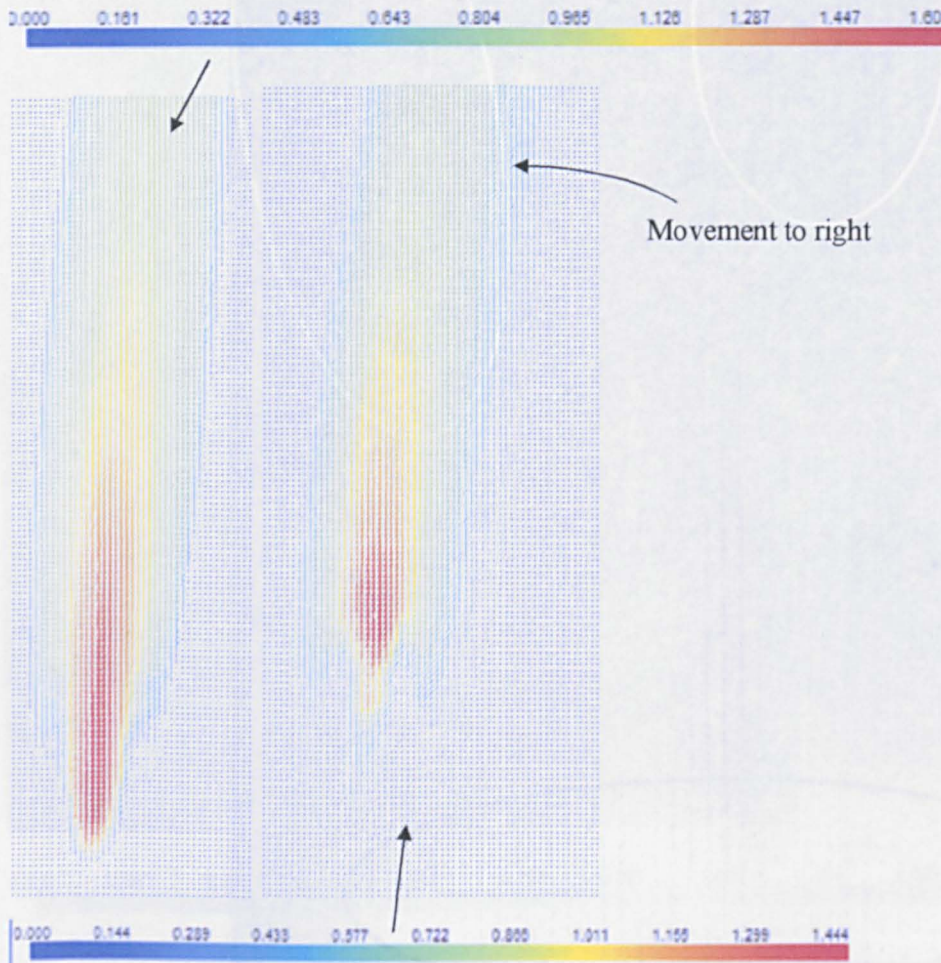


Figure 6.48 Comparison of PIV for rich flame no field and 10kV

The black circle indicated at the base of Figure 6.47 shows the area where the reflections of the laser light from the plate made the results unreliable. The PIV in this region has therefore been ignored. Further work is required in this area to establish how low in the premixed flame the ionic wind begins. This is important as the position where the ionic wind originates from will give an indication of the strength of effect that can be achieved. If the ionic wind begins low in the flame then the effect can be greater. It also gives an

impression of where there is a larger concentration of ionic species. This is important to know as any chemical changes caused by pulses or AC fields will be greater for higher concentrations of ions. The range of chemical effects that can be caused are greater the further upstream ions are produced. The reason for this is that the effect can only be applied after the ions are created. Therefore, the earlier in the combustion process the ions are produced the more reactions they can alter.

6.4 Particle tracking

6.4.1 Method

One of the constraints of PIV is that it assumes a 2D flow. To show that this was occurring and to verify the results the experiment has been repeated and the method of particle tracking has been used in 3D. The results from this do not provide as good an interpretation as the PIV but can be used to show that the flow is 2D and give an approximation of the flow, which is similar to that formed by PIV.

The set up can be seen in Figure 6.49. The cameras were spaced about 90° apart and at approximately the same level. Both cameras were synchronised with each other so that they took frames at the same time. The cameras were phantom V4, photosonics, USA capable of digitally recording 10,000 fps.

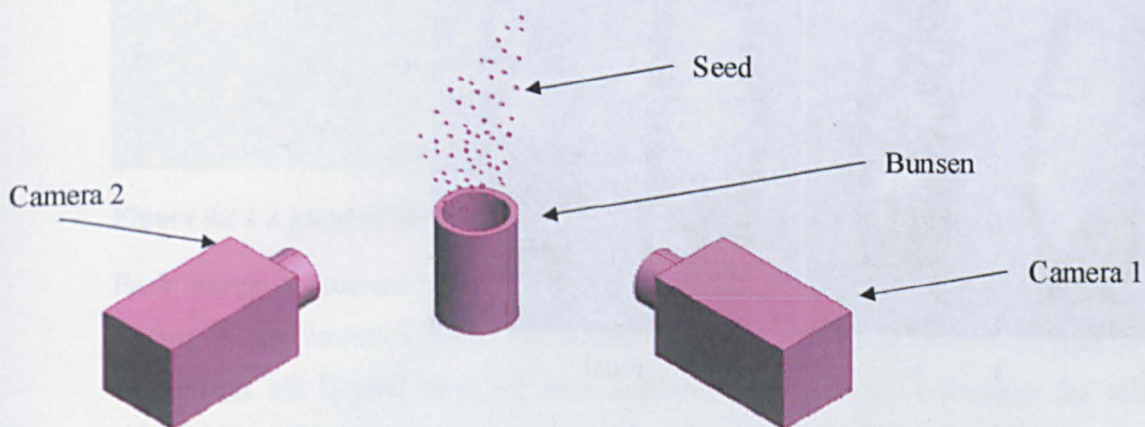


Figure 6.49 Camera set up for particle tracking

A program produced by the Sports Engineering Research Group [123-5] was used to give the pixel coordinates of a particle as it moved through the flame. A bright particle was chosen so that it could be ensured that the same particle was tracked for both cameras. Each particle was manually selected on each frame at its centre point on both the left and the right camera pictures. An example of this can be seen below in Figure 6.50. The particle tracks can be seen as red crosses. The first three sets are shown as well as the final result.

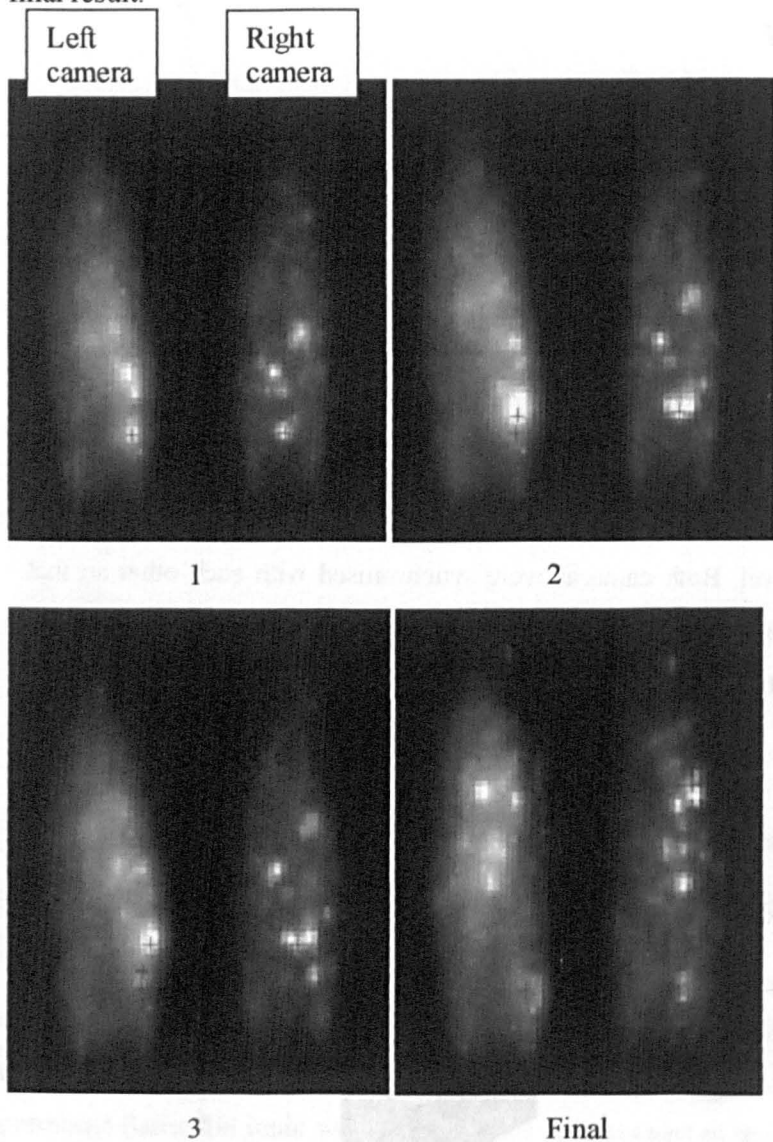


Figure 6.50 Particle tracking

A list of 2D coordinates in pixels was then created for both the left and right cameras. The selection of the centre of the seed was subject to human error. It was also difficult to identify the same particle on both cameras.

In order to transfer the position in pixels to mm, the positioning of the cameras relative to each other and to the flame, as well as the conversion factor from pixels to mm, needs to be known. To find this, a procedure developed by the Sports Engineering Research Group at Sheffield University [126] was used.

A chequer board was photographed on both cameras simultaneously in a variety of positions and orientations (see Figure 6.51 for an example of two image pairs). The checkerboard was perfectly flat and had black and white squares of known dimensions (2mmx2mm).

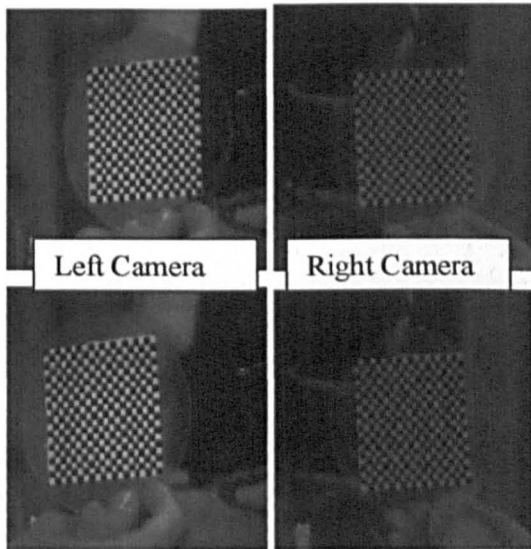


Figure 6.51 2 pairs of checker board images

Each image is processed so that the coordinates of each black/white intersection are known in the camera's frame of reference. For each board position a pair of 2D coordinates are formed (one for each camera). An algorithm calculates the relative orientations of each board to each camera and to the other boards, from the known spacing of the checkers. The positioning of the second set of board positions is compared

to the first set (by an algorithm) and then the position of the second camera relative to the first is calculated (see Figure 6.52). Five board positions are shown in Figure 6.52. Note that the left camera is given 0,0,0 coordinates and the position of the right camera is then calculated from this. This method provides a means to convert two sets of 2D coordinates (in pixels) from each camera into a single set of 3D coordinates (in mm to an accuracy of $\pm 0.5\text{mm}$).

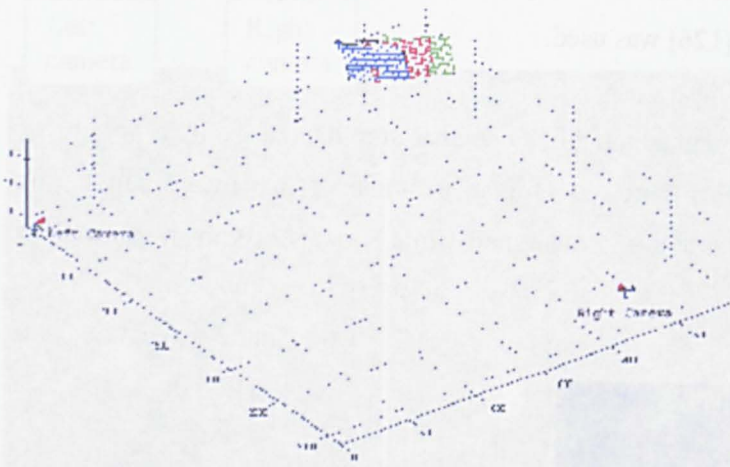


Figure 6.52 Alignment of the right camera to the left camera

6.4.2 Results

The results for the particle tracking are shown below (Figure 6.53). Each set of points should represent a streamline as the seed particles should not move across a streamline (by the definition of a streamline). This assumes that the seed was small enough to be carried by the fluid and that the seed follows the mass flow accurately. The axis has been included to show the scale. The units are in mm and begin from an arbitrary point.

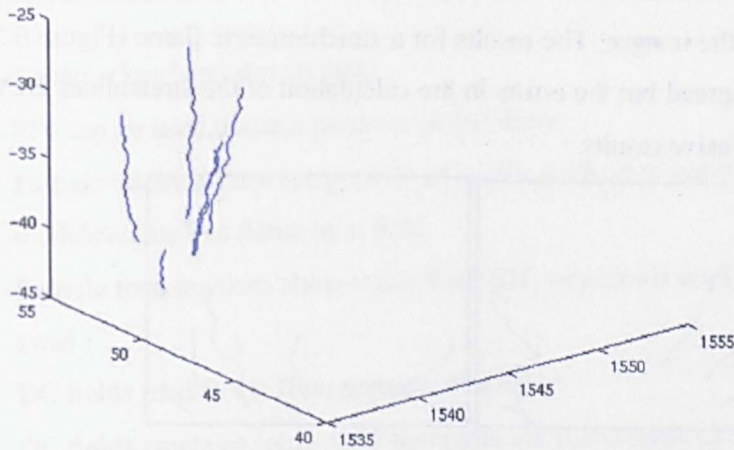


Figure 6.53 Lean no field 3D

From the results above it can be seen that the flow does not swirl and appears to follow a uniform expansion. This means that the assumption of 2D flow, made when using the PIV are accurate.

The lines plotted are the lines between the points measured. Variations from a smooth line are due to the inaccuracy of measuring the points (marking the centre of the seed) and errors in the algorithm that calculates the position in 3D (this is $\pm 0.5\text{mm}$).

The results from this can be compared for a lean flame with no field and an applied field of 10kV Figure 6.54.



Figure 6.54 Lean no field (left), applied 10kV (right)

The results do not show a conclusive effect. It may be possible that the flame is spreading out but it is unclear from the images. The results for a stoichiometric flame (Figure 6.55) appear to show a clearer spread but the errors in the calculation of the streamlines are too large to provide any conclusive results.



Figure 6.55 Stoichiometric no field (left), 5kV (centre) and 10kV (right)

The results for a rich flame and for applied pulses do not show any change between when a field is applied and when no field is applied, but this is probably due to the errors in calculation. The results have therefore been considered unreliable other than to show that the flow is 2D. The remaining results have therefore not been included but can be found in Appendix 4.

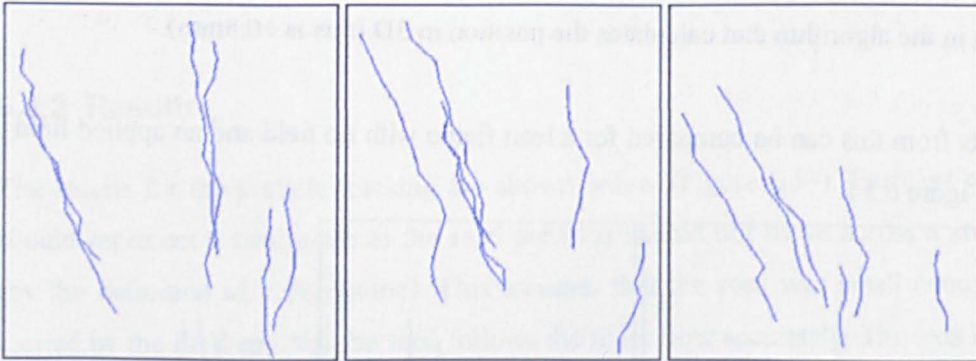


Figure 6.56 Rich no field (left), 5kV (centre) and 10kV (right)

6.5 Conclusions

In this chapter it has been shown that;

- PIV can be used to track particles in the flame
- Particle tracking does not provide a reliable method to observe aerodynamic modifications to a flame by a field
- Particle tracking does show that a field (DC or pulsed) does not cause the flame to swirl
- DC fields modify the flow patterns of a flame
- DC fields create an ionic wind that pulls the flame back down towards the base
- Pulsed fields do not appear to modify the flow of a flame but further work needs to be done to fully prove this
- The mass flow rates from experimental data are confirmed by PIV
- Further work is required to identify why the seeding is not present in all areas of the flame
- Further work is required to eliminate the reflections from the Bunsen and plate, ensuring that velocities and the ionic wind in the lower part of the flame can be calculated
- Further work is require to use PIV with pulsed and AC fields to measure any ionic wind disturbances caused by the field

Chapter 7 Conclusions

In the literature different researchers have used various apparatus geometries. Full modelling of the field is not possible due to technical difficulties in predicting the interaction between the flame and the field. However, an accurate model of the field without a flame can be produced. This modelling has shown the apparatus used by the different researchers produces very different fields.

For practical situations the best model is produced by a boundary set to ground an infinite distance away from the model. This best represents the use of a Faraday cage which is also required for safety and electrical isolation from other potential sources. The use of a Faraday cage will prevent a lot of this interference. Using a Faraday cage provides the best practical means to create a repeatable field and all future experiments should be conducted within one. This will allow results to be compared between different researchers. It will also permit a more accurate model of the flame field interaction to be developed in the future.

The modelling work showed that the most uniform field is produced by two parallel plates. It was therefore chosen to use this set up for further experiments. A mesh was used as the top electrode instead of a plate as this allowed the gas to flow through with minimal aerodynamic disturbance.

The modelling work was supported by experimental work. The experiments showed that the effect of an applied field was amplified when apparatus was used that increased the local field strength in the region of the flame.

When a DC field was applied to the flame the blow off/lift velocity of the flame was increased beyond the flammability limits for a flame without an applied field. It was also still possible to ignite the flame with an ignition source beyond the normal flammability boundaries when a field was applied, up to the new flammability boundary. The increase

in the flammability limits only occurred when the positive electrode was above the burner. With the positive electrode below the burner there was very little modification to the flammability limits.

It was shown with particle image velocimetry (PIV) that the DC field introduces a flow velocity towards the negative electrode (away from the positive). This velocity (called an ionic wind) can easily explain the increased flammability limits observed when a DC field was applied. The ionic wind will obstruct the upwards propagation of the flow when the positive electrode is above the burner, slowing it down. This means that the flame will still be able to burn for a higher flow velocity at the burner exit as the ionic wind will slow the velocity down to a point at which the flame can be sustained.

Modelling work confirmed by experimental results from PIV showed the ionic wind was not created uniformly. The flame created higher field strengths at its tip where the ionic wind was strongest, blowing vertically downwards. The ionic wind then followed the boundary of the flame to the base where it then spreads out towards to the plate. It was expected that the ionic wind acts from one electrode to the other. These new findings are important as they show that the ionic wind does not flow directly from one electrode to the other but that it can be predicted by electrostatic modelling.

An increase in the flammability limits occurs for pulses as short as 500ns and frequencies as low as 16Hz. However the greatest increase was observed when the pulse duration was 50% of the time between the pulses (square wave with equal “on” and “off times”). The effect peaked at a 50% “on time” but was almost as large when the “on time” was between 25% and 75% of the time between pulses. The effect also increased for higher frequencies, up to the maximum of the equipment (5kHz).

When a pulsed field is applied the increase in the flammability limits is even larger than for DC fields. The increase in flammability limits occurs when the positive electrode is above or below the flame (unlike for DC fields). However, the effect is stronger when the positive electrode is above the burner. These results cannot be explained by the ionic

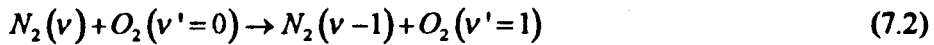
wind as the pulse duration is too short for the aerodynamic movement of the ionic wind to be created. The effect was also observed with the electrodes in an orientation that would cause the ionic wind to flow in the same direction as the flow as well as against it (retarding it). The effects observed must be due to the pulse increasing the chemical reaction rates inside the flame and therefore increasing the flame speed. There are two possible methods for the enhancement to the reaction rates:

1. The mechanism such as the method below suggested by Shebeko [95];

The field excites nitrogen particles



The excited N_2 then transfer their oscillatory energy to O_2



The excitation of O_2 increases the reaction rate of



2. The method proposed by Marcum and Ganguly [39] and Wiseman et al [40].

Ionic species such as H_3O^+ are pulled into the premix region of the flame where they dissociatively recombine to form radicals such as OH which are deficient in this region.

Both mechanisms result in an increase in the concentrations of OH in the preliminary stages of combustion. Either by speeding up the rate of the reaction (7.3), which often limits the rate of combustion (as it is the mechanism for OH production). Or by creating OH by other methods, reducing the importance of reaction (7.3). However, research showing that the effects of an electric field on a flame were reduced when air (containing N_2) was replaced by an Ar/ O_2 mix [64]. This theory is also supported by modelling work that suggests that the majority of energy from free electrons is absorbed by N_2 [48]. This work also did not show any ionic wind in the early stages of combustion which means that it is less likely that ions are pulled down into the early combustion region, supporting theory 1 above.

Particle tracking of the flame showed the flow to be laminar at the burner exit. It also showed the field did not introduce any additional swirl. However, the particle tracking did not provide accurate results due to the limited number of streamlines that it could produce. Further work therefore needs to be conducted to quantify the aerodynamic effect of the field when a pulse is applied.

7.1 Future work

In order to fully prove that the source for the changes to the flammability limits for pulse fields was chemical and not aerodynamic in source, PIV modelling needs to be conducted over the duration of the pulse. This will show whether any aerodynamic effects can be observed due to the pulse.

A full chemical scheme needs to be developed that includes ions and the influence that they can exert on a flame. There have been some ionic chemical models developed but they are not currently sophisticated enough to model the effects observed in this report. The development of a more advanced scheme may be difficult as one of the proposed reaction enhancement methods by ions (see the conclusions above) does not directly influence the chemistry of the flame; the ions excite nitrogen, which goes on to excite oxygen, which in turn speeds up the rate of reaction (7.3). It is possible to modify the reaction rates for the reaction $H^- + O_2 \rightarrow OH^- + O$ and see if it is comparable to the results observed in this report. It would also be possible to repeat the experiments conducted in this report without nitrogen present to see if the effect is the same without it and therefore whether nitrogen could be a significant factor.

The effect of DC fields needs to be compared with other recirculation methods such as a swirler. A design for an appropriate swirler for these flow rates has been developed with the use of CFD modelling to ensure that sufficient swirl is created to cause recirculation. However, these experiments were not considered important for this work. The results of this should be compared with PIV and the flammability limits plotted to show whether

the effect is comparable over a range of equivalence ratios. This will add further weight to the conclusions that the DC effect has an aerodynamic origin rather than chemical.

The presence of OH in the premixed zone could be detected with the use of a spectrometer. This would allow the concentration of OH to be measured directly without perturbing the flow. This technique has been used by several authors such as Schafer et al [127] and Hilton et al [128] to measure the composition of flame gases. The concentration of H_3O^+ could also be measured to discover which of the previously mentioned effects is dominant.

Currently it is unknown whether the effect can be applied to larger flames (with both DC and pulse fields). It is important to establish whether the effect can be scaled up to larger flames. It may be that the effect increases as more ions are present or it may be that for higher velocity flames the velocity change does not increase and the effect becomes insignificant.

This also leads onto work with atomised flames where the fuel is liquid and is vapourised into droplets in the combustor. If the pulsed fields can cause chemical changes to the flame then the effect should still be observed with these droplets. The use of a DC field could also be applied to this type of combustor as the local flow patterns could be altered. This would be advantageous to the combustion process for recirculating heat and other combustion products ensuring complete combustion.

The reasons for a loss in the signal for PIV experiments need to be further examined. Current data suggests that this could be due to a phase or crystalline change in the titanium dioxide. However, this has not been proved and this type of seeding method needs further confirmation before it can be widely used as a method for seeding low flow rates.

The work from PIV was unable to identify the earliest point of the ionic wind. This was due to reflections from the plate and Bunsen. An experiment has been designed with a

black metal plate and black Bunsen to try and eliminate the light reflections that have distorted the results.

Aircraft fuels have electrostatic inhibitors added to prevent static sparks that could cause explosions. The effect of these inhibitors on any electric field generation or the production of ions in the flame needs to be analysed. The addition of these inhibitors is likely to change the ionic reaction mechanisms and will alter the effects that a field can have on a flame.

References

- [1] Griffiths J and Bamard J – “Flame and Combustion”, third edition, Blackie Academic and Professional, London 1995
- [2] Tums S – “An introduction to combustion: concepts and applications”, first edition (international), McGraw-Hill International editions. Singapore. 1996
- [3] Gilbert W – “1600 De Magnete”, Book 2, Chap 2, Translated Mottelay, 1958
- [4] Hauksbee F – “Physico-mechanical experiments on various subjects”, London, 1709, (2nd edn 1719)
- [5] Brande W – “The Bakerian Lecture: on some new electrochemical phenomina”. Philosophical Transactions of the Royal Society, 104, P51-61, 1814
- [6] Chattock A – “On the velocity and Mass of the ions in the electric wind in air”. Philosophical Magazine, 48, p401-420, 1899
- [7] Lawton J and Weinberg F – “Electrical Aspects of Combustion”, Clarendon Press, Oxford, 1969
- [8] Fialkov A, Kalinich K and Fialkov B – “Experimental determination of primary ions in flame”. 24th Symposium (International) on Combustion, P785-93, 1992
- [9] Payne K and Weinberg F – “Measurements on field-induced ion flows from plane flames”. 8th Symposium (international) on Combustion, P207-17, 1962
- [10] Sandhu S and Weinberg F – “Laser interferometric studies of the control of heat transfer from flame gases by electric fields”. Combustion and Flame, 25, P321-334, 1975
- [11] NASA press release – “Ion propulsion – 50 years in the making”. Release number 46, 6th April 1999. Can be accessed online at; http://science.nasa.gov/newhome/headlines/prop06apr99_2.htm [last accessed 30th March 2008]
- [12] Fialkov A – “Investigations of ions in flames”. Progress in Energy and Combustion Science 23, P399-527, 1997
- [13] Huneiti Z and Balachandran W – “Effect of Electric Field on Flames”. Department of Systems Engineering, Brunel University, Unpublished, internal report. 2002

- [14] Pedersen T – “Ionic Structure of Methane Flames”. Thesis, PhD, Iowa State University, 1991
- [15] Pederson T and Brown R – “Simulation of electric field effects in premixed methane flames”, *Combustion and Flame*, 94, P433-88, 1993
- [16] Calcote H – “Mechanisms for the formation of ions in flames”. *Combustion and Flame*. 1, P385-403, 1957
- [17] Peeters J, Vinckier C and Van Tiggelen A – “Formation and behaviour of chemi-ions in flames”, *Oxid. Combust. Rev.* 4, P93-132, 1969
- [18] Calcote H and King I – “Study of ionisation in flames by mean of langmuir probes”. 5th symposium on Combustion, P423-34. New York: Reinhold Publishing Corporation, 1955
- [19] Sturgen T and Belcher H – “Studies on the ionisation produced by metallic salts in flames I”. The determination of the collision frequency of electrons in coal-gas/air flames. *Proceedings of the Royal Society A*, 201, P480-8, 1950
- [20] Wilson H – “Electrical conductivity of flames”. *Reviews of Modern Physics*, 3, P156-89, 1931
- [21] Mitchell J and Wright F – “Effects in diffusion flames by radial electric fields”. *Combustion and flame* 13, P413-8, 1969
- [22] Proskudin V, Berezhko P, Belyaev E, Tarakanov V, Polovinkin P, and Leshchinskaya A – “Chain-Thermal Explosion and Degree of Ionisation of Hydrogen–Air Flames”. *Combustion, Explosion, and Shock Waves*, 41, No. 1, P12-9, 2005
- [23] Green J and Sugden T – “Some observations on the mechanism of ionization in flames containing hydrocarbons”, in: 9th Symposium (International) on Combustion, Academic Press, New York, 1963, P607-21, 1964
- [24] Hu J, Rivin B and Sher E – “The effect of an electric Field on the shape of co-flowing and Candle-type methane-air flames”. *Experimental Thermal and Fluid Science* 21 p124-133, 2000
- [25] Lawton J and Weinberg F – “Maximum ion current from flames and the maximum practical effects of applied electric fields”. *Proceedings of the royal Society (London) A*, 277, P469-97, 1964

- [26] Jagers H and von Engel A – “The effect of electric fields on the Burning Velocity of Various Flames”. *Combustion and Flame*, 16, p275-285, 1971
- [27] Fialkov A and Fialkov B – “Ion content of Propane-Butane-Air flames at Reduced Pressure”. Translated from *Fizika Goreniya i Vzryva*, 21, (3), P32-42, 1985
- [28] Ketvirtis A and Simons J – “Dissociative Recombination of H_3O^+ ”. *Journal of Physical Chemistry (American Chemical Society)*, 103, P6552-63, 1999
- [29] Kinbara T and Nakamura J – “On ions in diffusion flames”. 5th Symposium on Combustion, P285. New York: Reinhold Publishing Corporation P285-89, 1955
- [30] Sugden T, Goodings J and Bohme K – “Positive ion probe of Methane-Oxygen combustion”. 16th Symposium (International) on Combustion, P891-903, 1976
- [31] Vinckier C, Gardner M and Bayes K – “A study of some primary and secondary chemi-ionisation reactions in hydrocarbon oxidations”. 16th Symposium (International) on Combustion, P881-9, 1976
- [32] Starik A and Titova N – “Kinetics of Ion Formation in the Volumetric Reaction of Methane with Air”. *Combustion, Explosion, and Shock Waves*, 38, No. 3, P253-68, 2002
- [33] Payne K and Weinberg F – “A preliminary investigation of field induced ion movement in flame gases and its applications”. *Proceedings of the Royal Society A*, 250, P316-36, 1959
- [34] Kinbara T and Ikegami H – “On the positive and negative ions in diffusion flames”. *Combustion and Flame*, 1, issue 2, P199-211, 1957
- [35] Yuan Z, Uday H and Faeth G – “Effect of electric fields on non-buoyant spherical diffusion flames. *Combustion and Flame*”, 124, P712-716, 2001
- [36] Sher E, Pinhasi G and Pokryvailo, Bar-on R - Extinction of pool flames by means of a DC field. *Combustion and Flame*, 94, p244-252, 1993
- [37] Rickard M, Dunn-Rankin D, Weinberg F and Carleton F – “Characterization of ionic wind velocity”. *Journal of electrostatics*, 63, P711-716, 2005
- [38] Bradley D and Nasser S - Electrical coronas and burner flame stability. *Combustion and Flame*, 55, P53-58, 1984

- [39] Marcum S and Ganguly B – “Electric field induced flame speed modification”. *Combustion and Flame*, 143, P27-36, 2005
- [40] Wisman D, Marcum S and Ganguly B – Electrical control of the thermodiffusive instability in premixed propane-air flames. *Combustion and Flame*, 151, P639-648. 2007
- [41] Saito M, Arai M and Arai T – “Control of Soot Emitted from Acetylene Diffusion Flames by Applying an Electric Field”. *Combustion and Flame*, 119, P356-366, 1999.
- [42] Lawton J, Mayo P and Weinberg F – “Electrical control of gas flows in combustion processes”, *Proceedings of the Royal Society A*, 303, P275-298, 1968
- [43] Nakamura J – “Effect of the electric Field upon the spectra of the hydrocarbon diffusion flame”, *Combustion and Flame*, 3, P277-84, 1959
- [44] Kono M, Carlton F, Jones A and Weinberg F – “The effect of Nonsteady Electric Fields on Sooting Flames”. *Combustion and Flame*, 78, P357-364, 1989
- [45] Bowser R and Weinberg F – “The effect of Direct Electric Fields on Normal Burning Velocity”. *Combustion and Flame*, 18, P296-300, 1972
- [46] Jagers H, Bowser R and Weinberg F – “The effect of electric fields on burning velocity”, *Combustion and Flame*, 19, P135-6, 1972
- [47] Weinberg F – “Electrical Intervention in the Sooting of Flames”. NATO Workshop on Soot in Combustion Systems and its Toxic Properties, P243-257, 1981
- [48] Bradley D and Ibrahim S – “The effects of electrical fields upon electron energy exchanges in flame gases”. *Combustion and Flame*, 22, P43-52, 1974
- [49] Bradley D and Ibrahim S – Electron-gas Energy Exchanges in a.c. Fields and their Relevance in Lasers. *Combustion and Flame*, 27, P353-362, 1976
- [50] Starikovskii A – “Plasma supported combustion”. *Proceedings of the Combustion Institute*, 30, P2405-17, 2005
- [51] Gulyaev G, Popkov G and Shebeko Yu – “Effect of a constant electric field on combustion of a propane-butane mixture with air”. *Combustion, Explosion and Shockwaves*, 21, (4), P401-3, 1985

- [52] Panteleev A, Popkov G, Shebeko Yu and Tsarichenko S – “Effect of ac field on the limiting blow-off flow-rate for a diffusion propane-hydrogen flame”. *Combustion, Explosion and Shockwaves*, 29, (1), P34-5, 1993
- [53] Bozhenkov S, Starikovskaia S and Starikovskii A – “Nanosecond gas discharge ignition of H_2 and CH_4 containing mixtures”. *Combustion and Flame*, 133, P133-46, 2003
- [54] Criner K, Cessou A, Louiche J and Vervisch P – “Stabilization of turbulent lifted jet flames assisted by pulsed high voltage discharge”. *Combustion and Flame*, 144, issue 1-2, P422-25, 2006
- [55] Lee S, Park C, Cha M and Chung S – “Effect of Electric fields on the liftoff of non premixed turbulent Jet flames”. *IEEE Transactions on Plasma Science*, 33, (5), P1703-9, 2005
- [56] Devonshire R, Healey T, Stone D and Tozer R - Relative Enhancement of near-UV Emission from a low-pressure mercury-rare-gas discharge lamp, for an LCD backlighting application. *Measurement Science and Technology*, 11, P547-553, 2000
- [57] Kono M, Inuma K and Kumagai – “The effect of DC to 10 MHz electric field on flame luminosity and carbon formation”. 18th Symposium on Combustion, the combustion Institute, Pittsburg, P1167-74, 1981
- [58] Calcote H and Pease R – “Electrical Properties of Flames”. *Burner Flames in Longitudinal Electric Fields. Industrial and Engineering Chemistry*, 43, P2726-31, 1951
- [59] Calcote H and Berman C – “Increased methane-air stability limits by a DC electric field”. *ASME (PD) 25*, P25-31, 1989
- [60] Dolman T (now Dolmansley) - *Dancing Flames*. Unpublished MEng Dissertation, Sheffield University, 2004
- [61] Glarborg P, Kee R, Grear J and Miller J – “A fortran program for modelling well stirred reactors”. SAND86-8209. 1986
- [62] Kee R, Grear J, Smooke M and Miller J – “A fortran program for modelling steady laminar one dimensional premixed flames”. SAND85-8240. 1985

- [63] Gregory P. Smith, David M. Golden, Michael Frenklach, Nigel W. Moriarty, Boris Eiteneer, Mikhail Goldenberg, C. Thomas Bowman, Ronald K. Hanson, Soonho Song, William C. Gardiner, Jr., Vitali V. Lissianski, and Zhiwei Qin – “GRI-Mech3.0” [online]. Published by the Department of Mechanical Engineering at Berkeley University of California. Available from: http://www.me.berkeley.edu/gri_mech/ [accessed on 13 August 2007]
- [64] Gulyaev G, Popkov G and Shebeko Yu – “Synergism effects in combined action of electric field and inert diluent on gas-phase flames”. *Combustion, Explosion and Shockwaves*, 23, (2), P170-2, 1987
- [65] Heinsohn R, Wulfhurst D and Becker P – “The effects of an electric field on an opposed-jet diffusion flame”. *Combustion and Flame*, 11, P288-96, 1967
- [66] Berman C, Gill R and Calcote H – “NO_x reduction in flames stabilized by an electric field”. *ASME (PD) 33*, P71-75, 1991
- [67] Noorani R and Holmes R – “Effects of Electric fields on the blowoff limits of a methane-air flame”. *American Institute of Aeronautics and Astronautics*, 23, (9), P1422-54, 1985
- [68] Brundish K, Wilson C, Nash S, Trippetts J and Woolhouse R – “The Initial design of a fluidically controlled variable geometry fuel injector for gas turbine combustion systems”. *AIAA/ASME/SAE/ASEE Joint propulsion conference and exhibit*, 34th, 1998.
- [69] Brundish K, Wilson C, Tippetts J and Woolhouse R – “Initial optimisation of a fluidically controlled variable swirl fuel injector”. *AIAA/ASME/SAE/ASEE Joint propulsion conference and exhibit*, 35th, 1999
- [70] Gardiner W Jr. (ed) – “Gas-phase combustion chemistry”. 2nd edition. Springer-Verlag New York Inc.
- [71] Echekki T and Chen J – “Unsteady strain rate and curvature effects in turbulent premixed methane air flames”. *Combustion and Flame*, 106, P184-90, 1996
- [72] Echekki T, Chen J and Kollmann W – “The Mechanism of Two-Dimensional Pocket Formation in Lean Premixed Methane-Air Flames with Implications to Turbulent Combustion”. *Combustion and Flame*, 116, P15-48, 1999

- [73] Bradley D, Sheppard C, Woolley R, Greenhalgh D and Lockett R – “The development and Structure of Flame instabilities and cellularity at low markstein numbers in explosions”. *Combustion and Flame*, 122, P195-209, 2000
- [74] Andrews G and Bradley D – “Determination of burning velocities: A critical review”. *Combustion and Flame*, 18, P133-53, 1972
- [75] Gulyaev G, Popkov G, Shebeko Yu and Korolenok A – “Joint action of an inert diluent and electric field on gas-phase flames”. *Combustion, Explosion and Shockwaves*, 24, (6), P700-2, 1988
- [76] Tewari G and Wilson J – “An experimental study of the effects of high frequency electric fields on laser-induced flame propagation”. *Combustion and Flame*, 24, P159-67, 1975
- [77] Saito M, Sato M and Sawada K – “Variation of Flame shape and soot emission by applying electric field”. *Journal of Electrostatics*, 39, P305-311, 1997
- [78] Wager H – “Soot formation in Combustion”. Plenary Lecture to 17th Symposium (International) on Combustion, the combustion Institute, Pittsburg, P3, 1979
- [79] Mizatani Y, Fuchihata M and Ohkura Y – “Premixed laminar flames in a uniform magnetic field”. *Combustion and Flame*, 125, P1071-1073. 2001
- [80] Calcote H, Olson D and Keil D – “Are ions important in soot formation?”. *Energy and Fuels*, 2, (4), P494-504, 1988
- [81] Hall-Roberts V, Hayhurst A, Knight D and Taylor S – “The Origin of Soot in Flames: Is the nucleus an Ion?”. *Combustion and Flame*, 120, P578-84, 2000
- [82] Hardesty D and Weinberg F – “Electrical control of particulate pollutants from flames”. *Proceedings of the 14th (International) Symposium on Combustion*, P907-18, 1967
- [83] Place E and Weinberg F – “Electrical control of flame carbon”. *Proceedings of the Royal Society A*, 289, P192-205, 1965
- [84] Lester T and Wittig S – “Soot nucleation kinetics in premixed methane combustion”. *16th Symposium (international) on combustion*, P671-81, 1977
- [85] Bowser R and Weinberg F – “Electrons and the emission of soot from flames”. *Nature*, 249, P339-41, 1974

- [86] Bowser R and Weinberg F – “Chemi-ionisation during Pyrolysis”. *Combustion and Flame*, 27, P21-32, 1976
- [87] Pratsinis S – “Flame synthesis of Nanosize particles: Precise control of Particle size”. *Journal of Aerosol science*, 27 supplement 1, P153-154, 1996
- [88] Jaworek A, Balachandran W, Lackowski M, Kulon J and Krupa A – “Multi-nozzle electrospray system for gas cleaning processes”. *Journal of Electrostatics*, 64, P194-202. 2006.
- [89] Vatazhin A, Likhter V, Sepp V and Shulgin V – “Electric Field Influence in Nitrogen oxides Emission in Laminar Diffusion Flames”. *Journal of Aerosol Science*, 26 supplement 1, PS651-S652, 1996
- [90] Rosocha L, Kim Y, Anderson G, Lee J and Abbate S – “Decomposition of Ethane in Atmospheric-pressure dielectric-barrier discharges: Experiments”. *IEEE Transactions on Plasma Science*, 34, (6), P2526-31, 2006
- [91] Sher E, Pokryvailo A, Jacobson E and Mond M – “Extinction of flames in a nonuniform electric field”. *Combustion Science and technology*, 87, P59-67, 1991
- [92] Gulyaev G, Popkov G and Shebeko Yu – “Effect of a constant electric field on self ignition temperature of organic materials in air”. *Combustion, Explosion and Shockwaves*, 21, (4), P403-4, 1985
- [93] Panteleev A, Popkov G, Shebeko Yu and Tsarichenko S – “Effect of an electric field on flame propagation over a solid material surface”. *Combustion, Explosion and Shockwaves*, 28, (3), P244-6, 1992
- [94] Panteleev A, Popkov G and Shebeko Yu – “Effect of an electric field on the vaporization and burning of combustible liquids”. *Combustion, Explosion and Shockwaves*, 28, (3), P242-4, 1992
- [95] Shebeko Yu – “Effect of an ac electric field on normal combustion rate of organic compounds in air”. *Combustion, Explosion and Shockwaves*, 18, (4), P427-9, 1982
- [96] Gulyaev G, Popkov G and Shebeko Yu – “Effect of inert gas dilution on electrical potential distribution in a propane-butane flame”. *Combustion, Explosion and Shockwaves*, 25, (5), P552-4, 1989

- [97] Fowler R and Corrigan S – “Burning wave speed enhancement by electric fields”. *Physics of Fluids*, 9, P2073-4, 1966
- [98] Jones F, Becker P and Heinsohn R – “A mathematical model of the opposed-jet diffusion flame: effect of an electric field on concentration and temperature profiles”. *Combustion and Flame*, 19, P351-62, 1972
- [99] Smook M, Lin P, Lam J and Long M – “Computational and experimental study of a laminar axisymmetric methane air diffusion flame”, in: 23rd Symposium (International) on Combustion, The Combustion Institute, Pittsburgh, P575-82, 1990
- [100] Hu J, Rivin B and Sher E – “Experimental and numerical study of the effect of an electric field on a Bunsen-type flame”. *Israel Journal of Chemistry*, 39, P87-96, 1999
- [101] Ansoft Corporation, Pittsburg, PA – “Ansoft Maxwell 2D Electromagnetic-field simulation”, program available online: <http://www.ansoft.com/products/em/max2d> [accessed 13th August 2007], 2006
- [102] Meeker D – “Manual for Finite Element Method Magnetics”, available online: <http://femm.foster-miller.net/wiki/Documentation/> [accessed 24th October 2007], 2007
- [103] Zolgharni M, Azimi S, Bahmanyar M and Balachandran W – “A numerical design study of chaotic mixing of magnetic particles in a microfluidic bio-separator”. *Microfluid Nanofluid*, 3, P677-687. 2007
- [104] Cecelja F, Bordovsky M and Balachandran W – “Lithium niobate sensor for measurement of DC electric fields”. *IEEE Transactions on instrumentation and measurement*, 50, no. 2, P465-469. 2001
- [105] Christopoulos C – “An Introduction to Applied Electromagnetism”, John Wiley & Sons Ltd. Chichester, 1990
- [106] Djuric Z, Balachandran W and Wilson C – “Electrical field and space charge modelling in a viscous flow in a nozzle”. *Journal of Physics D: Applied Physics*, 31, P2132-44, 1998
- [107] Heinsohn R, Wilhelm C and Becker P – “Effect of electric fields on ducted diffusion flames”. *Combustion and Flame*, 14, P341-9, 1970

- [108] Weinberg F – “Electrical aspects of aerosol formation and control”.
Proceedings of the Royal Society A, 307, P195-208, 1968
- [109] Place E and Weinberg F – “The nucleation of flame carbon by ions and the effect of electric fields”. 11th Symposium on Combustion, the combustion Institute, Pittsburg, P245-55, 1967
- [110] Panteleev A, Popkov G, Shebeko Yu, Tsarichenko S and Gorshkov V – “Effect of an electric field on concentration limits for propane flame propagation in air”. Combustion, Explosion and Shockwaves, 27, (1), P22-4, 1991
- [111] Carleton F, Dunn-Rankin D and Weinberg F – “The optics of small diffusion flames in microgravity”. Proceedings of the Combustion Institute, 27, P2567-72, 1998
- [112] Carleton F and Weinberg F – “Electric field-induced flame convection in the absence of gravity”. Nature, 330, P365-6, 1987
- [113] Mayo P and Weinberg F – “On the size, charge and number rate of formation of carbon particles in flames subjected to electric fields”. Proceedings of the Royal Society A, 319, P351-71, 1970
- [114] Rogers G and Mayhew Y – “Thermodynamic and Transport Properties of Fluids, SI units”. Fifth Edition. Blackwell Publishers Ltd., Oxford. 1995
- [115] Beck S, Brown M, Chin S, Dwyer-Joyce R, Niccoleau F and Wilson C – “The little book of thermo fluids”. 3rd Edition. University of Sheffield. 2006
- [116] Cengel Y and Boles M – “Thermodynamics: an engineering approach”. 3rd Edition. McGraw-Hill (International Editions), Maidenhead. 1998
- [117] Press release for E.ON UK – “E.ON UK returns Grain power station unit 4 to service amid security of supply concerns”. Available at <http://pressreleases.eon-uk.com/blogs/eonukpressreleases/archive/2005/09/22/e-on-uk-returns-grain-power-station-unit-4-to-service-amid-security-of-supply-concerns.aspx>. [accessed 25th February 2008], September, 2005
- [118] La vision – “Manual for PIV software”, available at <http://www.piv.de/> [accessed 8th December 2007], 2007

- [119] Dantec Dynamics – “Manual for PIV”, available at <http://www.dantecdynamics.com/Default.aspx?ID=651> [accessed 20th December 2007], 2007
- [120] Ahonen P, Moisala A, Brown D, Jokiniemi J and Kauppinen E – “Gas-phase crystallisation of titanium dioxide nanoparticles”. *Journal of Nanoparticle Research*, 4 (1-2), P43-52. 2002
- [121] Nelson K and Deng Y – “Effect of polycrystalline structure of TiO₂ particles on the light scattering efficiency”. *Journal of Colloid and Interface SCIENCE*, 319, P130-139. 2008
- [122] Massy B and Ward-Smith J (ed) – *Mechanics of fluids*. Seventh Edition. Stanley Thomes Ltd., Cheltenham, 1989.
- [123] Dignall R – “Modelling the Impact of Tennis Balls on Court Surfaces”. Thesis, PhD, Department of Mechanical Engineering, The University of Sheffield. 2005.
- [124] Goodwill S – “The dynamics of tennis ball impacts on tennis rackets”. Thesis, PhD. Department of Mechanical Engineering. The University of Sheffield. 2003
- [125] Dignall R and Haake S – “Analytical modelling of the impact of tennis balls on court surfaces”. *Tennis science and technology*. Roehampton University, London. Blackwell Science, London. 2000
- [126] Choppin S and Whyld N – “3D impact analysis in tennis. The Impacts of Technology on Sport”. *Tokyo Institute of Technology* P373-378. 2005
- [127] Schafer K, heland J, Lister D, Wilson C, Howes R, Falk R, Lindermeir E, Birk M, Wagner G, Haschberger P, Bernard M, Legras O, Wiesen P, kurtenbach R, Brokmann K, Kriesche V, Hilton M, Bishop G, Clarke R, Workman J, Caola M, Geatches R, Burrows R, Black J, Herve P and Vally J – “Nonintrusive optical measurements of Aircraft engine exhaust emissions and comparison with standard intrusive techniques”. *Applied Optics*, 39, P441-455, 2000
- [128] Hilton M, Lettington A and Wilson C – “Gas turbine Exhaust Emissions Monitoring Using non intrusive Infrared Spectroscopy”. *ASME*, 120, P514-518, 1998

Appendices

Appendix 1

The data for the ionic species known to be present in flames and their molecular weights is given here.

Appendix 2

Additional data from DC work. Particularly for 5kV where the results were very similar to 10kV and were therefore not included in the main report.

Appendix 3

Additional PIV results which have not been included in the main report have been included here. The individual flames, cross correlation, moving average and average PIV results are shown for lean rich and stoichiometric flames with no field, 5kV and 10kV applied.

Appendix 4

The majority of the particles tracking results are included here as they did not provide reliable enough results to be included in the main report.

Appendix 1

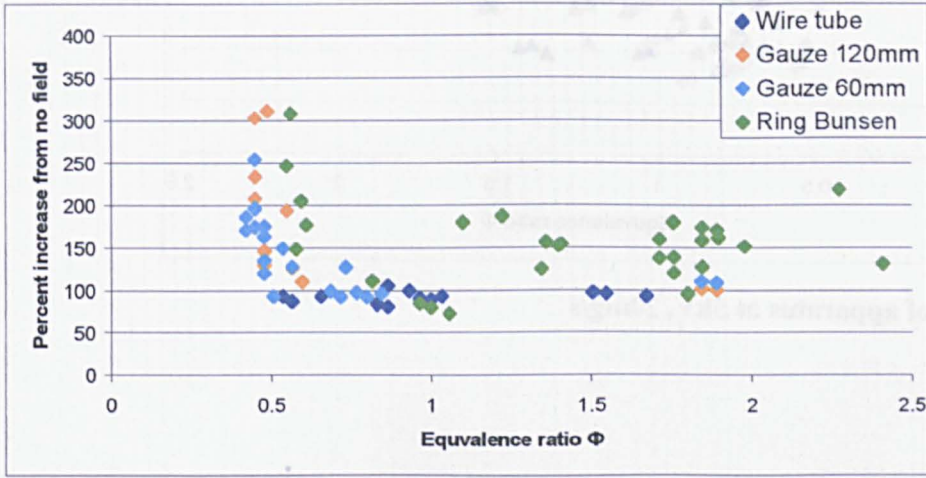
Ionic Species in Flames

Mass no.	Identity	Mass no.	Identity
1	H ⁺	41	C ₃ H ₅ ⁺ C ₂ H ₀ ⁺
2	H ₂ ⁺	42	C ₂ H ₂ O ⁺
3	H ₃ ⁺		C ₃ H ₆ ⁺
12	C ⁺	43	C ₂ H ₃ O ⁺
13	CH ⁺		C ₃ H ₇ ⁺
14	CH ₂ ⁺	45	C ₂ H ₅ O ⁺
15	CH ₃ ⁺		C ₃ H ₀ O ₂ ⁺
17	OH ⁺	46	CH ₂ O ₂ ⁺
18	H ₂ O ⁺	47	C ₂ H ₇ O ⁺
18	NH ₄ ⁺		CH ₃ O ₂ ⁺
19	H ₃ O ⁺	48	CH ₄ O ₂ ⁺
24	C ₂ ⁺	49	CH ₂ O ₂ ⁺
25	C ₂ H ⁺		C ₄ H ⁺
26	C ₂ H ₂ ⁺	51	C ₄ H ₃ ⁺
	CN ⁺	53	C ₄ H ₅ ⁺
27	C ₂ H ₃ ⁺		C ₃ H ₀ ⁺
28	C ₂ H ₄ ⁺ ,	54	C ₄ H ₆
	CO ⁺		C ₃ H ₂ O ⁺
29	CHO ⁺	55	H ₃ O ⁺ .2H ₂ O
30	NO ⁺	58	C ₂ H ₂ O ₂ ⁺
31	CH ₃ O ⁺		C ₃ H ₆ O ⁺
32	CH ₄ O ⁺	59	C ₂ H ₃ O ₂ ⁺
33	CH ₅ O ⁺	61	C ₂ H ₅ O ₂ ⁺
	HO ₂ ⁺		C ₅ H ₃ ⁺
36	NH ₄ ⁺ .H ₂ O	63	C ₂ H ₇ O ₂ ⁺
37	H ₅ O ₂ ⁺	65	C ₅ H ₅ ⁺

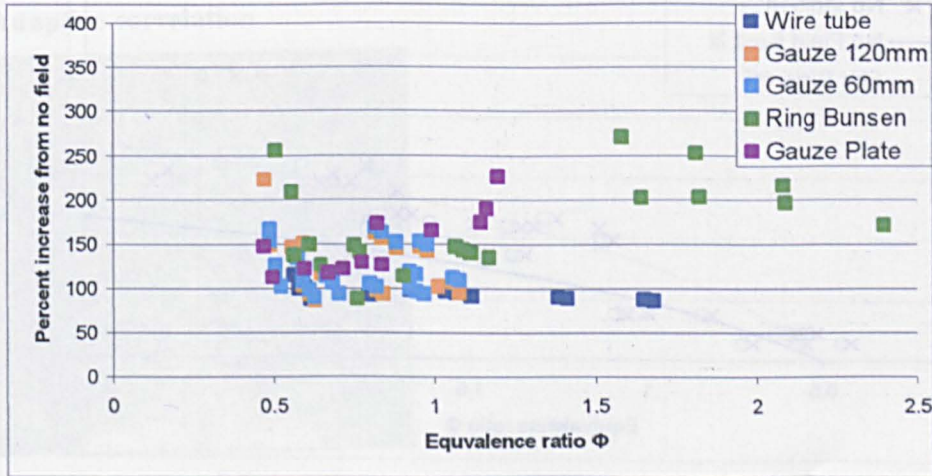
Appendix 2

5kV comparison of apparatus

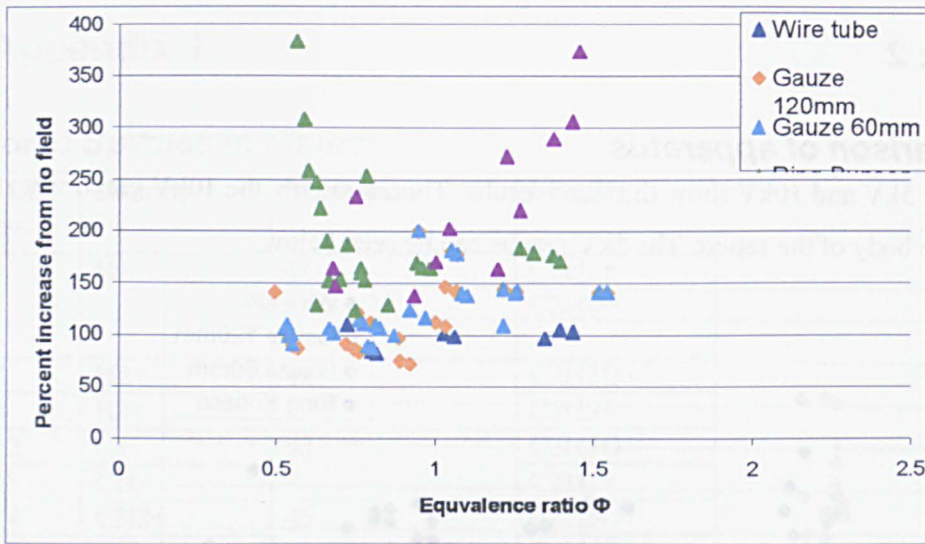
The results for 5kV and 10kV show the same results. Therefore only the 10kV graph was included in the body of the report. The 5kV graphs can be seen below.



Comparison of apparatus at 5kV, 5mg/s

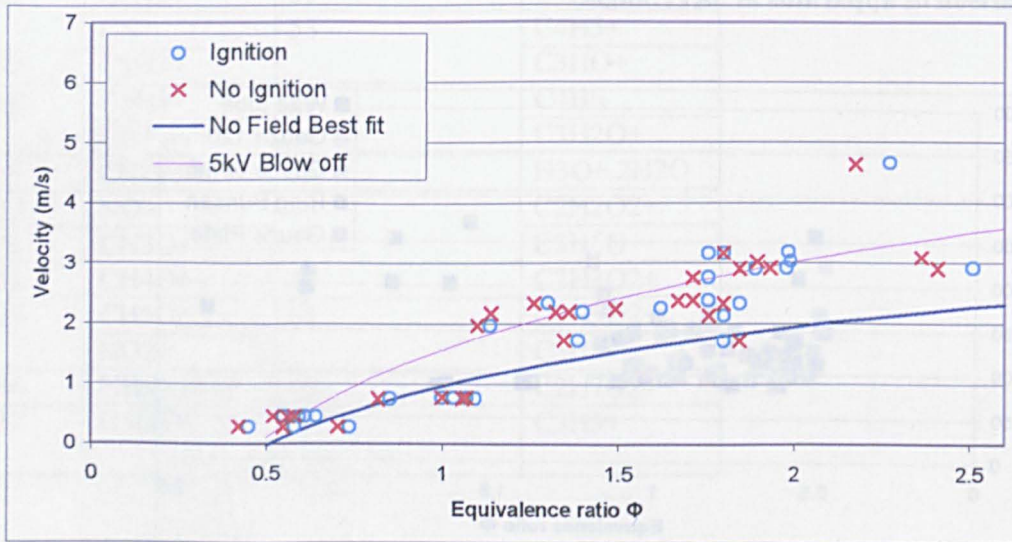


Comparison of apparatus at 5kV, 10mg/s



Comparison of apparatus at 5kV, 20mg/s

5kV Ignition tests

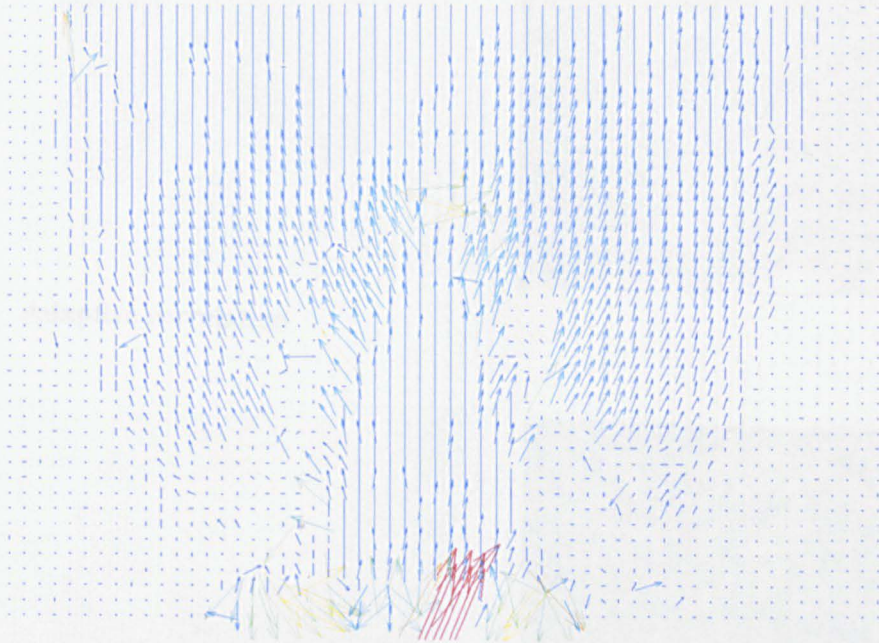


5kV ignition point, 5mg/s

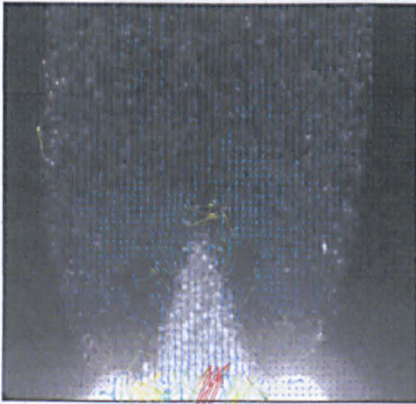
Appendix 3

Particle Image Velocimetry (PIV)

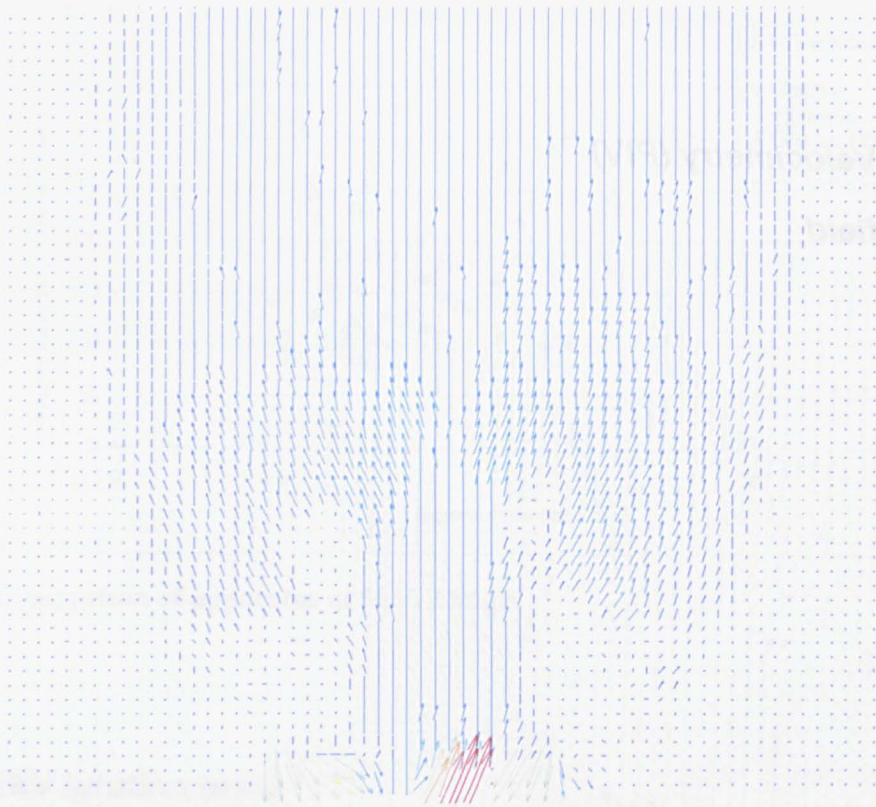
Lean flame no field



Adaptive correlation



Adaptive on top of image

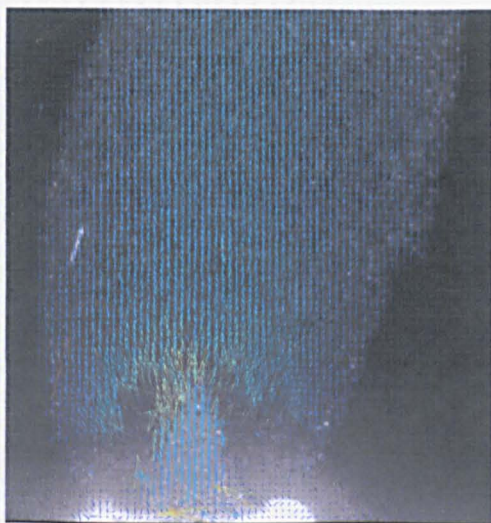
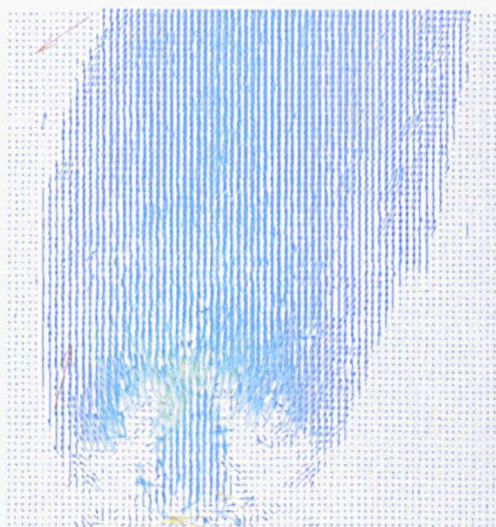


Moving average

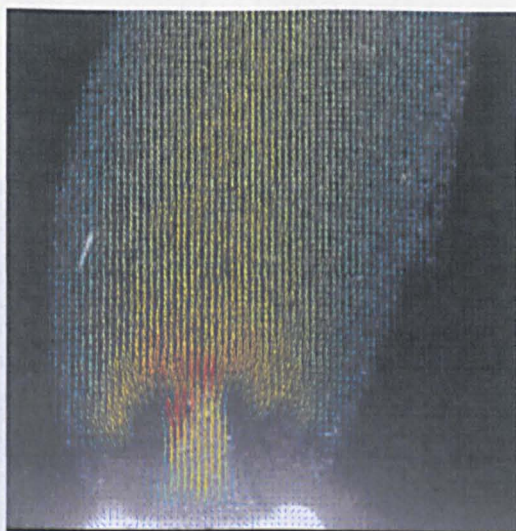
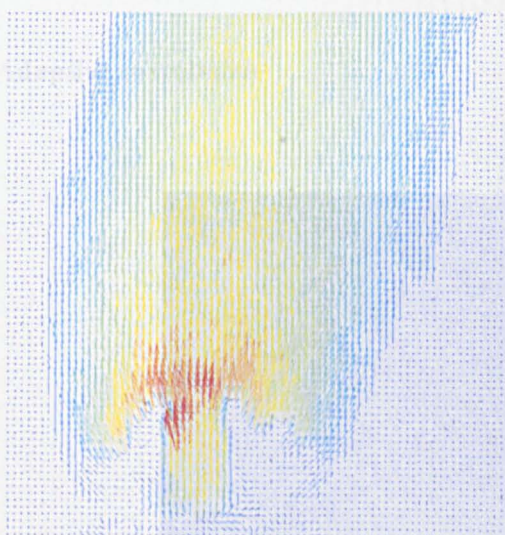
5kV DC lean flame



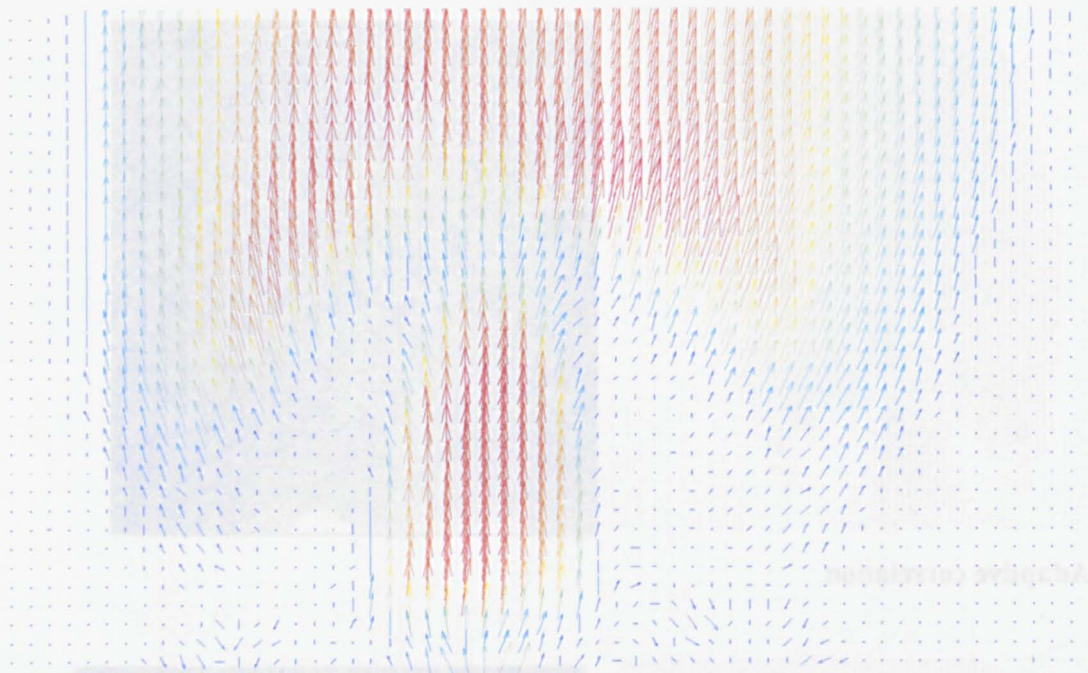
Frame 1 (left) and frame 2 (right)



Adaptive correlation

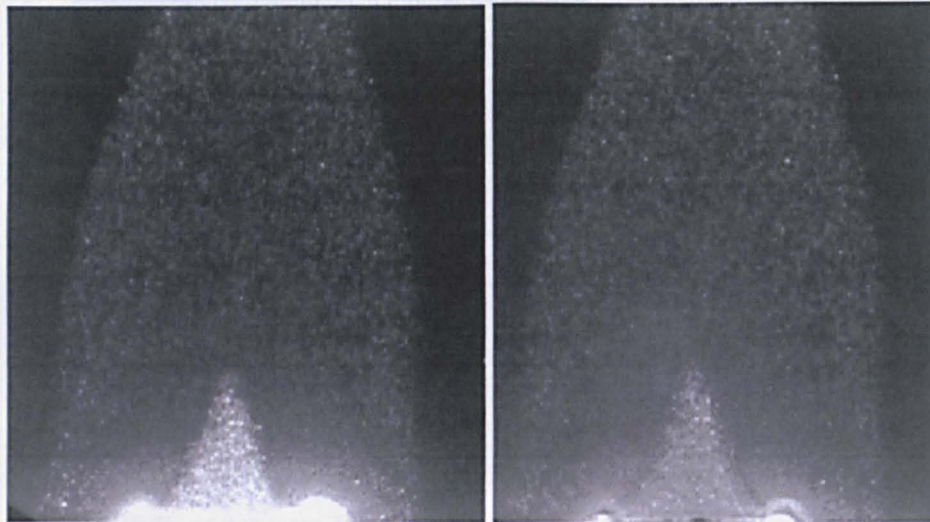


Moving average

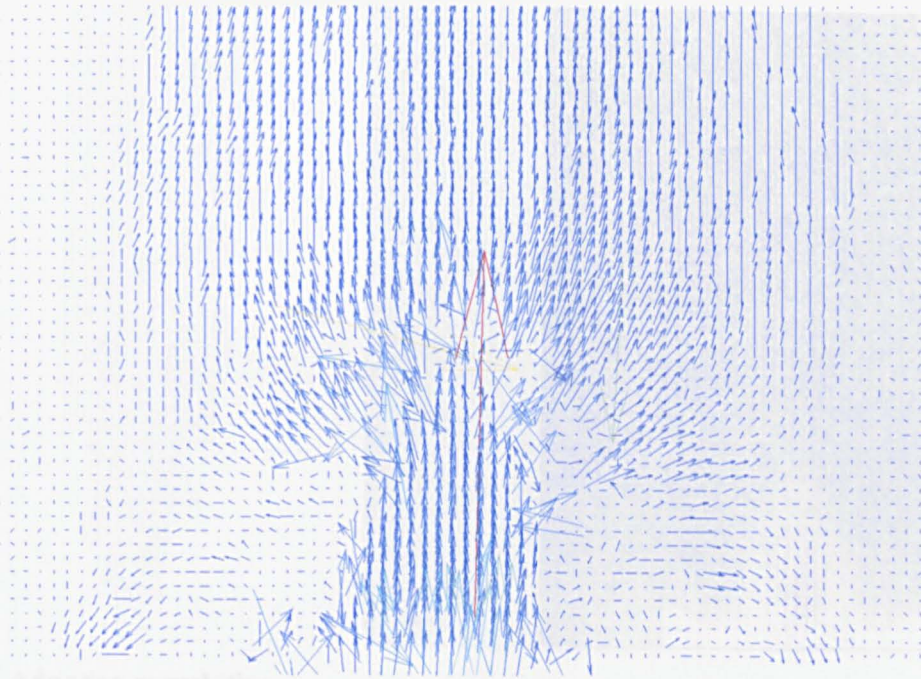


5kV Average expanded

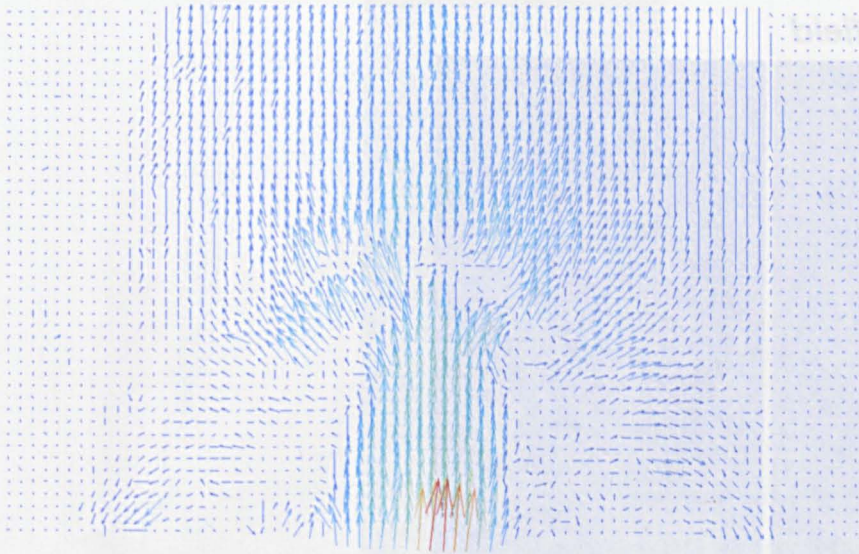
10kV DC lean flame



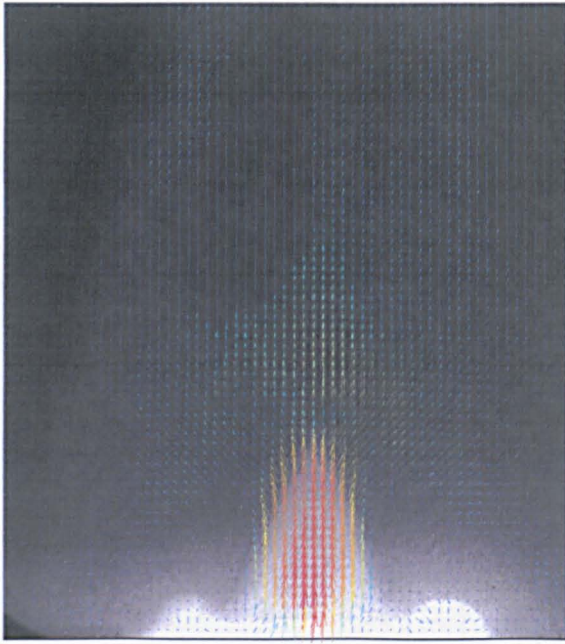
Frame 1 (left) and frame 2 (right)



Adaptive correlation

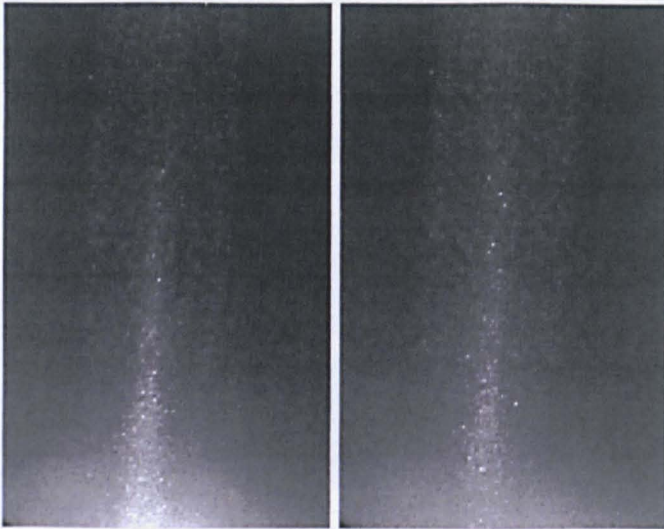


Moving average

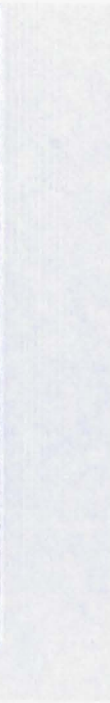
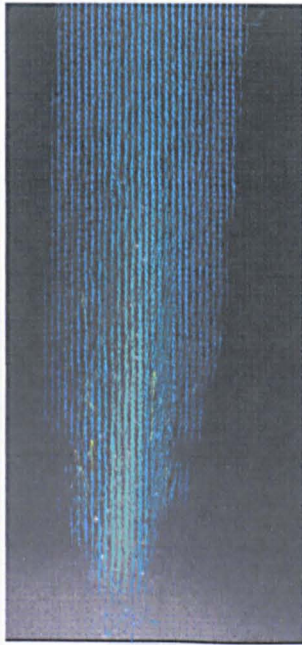
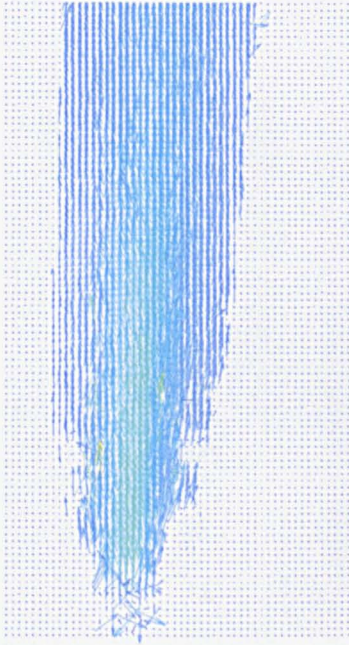


Average PIV

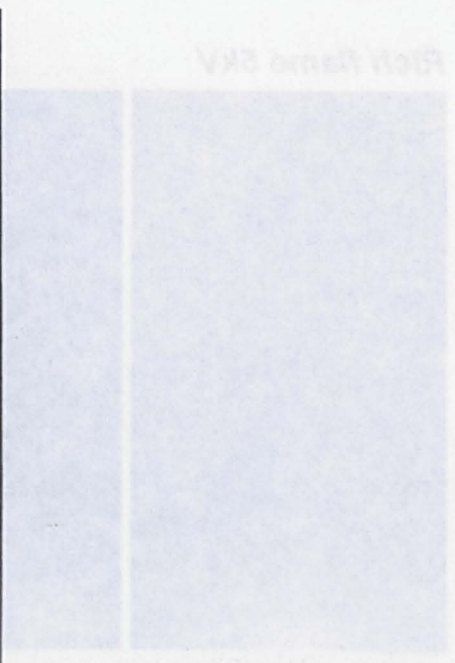
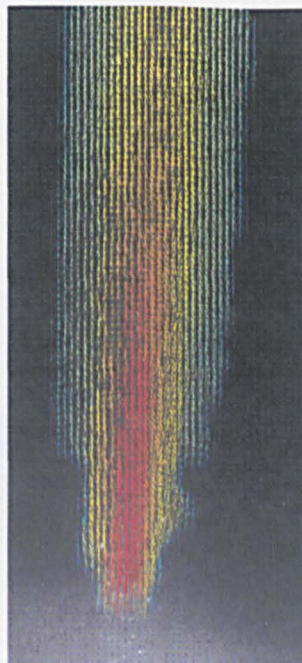
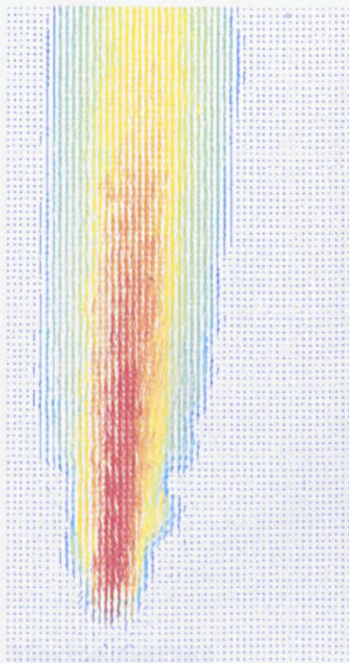
Rich flame no field



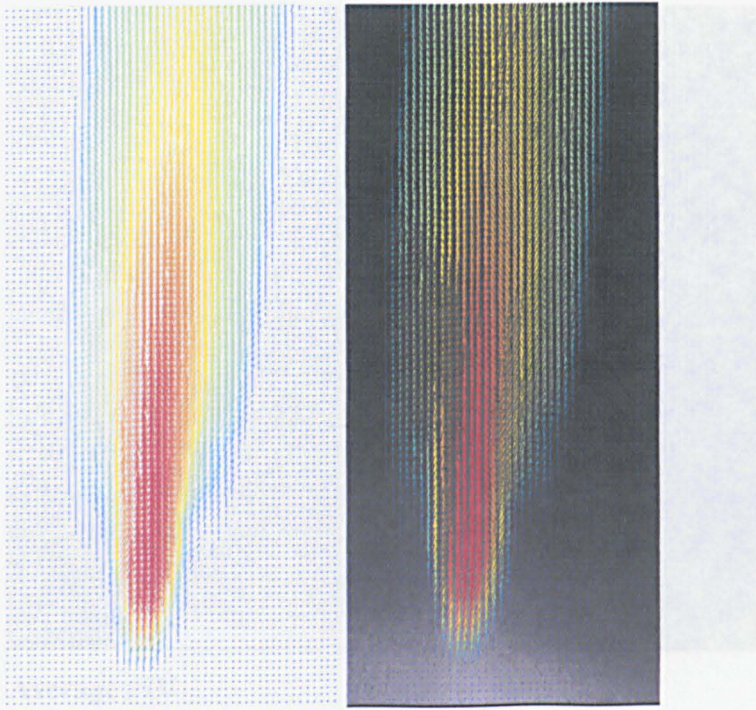
Frame 1 (left) and frame 2 (right)



Adaptive correlation

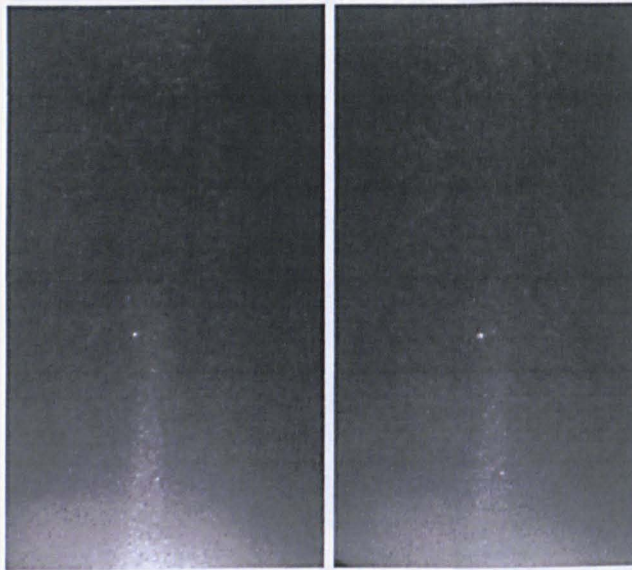


Moving average

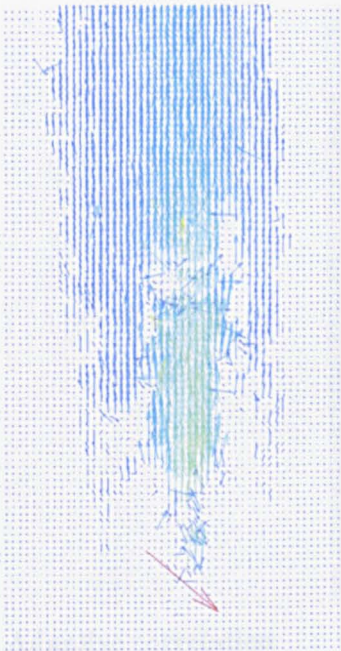


Average PIV

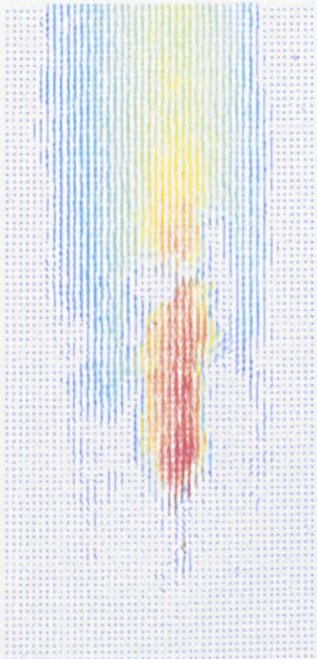
Rich flame 5kV



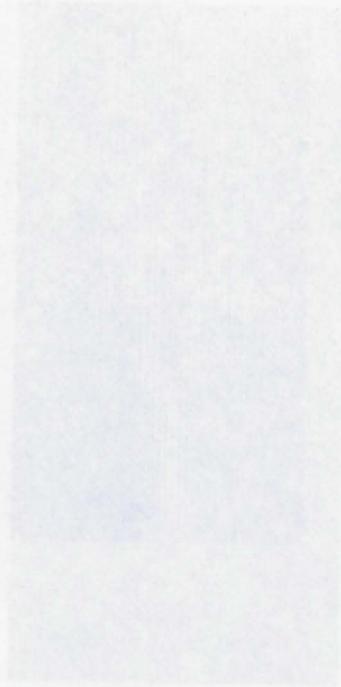
Frame 1 (left) and frame 2 (right)



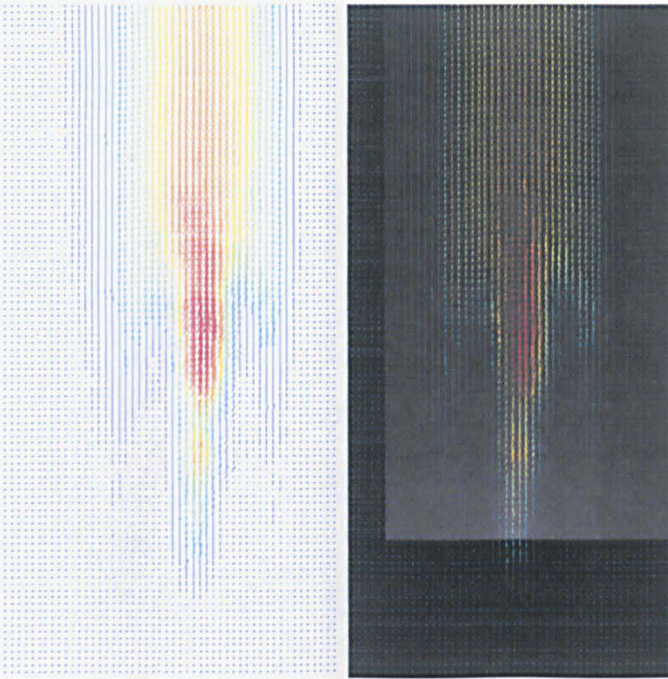
Adaptive correlation



Moving average

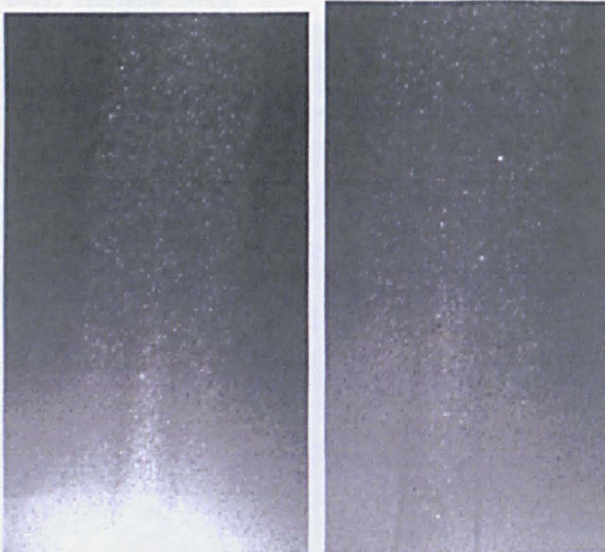


Average
 Rich time 10kV
 Frame 1 (left) and Frame 2 (right)

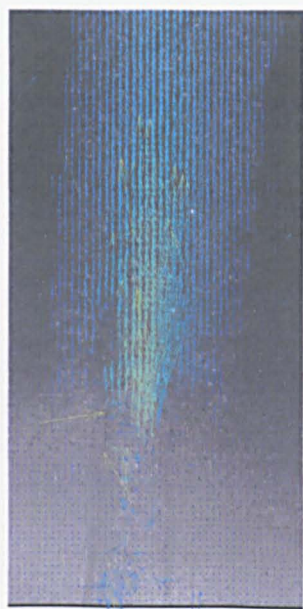
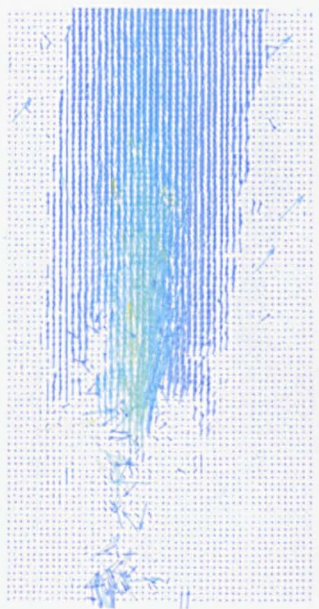


Average

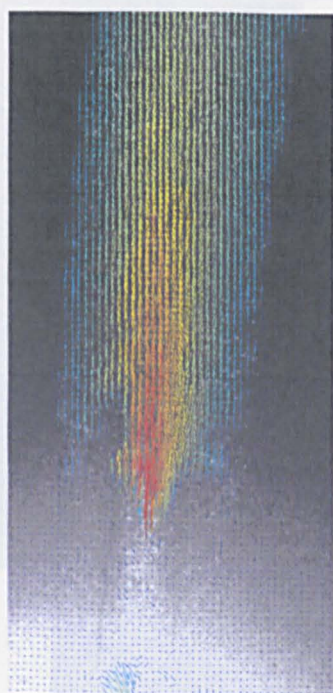
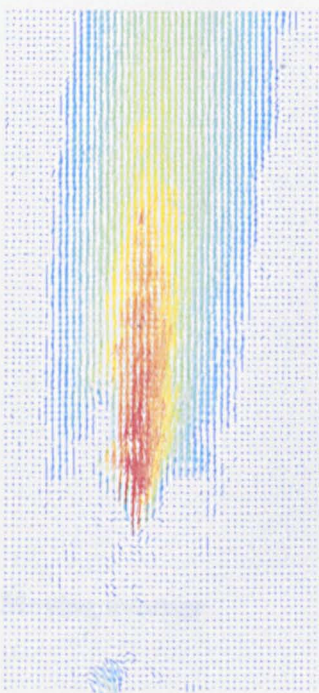
Rich flame 10kV



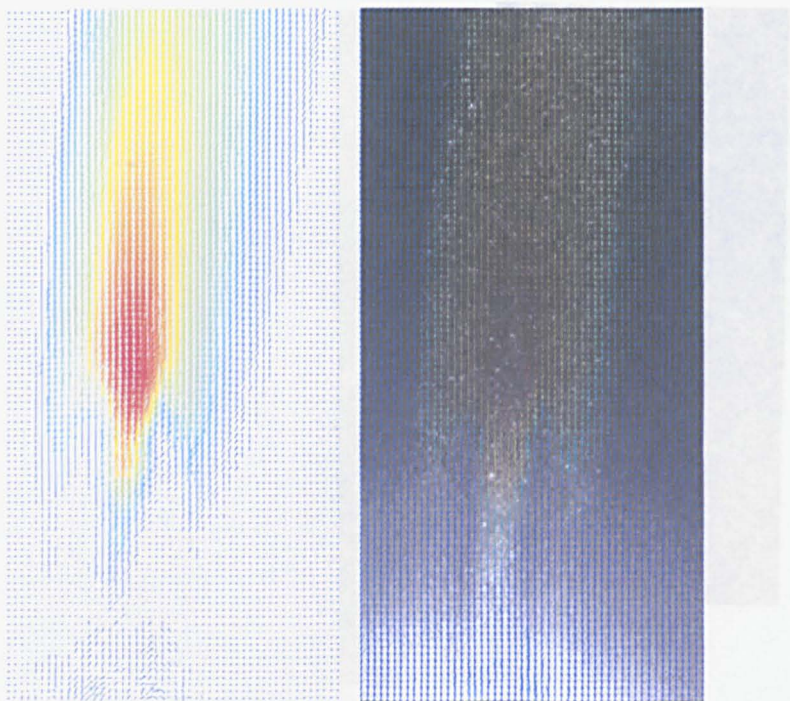
Frame 1 (left) and frame 2 (right)



Adaptive correlation

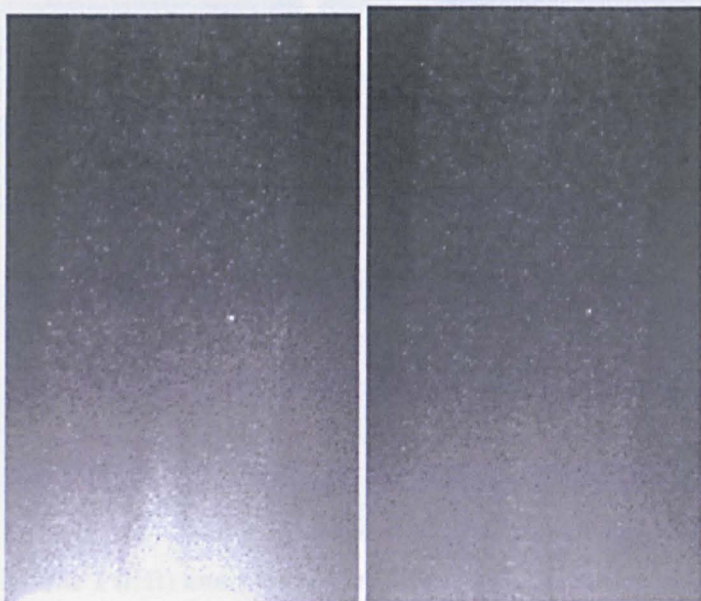


Moving average



Average

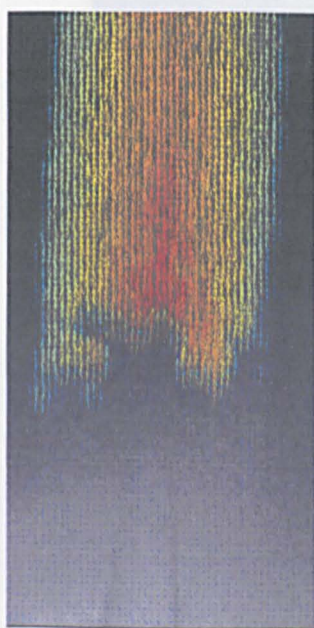
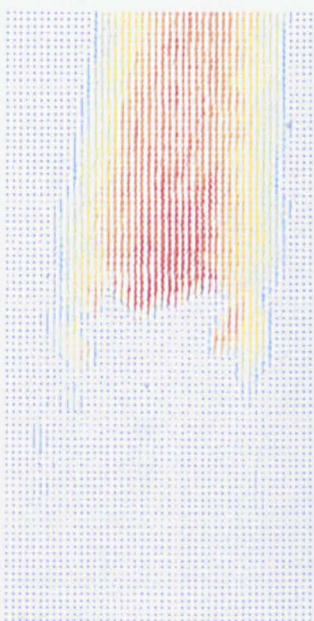
Stoichiometric flame no field



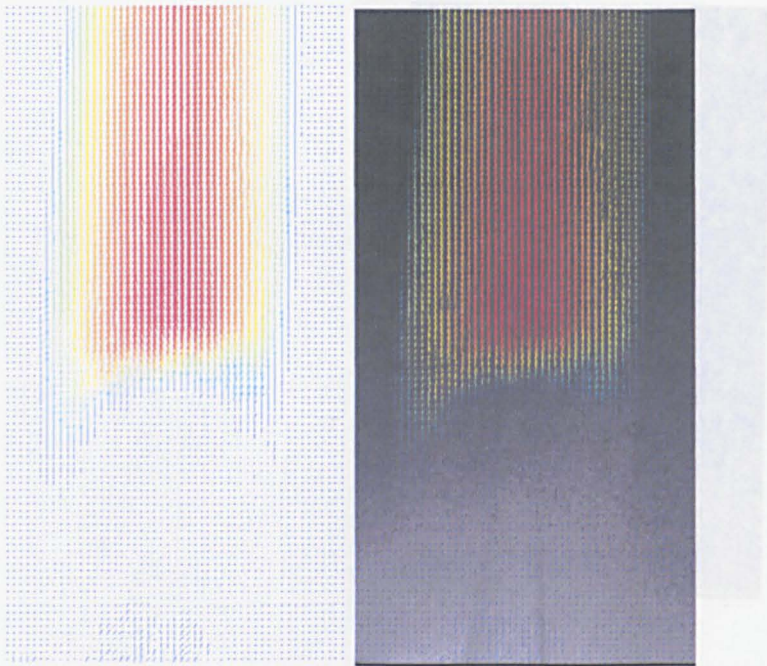
Frame 1 (left) and frame 2 (right)



Adaptive correlation

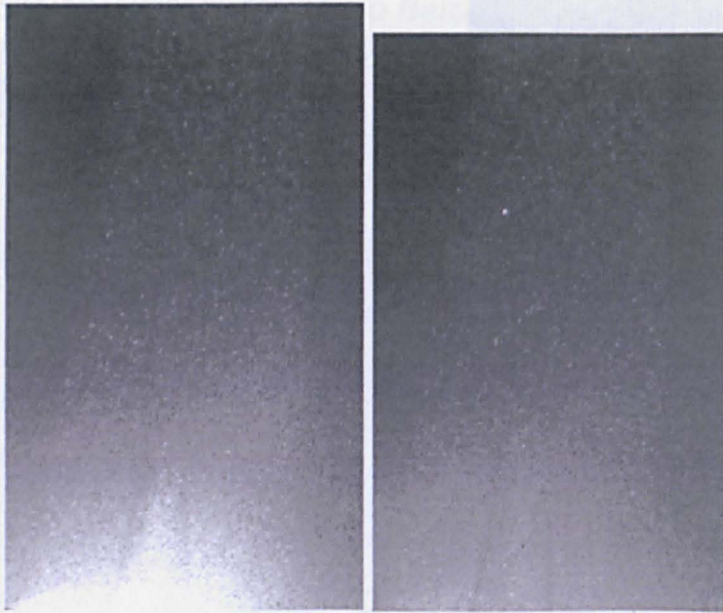


Moving average

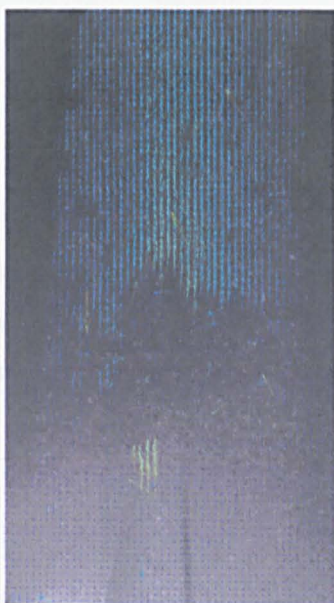
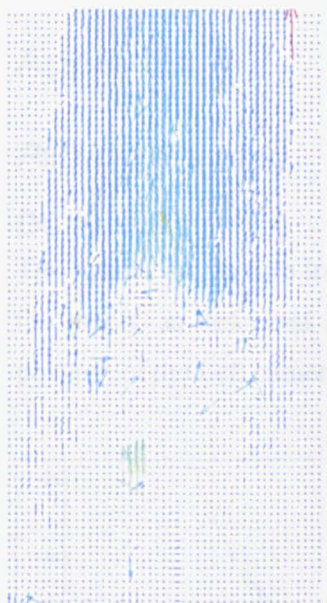


Average

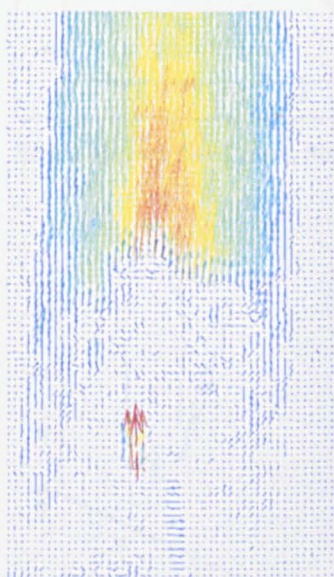
Stoichiometric flame 10kV



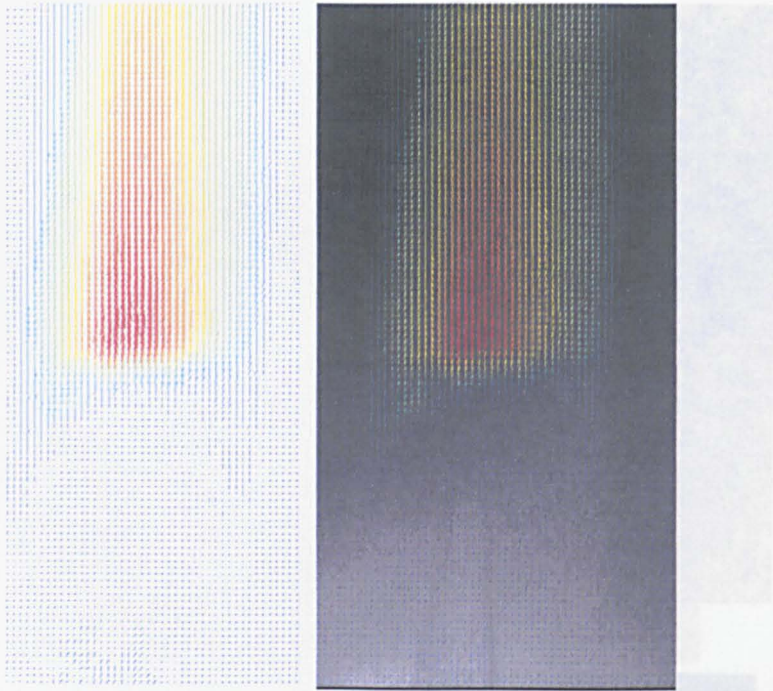
Frame 1 (left) frame 2 (right)



Adaptive



Moving average



Average PIV

Stoichiometric ratio 100%

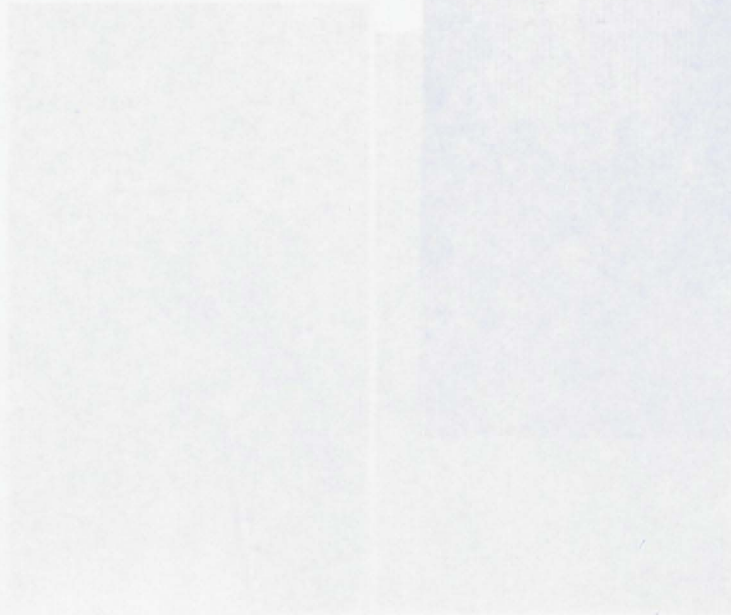


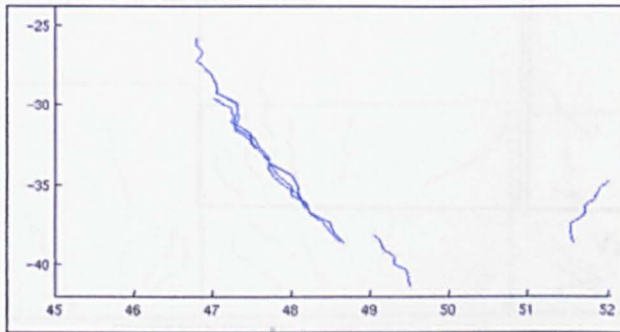
Figure 1 (left), Figure 2 (right)

Appendix 4

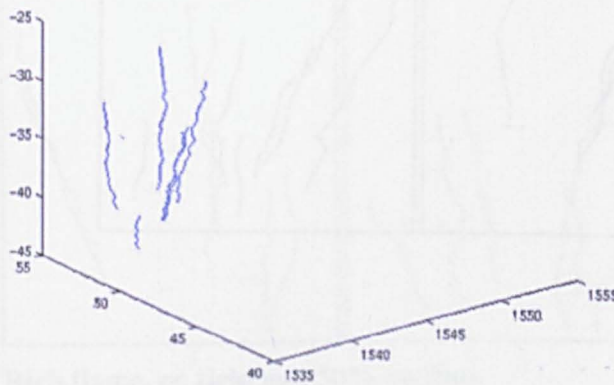
Particle tracking

DC Results

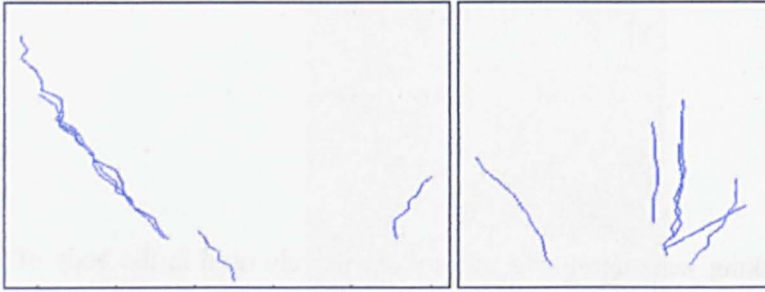
The results from particle tracking were unreliable and not extensively used in the body of the report, as described in Chapter 6. The scale is in mm, with the origin being the position of the Left camera.



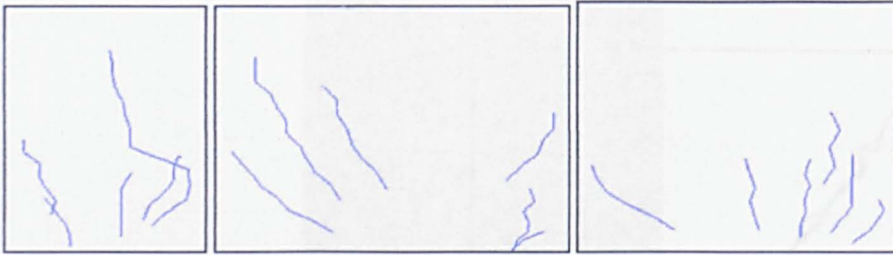
Scale shown for Lean, No field flame



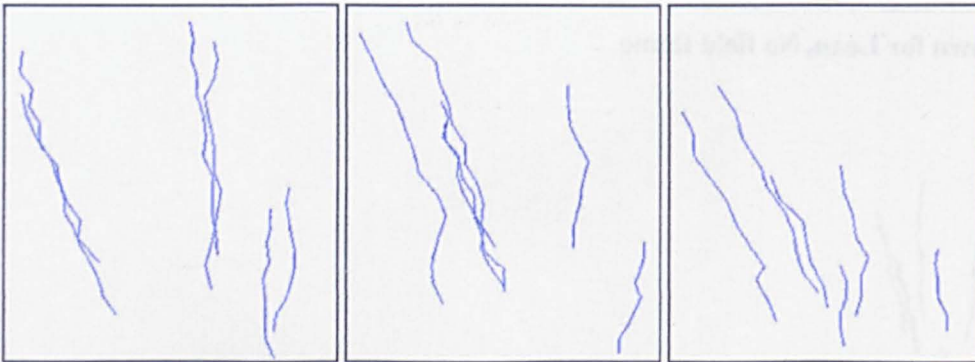
3D graph of a lean flame with no applied field



Lean, no field, 10kV



Stoichiometric, No field, 5kV and 10kV

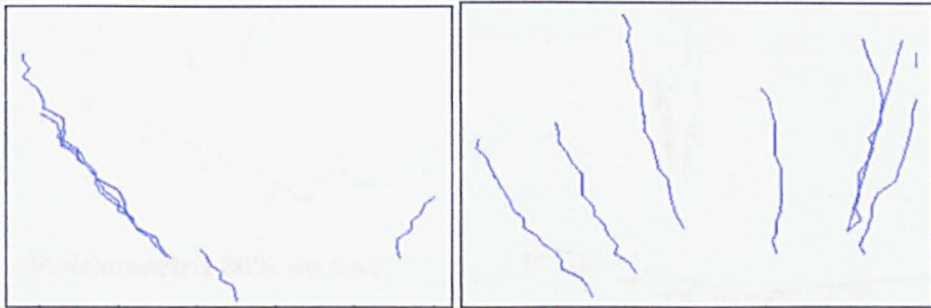


Rich No field, 5kV, 10kV

Pulse Results

The PIV equipment was not available to conduct tests with a pulse applied due to the difficulties in linking the pulse generator with the PIV imaging equipment. This should be possible in the future and is an important area of further work. The tests were conducted with particle tracking but the camera was not fast enough to record significantly any aerodynamic changes through the pulse duration. However, the main

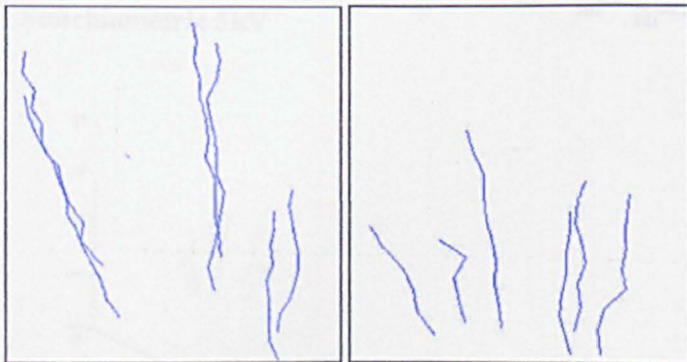
flow velocity should show distortions if the pulse changed the flame aerodynamically. The results are presented below.



Lean 0.5% on time pulse

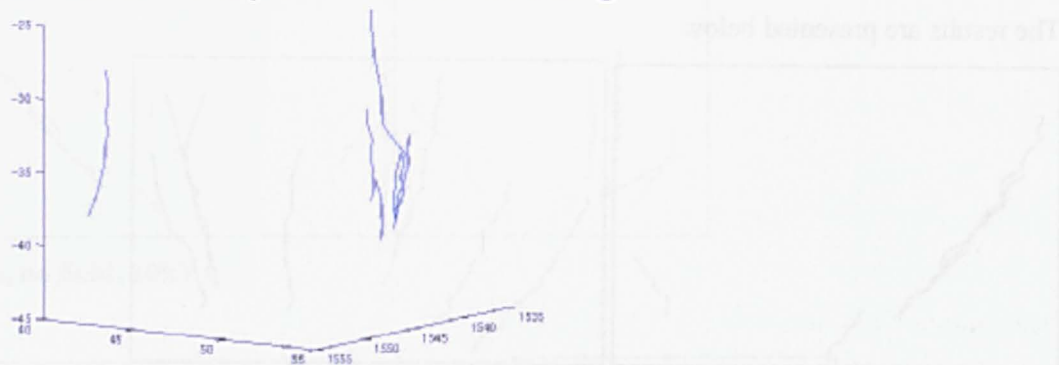


Stoichiometric flame No field, 20%, 50% and 80% on times

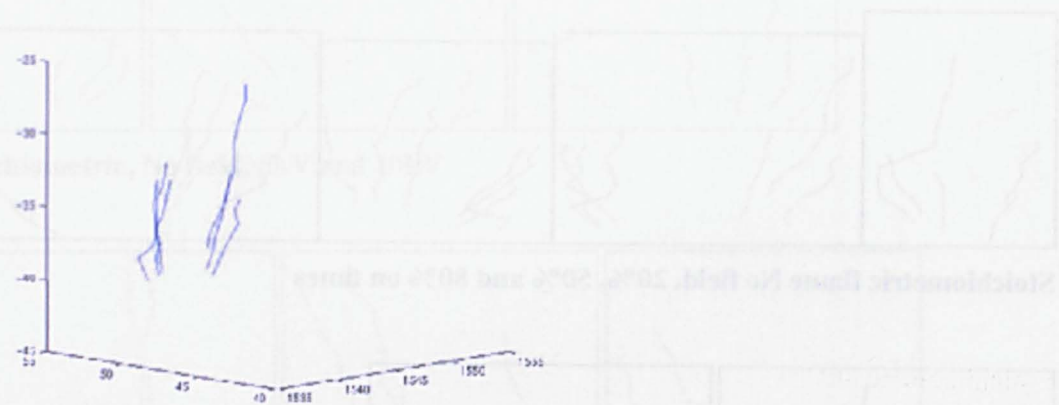


Rich flame, no field and 50% on time

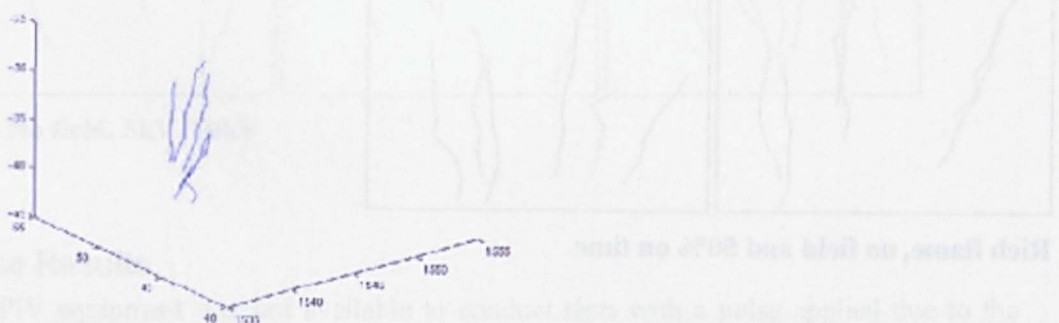
3 Dimensional Graphs of Particle Tracking



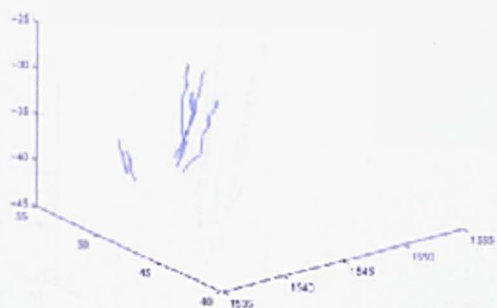
Stoichiometric No field



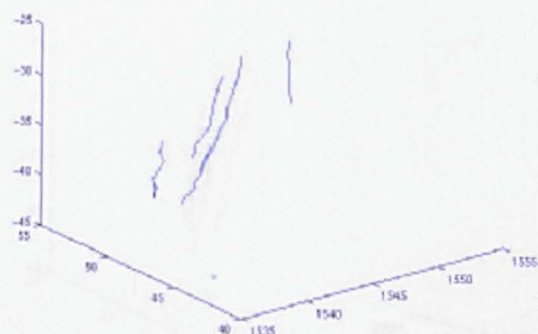
Stoichiometric 20% on time



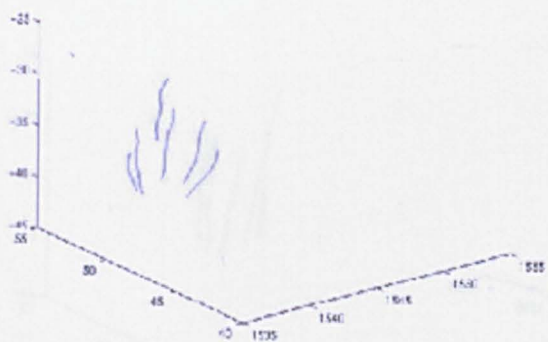
Stoichiometric 50% on time



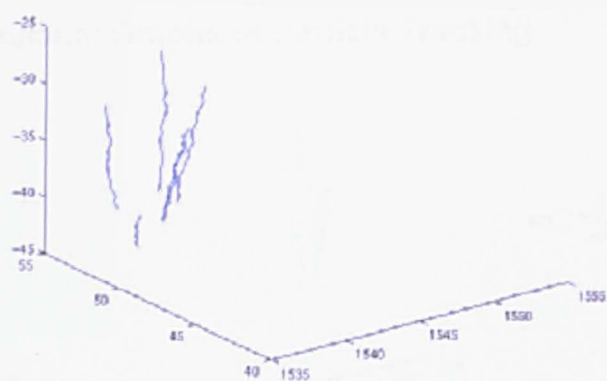
Stoichiometric 80% on time



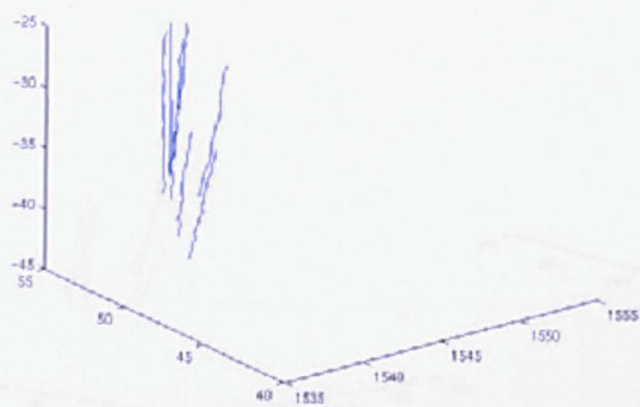
Stoichiometric 5kV



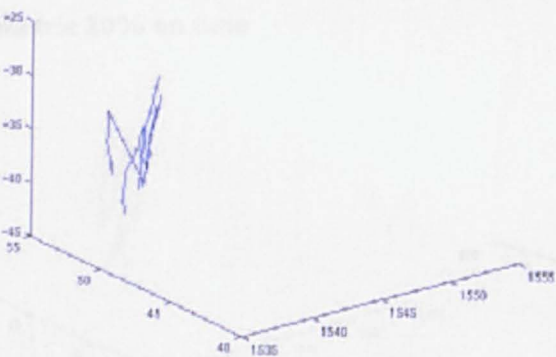
Stoichiometric 10kV



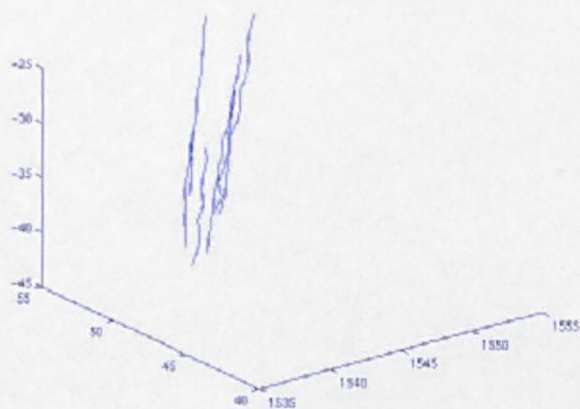
Lean No field



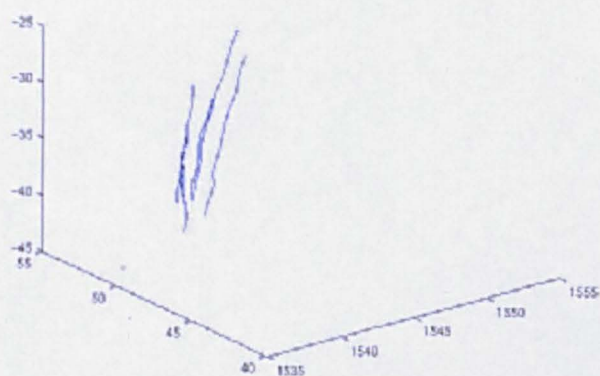
Lean 50% on time



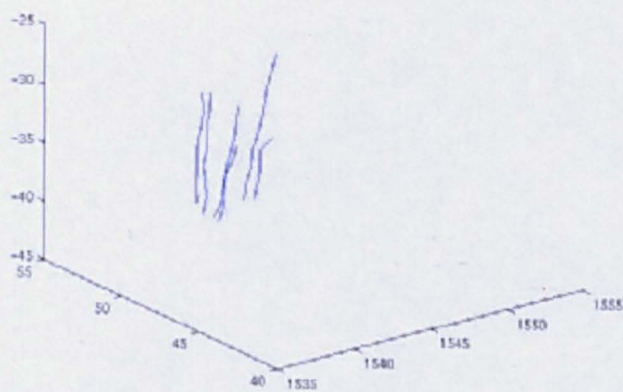
Lean 10 kV



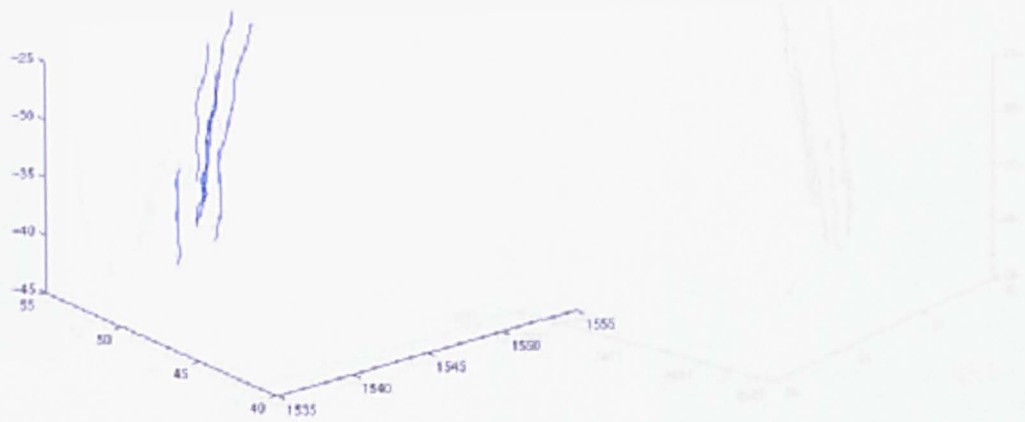
Rich No field



Rich 50% on time



Rich 5kV



Rich 10kV

